

The Generation and Characterisation of Low Fouling, Uniform, Gradient and Micropatterned Surfaces via Plasma Polymerisation

Donna Jade Menzies B.Sc (Hons 1)

Submitted in total fulfilment of the degree of Doctor of Philosophy

July 2011

Department of Materials Engineering

Monash University

Abstract

This thesis is focused on the generation, characterisation and application of PEG-like, low fouling surfaces deposited by plasma polymerisation of diethylene glycol dimethyl ether. The first part of the thesis focused on uniform films, where the ideal deposition parameters were identified for the fabrication of robust low fouling plasma polymer films, particularly with regards to the W/FM parameter by varying the plasma load power. A number of complimentary surface sensitive analytical tools were employed in film characterisation including, including XPS, NEXAFS and neutron reflectometry. A combination of these analytical techniques enabled us to determine that films deposited at lower load power retained a higher degree of monomer “PEG-like” functionality, particularly with regards to the ether content and these films displayed the most efficient low-fouling characteristics against BSA and lysozyme protein adsorption. Further to this, HeLa cell attachment was largely resisted by the lower-fouling higher ether containing plasma polymer surfaces. The use of neutron reflectometry in the analysis of the uniform plasma polymer films enabled us to further identify the densities and H content of the film, not otherwise determinable with XPS and ToF-SIMS. Using the scattering length densities we were also able to identify the full empirical formula of the plasma polymer films, where the lower load power that was shown to be most protein resistant (QCM-d) showed to have a chemical composition most similar to that of a typical PEG-grafted surface.

The second part of the results component of the thesis was focused on the generation and characterisation of gradient PEG-like plasma polymer surfaces. These surfaces are ideal for the high throughput analysis of material-biological interactions, and were shown to be

successful in the formation of chemical gradients of BSA, Lysozyme, IgG, human serum albumin (HAS) and fetal bovine serum (FBS). The gradient surfaces were analysed using complimentary techniques such as NEXAFS, XPS, synchrotron source gi FTIR microspectroscopy and ToF-SIMS and it was shown that more proteins adsorbed in regions of the gradients that displayed a lower ether and higher hydrocarbon and carbonyl content. Cell attachment was also investigated across the gradients, which appeared to be dictated by the adsorption of FBS which was present during the cell culture experiments. Time was shown to be a critical factor for the relative adsorption of FBS with the central region of the lower powered gradients showing to be FBS resistant (within XPS detection limits), while after a 24 hour adsorption period, proteins were measured across the entire length of the gradients.

The generation and application of chemically micropatterned surfaces is discussed in the final results chapter of this thesis. By controlling the electrode geometry, we were able to deposit functional, chemically micro-patterned surfaces in one step using plasma polymerisation of diethylene glycol dimethyl ether. By etching patterned holes in the top, active electrode, and placing it to sit 1 mm above the substrate in the plasma reactor, variation to the plasma flow and resulting sheath leads to a low-fouling surrounding coating, while the patterned features (deposited under the holes of the electrode) are more fragmented with a higher proportion of carbonyl and hydrocarbon species. The controlled spatial variation to surface chemistry was analysed and imaged using ToF-SIMS imaging and gi-FTIR microspectroscopy and the size and shape of the patterned features can be controlled with the design of the electrode. The biological applications of these chemically patterned surfaces was displayed by spatial control of protein (BSA) adsorption and cell (HeLa) attachment, as well as the spatial confinement of enzyme mediated self-assembled peptides.

ERRATA

- p. 71 Fifth and sixth sentences: replace Figures “3.3.1 and 3.3.2” with “Figures 3.1 and 3.2”
- p. 73 Third sentence: replace “Figure 3.3.2” and “Figure 3.3.3” with “Figure 3.2 and Figure 3.3”
- p. 74 First sentence: replace “Figure 3.3.4” with “Figure 3.4”
- p. 75 last sentence: “Figure 3.3.4” with “Figure 3.4”
- p. 76 Second and third sentences: replace “Table 3.3.1” with “Table 3.1”
- p. 77 second sentence: replace “Figure 3.3.5A” with “Figure 3.5A”
- p. 77 last sentence: replace “Figure 3.3.5B” with “Figure 3.5 B”
- p. 79 third and last sentence of second paragraph: replace “Figures 3.3.6” with “Figures 3.6”
- p. 81 fourth sentence replace “Figures 3.3.7 A” with “Figures 3.7 A”
- p. 81 fifth sentence replace “(Fig. 3.3.5A)” with “(Figure 3.5A)”
- p. 81 first sentence second paragraph replace “Figures 3.3.8” with “Figures 3.8 A and B”
- p. 82 second and third sentence replace: “(Figure 3.3.8)” with “Figure 3.8”
- p. 82 Figure 3.7 caption replace “immersion in PBS” with “ incubation in PBS overnight” so it reads “XPS C 1s curve fit for 5 (bottom spectra) to 50 W (top spectra) DGpp’s (dry; left spectra) and after “ incubation in PBS overnight (wet; right spectra)
- p. 83 first sentence replace “Figure 3.3.8” with “Figure 3.8”
- p. 83 first sentence second paragraph replace “Figure 3.3.9” with “Figure 3.9”
- p. 85 second sentence replace “Figure 3.3.10A” with “Figure 3.10A”
- p. 86 second sentence replace “Figure 3.3.10B” with “Figure 3.10B”
- p. 87 second sentence second paragraph replace “Figures 3.3.10” with “Figures 3.10.”
- p. 88 third sentence second paragraph replace “Figure 3.3.11” with “Figure 3.11”
- p. 88 fifth sentence: add in the nitrogen abbreviation “N” and read “less than 1 % N”
- p. 89 second sentence and p 92 first sentence: replace “DG” for “DEGDME”
- p. 90 section heading replace “3.2.4 Cell adhesion studies” with “3.3.4 Cell adhesion studies”
- p. 90 fifth sentence second paragraph replace “Table 3.3.3 and Figure 3.3.12” with “Table 3.2 and Figure 3.12”
- p. 90 eighth sentence second paragraph replace “Figure 3.3.12” and “Figure 3.2.12A” with “Figure 3.12” and “Figure 3.12A” respectively
- p. 91 first sentence replace “Table 3.3.3 and Figure 3.3.13” with “Table 3.2 and Figure 3.13”
- p. 91 Table legend replace “Table 3.3.3” with “Table 3.2”

ADDENDUM

- p. 23 line 5: delete “excited” and read “collides with the gaseous molecules.”
- p. 78 Figure 3.5 A figure caption: delete the words “with normalised absorbance units” and read “Overlay of FTIR spectra of DGpp films”
- p. 121 Table 4.2 is amended to include errors as shown below.
Table 4.2. Average film thickness, roughness, scattering length density and composition of PEG-like plasma polymer films as determined by AFM, X-ray and neutron reflectometry. Parameter uncertainties are reported as 1 s.d. Uncertainties in derived values (mass density and atomic composition) are approximate.

Table 2. Average film thickness, roughness, scattering length density and composition of PEG-like plasma polymer films as determined by AFM, X-ray and neutron reflectometry. Parameter uncertainties are reported as 1 s.d. Uncertainties in derived values (mass density and atomic composition) are approximate.

	10 W load power	20 W load power	50 W load power
film thickness (\AA)			
X-ray reflectometry	358.0 + 0.1	247.8 + 1.1	197 + 2
neutron reflectometry	369.5 + 0.4	245.4 + 0.4	226 + 3
scattering length density ^a , r ($\times 10^6 \text{\AA}^2$)			
X-ray reflectometry	10.9 + 0.6	11.3 + 0.9	8.9 + 0.6
neutron reflectometry	1.09 + 0.13	1.00 + 0.04	1.56 + 0.26
monomer atomic composition	$\text{C}_2\text{H}_{4.7}\text{O}_1$		
plasma polymer atomic composition ^a	$\text{C}_2\text{H}_{3.3+0.13}\text{O}_{0.9}$	$\text{C}_2\text{H}_{3.3+0.06}\text{O}_{0.78}$	$\text{C}_2\text{H}_{2.0+0.2}\text{O}_{0.6}$
mass density (g cm^{-3}) ^a	1.19 + 0.07	1.23 + 0.1	0.99 + 0.07

^aExcluding layer closest to air.

p. 157 sixth sentence. Add at the end of the sentence “ (please refer to Appendix 1 Figure 8 for the XPS survey scans to show the absence of any elemental F across the 5 and 30 W gradients prior to TFAA derivatisation)” so it reads “Figure 5.5A presents the F/C plots from quantified XPS survey spectra across the 5 and 30W DGpp gradient films after derivatisation with TFAA (please refer to Appendix 1 Figure 8 for the XPS survey scans to show the absence of any elemental F across the 5 and 30 W gradients prior to TFAA derivatisation).

p. 181 at the end of section 6.3.4 add “The complex mass spectra were analysed by detecting differences in the fragmentation patterns. This was achieved with the aid of Principal Component Analysis (PCA). Briefly, several fragments are selected from the ToF-SIMS spectra. The peaks are normalised to the sum of the intensities of the selected peaks and mean-centred prior to analysis. The input to PCA is a matrix where the rows are samples (i.e. spectra) and the columns are variables (i.e. peak intensities). The process of data decomposition by PCA results in the formation of two new matrices: a score matrix and a loading matrix. The scores show the relationship between the samples in the new coordinate (PC defined) space, whilst the loadings illustrate the relationship between the original variables and the principal components.

The primary task of PCA is to compress the original dataset in a way that most essential and useful information was retained. In the case of static SIMS spectra the original dataset, consisting of hundreds of variables, can be adequately described by few uncorrelated principal components. If one, two or three principal components form a satisfactory model, then data processed by PCA can be visualised. PCA was accomplished using PLS_Toolbox version 3.0 (Eigenvector Research, Inc., Manson, WA) along with MATLAB software v. 6.5, (MathWorks Inc., Natick, MA).”

p. 238 Appendix 1. Add to the end of the Appendix 1 the following figure

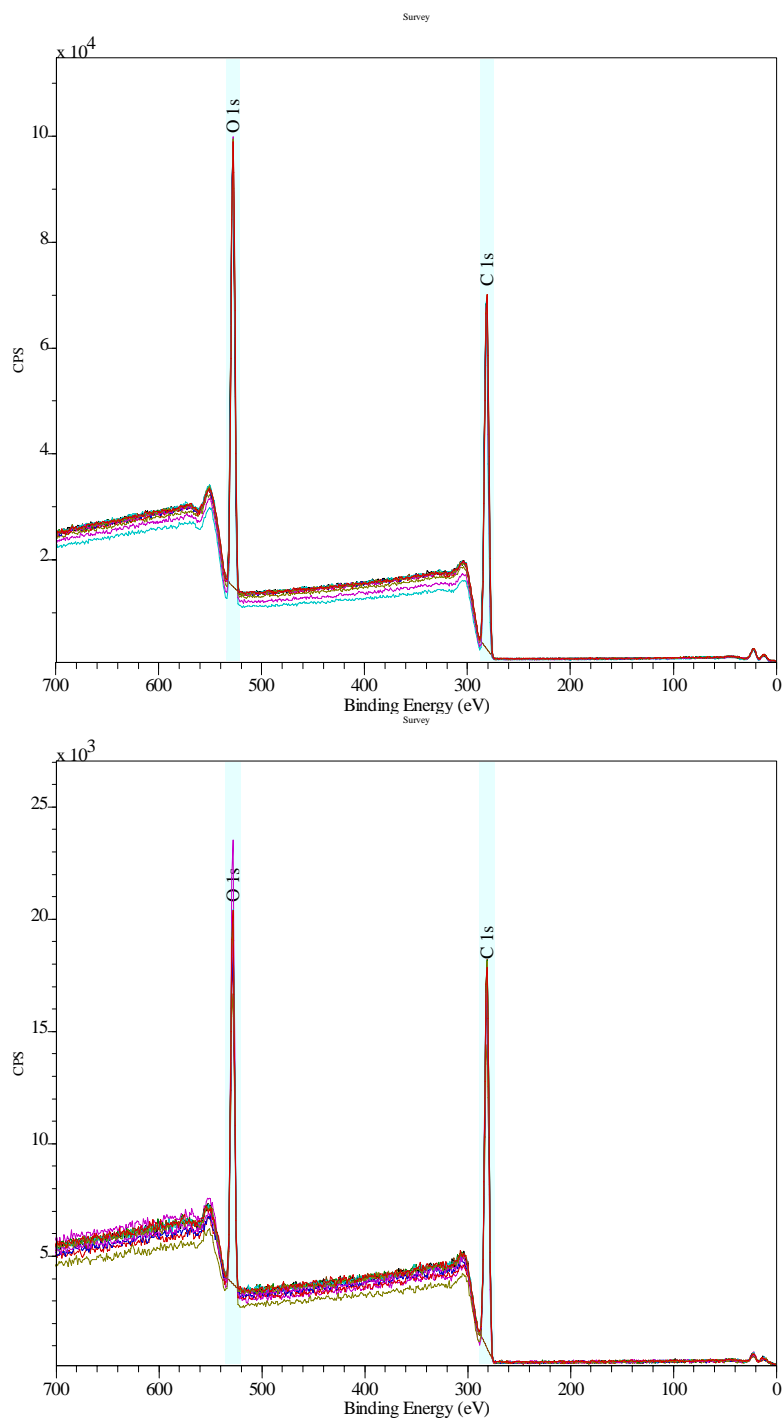


Figure 8. XPS elemental survey scans across 0 to 10 mm of the 5 W (top overlaid spectra) and 30 W (bottom overlaid spectra) gradient films. Only carbon and oxygen was detected.

Notice 1

Under the Copyright Act 1968, this thesis must be used only under the normal conditions of scholarly fair dealing. In particular no results or conclusions should be extracted from it, nor should it be copied or closely paraphrased in whole or in part without the written consent of the author. Proper written acknowledgement should be made for any assistance obtained from this thesis.

Notice 2

I certify that I have made all reasonable efforts to secure copyright permissions for third-party content included in this thesis and have not knowingly added copyright content to my work without the owner's permission.

PART A: General Declaration

Monash University

Monash Research Graduate School

Declaration for thesis based or partially based on conjointly published or unpublished work

General Declaration

In accordance with Monash University Doctorate Regulation 17/ Doctor of Philosophy and Master of Philosophy (MPhil) regulations the following declarations are made:

I hereby declare that this thesis contains no material which has been accepted for the award of any other degree or diploma at any university or equivalent institution and that, to the best of my knowledge and belief, this thesis contains no material previously published or written by another person, except where due reference is made in the text of the thesis.

This thesis includes 1 original paper published in a peer reviewed journal and 3 unpublished publications. The core theme of the thesis is the design, generation and characterisation of low fouling uniform, gradient and micropatterned plasma polymers surfaces. The ideas, development and writing up of all the papers in the thesis were the principal responsibility of myself, the candidate, working within the Department of Materials Engineering, under the supervision of Associate Professor John Forsythe and Dr. Ben W. Muir of CSIRO Material Science and Engineering.

The inclusion of co-authors reflects the fact that the work came from active collaboration between researchers and acknowledges input into team-based research.

In the case of chapters 4, 5, 6 and 7 my contribution to the work involved the following:

Thesis chapter	Publication title	Publication status*	Nature and extent of candidate's contribution
4	An X-ray and neutron reflectometry study of 'PEG-like' plasma polymer films	Submitted	Experimental design, conduct, data processing and writing
5	A one-step method for generating PEG-like plasma polymer gradients: Chemical characterisation and analysis of protein interactions	Published	Experimental design, conduct, data processing and writing
6	An XPS and TOF-SIMS study of protein and cell adsorption across PEG-like plasma polymer films with lateral compositional gradients	In draft	Experimental design, conduct, data processing and writing
7	One step multifunctional micropatterning of surfaces using asymmetric glow discharge plasma polymerisation	Submitted	Experimental design, conduct, data processing and writing

I have/ have not (circle that which applies) renumbered sections of submitted or published papers in order to generate a consistent presentation within the thesis.

Signed:

Date:

Statement of originality

I hereby declare that, to the best of my knowledge, this thesis contains no material previously published or written by another person, except where due reference is made in the text of this thesis. I also declare that the material has not been submitted, either in whole or part, for any degree at this or any other university.

.....
Donna J. Menzies

Acknowledgments

I would like to thank my supervisor Dr Ben Muir, for his endless encouragement and support throughout my entire PhD and for his valuable, knowledgeable feedback and advice. Ben, you have been an awesome mentor to me for the last four years of my life and I'm grateful for everything that you've done for me. I will continue to utilize the knowledge that you have instilled in me throughout the rest of my career.

I was also fortunate enough to have Associate Professor John Forsythe as my supervisor from Monash University, who has been very supportive, patient and helpful. I miss our Monash, Biomaterials group meetings, and would like to thank all of the students involved for making it a friendly and conducive environment.

I would like to also acknowledge the people who have helped me throughout my PhD, Celesta Fong and Thomas Gengenbach not only for their ongoing technical advice but also for their moral support on those late night synchrotron experiments. I appreciate the financial support from the OCE scholarship through CSIRO. I also appreciate the company and support of all my friends from "The Ballroom" at CSIRO.

Finally thank you to my family, Paul and friends for their constant support and encouragement throughout my PhD.

Publications Obtained during PhD

Muir BW, Tarasova A, Gengenbach TR, **Menzies DJ**, Meagher L, Rovere F, Fairbrother A, McLean KM, Hartley PG. Characterization of Low-Fouling Ethylene Glycol Containing Plasma Polymer Films. *Langmuir* **2008**, 24, (8), 3828-3835. Published

Menzies DJ, Cowie BC, Fong C, Forsythe J, Gengenbach T, Mc Lean K, Puskar L, Textor, M, Thomsen L, Tobin M., Muir B. A one-step method for generating PEG-like plasma polymer gradients: Chemical Characterisation and Analysis of protein interactions. *Langmuir* **2010**, 26, (17), 13987-13994. Published

Menzies DJ, Forsythe J, Birbilis N, Johnson G, Charles C, McFarland G, Williams R, Fong C, Leech P, McLean K, Muir B. One step multifunctional micropatterning of surfaces using asymmetric glow discharge plasma polymerisation. *Advanced Materials*, submitted

Menzies DJ, Shen H, McLean K, Forsythe J, Gengenbach T, Fong C, Muir B. An X-ray and neutron reflectometry study of 'PEG-like' plasma polymer films. *Interface*, submitted

Menzies DJ, Jasieniak M, Griesser H, Forsythe J, Johnson G, McFarland G, Muir B. An XPS and TOF-SIMS study of protein and cell adsorption across PEG-like plasma polymer films with lateral compositional gradients. *Surface Science*, In preparation

TABLE OF CONTENTS

1. GENERAL INTRODUCTION, MAJOR AIMS AND SCOPE OF THE THESIS	1
1.1 AN INTRODUCTION TO PLASMA POLYMERIZATION IN BIOMATERIALS	1
1.2 MAJOR AIMS AND SCOPE OF THIS PHD RESEARCH THESIS.....	3
1.3 REFERENCES	7
 2. SCIENTIFIC BACKGROUND AND LITERATURE REVIEW	 9
2.1 POLY(ETHYLENE GLYCOL)	9
2.1.1 Theories of protein resistance	10
2.1.2 Methods of fabrication PEG films	16
2.1.3 Applications of PEG based materials	16
2.2 PLASMA POLYMERISATION.....	20
2.2.1 Plasma Fundamentals	20
2.2.2 The Plasma Sheath.....	22
2.2.3 Glow discharge plasmas and excitation sources	22
2.2.4 Pulsed and continuous wave glow discharges	24
2.2.5 Plasma Polymerisation, Parameters and use in Biomaterials.....	25
2.3 METHODS OF THIN FILM ANALYSIS	29
2.3.1 Fourier transform infra red spectroscopy (FTIR)	30
2.3.2 X-ray Photoelectron Spectroscopy (XPS).....	31
2.3.3 Near Edge X-ray Absorption Fine Structure (NEXAFS)	32
2.3.4 Time of Flight Secondary Ion Mass Spectrometry (ToF-SIMS)	33
2.3.5 Neutron Reflectometry	34
2.3.6 Contact Angle Goniometry	35
2.3.7 Atomic Force Microscopy (AFM)	36
2.4 SURFACE BOUND CHEMICAL GRADIENTS IN BIOMATERIALS RESEARCH	36
2.4.1 Types of Gradient surfaces	39
2.4.2 Methods of gradient fabrication.....	39
2.5 MICROPATTERNED SURFACES	42
2.5.1 Methods for Generating Micropatterned Surfaces	44
2.5.2 Surface Analysis of Micropatterned Surfaces.....	45
2.6 REFERENCES	46

Results Part 1: Investigating the Properties of Uniform PEG-like Plasma polymers

3. A STUDY INTO OF THE EFFECTS OF PLASMA PROCESSING PARAMETERS ON THE PRODUCTION OF UNIFORM, LOW FOULING PEG-LIKE PLASMA POLYMER FILMS	63
3.1 INTRODUCTION	63
3.2 MATERIALS AND METHODS.....	64
3.2.1 Substrate Materials and Cleaning	64
3.2.2 Masking	64
3.2.3 Plasma Polymerisation.....	65
3.2.4 Monomer flow rate determination	65
3.2.5 Protein Adsorption.....	66
3.2.6 Atomic Force Microscopy	66
3.2.7 Grazing Incidence Fourier Transform Infra Red Spectroscopy	67
3.2.8 Contact Angle Goniometry	67
3.2.9 X-ray Photoelectron Spectroscopy	67

3.2.10 Near Edge X-ray Absorption Fine Structure.....	68
3.2.11 Cell Attachment Study.....	69
3.3 RESULTS AND DISCUSSION.....	71
3.3.1 Plasma Polymerisation.....	71
3.3.2 Film Thickness and Wettability.....	76
3.3.3 Film Chemistry.....	77
3.3.3 Protein Adsorption Studies.....	88
3.2.4 Cell adhesion studies.....	90
3.3 CONCLUSIONS.....	92
3.4 REFERENCES.....	94

4. AN X-RAY AND NEUTRON REFLECTOMETRY STUDY OF ‘PEG-LIKE’ PLASMA POLYMER FILMS..... 100

4.1 ABSTRACT.....	100
4.2 INTRODUCTION.....	101
4.3 MATERIALS AND METHODS.....	104
4.3.1 Substrates.....	104
4.3.2 Plasma Polymer Deposition.....	105
4.3.3 Atomic Force Microscopy.....	106
4.3.4 X-ray Photoelectron Spectroscopy.....	106
4.3.5 Contact angle measurements.....	107
4.3.6 Quartz crystal microbalance measurements.....	107
4.3.7 Reflectometry Measurements.....	108
4.4 RESULTS AND DISCUSSION.....	109
4.4.1 Characterisation of the films using Atomic Force Microscopy (AFM).....	109
4.4.2 Film stability, water uptake and protein resistant properties of the DGpp films characterised by QCM-D.....	111
4.4.3 Surface Chemistry.....	115
4.4.4 Characterisation of the films using X-ray and neutron reflectometry in air.....	117
4.5 CONCLUSIONS.....	128
4.6 ACKNOWLEDGEMENTS.....	130
4.7 REFERENCES.....	131

Results Part 2: Generation and Characterisation of Gradient PEG-like Plasma Polymers

5. A ONE-STEP METHOD FOR GENERATING PEG-LIKE PLASMA POLYMER GRADIENTS: CHEMICAL CHARACTERISATION AND ANALYSIS OF PROTEIN INTERACTIONS..... 139

5.1 ABSTRACT.....	139
Keywords: PEG gradient, plasma polymer, protein adsorption, NEXAFS.....	140
5.2 INTRODUCTION.....	140
5.3 MATERIALS AND METHODS.....	143
5.3.1 Substrates Preparation.....	143
5.3.2 Plasma Polymerisation.....	143
5.3.3 Profilometry.....	144
5.3.4 Grazing incidence FTIR microspectroscopy.....	144
5.3.5 X-ray Photoelectron Spectroscopy (XPS).....	145
5.3.6 Near Edge X-ray Adsorption Fine Structure (NEXAFS) spectroscopy.....	146
5.3.7 Surface Derivatisation.....	146
5.3.8 Protein adsorption.....	147
5.4 RESULTS AND DISCUSSION.....	148
5.4.1 Plasma Deposition.....	148

5.4.2 giFTIR microspectroscopy	149
5.4.3 X-Ray Photoelectron Spectroscopy	152
3.4.4 NEXAFS spectroscopy	154
5.4.5 Surface Derivatisation	157
5.4.6 Protein Adsorption	160
5.5 CONCLUSIONS	163
5.6 ACKNOWLEDGEMENTS	163
5.7 REFERENCES	165

6. AN XPS AND TOF-SIMS STUDY OF PROTEIN AND CELL ADSORPTION ACROSS PEG-LIKE PLASMA POLYMER FILMS WITH LATERAL COMPOSITIONAL GRADIENTS 172

6.1 ABSTRACT	172
6.2 INTRODUCTION	173
6.3 MATERIALS AND METHODS.....	178
6.3.1 Substrate Preparation	178
6.3.2 Plasma Polymerisation.....	178
6.3.3 X-Ray Photoelectron Spectroscopy (XPS)	179
6.3.4 Time-of-Flight Secondary Ion mass Spectroscopy (ToF-SIMS)	180
6.3.5 Serum protein adsorption.....	181
6.3.6 Cell attachment	181
6.4 RESULTS AND DISCUSSION.....	182
6.4.1 XPS analysis of gradient films.....	183
6.4.2 ToF-SIMS Chemistry	185
6.4.3 XPS and ToF-SIMS analysis of Protein Adsorption on gradient films (HSA)	189
6.4.4 Fetal Bovine Serum Adsorption and HeLa cell attachment.....	193
6.5 CONCLUSIONS	198
6.6 REFERENCES	199

Results Part 3: Generation and Characterisation of Chemically Micropatterned surfaces

7. ONE STEP MULTIFUNCTIONAL MICROPATTERNING OF SURFACES USING ASYMMETRIC GLOW DISCHARGE PLASMA POLYMERISATION 208

7.1 ABSTRACT	208
7.2 INTRODUCTION	209
7.3 MATERIALS AND METHODS.....	210
7.3.1 Plasma polymer deposition.....	210
7.3.2 Preparation of patterned plasma reactor electrodes	210
7.3.3 Optical images of patterns	210
7.3.4 Optical profilometry	211
7.3.5 giFTIR microspectroscopy	211
7.3.6 ToF-SIMS measurements	211
7.3.7 Protein adsorption.....	211
7.3.8 Cell culture	211
7.3.9 Site specific growth of self assembling peptides	212
7.4 RESULTS AND DISCUSSION.....	213
7.5 CONCLUSIONS	220
7.6 REFERENCES	221

8. CONCLUSIONS AND FUTURE WORKS	223
8.1 CONCLUSIONS	224
8.1.1 Uniform PEG like plasma polymers	224
8.1.2 PEG-like gradient plasma polymers	227
8.1.3 Chemically patterned plasma polymer surfaces.....	228
8.2 FUTURE DIRECTIONS	229
 APPENDIX 1	 231
SUPPORTING INFORMATION FOR CHAPTER 5.....	231
 APPENDIX 2	 239
SUPPORTING INFORMATION FOR CHAPTER 7.....	239

List of Abbreviations

AFM	Atomic force microscopy
BE	binding energy
DG	Diethylene glycol dimethyl ether
FTIR	Fourier Transform Infra red
gi	Grazing incidence
ITO	Indium tin oxide
HA	Heptylamine
NEXAFS	Near edge X-ray absorption fine structure
NR	Neutron reflectometry
PEG	poly(ethylene glycol)
PEY	partial electron yield
pp	Plasma polymer
QCM-d	Quartz crystal microscopy with dissipation
rfgd	radio frequency glow discharge
ToF-SIMS	time of flight secondary ion mass spectroscopy
XPS	X-ray Photoelectron Spectroscopy

Chapter 1:

General Introduction, Major Aims and Scope of the Thesis

1. General Introduction, Major Aims and Scope of the Thesis

1.1 An Introduction to Plasma Polymerization in Biomaterials

The research presented in this thesis has relied on a deposition process termed “plasma polymerisation” to produce a series of PEG-like surface bound films. These films firstly allowed us to study the critical film properties that impart a low-fouling nature into the PEG-like films. Secondly, they enabled the production of advanced biomaterials capable of studying, optimising and controlling material-biological interactions, in the form of both lateral surface gradients as well as micropatterned surfaces which rely on a defined distinction between fouling and non-fouling regions.

The ability to generate materials that are low fouling, that is resist the adsorption of non-specific proteins, is critical to the functioning of many biomaterials, biomedical devices, implants and in vitro diagnostics. In the case of blood contacting devices/materials, the adsorption of plasma proteins can result in platelet adhesion and possible thrombosis, while for tissue contacting devices, non-specific protein adsorption can result in a proliferation of macrophages and other inflammatory response cells, causing inflammation and possible rejection of the foreign device/material.¹

Plasma polymerisation is the formation of surface bound polymeric material. When an organic precursor or monomer is introduced into a reactor vessel and exposed to an electrical stimulus (such as radio-frequency or microwave), the monomer forms a plasma within the reactor; an electrically neutral, ionised gas species which have a characteristic

glow discharge, consisting of high energy, charged electrons, ions, radicals and neutrals.²

³ A series of complex molecular events occur leading to the grafted, pinhole free, highly crosslinked polymer like deposition. Firstly, ionisation of the monomer molecules occurs from collisions with the high energy electrons within the glow discharge, creating a series of energetic radicals, free electrons, ions and excited molecular fragments, which can form new molecular fragments uncommon to the monomer that was introduced into the plasma reactor. Condensation and polymerisation of these species occurs, initiated from reactions of the radicals with the substrate and other molecular fragments within the plasma, forming a highly crosslinked grafted polymer film, composed of a complex chemical structure. The plasma polymer differs from a conventional polymer, in that it does not consist of a series of repeated monomer units due to the complex ionisation, fragmentation and recombination processes occurring within the plasma, but rather a more disordered cross-linked system.

Plasma polymerisation, both for film deposition and surface modification has been studied extensively since around the 1960's.^{3,4} Since the emergence of nanotechnology in the 1990's the use of plasma polymerisation has become an increasingly popular applied technique within the biomaterials sector to create surfaces with specific chemical functionality and physical properties. The potential benefits of using plasma polymerisation in the field of biomaterials and biomedicine was noticed as early as the late 1960's by Hollahan et al.,⁵ who utilised plasma polymerisation to create reactive amine functionalities. The amines were exploited to immobilise heparin with the vision of creating blood compatible materials.

Some of the main advantages of using plasma polymerisation include the ability to dictate surface functionality by choice of monomer, the production of thin, pin-hole free, conformant film to almost any substrate, the deposition process is quick and easy, involving low costs, as well as providing a sterile environment within the reactor. Furthermore, the degree of ionisation to the monomer can be controlled to a degree, by careful manipulation of some of the processing parameters, primarily the Yasuda factor⁶ (refer to section 2.2.5.1) which considers the flow rate, input power and molecular weight of the gas.

1.2 Major Aims and Scope of this PhD Research Thesis

The overall aim of this research project is to obtain a more thorough understanding of the mechanisms responsible for the low protein adsorption characteristics of PEG-like plasma polymer films. In more specific terms, this research project will identify the critical processing and morphological characteristics for enhanced low-fouling plasma polymer films for biomedical applications. These are summarised below:

- Identify the critical process parameters of radio frequency glow discharge (rfgd) plasma polymerisation to yield low-fouling PEG-like surfaces
- Identify the important chemical and physical characteristics of the plasma polymer films that infer protein resistance
- Investigate the adsorption/resistance of the plasma polymer films and various proteins

- Identify and exploit potential applications for the protein resistant plasma polymer surfaces such as the generation of micropatterned and gradient surfaces

Chapter 1 of the thesis provides a general introduction and outline of the thesis, while **chapter 2** reports the background and literature review of the thesis topics. Most of the results chapters represent individual research papers (either published or in preparation) and is comprised of 3 parts, where **part I (chapters 3 and 4)** relates to the synthesis and characterisation of uniform PEG-like plasma polymer films. Initial research into the production of low fouling uniform PEG-like plasma polymer films, including a characterisation of the deposition processes such as flow rate, and inflow and outflow of the diglyme monomer is reported in **chapter 3**. A thorough chemical characterisation of the films was performed using a number of complimentary techniques including X-ray photoelectron spectroscopy (XPS), near-edge X-ray absorption fine structure (NEXAFS) and grazing incidence (gi) Fourier transform infra red (FTIR) spectroscopy, in order to understand the effect of plasma processing parameters, such as input power and deposition time. The effects of film thickness and wettability were also analysed and reported. The resulting film properties were correlated with the films ability to resist protein adsorption and cell attachment, in order to gain a better understanding of the requirements to produce robust, low fouling surfaces. **Chapter 4** also reports on the production and analysis of uniform PEG-like plasma polymer films, however this chapter is comprised of a publication submitted to *The Journal of the Royal Society Interface*, titled “An X-ray and Neutron reflectometry study of ‘PEG-like’ plasma polymer films”. The paper reports on the full chemical composition (empirical formula) of the films

including hydrogen content (not determinable by XPS or NEXAFS), mass densities, and wettability and swelling behaviour of the films. The surface morphology of the films is also reported as is the adsorption of a model protein, BSA, which was measured via changes in frequency responses using quartz crystal microbalance-dissipation. While the uniform PEG-like pp films reported in chapter 3 were deposited at a uniform 60 seconds with the load power being the only variable, in this chapter, due to the film thickness requirement of ~ 20 nm when using neutron reflectometry, optimisation of deposition time for each load power used was required to achieve the desired film thickness, where the effects of the resulting surface morphologies could be justified by data reported in Chapter 3, which measured changes in pressure over time as a function of plasma load power.

Part II, including **chapters 5 and 6** discusses the generation and characterisation of surface bound chemical gradients via a one step plasma polymerisation method. **Chapter 5** comprises of a paper published in *Langmuir* titled “One-step method for generating PEG-like plasma polymer gradients: chemical characterization and analysis of protein interactions”. This paper introduces the method of gradient generation, as well as reporting a thorough chemical characterisation, and discussion of protein adsorption using three proteins of varied size and charge. Furthermore, the versatility of the gradients was highlighted by using surface derivatization of a graft copolymer of poly (L-lysine) and poly(ethylene glycol) (PLL-g-PEG copolymer) to display the reactivity of the gradient films toward primary amine groups, which was correlated to residual aldehyde, ketone and carboxylic acid functionalities within the films. **Chapter 6** reports on the use

of the surface gradients as a tool for the investigation and control of biological interactions. Here, the attachment of FBS across the gradients was monitored and correlated with the residual ether content, and also showed to dictate HeLa cell attachment. Furthermore, the importance of serum incubation time is highlighted in dictating possible cell-material response.

Part III, consisting of **chapter 7** discusses the generation of a one-step plasma polymerisation micro-patterning technique, referred to as “plasma induced patterning via electrode templates”. To the best of our knowledge, this is the first ever described one-step micro-patterning technique. This chapter is comprised of a paper submitted to *Advanced Materials* titled “One step multifunctional micropatterning of surfaces using asymmetric glow discharge plasma polymerisation”. The paper shows the techniques ability to pattern a variety of different shapes and micro-environments, which were imaged using optical profilometry, as well showing surface chemical mapping across the patterns using time of flight secondary ion mass spectroscopy (ToF-SIMS) and synchrotron source g-FTIR. Cell attachment is shown to remain spatially confined to the patterned features with the surrounding high ether film remaining cell resistant. Furthermore, the applicability and versatility of the patterned films is highlighted by achieving spatially confined, enzyme mediated peptide self-assembly. Finally, **Chapter 8** summarises the outcomes and conclusions achieved from this body of research and highlights the particular areas of research related to the project that warrant further investigation.

1.3 References

1. Feng, W.; Nieh, M. P.; Zhu, S.; Harroun, T. A.; Katsaras, J.; Brash, J. L., Characterization of protein resistant, grafted methacrylate polymer layers bearing oligo(ethylene glycol) and phosphorylcholine side chains by neutron reflectometry. *Biointerphases* **2007**, 2, (1), 34-43.
2. Chu, P. K.; Chen, J. Y.; Wang, L. P.; Huang, N., Plasma-surface modification of biomaterials. *Materials Science and Engineering: R: Reports* **2002**, 36, (5-6), 143-206.
3. Förch, R.; Zhang, Z.; Knoll, W., Soft Plasma Treated Surfaces: Tailoring of Structure and Properties for Biomaterial Applications. *Plasma Processes and Polymers* **2005**, 2, (5), 351-372.
4. Yasuda, H., Glow-discharge polymerization. *Macromolecular Reviews Part D- Journal of Polymer Science* **1981**, 16, 199-293.
5. Hollahan, J. R.; Stafford, B. B.; Falb, R. D.; Payne, S. T., Attachment of amino groups to polymer surfaces by radiofrequency plasmas. *Journal of Applied Polymer Science* **1969**, 13, (4), 807-816.
6. Yasuda, H. K. H. K., Some important aspects of plasma polymerization. *Plasma processes and polymers* **2005**, 2, (4), 293-304.
7. Allen, S. J.; Curran, A. R.; Templer, R. H.; Meijberg, W.; Booth, P. J., Controlling the Folding Efficiency of an Integral Membrane Protein. *Journal of Molecular Biology* **2004**, 342, (4), 1293-1304.

Chapter 2:

Scientific Background and Literature Review

2. Scientific Background and Literature Review

2.1 Poly(ethylene glycol)

Poly(ethylene glycol) (PEG) is a material that is widely used in biomedical technologies due to its low fouling nature¹ and the fact that it is non-toxic and has been approved for use in humans by the FDA. It is composed of quite a simple chemical structure, containing carbon, oxygen and hydrogen (Figure 2.1) however the polymer has many complex and unique properties.

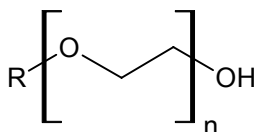


Figure 2.1 Chemical structure of poly(ethylene glycol), where R can either be an H or CH₃ and n is the number of ethylene oxide units in the polymer.

It has an inherent ability to resist the adsorption of non-specific proteins. This characteristic of PEG macromolecules provides many potential applications; it is of particular interest in the biomedical field since the design of many biomaterials is aimed at preventing the adsorption of blood proteins. The adsorption of these proteins *in-vivo*, followed by platelet adhesion can result in localised thrombosis.² It is reported that over half of hospital acquired bacterial infections are associated with implants or internal medical devices,³ so it is vital to design biomaterials with chemical and physical properties that can limit non-specific protein adsorption while remaining compatible with living cells.³⁻⁵ The low fouling nature of PEG-like molecules also lends itself to use in such applications in the biomedical and biotechnology fields including the design of

biosensor devices based on the specific immobilisation of biomolecules,^{6, 7} as cellular guides for tissue engineering⁷⁻¹⁰ and for drug delivery based devices¹¹⁻¹⁴ as well as being highly utilised in industrial applications such as surfactant production, food packaging and cosmetic production. Furthermore, the inertness of PEG-like coatings is also attractive from a fundamental research perspective, for example in the enhancement and development of high throughput screening utilising biomolecules,^{15, 16} micro-array technology^{17, 18} and micro-fluidic systems.¹⁹⁻²²

2.1.1 Theories of protein resistance

Many experimental studies^{2, 23-28} have been employed to investigate the mechanisms of protein resistance that PEG-based coatings display, however it remains an area of ongoing contention. Some of these theories include hydrophobic interactions and electrostatic double layer forces²⁹, but two of the most accepted theories proposed in the literature include the ‘steric repulsion’ theory and the effect of the ‘water barrier’. The steric repulsion theory was first proposed by DeGennes et al.³⁰ using free energy calculations. This theory proposes that an approaching protein causes compression of the PEG chains, which results in a conformational entropy loss making protein adsorption onto a PEG surface thermodynamically unfavourable. The steric repulsion theory has been applied to explain the inertness of longer chain ($n \geq 6$) PEG-based films, but does not provide a molecular level explanation for their protein resistant properties.

The effect of the ‘water barrier’ has been supported by many researchers.^{15, 31-33} The theory proposes that the tight, directional hydrogen bonding between the water molecules and the PEG chains provide a physical barrier against protein adsorption at the PEG-

water interface. The effect of the water barrier theory has been primarily applied to oligo(ethylene glycol) (OEG) self assembled monolayer's (SAMs) with shorter chains ($n=2-8$). The densely packed shorter OEG-SAMs have less freedom for conformational change upon protein exposure³⁴ allowing for a distinction between the importance of the steric component and the effect of the water barrier on protein resistance. Molecular simulations of the water structure at PEG interfaces indicate that bound water layers adjacent to the OEG-SAMs are largely responsible for the reported repulsive hydration forces along with a small steric contribution.^{31, 32, 35} Kim et al.³⁶ suggested that the effect of the water barrier was not sufficient to impart the protein resistance of OEG-SAMs and that some form of steric component must also be present. Grunze et al.³² suggested that the chain conformation of OEG-SAMs is an important determinant for protein resistance, but also highlighted the importance of both the steric and water barrier theories. They reported that OEG-SAMs existing in a helical conformation were more inert since the helical structure provides a template for water nucleation as opposed to OEG-SAMs of a trans configuration.

In work by Kim et al.³⁶ using a surface force apparatus (SFA) an interfacial water layer with a viscosity 6 orders of magnitude higher than bulk water on an OEG-SAM was reported. They postulated that the increased viscosity may be due to the formation of ice-like water up to 5nm from the 3 mer OEG-SAM. Schwendel et al.³⁷ observed a reduced density of water up to 4nm from the surface in which they suggest it may be caused by the formation of 'nanobubbles'. It was not seen however in an additional study of some OEG-SAMs by Fick et al.³⁸ A density depression in the structure of water was observed

in a SFA study by Heuberger et al.³⁹ In addition recent work suggests that protein resistance on OEG-SAMs could also be due in part to fixed dipoles and charging effects from hydroxide ion adsorption.⁴⁰

More recently, Latour has proposed a thermodynamic perspective on the inertness of PEG tethered surfaces²⁶. He suggested both entropic and enthalpic effects should be considered. Entropic penalties result from bond formation between a surface-tethered chain and a protein since this reduces the chains configurational space and freedom of gyration. The bond formation that occurs between water molecules and the tethered chains don't result in this entropic decrease since the small, mobile water molecules don't hinder the configurational space of the chains (Figure 2.2).

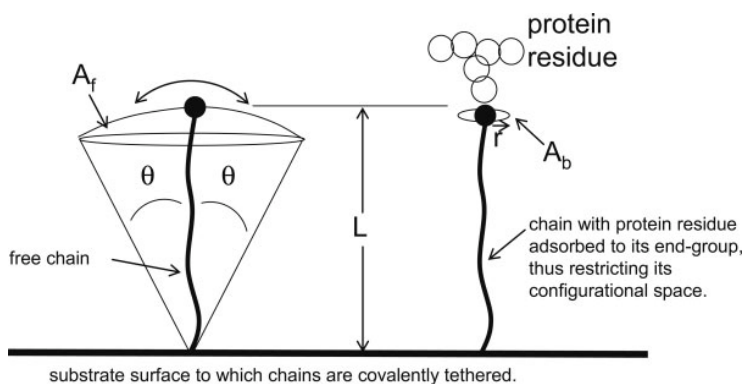


Figure 2.2 Restriction in the configurational space of the PEG chains once a protein has bound to the surface where: A_f is the area available for translational motion of the end group of the free chain A_b is the area available for translational motion when the chains end-group is bound by a protein r is the radius of translation available to maintain the bond between functional groups on the protein and the chain. Figure reproduced with permission from John Wiley & Sons.²⁶

The enthalpic contributions increase upon protein adsorption due to the intra-molecular strain energy of the tethered chains increasing upon exposure to a protein. The increased

strain energy is due to the alignment of the hydrogen bondable functional groups between a protein residue and the surface tethered chains. Latour therefore proposed that for a surface to be protein resistant, it should possess:

- well hydrated, long, flexible, surface tethered chains that are mobile but dense enough for sufficient surface coverage
- surface tethered chains that contain H-bondable groups that are readily accessible to water molecules but not the H-bonding groups of the protein

Film properties such as PEG chain length, molecular weight, density, functionality and ether retention are reported to affect the above mentioned interaction forces and hence the low-fouling nature of a PEG-like grafted films^{2, 30, 41, 42}. Jeon et al.³⁰, who performed pioneering work in this area investigated the relationship between steric repulsion and van der Waals attractions as a function of surface density and chain length of PEG grafted onto a hydrophobic surface. The protein resistant properties of PEG result firstly from the minimal van der Waals attraction between the polymer and protein. Secondly, an approaching protein will cause compression of the PEG chains enhancing the steric repulsion, which is of greater magnitude than the van der Waals attractions. The surface density was shown to have a greater effect on the protein resistant properties of PEG films, than the molecular weight of the PEG-like monomer.³⁰ Hydrophobic interactions between the substrate and protein were most repulsive when the PEG surface density was highest.

To summarise, the possible protein repulsive forces present on PEG grafted surfaces may include steric forces, enthalpic penalties for disruption of hydrogen bonds with water, electrostatic double layer forces, ice like water, hydroxide ion adsorption and hydrodynamic lubrication forces.⁴³ However, many of the assumptions from these theories are not particularly relevant to the highly cross-linked PEG-like surfaces produced from plasma polymerization described in this study, assuming the presence of PEG surfaces with long flexible surface-tethered chains having both a low packing density (to allow a high mobility) yet providing full coverage on the surface. Johnston et al.,³ plasma polymerised a series of short chain oligoglymes including mono, di, tri and tetraglymes, as well as dioxane and crown ethers to investigate the protein resistant nature of PEG-like films. They found that protein resistance increased with the length of the linear glymes and were most efficient at resisting radio-labelled fibrinogen, compared to the dioxane and crown ethers. They concluded that wettability was a poor determinant in predicting the protein resistant behaviour of the films, with the ether carbon content (detected from XPS) being a better indicator in correlating the protein resistant behaviour of the films. While this is generally true, it is important to note, however, that surfaces of a similar ether content adsorbed very different amounts of fibrinogen. They further postulated that since the increasing length of the linear brush like surfaces were more efficient at resisting protein adsorption than the dioxane or crown ethers, short chain mobility was a critical factor governing protein resistance in surface tethered films.

Ostuni et al. proposed that for surfaces to be protein resistant, they should be hydrophilic, include hydrogen bond acceptors but not hydrogen donors and have an overall neutral

charge which was concluded after analysing the protein resistant abilities of 48 surface groups covalently attached to carboxyl terminated SAMs. When comparing the findings of the TOF-SIMS data reported by Johnston et al.³ to the above set of criteria, there was some general agreement with the criteria in that the more protein resistant linear glyme films were primarily methyl terminated and generally free of hydroxyl groups, however the cyclic crowns which adsorbed more fibrinogen films also consisted primarily of intact methyl terminated groups, however these were attached to intact cyclic structures rather than more mobile chains. Further in line with Ostuni's criteria was that the dioxanes, which adsorbed the most fibrinogen (while having a lower ether and higher hydrocarbon content) appeared to contain pendant hydroxyl groups, which are hydrogen donors. Conflicts to Ostuni's criteria have been noted particularly when considering the findings of Kane et al.⁴⁴ who hypothesised that kosmotropes (i.e. those that are excluded from the protein-water interface) such as PEGs may behave similarly to osmolytes (i.e. those that remain more thermodynamically stable when bound to water rather than the surface of a protein). However, since many osmolytes are polyols^{45, 46} containing hydrogen donatable groups (-OH) and others possessing a negative charge, two of the four criteria proposed by Ostuni are challenged. Kane further postulated that the behaviour of osmolytes may be compromised when surface bound rather than free in solution, and that the mechanisms of osmolytes activity may in fact be quite different from the functioning of protein resistant films. As such the conflict between these findings and the number of varying proposed criteria to impart protein resistance into surface tethered films highlights the importance of the nanostructuring in protein resistant films, especially those deposited via plasma polymerisation. Furthermore, they indicate the

need for further investigation into the physical and chemical characteristics critical to impart protein adsorption resistant into surface bound films.

2.1.2 Methods of fabrication PEG films

There are numerous methods employed to fabricate PEG based films and coatings, including chemical immobilisation methods such as self-assembly⁴⁷⁻⁴⁹, chain grafting^{50, 51}, chemisorption immobilisation⁵², Langmuir-Blodgett techniques⁵³, atom transfer radical polymerisation⁵⁴ and plasma polymerisation^{3, 5, 55} as well as physisorption^{56, 57}. Regardless of the method used for the PEG surface generation or modification, the main focus over the last number of decades has been to optimise the resulting films in terms of its inherently inert nature, biocompatibility and stability by variations to such factors as PEG chain grafting density, molecular weight and conformation.⁵⁸ Furthermore, the variety of generation methods enables the fabrication of PEG surfaces with varying characteristics and conformational structures providing multiple parameters for one to investigate the mechanisms of PEGs protein repulsive effects.

2.1.3 Applications of PEG based materials

PEG based materials have been utilised in many different areas including cosmetics production, in industrial applications such as plastic generation for packaging, cleaning surfactants, and even as additives in food technology. I will focus this discussion to a few major applications of PEGs in the biomedical and biotechnology areas due to the topic of this thesis.

The non toxic nature of PEGs and the fact that it has been approved by the FDA for many uses in humans has made PEGs an ideal material to incorporate into injectable drug

carriers. Some of the crucial factors required from drug delivery systems, whether delivery is via oral ingestion, intra-venous or trans-dermal delivery routes, are sustainability of drug release and activity, the ability to deliver the drug to the specific site required and a non-immunogenic response to the delivery vesicle and drug/protein/peptide of interest. PEGs have shown to prolong the activity and presence of the drug in the blood, presumably due to its low fouling nature preventing the adsorption of plasma proteins^{11, 59} and by increasing the circulation time of the drug, the probability that the drug will reach the desired target site before being metabolised or excreted from the body as foreign material is increased.⁶⁰ It was recently reported that all polymer based stealth drug delivery systems available on the market in Europe and the US contain PEG-based material⁶⁰ highlighting the importance of PEG materials in drug delivery. Further benefits of PEGylation in drug delivery include a reduced immunogenicity of the carrier and or drug, as well as increased solubility.⁶¹

PEG based materials also play an integral role in biomaterials research and regenerative medicine. The trend in the research and generation of biomaterials has gone from the traditionally used metallic implants for such purposes as orthopaedic implants and coronary stents for example, towards biodegradable materials. PEGs previously discussed low fouling and biocompatible nature are integral to the introduction of synthetic materials into the body, and many studies aimed at generating various biomaterials have reported the incorporation of PEGs into the synthetic polymer structures. For example the acceptance of implanted stents, particularly coronary stents relies heavily on the prevention of thrombosis in the immediate area and as such a

number of researchers have incorporated PEG as a drug eluting stent coating⁶² to minimise the likeliness of thrombosis and implant rejection. In orthopaedic implant research, PEG has been used as a coating on both polyurethane based materials⁶³ and metal alloys⁶⁴ in an effort to maintain the mechanical properties, but enhance biocompatibility.

In a more recent example, PEG-based hydrogels have shown promise in their applications in reconstructive surgeries where researchers have shown their potential as stem cell culture vesicles, that can be grafted/transplanted to the required area in or on the body that are also capable of promoting mesenchymal stem cell growth and direct lineage differentiation. Park et al. encapsulated mesenchymal stem cells (MSCs) in a PEG based hydrogel with transforming growth factor- β 1 (TGF- β 1) loaded gelatin microparticles (MPs) to investigate the possibility of engineering functional cartilage tissue. The encapsulated MSCs remained viable over the culture period of 14 days and differentiated into chondrogenic-like cells confirmed by chondrogenic specific gene expression quantification.⁶⁵ Similarly, Alhadlaq et al.⁶⁶ photoencapsulated bone marrow derived human MSCs in a PEG diacrylate hydrogel after one week pre-conditioning of the cells in adipogenic inducing supplement. The shape and dimensions of the hydrogels were pre-defined and relevant to what would be required for reconstructive surgery. The PPAR- γ 2 adipogenic gene marker was expressed in the resulting tissue engineered adipose constructs but not in the control hydrogel that encapsulated undifferentiated human MSCs. While these results were positive the authors commented on the need to coincide gel degradation rates with differentiation for optimal adipose reconstruction. Its

also worth noting that on a fundamental research level, the ability to create micro-patterned surfaces relies heavily on the use of a low-fouling surrounding coating and PEG has been a widely exploited material for this purpose, however this application will be expanded on in section 2.5.

The susceptibility of PEGs to oxidative degradation should also be mentioned, where the resulting change in chain structuring and density can affect their non-adhesive properties. This is a characteristic that should be investigated on the application of PEG based materials in the biomaterials and regenerative medicine fields. Furthermore, it has been suggested that while PEG materials may reduce the adsorption of proteins in their localised materials (compared to other synthetic materials) it is potentially the conformation that a protein is bound with that may effect cellular attachment. For example, Shen et al⁶⁷ compared the adhesion of leukocytes in vitro on tetraglyme coated fluorinated ethylene propylene copolymer (FEP), compared to the bare FEP control. Previous studies in vivo had shown that the tetraglyme coated FEP significantly reduced the adsorption of fibrinogen (compared to the bare FEP control) and monocyte adhesion,⁶⁸ however results of the in vivo studies showed that after subcutaneous implantation in the backs of mice for four weeks, the tetraglyme surface resulted in a higher number of leukocytes attached, compared to the FEP control. The authors hypothesised that the differences could be due to a variation in protein conformation on the surfaces, where loosely bound proteins fail to spread on the “lower fouling” tetraglyme surface, resulting in the presentation of more cell binding active sites than on

the FEP control. Also, possible degradation of the tetraglyme surface was considered as a contributing factor to the loss of the “low-fouling” nature of the PEG-like material.

2.2 Plasma polymerisation

2.2.1 Plasma Fundamentals

Plasma is an overall neutrally charged collection of highly active, electrically charged, ionised gas molecules that move in random directions.⁶⁹ It consists of positive and negative ions, electrons, neutrons and radicals. A schematic of the chemical species existing in a plasma (ignited in a laboratory scenario), and their interaction with a substrate is presented in Figure 2.3. Ionisation of gas molecules occurs when the gas is exposed to energetic electric fields or radiation.⁷⁰ Plasmas are not unique to the laboratory, but are a phenomenon of nature, with visible matter such as lightening, the sun and stars being some examples. The state of plasma has been re-created by man and exploited in modern science and technologies. Plasma was initially identified in 1879 by Sir William Crookes which he described as ‘radiant matter’ and as ‘a world where matter may exist in a fourth state’. Then in 1928, Irving Langmuir was able to name this fourth state of matter, when he introduced the term ‘plasma’ in his studies of electrified gases in vacuum tubes.⁷¹

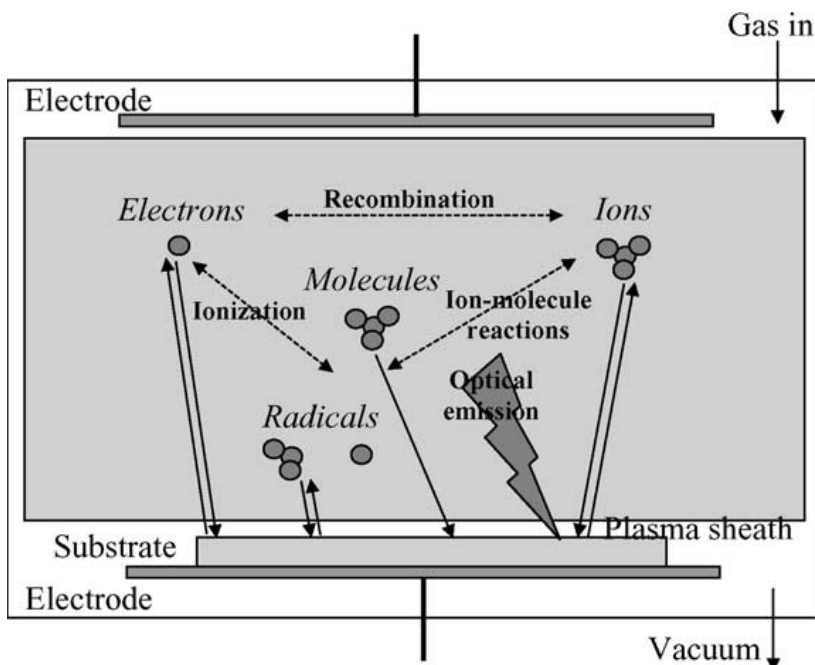


Figure 2.3 Schematic of the components generated in plasma and their interactions with the substrate. Figure reproduced with permission from Elsevier.⁷⁰

Plasmas may be classified as either high temperature or low temperature plasmas. High temperature plasmas result in a higher degree of ionisation ($> 100\%$) where the electron and molecule temperatures range from 4000 to 20000 K.⁷⁰ In this type of plasma the temperature of the electrons is closely equivalent to that of the ionised molecules; as such they are often referred to as near-equilibrium plasmas. Lightning is an example of high temperature plasma. Low temperature or non-equilibrium plasmas are categorised by lower temperatures, however, the temperature of the electrons within the plasma is far higher compared to that of the ionised molecules and as such these are often referred to as non-equilibrium plasmas. The degree of ionisation of these plasma is far lower than that of high temperature plasmas ranging from around 10^{-4} to 10% .⁷⁰ Examples of low-temperature plasmas include those resulting from low pressure direct current (DC), radio-frequency (RF) and corona discharges.⁷⁰ The type of plasma discussed throughout this

thesis will relate to radio-frequency induced low temperature, non-equilibrium plasmas. It is this low temperature, non-equilibrium form of plasma that results in a glow discharge and enables thin film deposition since the comparatively energetic electrons collide with gas molecules during acceleration resulting from a potential difference between two electrodes. The collision causes the ejection of electrons from the gas molecules resulting in the ionised molecules and radicals necessary for thin film deposition. This collision process is often referred to as collision induced energy transfer.⁷²

2.2.2 The Plasma Sheath

The sheath region of a plasma is an electrical boundary existing at the plasma-surface interface consisting primarily of positive ions.⁷³ It results from electron loss to the neighbouring surface of that plasma region. The positively charged sheath region repels electrons and negative ions,⁷⁴ while positive ions are accelerated from the plasma to the surface potential.⁷⁵ A concentrated electrical field is created in this region when an applied voltage travels across the sheath, and while the mobility of species in the main plasma body is controlled by diffusion, movement of ions in the sheath is directional and controlled primarily by the electric field. A recent publication by Zelzer et al.⁷⁵ has highlighted the importance of consideration of the plasma sheath on the deposition of plasma polymer films through masks. The pore size of a mask affected the length of the sheath, electron depletion, ion density and consequently the deposition rate.

2.2.3 Glow discharge plasmas and excitation sources

A glow discharge is a type of plasma formed, which occurs when a potential difference is applied between two conductive electrodes in the system. Electrodes can either be

inductively or capacitively coupled, with the main difference being that capacitively coupled electrodes are generally parallel and positioned inside the reactor while inductively coupled electrodes are generally external coils.⁷⁶ The potential difference applied between the electrodes results in an emission of electrons from the cathode region that then collides with the excited gaseous molecules. This excitation decays by means of emitting light, which results in the characteristic glow discharge. The various species then condense and polymerise on the surface substrate, resulting in highly cross-linked and adherent, pin hole free thin films.⁶ The power and excitation source to ignite and sustain a glow discharge plasma can be supplied by either an alternating (AC) or direct current (DC). DC plasmas are characterised by a constant current, generated from a continuous potential difference applied between the cathode and the anode. This type of plasma can result in decomposition of the glow discharge where one of the electrodes is non-conducting due to charging and are less commonly used for plasma polymer deposition.⁷⁶ AC plasma overcomes this issue by alternating the voltage between two electrodes, enabling any charge accumulation to be neutralised. Commonly used frequencies applied for AC power sources include radio frequency (RF) at 13.56 MHz and microwave at 2.45 GHz⁷⁷. Advantages of RF discharges over DC, particularly for the deposition of biomaterial intended surfaces include the ability to operate at lower pressures and to sustain themselves during depositing discharges. They are also reported to have a more efficient ionisation mechanism and to exist in a more spatially uniform manner.⁷⁰ The work carried out for the content of this thesis was performed using capacitively coupled RF plasma polymerisation in continuous wave mode which will be expanded on in the following paragraphs.

2.2.4 Pulsed and continuous wave glow discharges

Radio-frequency depositions can be separated into two types of supplied voltage. Firstly, as the name suggests, radio-frequency is supplied in a ‘continuous wave’ manner. The second approach is the ‘pulsed’ plasma, where the radio-frequency is applied in pulsed on time, generally in the millisecond time frame followed by a lag period. It is often characterised by the duty cycle which is the ratio of pulsed on time to total pulse time. The advantage of pulsed deposition is reported to be the ability to control film chemistry by being able to operate at higher peak voltages while maintaining a lower power input compared to that using continuous wave deposition. During pulsed discharges, reactive species are consumed during plasma off cycles resulting in films more chemically similar to that of the starting monomer.⁷⁶ While this is a generally supported concept, there are a number of other factors that can largely influence the resulting discharge and plasma polymer such as the reactor shape and size, electrode separation distance and geometry, W/FM Yasuda factor (expanded on in section 2.2.5.1), time of deposition, working pressure and substrate size and placement.^{5, 78-80}

A comparison of the ether retention of PEG-like plasma polymer films deposited from diethylene glycol dimethyl ether in a pulsed polymerisation process reported by Bretagnol et al.²⁵ to those reported in chapter 3 of this thesis has shown that at a load power of 5W, the pulsed films retained an ether content of 55 % (as measured by XPS) while those deposited at 5W under continuous wave processes in this research retained 70% (as measured by XPS) highlighting the ability to achieve chemically controlled films via continuous wave radio frequency plasma polymerisation.

2.2.5 Plasma Polymerisation, Parameters and use in Biomaterials

Plasma polymerisation is the deposition of ionised gas phase molecules, which results in nanoscale, highly crosslinked, adherent and pinhole free films that can be deposited onto a wide variety of substrates of various dimensions. It is a one step process that does not require solvents.^{55, 81} The process itself provides a clean environment within the reaction chamber,⁸² is fast, reproducible and most importantly the chemistry, thickness and many physical properties of plasma deposited films can be tailored by careful manipulation of the processing parameters such as flow rate, system geometry, plasma load power^{78, 81} and of course monomer choice. It is a process that has been widely studied since the 1950's⁷⁸ and has been applied in areas including microelectronics, paints, adhesives and protective layers,⁸² and more recently in providing surfaces for the biomedical and biotechnology areas. This technique is particularly beneficial to these fields due to its ability to deposit reactive functional groups on an otherwise non-reactive surface, enhancing specific biointeractions of a surface⁸³ and enabling the covalent immobilization of biomolecules,⁸⁴ as well as rendering a surface bio-inert by careful control of the chemistry and processing parameters.

2.2.5.1 The W/FM Yasuda factor

As previously mentioned plasma polymerisation has a number of variable parameters that can affect the resulting chemistry and physical properties of the film such as flow rate, plasma load power, electrode geometry, temperature, pressure and deposition times. One in particular is the 'Yasuda factor', or W/FM parameter (where W is the radiofrequency power input, F is the flow rate and M is the molecular weight of the monomer), and can be defined as the plasma power input per monomer mass unit⁸⁵⁻⁸⁷. A low W/FM value is reported to result in pp films with a high retention of the original monomer structure,

while films deposited under conditions of a high W/FM value result in films with a more complex chemistry and less like the original monomer structure⁸⁵.

2.2.5.2 Plasma Polymerisation in Biomaterials

The main benefits of plasma polymerisation and plasma treatment in the field of biomaterials are due to the ability to create specific chemical functionalities, and to vary the surface wettability, charge and morphology.⁸⁸ These chemical functionalities are either intended to enable specific biological interactions by the creation of such functionalities as amines, aldehydes and carboxylic acid, or to create low fouling surfaces by polymerising ether containing monomers such as those of the glyme family^{25, 27} and it is well reported that surface functionality can in turn alter the physical characteristics of a surface.

The creation of amine functionalised surfaces have been reported from the use of such monomers as allylamine and heptylamine and used for the immobilisation and study of such bioactive molecules as DNA⁸⁹⁻⁹¹, proteins^{92, 93}, polysaccharides,⁹⁴⁻⁹⁶ and enzymes^{97, 98} with the popular source of immobilisation methods being that of carbodiimide coupling. More specifically, a recent study published by Rebl⁹⁹ et al. has highlighted the importance of implant surface charge by creating amine functionalised surfaces via the plasma polymerisation of allylamine. Using GFP–vinculin transfected osteoblastic cells, the attachment and mobility of the cytoskeletally associated protein vinculin on the functionalized surfaces was shown to be significantly increased compared to collagen I coated surfaces during the initial adhesion phase. It was concluded that positive charges control the cell physiology which appeared to dominate over the integrin receptor binding to collagen I. As such, it was proposed that since the deciding factor for the ingrowth of

medical implants into human bones is their rapid acceptance by the cells that the ultimate function of implants could be optimized by these positively charge amino surfaces. Further in vivo studies showed no signs of localised inflammation in the back musculature of rats.

Aldehyde functionalised surfaces have also been applied in the field of biomaterials research¹⁰⁰ with the popular monomer choices including acetaldehyde and benzaldehyde. While the immobilisation of a number of bioactive molecules have been reported on these surfaces, for example DNA,¹⁰¹ NHS-PEG-Biotin for the consequential immobilisation of Neutravidin¹⁰² and PEG-albumin. A more recent publication utilising aldehyde functionalities was aimed at biological patterning. Hadjizadeh¹⁰⁰ functionalized fibers of polyethylene terephthalate with acetaldehyde plasma polymer, followed by carboxymethyl dextran (CMD) grafting onto the aldehyde-coated surfaces via a polyethyleneimine interlayer. It was shown that the CMD functionalised fibers resisted the attachment of human umbilical vein endothelial cells (HUVECs), while those terminated with polyethyleneimine facilitated HUVEC attachment, spreading and focal adhesion formation. It was hypothesised that being able to pattern fibres with endothelial cells would have implications in the development of 3D scaffolds for vascular prosthesis devices. Similarly, but related to amine functionalities via plasma polymerisation of allylamine, Hook et al.¹⁰³ created surface bound micropatterned surfaces utilising a low fouling PEG background and exposing amine functionalities in spatially patterned regions via laser ablation. The functionality of the exposed amines were utilised via the successful array of DNA, proteins and cells.

Carboxyl functionalised surfaces have also been generated via plasma polymerisation and are favoured for their ability to immobilise amine containing biological molecules via carbodiimide coupling.⁸⁴ Some recent examples of these include the generation of carboxyl density surface gradients for the culture and differentiation study of mouse embryonic stem cells,¹⁰⁴ and the generation of oligonucleotide patterns onto an acrylic acid plasma polymerised surface. The oligonucleotides were spatially immobilised using a microspotter and conjugated via carbodiimide coupling chemistry.¹⁰⁵ Examples of other biological molecules immobilised onto carboxyl functionalised plasma polymer surfaces include the cell adhesive RGDS peptide¹⁰⁶, collagen,¹⁰⁷ and an anticoagulant heparin-albumin conjugate.¹⁰⁸

While the studies are vast for the development of biomolecules immobilised onto plasma polymerised and plasma treated surfaces, there are a number of principle factors that should be considered; some of these include the covalent attachment (rather than physisorption) of biomolecules moieties to prevent their displacement when exposed to biological media, the directionality of their active site (i.e. the active site should not be involved in the covalent attachment), and their retained functionality after immobilisation (i.e. they should not denature or change their functional configuration).⁸⁴

The use of low fouling surfaces deposited by plasma polymerisation is also a critical factor in the development of biomaterials. As discussed in section 2.1, low fouling surfaces can dictate the success of a material or device for the prevention of thrombosis in the case blood contacting devices and inflammation and infection in the case of tissue contacting materials¹⁰⁹ as well as providing the contrasting low fouling background in

micropatterned surfaces used to study a number of complex biological phenomenon. Much of the work on low fouling materials to date has involved plasma polymerisation from ether containing monomers such as diglyme^{6, 17, 25, 27, 110-112} triglyme, tetraglyme,^{25, 113-118} as well as diethylene glycol monovinyl ether¹¹⁹, triethylene glycol monallyl ether¹²⁰ and allyl glycidal ether¹²¹. However a recent publication has reported on the generation of low fouling coatings plasma polymerised from 1H,1H,2H,2H-perfluorodecyl acrylate¹²², possibly opening up a new era of low fouling plasma polymer coatings. The protein resistant nature of these films were displayed against three model proteins including ovalbumin, human serum albumin and fibrinogen, where adsorption was significantly reduced compared to a gold control as measured by QCM.

As previously mentioned the use of plasma polymerisation in the fields of biomaterials and biomedicine has been extended into the generation of gradient and micropatterned surfaces for the study of biological behaviour and biological-material interactions and these topics will be expanded on in sections 2.4 and 2.5 respectively.

2.3 Methods of thin film analysis

Due to the complex chemistry of the resulting plasma polymer film, a number of complimentary techniques are commonly used to analyse their chemical structure and physical properties. Some of these techniques include X-ray photoelectron spectroscopy (XPS) and Fourier transform infra red spectroscopy (FTIR)^{1, 3, 6, 7, 85, 87, 123}, time of flight secondary ion mass spectroscopy (TOF-SIMS)^{1, 6, 83, 124-127}, near edge X-ray absorption fine structure (NEXAFS)^{87, 128-131} neutron reflectometry to analyse film chemistry and

structure. Atomic force microscopy (AFM)²³, surface plasmon resonance (SPR)^{34, 132} and quartz crystal microbalance (QCM)¹³³ have been used to investigate the interaction behaviour between a plasma polymer surface and various proteins, as well as investigating film morphology in the case of AFM^{5, 134-137}. Water contact angles have also been commonly used to investigate the wettability of thin films. In terms of chemical analysis, consideration must be given to the depth of analysis for each given technique, where for the analysis of plasma polymer films, FTIR will consider the bulk chemistry, while XPS, NEXAFS and TOF-SIMS are more surface sensitive. Following is an overview of the primary techniques of thin film analysis utilised throughout this thesis.

2.3.1 Fourier transform infra red spectroscopy (FTIR)

Fourier transform infra red spectroscopy is a non-vacuum chemical analysis technique used to identify the chemical functionality of a material. The technique relies on the vibrational modes of specifically chemically bonded species that are distinguished by their distinct vibrational energy level, often termed its fingerprint. Infra-red radiation is passed through a sample, with absorbed IR light exciting the various chemical functionalities into the vibrational energies of their specific fingerprints.¹³⁸ The FTIR uses an interferometer enabling the simultaneous detection of a range of wavelengths producing faster and more sensitive spectra. An interferogram is obtained which must then be converted to an infra red spectra, generally in the form of transmittance or absorbtion vs wavelength, via fourier transforms to obtain a single beam infra red spectrum.

Grazing incidence (gi), or ‘specular reflectance’ FTIR was used in the analysis of the plasma polymer films throughout this thesis due to their thin nature and secondly the low concentration of certain chemical functional groups, as the technique is known to enhance the signal to noise ratio. The requirements of this technique is that the films are deposited onto a reflective surface, such as indium tin oxide coated glass, and that the films are extremely flat so as to avoid scattering of the reflected infra red radiation. Synchrotron source gi-FTIR microspectroscopy was used throughout this thesis in the analysis of both gradient and micropatterned films. Benefits of this technique include the increased signal to noise ratio due to the intensity of the light source, decreased spot size, enabling greater resolution in the attained chemical maps and decreased collection time with automated analysis collection attainable.

2.3.2 X-ray Photoelectron Spectroscopy (XPS)

XPS is a surface sensitive, quantitative elemental detection technique which not only identifies the specific elements present, but also their oxidation states. When a sample is irradiated with a monochromated X-ray source, the core shell electrons of the surface atoms are excited and eject photoelectrons. For a photoelectron to be ejected, the binding energy must be lower than the X-ray energy. Elemental detection is achieved as the binding energy at which photoelectrons are emitted and is specific to each element. Typically, an elemental survey scan is acquired by scanning a binding energy range, where the ‘counts’ or intensity of the peaks can be fitted to acquire quantitative data. Furthermore, the peaks can be scanned in a narrower energy range (specific to each element) to obtain high resolution curves, which provide the information related to the elements oxidation state and bonding environment. The angle of incidence of the X-ray

beam relative to the surface normal can be varied to attain depth dependant data of surface chemistry. For thin film analysis, the combination of XPS with FTIR is advantageous, as information regarding both the surface and bulk chemistry can be acquired, respectively. XPS was a vital characterization instrument utilized throughout the course of this thesis. XPS analysis was applied to the uniform, gradient and micropatterned surfaces; however the spot size (resolution) was a limiting factor in analysing the small patterned features.

2.3.3 Near Edge X-ray Absorption Fine Structure (NEXAFS)

The use of NEXAFS for the characterisation remains in its early years and thus warrants a brief explanation of how the technique can be applied for the characterisation of thin films. NEXAFS is a surface sensitive, element specific technique that analyses in the soft X-ray region therefore detecting the low Z molecules including S, C, N, O and F^{131, 139}. It relies on the ejection of excited electrons from a core orbital (at the K-edge) into unoccupied orbitals via dipole transitions. The probing depth can be varied depending on the detection method used, for example it is estimated that a typical total electron yield experiment would probe the top 2-4 nm while analysing in the partial electron yield mode (PEY), this depth analysis would be further reduced.¹³¹

NEXAFS also has the ability to detect the orientation of surface tethered molecules by using the polarized synchrotron light source. The first reported finding of orientation of plasma polymer films was reported by Castner et al. who analysed tetrafluoroethylene based plasma polymer films.¹⁴⁰ The intensity associated with a specific molecular orbital final state is at its maximum when X-ray incidence points in its direction, and the

intensity vanishes when the X-ray incidence points perpendicular to the orbital.¹³⁹ Therefore, by using a polarised light source and obtaining spectra at various incidence angles it is possible to observe any structural orientation of the sample in question. The intensity of the π^* and σ^* resonances will change where there is an angular dependence.

The use of NEXAFS as a spectroscopic tool for the structural determination of complex molecules and polymers remains in its infancy. While the spectral NEXAFS library of condensed molecules is developing, the use of complimentary techniques, such as XPS and FTIR is extremely beneficial to aid in the assignment of relevant spectral features. NEXAFS was employed as a characterisation tool for both the uniform and gradient surfaces and is reported in chapters 3 and 5 of this thesis, respectively.

2.3.4 Time of Flight Secondary Ion Mass Spectrometry (ToF-SIMS)

ToF-SIMS is a surface sensitive chemical analysis technique that uses a pulsed beam to remove molecules at the surface of a material, in a high vacuum environment. Once the sample is bombarded with the ion beam (primary ions), charged ions and molecules (secondary ions) are emitted and accelerated into a flight tube, where the time taken for the ion to travel is distinct for each ions mass to charge ratio (m/z).¹⁴¹ The technique requires the sample of interest to be very smooth and flat (as with most surface sensitive techniques) since distance of travel of the emitted the secondary ions must be the same to avoid confusion in identifying the fragments based on their mass to charge ratio. ToF-SIMS is often used as a complimentary technique in conjunction with XPS since the resulting spectra are often extremely complex. Furthermore, principle components analysis (PCA) has more recently been applied in ToF-SIMS data interpretation^{142, 143}

PCA is a statistical transformation of data, which when applied to the complex TOF-SIMS spectra, reduces the dimensionality and random variables of the raw data, enabling a more accurate comparison of ion peak trends not necessarily otherwise apparent between datasets. The high spatial resolution of this technique ($50\text{ nm} - 5\text{ }\mu\text{m}$)¹⁴⁴ makes it ideal for chemical imaging and as such has been a popular tool in imaging the chemistry of micropatterned surfaces.^{17, 143, 145} ToF-SIMS was utilised in the characterisation of both the gradient and micropatterned surfaces reported in this thesis, discussed in chapter 6 and 7 respectively. Across the gradient surfaces spectral data was acquired while TOF-SIMS imaging was utilised for the patterns.

2.3.5 Neutron Reflectometry

While techniques such as XPS and FTIR can provide certain information on the complex structure of plasma polymer films, defining the empirical formula using these techniques is not possible. FTIR provides information on the presence of certain chemical functionalities throughout the film and XPS does not provide information on the hydrogen content. Therefore, in chapter 4 of this thesis the uniform PEG-like films were characterised using complimentary techniques XPS, X-ray and neutron reflectometry, enabling the full chemical composition of the films to be defined. The film thickness, density and roughness can also be determined. Film requirements for neutron analysis are that they should be around $200\text{ }\text{\AA}$ thick and must be extremely smooth to retain the specular reflectance, where the angle of incidence equals the angle of reflectance.

During a neutron reflectometry experiment, a highly collimated neutron beam bombards and reflects off a surface and the intensity of the specularly reflected beam can be

measured as a function of the angle.¹⁴⁶ The reflectivity is related to both the angle of incidence and the wavelength of the neutrons, which is often described in terms of a momentum transfer, Q .¹⁴⁶ This term relates to the change in momentum of the surface approaching neutrons once they are reflected from a material. The resulting neutron reflectometry plot shows the reflected intensity as a function of Q . The basic principles of X-ray and neutron reflectometry are similar, however neutrons interact with the nucleus of an atom, while X-rays with the electron.¹⁴⁷ Furthermore, neutron reflectometry has the distinct advantage of being able to analyse lower Z elements such as hydrogen, and the utilisation of deuterated isotopes can provide contrasts between the film, substrate and solution.¹³⁵

2.3.6 Contact Angle Goniometry

Measuring the contact angle of a material provides information of its wettability and can be defined as the angle at which a liquid interface meets the solid surface.¹⁴⁸ When designing biomaterials this information is particularly important since the wettability of a film is reported to effect the interactions between the surface and proteins,¹³⁶ where a higher level of oxygen functionality is reported to increase the wettability of a film.^{78, 149} A water droplet on a completely hydrophilic surface will result in a contact angle of 0° where there is a strong attraction between the liquid and surface. A more moderately wettable or hydrophilic surface will yield contact angles of up to 90° and a hydrophobic material will have contact angles above 90° .¹⁴⁸ Contact angle goniometry data is reported in chapters 3 and 4 of this thesis related to the uniform plasma polymerised films.

2.3.7 Atomic Force Microscopy (AFM)

AFM is an excellent characterisation tool for attaining 3 dimensional topographical images and information related to a sample such as surface roughness, homogeneity and film thickness. In contact mode, a tip or 'cantilever' is scanned across the sample surface and the force between the tip and surface is measured. The sample is positioned on a piezo-electric ceramic which controls the scanning movement in the x, y or z directions and a laser light is focussed onto the end of the cantilever and is reflected into a photodiode. The height of the piezo electric ceramic is adjusted by a feedback signal from the photodiode and height adjustments occurring while the sample is scanning provides information on the topographical features of the sample.¹⁵⁰ AFM can be used for both acquiring surface images as well as measuring forces between the sample surface and a cantilever. Furthermore, the cantilever can be loaded with materials, proteins or biomolecules of interest to attain information on the forces occurring between the objects of interest. AFM was used as a characterisation technique to analyse film thickness and roughness for both the uniform and gradient films analysed in this thesis, presented in chapters 4 and 5 respectively.

2.4 Surface bound chemical gradients in biomaterials research

Gradient surfaces are those that display a spatial variation in one or more physicochemical property such as chemistry, topography, nanostructuring, wettability and surface charge. Gradient surfaces provide a high throughput and/or combinatorial approach for optimising the interactions of various proteins, biomolecules and cells with a material of interest,¹⁵¹ vastly reducing the need for multiple surface preparations. The chemistry of a surface can largely dictate biological interaction leading to variations in

film/surface properties such as wettability, cross-link density, swelling, solvation and roughness. Gradient surfaces provide a more physiologically relevant environment for biomolecules, since cell migration, differentiation and chemotaxis are driven by gradients of specific biomolecules that provide directional cues.¹⁵²

Zelzer *et al.*¹⁵³ formed chemical gradients from the plasma polymerisation of hexane and allylamine (via diffusion of the gaseous monomers under a fixed mask) and used them to investigate the attachment and proliferation of fibroblast cells. They further indicated that the initial attached cell density differed as a function of the specific chemistry across the gradient environment which contrasts with their attachment upon a chemically equivalent, uniform surface. They suggest this could be due to differences in cell-cell signalling or a greater number of proteins produced from the surrounding cells between the different substrate types. This is an interesting finding and is something that should be considered when using surface gradients as a high throughput method for optimising surface-biological interactions. Robinson *et al.*¹⁵⁴ also reported on the generation of chemical gradients formed via plasma polymerisation, however they used a mixture of allylamine and octadiene monomers. They were able to form functional heparin gradients, where the adsorption and function varied as a product of the allylamine gradient. However the adsorption of higher amounts of heparin did not correspond to a continued increase in functionality.

The use of PEG based gradients has been relatively limited, however more recently Vasilev *et al.*¹⁵⁵ has demonstrated the use of these to create gradients of two proteins of

differing size (lysozyme and fibrinogen). Jeong et al.¹⁵⁶ formed gradients in the density of comb-like PEO chains prepared on low density polyethylene (PE) sheets by corona discharge treatment that were subsequently grafted with poly(ethylene glycol) monomethacrylate (PEG-MA) with PEO chain lengths of 1, 5, and 10 monomer units. The authors envisioned that these gradient surfaces could be used to provide useful information on the interaction behaviours of blood components such as plasma proteins. Wang et al.¹⁵⁷ utilised PEG molecules in the formation of a two component chemical gradient used to control protein adsorption. A PEG thiol and 11-amino-1-undecanethiol was used to form covalently linked gradients of epidermal growth factor (EGF) a signalling molecule, via carbodiimide coupling chemistry. Lower EGF adsorption occurred at higher PEG concentrations.

PEG gradient surfaces are also becoming an increasingly popular tool for the study and optimisation of cell attachment, proliferation and viability. Furthermore, they are a rapidly developing area within the biomaterials industry since the gradients can be generated to mimic a number of physiological gradients that drive specific biological events. Delong et al.¹⁰ used PEG-based hydrogels with a gradient of covalently immobilized RGDS to study the effect of fibroblast growth migration and alignment. It was found that the fibroblasts changed their morphology to align in the direction of increasing RGDS concentration and that the slope of the gradient further affected this response. Bhat *et al.*¹⁵⁸ used gradients of molecular weight (Mw) and/or grafting density of surface bound poly(2-hydroxyethyl methacrylate) (PHEMA) with physisorbed gradients of fibronectin to investigate changes in the behaviour and morphology of

osteoblastic cells as a function of their chemical environment. Furthermore, the use of gradients to probe the growth and differentiation of stem cells has also been reported. Wells et al.¹⁰⁴ used chemical gradients of plasma polymerised octadiene and acrylic acid in order to probe the response of E14 and R1 mouse embryonic stem cells to a range of carboxylic acid concentrations on a single sample. They were able to show that the self-renewal capacity was maintained if the cells were restricted in their spreading to $<120\text{ }\mu\text{m}^2$, indicating that the degree of spreading was the critical parameter rather than the exact surface acid density.

2.4.1 Types of Gradient surfaces

The directionality and dimensionality are two distinct ways to classify a gradient. In terms of dimension, gradients can be 1, 2 or 3D, meaning that the physicochemical variation occurs in the X, XY or XY and Z dimensions.

2.4.2 Methods of gradient fabrication

There are a number of methods used to produce surface chemical gradients with a vast number of these relying on the modification of self assembled monolayer's (SAMs). Other reported techniques include various diffusion process techniques^{26, 151, 152, 159} such as UV-initiated free-radical polymerisation¹⁶⁰ and grafting¹⁶¹, corona discharge^{162-164, 156, 165, 166}, corona-induced graft copolymerisation¹⁵⁶, adsorption¹⁶⁷ and plasma copolymerisation.¹⁶⁸ The use of radio frequency plasma polymerisation (RFpp) has also been reported for gradient generation^{104, 153, 154, 169}, but to date have required the use of a moving sample stage or shutter. In chapter 5 and 6 of this thesis a one-step method of gradient generation uses radio frequency plasma polymerisation without the need for any moving components is presented and discussed. The use of corona discharge and radio-

frequency plasma treatment have the distinct advantage over other deposition methods since it is not restricted to a specific substrate or attachment functionality,⁷⁵ are solvent free processes that are easily reproducible. Furthermore, the chemistry of the films generated can be systematically varied by manipulation of the deposition parameters including load power and monomer flow rate and the films produced are generally extremely smooth, making them ideal model surfaces to investigate the effects of surface chemistry on protein and cellular interactions.

Genzer and Bhat¹⁵¹ have recently published a review on surface bound soft matter gradients that provides an excellent overview of the methods used for gradient generation, and Figure 2.4 is extracted from the article to display the many reported techniques used for gradient generation.

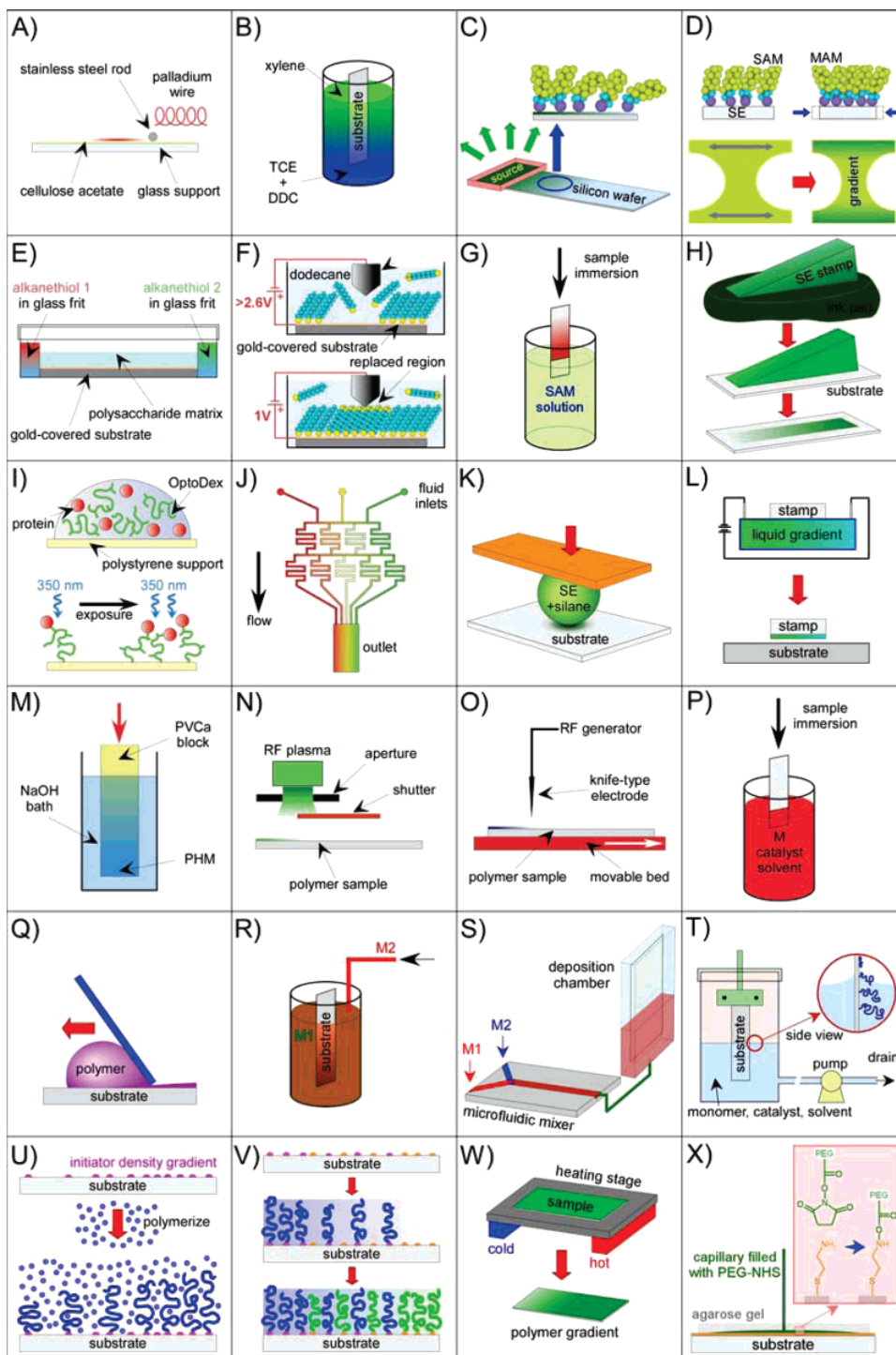


Figure 2.4 An overview of the various techniques used to create surface bound gradients. (A) deposition using a palladium wire on an acetate film;¹⁷⁰ (B) liquid diffusion of organosilanes;¹⁷¹ (C) vapor diffusion of organosilanes;¹⁷² (D) depositing self-assembled monolayer on top of a mechanically predeformed substrate;¹⁷³ (E) diffusion of alkanethiols in a polysaccharide matrix;¹⁷⁴ (F) replacement lithography of alkanethiols;¹⁷⁵ (G) immersion technique applied to self-assembled monolayers;¹⁶⁷ (H) printing alkanethiols from stamps of variable thickness;¹⁷⁶ (I) gradients of proteins by means of heterobifunctional photolinkers;¹⁷⁷ (J) solution and surface gradient using microfluidics;¹⁷⁸ (K) deposition of organosilanes by means of silicone elastomer stamps with different curvatures;¹⁷⁹ (L)

forming a concentration gradient of two charged molecules in a solution and imprinting them onto a stamp, which could then transfer the gradient pattern onto a substrate;¹⁸⁰ (M) hydrolysis of poly(vinylene carbonate);¹⁸¹ (N) radio frequency plasma discharge;¹⁸² (O) corona discharge;¹⁸³ (P) immersion of substrates into polymerization media;¹⁸⁴ (Q) knife-edge coating technology;¹⁸⁵ (R) preparing random copolymer brushes by steadily adding a new monomer (M2) to the polymerization mixture containing another monomer (M1);¹⁸⁶ (S) preparing statistical copolymers by the microfluidic mixing of two monomers followed by chamber filling method;¹⁸⁷ (T) solution draining method for preparing polymer brushes;¹⁸⁸ (U) forming a molecular gradient of an initiator on a substrate followed by grafting-from polymerization;¹⁸⁹ ¹⁹⁰ (V) opposite grafting density counter gradients of two polymers formed by sequential grafting from two different set of initiators;¹⁹¹ (W) grafting-onto method in conjunction with temperature gradient heating of the substrate;¹⁹² and (X) immobilization of PEG by diffusion and grafting.¹⁹³ Reproduced with permission from the American Chemical Society.¹⁵¹

2.5 Micropatterned Surfaces

Engineering chemically micropatterned surfaces generally relies on achieving a spatial distinction between fouling and non-fouling regions on a surface. While the term micropatterning can have a broader definition, in terms of what is being patterned, for example, enzymes, DNA, proteins and cells, this discussion of micropatterning will refer to the chemical patterning of substrates. Traditionally, polymer and solid state micropatterning techniques generally require a number of steps to produce the desired substrate surface chemistries and geometries.^{9, 17, 194-197} Innovation is driven by the aim of increasing pattern fidelity, resolution, miniaturisation and cost effectiveness while maintaining suitable mechanical properties and scalability. The micropatterning research presented in chapter 6 of this thesis introduces a novel technique by which the deposition of chemically micropatterned surfaces can be achieved in one simple step via plasma polymerisation.

The generation of regular arrays of two or more polymer surface chemistries, features or structures on a surface is routinely used in a number of research fields. This includes the

production of light-emitting displays (LEDs), semiconductor & optoelectronic devices¹⁹⁸⁻²⁰⁰, biomedical and 'life science' related research including the study of cells,²⁰¹⁻²⁰³ tissue engineered devices,²⁰⁴ fundamental surface science research and high-throughput screening research.²⁰⁵

Of particular importance in the fields of biomaterials and tissue engineering is the use of micropatterned surfaces to control and understand the effects of the microenvironment on cell behaviour such as chemistry, topography, varying ligand, growth factor and protein density, and the effects of spatial distribution on cell-cell interactions. For example, a recent study reported by Cheng et al.⁹ who produced patterned surfaces by combining plasma polymerisation and deposition with plasma etching through the window arrays of a shadow mask fabricated by photolithography was able to form single cell patterns and study the effects of the pattern shape and size on the morphology of the attached human mesenchymal stem cells (hMSCs). Cell spreading was shown to be controlled by the shape of the patterns. Actin and nuclei staining showed a strong dependence of the hMSC morphology on the size and shape of the cell spreading area, with circular features producing rounded nuclei and actin alignment along the radial direction, while thin, elongated features yielded nucleus elongation and actin alignment along the major axis of their elliptical shape. With the increasing investigation into the use of stem cell research and related therapies, this finding highlights the importance of further investigation into the optimised microenvironment for stem cell culture and research. In regards to the effects of growth factor and protein density, Ito et al.²⁰⁶ were able to highlight the importance of the combination of heparin density and the presence of basic fibroblast

growth factor (bFGF) for the growth of NIH3T3 cells on gradient-micropatterned immobilised heparin surfaces. Results indicated that while the high density of heparin failed to enhance cell growth in the absence of bFGF, it did enhance cell growth in the presence of bFGF. The authors were able to conclude that the concentration of immobilised heparin was critical to the activation of bFGF, and consequently the enhancement of NIH3T3 cell growth.

2.5.1 Methods for Generating Micropatterned Surfaces

There are a large number of methods used to obtain micropatterned surfaces including photolithography²⁰⁷ and other photochemical techniques²⁰⁸, soft lithography²⁰⁹, laser ablation/lithography²¹⁰, ion-beam lithography²¹¹, ion implantation²¹² and pattern deposition with atomic force microscopy.^{213, 214} With the exception of a small number of emerging patterning techniques,²¹⁵ these methods result in surfaces that contain both modified and unmodified regions which then require further chemical derivatisation to block or modify the untreated region on the substrate surface to optimise its performance.^{17, 202, 215}

The use of plasma polymerisation has also been reported for the generation of chemically patterned surfaces, however to date have also required the combination of two or more steps, or in a single step by the use of a physical mask placed over the substrate during deposition.^{216, 217} In terms of the masking process, problems can be associated with achieving a close enough contact between the mask and substrate to produce defined chemical patterns.⁶ In terms of the multiple step processes, while good patterning can be achieved the multiple step process for each patterned substrate can be laborious and time

consuming. Chapter 7 of this thesis introduces a novel one-step patterning technique that produces well defined and functional micropatterned surfaces. Much of the work reported on the generation of micropatterned surfaces via plasma polymerisation, relies on the deposition of a low fouling coating followed by spatially specific removal of regions of the film to expose an underlying reactive surface, via photolithographic methods.^{6, 218, 219}

2.5.2 Surface Analysis of Micropatterned Surfaces

Due to the focus on pattern miniaturisation, the capabilities of spatially resolved chemical surface imaging techniques are required.¹⁴⁴ ToF-SIMS imaging has proven to be an excellent technique in imaging patterns due to its excellent spatial resolution as discussed in section 2.3.4, with many micropatterning focused researchers relying on the technique^{6, 143, 196, 217}. While XPS has the capability of imaging, generally the lateral resolution is limited to a few microns, limiting the quality and ability to resolve patterns in the nano-range. AFM²²⁰ and SEM²¹⁷ (scanning electron microscopy) are also well resolved topographical and structural imaging techniques for patterned surfaces, however are limited to topographical information rather than chemical. There are a vast number of imaging techniques available, and with the enhancement of synchrotron technology, highly resolved giFTIR microspectroscopic imaging is also available to provide chemical information as presented and discussed in chapter 7 of this thesis.

2.6 References

1. Ademovic, Z.; Wei, J.; Winther-Jensen, B.; Hou, X.; Kingshott, P., Surface Modification of PET Films Using Pulsed AC Plasma Polymerisation Aimed at Preventing Protein Adsorption. *Plasma Processes and Polymers* **2005**, 2, (1), 53-63.
2. Szleifer, I., Polymers and proteins: interactions at interfaces. *Current Opinion in Solid State & Materials Science* **1997**, 2, (3), 337-344.
3. Johnston, E. E.; Bryers, J. D.; Ratner, B. D., Plasma Deposition and Surface Characterization of Oligoglyme, Dioxane, and Crown Ether Nonfouling Films. *Langmuir* **2005**, 21, (3), 870-881.
4. Klein, E.; Kerth, P.; Lebeau, L., Enhanced selective immobilization of biomolecules onto solid supports coated with semifluorinated self-assembled monolayers. *Biomaterials* **2008**, 29, (2), 204-214.
5. Bremmell, K. E.; Kingshott, P.; Ademovic, Z.; Winther-Jensen, B.; Griesser, H. J., Colloid Probe AFM Investigation of Interactions between Fibrinogen and PEG-Like Plasma Polymer Surfaces. *Langmuir* **2006**, 22, (1), 313-318.
6. Brétagne, F.; Ceriotti, L.; Lejeune, M.; Papadopoulou-Bouraoui, A.; Hasiwa, M.; Gilliland, D.; Ceccone, G.; Colpo, P.; Rossi, F., Functional Micropatterned Surfaces by Combination of Plasma Polymerization and Lift-Off Processes. *Plasma Processes and Polymers* **2006**, 3, (1), 30-38.
7. Silván, M. M.; Valsesia, A.; Gilliland, D.; Ceccone, G.; Rossi, F., An evaluation of poly(ethylene-glycol) films stabilized by plasma and ion beam methods. *Applied Surface Science* **2004**, 235, (1-2), 119-125.
8. Ademovic, Z. Z., The method of surface PEGylation influences leukocyte adhesion and activation. *Journal of materials science. Materials in medicine* **2006**, 17, (3), 203-211.
9. Cheng, Q.; Li, S.; Komvopoulos, K., Plasma-assisted surface chemical patterning for single-cell culture. *Biomaterials* **2009**, 30, (25), 4203-4210.
10. DeLong, S. A.; Gobin, A. S.; West, J. L., Covalent immobilization of RGDS on hydrogel surfaces to direct cell alignment and migration. *J. Control. Release* **2005**, 109, (1-3), 139-148.
11. Gref, R.; Lück, M.; Quellec, P.; Marchand, M.; Dellacherie, E.; Harnisch, S.; Blunk, T.; Müller, R. H., 'Stealth' corona-core nanoparticles surface modified by polyethylene glycol (PEG): influences of the corona (PEG chain length and surface density) and of the core composition on phagocytic uptake and plasma protein adsorption. *Colloids and Surfaces B: Biointerfaces* **2000**, 18, (3-4), 301-313.
12. Caliceti, P.; Veronese, F. M., Pharmacokinetic and biodistribution properties of poly(ethylene glycol)-protein conjugates. *Advanced Drug Delivery Reviews* **2003**, 55, (10), 1261-1277.
13. Roberts, M. J.; Bentley, M. D.; Harris, J. M., Chemistry for peptide and protein PEGylation. *Advanced Drug Delivery Reviews* **2002**, 54, (4), 459-476.
14. Szleifer, I.; Gerasimov, O. V.; Thompson, D. H., Spontaneous liposome formation induced by grafted poly(ethylene oxide) layers: theoretical prediction and experimental verification. *Proceedings of the National Academy of Sciences of the United States of America* **1998**, 95, (3), 1032-7.

15. Ostuni, E.; Chapman, R. G.; Holmlin, R. E.; Takayama, S.; Whitesides, G. M., A Survey of Structure-Property Relationships of Surfaces that Resist the Adsorption of Protein. *Langmuir* **2001**, 17, (18), 5605-5620.
16. Larsson, A.; Liedberg, B., Poly(ethylene glycol) gradient for biochip development. *Langmuir* **2007**, 23, (22), 11319-11325.
17. Brétagnot, F.; Kylián, O.; Hasiwa, M.; Ceriotti, L.; Rauscher, H.; Ceccone, G.; Gilliland, D.; Colpo, P.; Rossi, F., Micro-patterned surfaces based on plasma modification of PEO-like coating for biological applications. *Sensors & Actuators: B. Chemical* **2007**, 123, (1), 283-292.
18. Angenendt, P.; Glökler, J.; Sobek, J.; Lehrach, H.; Cahill, D. J., Next generation of protein microarray support materials. *Journal of Chromatography A* **2003**, 1009, (1-2), 97-104.
19. Cuchiara, M. P.; Allen, A. C. B.; Chen, T. M.; Miller, J. S.; West, J. L., Multilayer microfluidic PEGDA hydrogels. *Biomaterials* 31, (21), 5491-5497.
20. Turri, S.; Levi, M.; Emilietri, E.; Suriano, R.; Bongiovanni, R., Direct Photopolymerisation of PEG-Methacrylate Oligomers for an Easy Prototyping of Microfluidic Structures. *Macromolecular Chemistry and Physics* 211, (8), 879-887.
21. Vasdekis, A. E.; O'Neil, C. P.; Hubbell, J. A.; Psaltis, D., Microfluidic Assays for DNA Manipulation Based on a Block Copolymer Immobilization Strategy. *Biomacromolecules* 11, (3), 827-831.
22. Zhou, J. H.; Yan, H.; Ren, K. N.; Dai, W.; Wu, H. K., Convenient Method for Modifying Poly(dimethylsiloxane) with Poly(ethylene glycol) in Microfluidics. *Analytical Chemistry* **2009**, 81, (16), 6627-6632.
23. Sharma, S.; Johnson, R. W.; Desai, T. A., XPS and AFM analysis of antifouling PEG interfaces for microfabricated silicon biosensors. *Biosensors and Bioelectronics* **2004**, 20, (2), 227-239.
24. Sheth, S. R.; Leckband, D., Measurements of attractive forces between proteins and end-grafted poly(ethylene glycol) chains. *Proceedings of the National Academy of Sciences of the United States of America* **1997**, 94, (16), 8399-8404.
25. Brétagnot, F.; Lejeune, M.; Papadopoulou-Bouraoui, A.; Hasiwa, M.; Rauscher, H.; Ceccone, G.; Colpo, P.; Rossi, F., Fouling and non-fouling surfaces produced by plasma polymerization of ethylene oxide monomer. *Acta Biomaterialia* **2006**, 2, (2), 165-172.
26. Latour, R. A., Thermodynamic perspectives on the molecular mechanisms providing protein adsorption resistance that include protein-surface interactions. *Journal of Biomedical Materials Research Part A* **2006**, 78A, (4), 843-854.
27. Muir, B. W.; Tarasova, A.; Gengenbach, T. R.; Menzies, D. J.; Meagher, L.; Rovere, F.; Fairbrother, A.; McLean, K. M.; Hartley, P. G., Characterization of Low-Fouling Ethylene Glycol Containing Plasma Polymer Films. *Langmuir* **2008**, 24, (8), 3828-3835.
28. Leckband, D., Measuring the forces that control protein interactions *Annual Review of Biophysics and Biomolecular Structure* **2000**, 29, (1), 1-26.
29. Malmsten, M., Biopolymers at Interfaces In 2 ed.; Malsmten, M., Ed. 2003; Vol. 110, p 908.

30. Jeon, S. I.; Lee, J. H.; Andrade, J. D.; De Gennes, P. G., Protein--surface interactions in the presence of polyethylene oxide : I. Simplified theory. *Journal of Colloid and Interface Science* **1991**, 142, (1), 149-158.
31. Li, L.; Chen, S.; Zheng, J.; Ratner, B. D.; Jiang, S., Protein Adsorption on Oligo(ethylene glycol)-Terminated Alkanethiolate Self-Assembled Monolayers: The Molecular Basis for Nonfouling Behavior. *The Journal of Physical Chemistry B* **2005**, 109, (7), 2934-2941.
32. Pertsin, A. J.; Grunze, M., Computer Simulation of Water near the Surface of Oligo(ethylene glycol)-Terminated Alkanethiol Self-Assembled Monolayers. *Langmuir* **2000**, 16, (23), 8829-8841.
33. Archambault, J. G.; Brash, J. L., Protein resistant polyurethane surfaces by chemical grafting of PEO: amino-terminated PEO as grafting reagent. *Colloids and Surfaces B: Biointerfaces* **2004**, 39, (1-2), 9-16.
34. Zhang, Z.; Menges, B.; Timmons, R. B.; Knoll, W.; Förch, R., Surface Plasmon Resonance Studies of Protein Binding on Plasma Polymerized Di(ethylene glycol) Monovinyl Ether Films. *Langmuir* **2003**, 19, (11), 4765-4770.
35. Besseling, N. A. M., Theory of Hydration Forces between Surfaces. *Langmuir* **1997**, 13, (7), 2113-2122.
36. Kim, H. I.; Kushmerick, J. G.; Houston, J. E.; Bunker, B. C., Viscous "Interphase" Water Adjacent to Oligo(ethylene glycol)-Terminated Monolayers. *Langmuir* **2003**, 19, (22), 9271-9275.
37. Schwendel, D.; Hayashi, T.; Dahint, R.; Pertsin, A.; Grunze, M.; Steitz, R.; Schreiber, F., Interaction of Water with Self-Assembled Monolayers: Neutron Reflectivity Measurements of the Water Density in the Interface Region. *Langmuir* **2003**, 19, (6), 2284-2293.
38. Fick, J.; Steitz, R.; Leiner, V.; Tokumitsu, S.; Himmelhaus, M.; Grunze, M., Swelling Behavior of Self-Assembled Monolayers of Alkanethiol-Terminated Poly(ethylene glycol): A Neutron Reflectometry Study. *Langmuir* **2004**, 20, (10), 3848-3853.
39. Heuberger, M.; Drobek, T.; Spencer, N. D., Interaction Forces and Morphology of a Protein-Resistant Poly(ethylene glycol) Layer. *Biophysical Journal* **2005**, 88, (1), 495.
40. Chan, Y. H. M.; Schweiss, R.; Werner, C.; Grunze, M., Electrokinetic Characterization of Oligo- and Poly(ethylene glycol)-Terminated Self-Assembled Monolayers on Gold and Glass Surfaces. *Langmuir* **2003**, 19, (18), 7380-7385.
41. Unsworth, L. D.; Sheardown, H.; Brash, J. L., Protein resistance of surfaces prepared by sorption of end-thiolated poly(ethylene glycol) to gold: Effect of surface chain density. *Langmuir* **2005**, 21, (3), 1036-1041.
42. Xu, Z. K.; Nie, F. Q.; Qu, C.; Wan, L. S.; Wu, J.; Yao, K., Tethering poly(ethylene glycol)s to improve the surface biocompatibility of poly(acrylonitrile-co-maleic acid) asymmetric membranes. *Biomaterials* **2005**, 26, (6), 589-598.
43. Zhu, B.; Eurell, T.; Gunawan, R.; Leckband, D., Chain-length dependence of the protein and cell resistance of oligo(ethylene glycol)-terminated self-assembled monolayers on gold. *Journal of Biomedical Materials Research* **2001**, 56, (3), 406-416.
44. Kane, R. S.; Deschatelets, P.; Whitesides, G. M., Kosmotropes Form the Basis of Protein-Resistant Surfaces. *Langmuir* **2003**, 19, (6), 2388-2391.

45. Davis-Searles, P. R.; Saunders, A. J.; Erie, D. A.; Winzor, D. J.; Pielak, G. J., Interpreting the effects of small uncharged solutes on protein-folding equilibria. *Annual Review of Biophysics and Biomolecular Structure* **2001**, 30, 271-306.
46. Timasheff, S. N., Control of protein stability and reactions by weakly interacting cosolvents: The simplicity of the complicated. In *Advances in Protein Chemistry, Vol 51*, 1998; Vol. 51, pp 355-432.
47. Hoffmann, C.; Tovar, G. E. M., Mixed self-assembled monolayers (SAMs) consisting of methoxy-tri(ethylene glycol)-terminated and alkyl-terminated dimethylchlorosilanes control the non-specific adsorption of proteins at oxidic surfaces. *Journal of Colloid And Interface Science* **2006**, 295, (2), 427-435.
48. Holmlin, R. E.; Chen, X.; Chapman, R. G.; Takayama, S.; Whitesides, G. M., Zwitterionic SAMs that Resist Nonspecific Adsorption of Protein from Aqueous Buffer. *Langmuir* **2001**, 17, (9), 2841-2850.
49. Knerr, R.; Weiser, B.; Drotleff, S.; Steinem, C.; Göpferich, A., Measuring cell adhesion on RGD-modified, self-assembled PEG monolayers using the quartz crystal microbalance technique. *Macromolecular Bioscience* **2006**, 6, (10), 827-838.
50. Kidane, A.; McPherson, T.; Shim, H. S.; Park, K., Surface modification of polyethylene terephthalate using PEO-polybutadiene-PEO triblock copolymers. *Colloids and Surfaces B: Biointerfaces* **2000**, 18, (3-4), 347-353.
51. Szleifer, I.; Carignano, M. A., Tethered polymer layers: Phase transitions and reduction of protein adsorption. *Macromolecular Rapid Communications* **2000**, 21, (8), 423-448.
52. Unsworth, L. D.; Sheardown, H.; Brash, J. L., Polyethylene oxide surfaces of variable chain density by chemisorption of PEO-thiol on gold: Adsorption of proteins from plasma studied by radiolabelling and immunoblotting. *Biomaterials* **2005**, 26, (30), 5927-5933.
53. Bosker, W. T. E.; Iakovlev, P. A.; Norde, W.; Cohen Stuart, M. A., BSA adsorption on bimodal PEO brushes. *Journal of Colloid and Interface Science* **2005**, 286, (2), 496-503.
54. Tsukagoshi, T.; Kondo, Y.; Yoshino, N., Preparation of thin polymer films with drug release and protein adsorption resistance. *Colloids and Surfaces B: Biointerfaces* **2007**, 55, (1), 19-25.
55. Bretagnol, F.; Lejeune, M.; Papadopoulou-Bouraoui, A.; Hasiwa, M.; Rauscher, H.; Ceccone, G.; Colpo, P.; Rossi, F., Fouling and non-fouling surfaces produced by plasma polymerization of ethylene oxide monomer. *Acta Biomaterialia* **2006**, 2, (2), 165-172.
56. Caldwell, K. D., Surface modifications with adsorbed poly(ethylene oxide)-based block copolymers. In *Poly(Ethylene Glycol) - Chemistry and Biological Applications*, Harris, J. M.; Zalipsky, S., Eds. Amer Chemical Soc: Washington, 1997; Vol. 680, pp 400-419.
57. Li, J. T.; Carlsson, J.; Huang, S. C.; Caldwell, K. D., Adsorption of poly(ethylene oxide)-containing block copolymers - A route to protein resistance. In *Hydrophilic Polymers - Performance with Environmental Acceptance*, Glass, J. E., Ed. Amer Chemical Soc: Washington, 1996; Vol. 248, pp 61-78.
58. Gong, P.; Grainger, D. W., Nonfouling Surfaces. In 2007; Vol. 381, pp 59-92.

59. Leroux, J. C.; Allemann, E.; DeJaeghere, F.; Doelker, E.; Gurny, R., Biodegradable nanoparticles - From sustained release formulations to improved site specific drug delivery. *J. Control. Release* **1996**, 39, (2-3), 339-350.
60. Knop, K.; Hoogenboom, R.; Fischer, D.; Schubert, U. S., Poly(ethylene glycol) in Drug Delivery: Pros and Cons as Well as Potential Alternatives. *Angewandte Chemie-International Edition* **2010**, 49, (36), 6288-6308.
61. Harris, J. M., *Poly(Ethylene Glycol) Chemistry Biotechnical and Biomedical Applications*. Plenum Press: New York 1992; p 385.
62. Alt, E.; Haehnel, I.; Beilharz, C.; Prietzel, K.; Preter, D.; Stemberger, A.; Flidner, T.; Erhardt, W.; Schomig, A., Inhibition of neointima formation after experimental coronary artery stenting - A new biodegradable stent coating releasing hirudin and the prostacyclin analogue iloprost. *Circulation* **2000**, 101, (12), 1453-1458.
63. Park, K. D.; Kim, Y. S.; Han, D. K.; Kim, Y. H.; Lee, E. H. B.; Suh, H.; Choi, K. S., Bacterial adhesion on PEG modified polyurethane surfaces. *Biomaterials* **1998**, 19, (7-9), 851-859.
64. Khoo, X.; Hamilton, P.; O'Toole, G. A.; Snyder, B. D.; Kenan, D. J.; Grinstaff, M. W., Directed Assembly of PEGylated-Peptide Coatings for Infection-Resistant Titanium Metal. *Journal of the American Chemical Society* **2009**, 131, (31), 10992-10997.
65. Park, H.; Temenoff, J. S.; Tabata, Y.; Caplan, A. I.; Mikos, A. G., Injectable biodegradable hydrogel composites for rabbit marrow mesenchymal stem cell and growth factor delivery for cartilage tissue engineering. *Biomaterials* **2007**, 28, (21), 3217-3227.
66. Adel Alhadlaq, M. T., Jeremy J. Mao, Engineered Adipose Tissue from Human Mesenchymal Stem Cells Maintains Predefined Shape and Dimension: Implications in Soft Tissue Augmentation and Reconstruction. *Tissue Engineering* **2005**, 11, (3-4), 556-566.
67. Shen, M. M., Laura; Wagner, Matthew S.; Castner, David G.; Ratner, Buddy D.; Horbett, Thomas A., PEO-like plasma polymerized tetraglyme surface interactions with leukocytes and proteins: in vitro and in vivo studies. *Journal of Biomaterials Science, Polymer Edition* **2002**, 13, 367-390.
68. Shen, M.; Pan, Y. V.; Wagner, M. S.; Hauch, K. D.; Castner, D. G.; Ratner, B. D.; Horbett, T. A., Inhibition of monocyte adhesion and fibrinogen adsorption on glow discharge plasma deposited tetraethylene glycol dimethyl ether. *Journal of Biomaterials Science, Polymer Edition* **2001**, 12, 961-978.
69. Lieberman, M. A.; Lichtenberg, A. J., Principles of Plasma Discharges and Materials Processing. In John Wiley & Sons: New York, 2005.
70. Denes, F. S.; Manolache, S., Macromolecular plasma-chemistry: an emerging field of polymer science. *Progress in Polymer Science* **2004**, 29, (8), 815-885.
71. Boenig, H. V., *Fundamentals of Plasma Chemistry and Technology*. Technomic Publishing Co, Inc: Lancaster, PA, 1988.
72. d'Agostino, R.; Favia, P.; Oehr, C.; Wertheimer, M. R., Low-Temperature Plasma Processing of Materials: Past, Present, and Future. *Plasma Processes and Polymers* **2005**, 2, (1), 7-15.
73. Allen, J. E., The plasma-sheath boundary: its history and Langmuir's definition of the sheath edge. *Plasma Sources Science & Technology* **2009**, 18, (1).

74. Lieberman, M. A.; Lichtenberg, A. J., *Principles of plasma discharges and materials processing*. John Wiley & Sons Inc: New York, 2005.
75. Zelzer, M.; Scurr, D.; Abdullah, B.; Urquhart, A. J.; Gadegaard, N.; Bradley, J. W.; Alexander, M. R., Influence of the plasma sheath on plasma polymer deposition in advance of a mask and down pores. *Journal of Physical Chemistry B* **2009**, 113, (25), 8487-8494.
76. Biederman, H., Plasma polymer films. In Biederman, H., Ed. Imperial College Press: London, 2004.
77. Desmet, T.; Morent, R.; De Geyter, N.; Leys, C.; Schacht, E.; Dubruel, P., Nonthermal plasma technology as a versatile strategy for polymeric biomaterials surface modification: A review. *Biomacromolecules* **2009**, 10, (9), 2351-2378.
78. Biederman, H.; Slavínská, D., Plasma polymer films and their future prospects. *Surface and Coatings Technology* **2000**, 125, (1-3), 371-376.
79. Kühn, G.; Retzko, I.; Lippitz, A.; Unger, W.; Friedrich, J., Homofunctionalized polymer surfaces formed by selective plasma processes. *Surface and Coatings Technology* **2001**, 142-144, 494-500.
80. Swaraj, S.; Oran, U.; Lippitz, A.; Friedrich, J. F.; Unger, W. E. S., Study of influence of external plasma parameters on plasma polymerised films prepared from organic molecules (acrylic acid, allyl alcohol, allyl amine) using XPS and NEXAFS. *Surface & Coatings Technology* **2005**, 200, (1-4), 494-497.
81. Shi, F. F., Recent advances in polymer thin films prepared by plasma polymerization Synthesis, structural characterization, properties and applications. *Surface and Coatings Technology* **1996**, 82, (1-2), 1-15.
82. Förch, R.; Zhang, Z.; Knoll, W., Soft Plasma Treated Surfaces: Tailoring of Structure and Properties for Biomaterial Applications. *Plasma Processes and Polymers* **2005**, 2, (5), 351-372.
83. Brétagne, F.; Valsesia, A.; Ceccone, G.; Colpo, P.; Gilliland, D.; Ceriotti, L.; Hasiwa, M.; Rossi, F., Surface Functionalization and Patterning Techniques to Design Interfaces for Biomedical and Biosensor Applications. *Plasma Processes and Polymers* **2006**, 3, (6-7), 443-455.
84. Siow, K. S.; Britcher, L.; Kumar, S.; Griesser, H. J., Plasma methods for the generation of chemically reactive surfaces for biomolecule immobilization and cell colonization - A review. *Plasma Processes and Polymers* **2006**, 3, (6-7), 392-418.
85. Gengenbach, T. R.; Griesser, H. J., Deposition conditions influence the postdeposition oxidation of methyl methacrylate plasma polymer films. *Journal of Polymer Science Part A: Polymer Chemistry* **1998**, 36, (6), 985-1000.
86. Ward, A. J.; Short, R. D., A t.o.f.s.i.m.s. and x.p.s. investigation of the structure of plasma polymers prepared from the methacrylate series of monomers: 2. The influence of the W/F parameter on structural and functional group retention. *Polymer* **1995**, 36, (18), 3439-3450.
87. Retzko, I.; Friedrich, J. F.; Lippitz, A.; Unger, W. E. S., Chemical analysis of plasma-polymerized films: The application of X-ray photoelectron spectroscopy (XPS), X-ray absorption spectroscopy (NEXAFS) and fourier transform infrared spectroscopy (FTIR). *Journal of Electron Spectroscopy and Related Phenomena* **2001**, 121, (1-3), 111-129.

88. Gomathi, N.; Sureshkumar, A.; Neogi, S., RF plasma-treated polymers for biomedical applications. *Current Science* **2008**, 94, (11), 1478-1486.
89. Zhang, Z. H.; Chen, Q.; Knoll, W.; Foerch, R.; Holcomb, R.; Roitman, D., Plasma polymer film structure and DNA probe immobilization. *Macromolecules* **2003**, 36, (20), 7689-7694.
90. Zhang, Z.; Knoll, W.; Foerch, R.; Holcomb, R.; Roitman, D., DNA hybridization on plasma-polymerized allylamine. *Macromolecules* **2005**, 38, (4), 1271-1276.
91. Hook, A. L.; Thissen, H.; Quinton, J.; Voelcker, N. H., Comparison of the binding mode of plasmid DNA to allylamine plasma polymer and poly(ethylene glycol) surfaces. *Surface Science* **2008**, 602, (10), 1883-1891.
92. Volcke, C.; Gandhiraman, R. P.; Gubala, V.; Raj, J.; Cummins, T.; Fonder, G.; Nooney, R. I.; Mekhalif, Z.; Herzog, G.; Daniels, S.; Arrigan, D. W. M.; Cafolla, A. A.; Williams, D. E., Reactive amine surfaces for biosensor applications, prepared by plasma-enhanced chemical vapour modification of polyolefin materials. *Biosensors & Bioelectronics* **25**, (8), 1875-1880.
93. Sano, S.; Kato, K.; Ikada, Y., Introduction of functional-groups onto the surface of polyethylene for protein immobilization. *Biomaterials* **1993**, 14, (11), 817-822.
94. Dai, L. M.; StJohn, H. A. W.; Bi, J. J.; Zientek, P.; Chatelier, R. C.; Griesser, H. J., Biomedical coatings by the covalent immobilization of polysaccharides onto gas-plasma-activated polymer surfaces. *Surface and Interface Analysis* **2000**, 29, (1), 46-55.
95. McLean, K. M.; Johnson, G.; Chatelier, R. C.; Beumer, G. J.; Steele, J. G.; Griesser, H. J., Method of immobilization of carboxymethyl-dextran affects resistance to tissue and cell colonization. *Colloids and Surfaces B-Biointerfaces* **2000**, 18, (3-4), 221-234.
96. McArthur, S. L.; McLean, K. M.; Kingshott, P.; St John, H. A. W.; Chatelier, R. C.; Griesser, H. J., Effect of polysaccharide structure on protein adsorption. *Colloids and Surfaces B-Biointerfaces* **2000**, 17, (1), 37-48.
97. Abbas, A.; Vercaigne-Marko, D.; Supiot, P.; Bocquet, B.; Vivien, C.; Guillochon, D., Covalent attachment of trypsin on plasma polymerized allylamine. *Colloids and Surfaces B-Biointerfaces* **2009**, 73, (2), 315-324.
98. Gancarz, I.; Bryjak, J.; Bryjak, M.; Tylus, W.; Pozniak, G., Poly(phenylene oxide) films modified with allylamine plasma as a support for invertase immobilization. *European Polymer Journal* **2006**, 42, (10), 2430-2440.
99. Rebl, H.; Finke, B.; Ihrke, R.; Rothe, H.; Rychly, J.; Schroeder, K.; Nebe, B. J., Positively Charged Material Surfaces Generated by Plasma Polymerized Allylamine Enhance Vinculin Mobility in Vital Human Osteoblasts. *Advanced Engineering Materials* **2010**, 12, (8), B356-B364.
100. Hadjizadeh, A., Acetaldehyde plasma polymer-coated PET fibers for endothelial cell patterning: Chemical, topographical, and biological analysis. *Journal of Biomedical Materials Research Part B-Applied Biomaterials* **2010**, 94B, (1), 11-21.
101. McGettrick, J. D.; Schofield, W. C. E.; Garrod, R. P.; Badyal, J. P. S., A Substrate-Independent Approach for the Surface Immobilization of Oligonucleotides using Aldehyde Functionalized Surfaces. *Chemical Vapor Deposition* **2009**, 15, (4-6), 122-127.
102. Vermette, P.; Gengenbach, T.; Divisekera, U.; Kambouris, P. A.; Griesser, H. J.; Meagher, L., Immobilization and surface characterization of NeutrAvidin biotin-binding

protein on different hydrogel interlayers. *Journal of Colloid and Interface Science* **2003**, 259, (1), 13-26.

103. Hook, A. L.; Voelcker, N. H.; Thissen, H., Plasma polymer and PEG-based coatings for DNA, protein and cell microarrays. *Methods Mol Biol* **2011**, 706, 159-70.

104. Wells, N.; Baxter, M. A.; Turnbull, J. E.; Murray, P.; Edgar, D.; Parry, K. L.; Steele, D. A.; Short, R. D., The geometric control of E14 and R1 mouse embryonic stem cell pluripotency by plasma polymer surface chemical gradients. *Biomaterials* **2009**, 30, (6), 1066-1070.

105. Jafari, R.; Arefi-Khonsari, F.; Tatouliau, M.; Le Clerre, D.; Talini, L.; Richard, F., Development of oligonucleotide microarray involving plasma polymerized acrylic acid. *Thin Solid Films* **2009**, 517, (19), 5763-5768.

106. Ito, Y.; Kajihara, M.; Imanishi, Y., Materials for enhancing cell adhesion by immobilization of cell-adhesive peptide. *Journal of Biomedical Materials Research* **1991**, 25, (11), 1325-1337.

107. Gupta, B.; Plummer, C.; Bisson, I.; Frey, P.; Hilborn, J., Plasma-induced graft polymerization of acrylic acid onto poly(ethylene terephthalate) films: characterization and human smooth muscle cell growth on grafted films. *Biomaterials* **2002**, 23, (3), 863-871.

108. vanDelden, C. J.; Lens, J. P.; Kooyman, R. P. H.; Engbers, G. H. M.; Feijen, J., Heparinization of gas plasma-modified polystyrene surfaces and the interactions of these surfaces with proteins studied with surface plasmon resonance. *Biomaterials* **1997**, 18, (12), 845-852.

109. Feng, W.; Nieh, M. P.; Zhu, S.; Harroun, T. A.; Katsaras, J.; Brash, J. L., Characterization of protein resistant, grafted methacrylate polymer layers bearing oligo(ethylene glycol) and phosphorylcholine side chains by neutron reflectometry. *Biointerphases* **2007**, 2, (1), 34-43.

110. Menzies, J. D.; Cowie, C. C. B.; Fong, C.; Forsythe, J.; Gengenbach, T.; Mc Lean, K.; Puskar, L.; Textor, M.; Thomsen, L.; Tobin, M.; Muir, B., A one-step method for generating PEG-like plasma polymer gradients: Chemical Characterisation and Analysis of protein interactions. *Langmuir* **2010**.

111. Sardella, E.; Gristina, R.; Senesi, G. S.; d'Agostino, R.; Favia, P., Homogeneous and Micro-Patterned Plasma-Deposited PEO-Like Coatings for Biomedical Surfaces. *Plasma Processes and Polymers* **2004**, 1, (1), 63-72.

112. Sardella, E.; Detomaso, L.; Gristina, R.; Senesi, G. S.; Agheli, H.; Sutherland, D. S.; d'Agostino, R.; Favia, P., Nano-structured cell-adhesive and cell-repulsive plasma-deposited coatings: Chemical and topographical effects on keratinocyte adhesion. *Plasma Processes and Polymers* **2008**, 5, (6), 540-551.

113. Hurley, C. R.; Ducker, R. E.; Leggett, G. J.; Ratner, B. D., Fabrication of Submicrometer Biomolecular Patterns by Near-Field Exposure of Plasma-Polymerized Tetraglyme Films. *Langmuir* **2000**, 16, (12), 10203-10209.

114. Zhang, M.; Horbett, T. A., Tetraglyme coatings reduce fibrinogen and von Willebrand factor adsorption and platelet adhesion under both static and flow conditions. *Journal of Biomedical Materials Research Part A* **2009**, 89A, (3), 791-803.

115. Salim, M.; Mishra, G.; Fowler, G. J. S.; O'Sullivan, B.; Wright, P. C.; McArthur, S. L., Non-fouling microfluidic chip produced by radio frequency tetraglyme plasma deposition. *Lab on a Chip* **2007**, 7, (4), 523-525.

116. Cao, L.; Chang, M.; Lee, C. Y.; Castner, D. G.; Sukavaneshvar, S.; Ratner, B. D.; Horbett, T. A., Plasma-deposited tetraglyme surfaces greatly reduce total blood protein adsorption, contact activation, platelet adhesion, platelet procoagulant activity, and in vitro thrombus deposition. *Journal of Biomedical Materials Research Part A* **2007**, 81A, (4), 827-837.
117. Kitching, K. J.; Cao, L.; Ratner, B. D.; Horbett, T. A.; Solen, K., Improving the blood compatibility of polyethylene tubing by plasma polymerization of tetraglyme. *Abstracts of Papers of the American Chemical Society* **2003**, 225, 319-POLY.
118. Cao, L.; Sukavaneshvar, S.; Ratner, B. D.; Horbett, T. A., Glow discharge plasma treatment of polyethylene tubing with tetraglyme results in ultralow fibrinogen adsorption and greatly reduced platelet adhesion. *Journal of Biomedical Materials Research Part A* **2006**, 79A, (4), 788-803.
119. Chu, L.-Q.; Knoll, W.; Förch, R., Plasma polymerized non-fouling thin films for DNA immobilization. *Biosensors and Bioelectronics* **2009**, 25, (2), 519-522.
120. Beyer, D.; Knoll, W.; Ringsdorf, H.; Wang, J. H.; Timmons, R. B.; Sluka, P., Reduced protein adsorption on plastics via direct plasma deposition of triethylene glycol monoallyl ether. *Journal of Biomedical Materials Research* **1997**, 36, (2), 181-189.
121. Vreuls, C.; Zocchi, G.; Thierry, B.; Garitte, G.; Griesser, S. S.; Archambeau, C.; Van de Weerd, C. V.; Martial, J.; Griesser, H., Prevention of bacterial biofilms by covalent immobilization of peptides onto plasma polymer functionalized substrates. *Journal of Materials Chemistry* **20**, (37), 8092-8098.
122. Kumar, V.; Pulpytel, J.; Rauscher, H.; Mannelli, I.; Rossi, F.; Arefi-Khonsari, F., Fluorocarbon Coatings Via Plasma Enhanced Chemical Vapor Deposition of 1H,1H,2H,2H-perfluorodecyl Acrylate-2, Morphology, Wettability and Antifouling Characterization. *Plasma Processes and Polymers* **2010**, 7, (11), 926-938.
123. Oran, U.; Swaraj, S.; Lippitz, A.; Unger, W. E. S., Surface Analysis of Plasma Deposited Polymer Films, 7. *Plasma Processes and Polymers* **2006**, 3, (3), 288-298.
124. Swaraj, S.; Oran, U.; Lippitz, A.; Schulze, R. D.; Friedrich, J. F.; Unger, W. E. S., Surface Analysis of Plasma-Deposited Polymer Films, 2. *Plasma Processes and Polymers* **2004**, 1, (2), 134-140.
125. Unger, W. E. S.; Swaraj, S.; Oran, U.; Lippitz, A., Radio frequency (r.f.) plasma-deposited polymer films: influence of external plasma parameters as viewed by comprehensive in-situ surface chemical analysis by XAS, XPS and ToF-SIMS. *Surface and Interface Analysis* **2006**, 38, (4), 522-525.
126. Gray, J. J., The interaction of proteins with solid surfaces. *Current Opinion in Structural Biology* **2004**, 14, (1), 110-115.
127. Swaraj, S.; Oran, U.; Friedrich, J. F.; Lippitz, A.; Unger, W. E. S., Surface Chemical Analysis of Plasma-Deposited Copolymer Films Prepared from Feed Gas Mixtures of Ethylene or Styrene with Allyl Alcohol. *Plasma Processes and Polymers* **2007**, 4, (4), 376-389.
128. Shard, A. G.; Whittle, J. D.; Beck, A. J.; Brookes, P. N.; Bullett, N. A.; Talib, R. A.; Mistry, A.; Barton, D.; McArthur, S. L., A NEXAFS Examination of Unsaturation in Plasma Polymers of Allylamine and Propylamine. *The Journal of Physical Chemistry B* **2004**, 108, (33), 12472-12480.

129. Swaraj, S.; Oran, U.; Lippitz, A.; Friedrich, J. F.; Unger, W. E. S., Surface analysis of plasma deposited polymer films, 6 Analysis of plasma deposited allyl alcohol films before and after aging in air. *Plasma Processes and Polymers* **2005**, 2, (7), 572-580.
130. Swaraj, S.; Oran, U.; Lippitz, A.; Schulze, R. D.; Friedrich, J. F.; Unger, W. E. S., Surface analysis of plasma-deposited polymer films, 4a: In situ characterization of plasma-deposited ethylene films by XPS and NEXAFS. *Plasma Processes and Polymers* **2005**, 2, (4), 310-318.
131. Unger, W. E. S.; Lippitz, A.; Wöll, C.; Heckmann, W., X-ray absorption spectroscopy (NEXAFS) of polymer surfaces. *Fresenius' Journal of Analytical Chemistry* **1997**, 358, (1/2), 89-92.
132. Zhi-Hong Zhang, C.-L. F., The investigation of protein adsorption behaviors on different functionalized polymers films. *Biotechnology Journal* **2007**, 2, (6), 743-751.
133. Blümmel, J.; Perschmann, N.; Aydin, D.; Drinjakovic, J.; Surrey, T.; Lopez-Garcia, M.; Kessler, H.; Spatz, J. P., Protein repellent properties of covalently attached PEG coatings on nanostructured SiO₂-based interfaces. *Biomaterials* **2007**, 28, (32), 4739-4747.
134. Thissen, H.; Johnson, G.; Hartley, P. G.; Kingshott, P.; Griesser, H. J., Two-dimensional patterning of thin coatings for the control of tissue outgrowth. *Biomaterials* **2006**, 27, (1), 35-43.
135. Muir, B. W.; Nelson, A.; Fairbrother, A.; Fong, C.; Hartley, P. G.; James, M.; McLean, K. M., A Comparative X-Ray and Neutron Reflectometry Study of Plasma Polymer Films Containing Reactive Amines. *Plasma Processes and Polymers* **2007**, 4, (4), 433-444.
136. Xu, L. C.; Siedlecki, C. A., Effects of surface wettability and contact time on protein adhesion to biomaterial surfaces. *Biomaterials* **2007**, 28, (22), 3273-3283.
137. Zheng, J.; Li, L.; Tsao, H. K.; Sheng, Y. J.; Chen, S.; Jiang, S., Strong repulsive forces between protein and oligo (ethylene glycol) self-assembled monolayers: A molecular simulation study. *Biophysical Journal* **2005**, 89, (1), 158-166.
138. Dee, K. C.; Puleo, D. A.; Bizios, R., *An introduction to tissue-biomaterial interactions*. John Wiley & Sons: New Jersey, 2002.
139. Stohr, J., *NEXAFS Spectroscopy*. Springer: New York, 1996.
140. Castner, D. G.; Lewis, K. B.; Fischer, D. A.; Ratner, B. D.; Gland, J. L., Determination of surface structure and orientation of polymerized tetrafluoroethylene films by near-edge x-ray absorption fine structure, x-ray photoelectron spectroscopy, and static secondary ion mass spectrometry. *Langmuir* **1993**, 9, (2), 537-542.
141. Stamm, M., Polymer surfaces and interfaces: characterization, modification and applications
In First edition ed.; Springer: Berlin, 2008.
142. Lee, C. Y.; Harbers, G. M.; Grainger, D. W.; Gamble, L. J.; Castner, D. G., Fluorescence, XPS, and TOF-SIMS surface chemical state image analysis of DNA microarrays. *Journal of the American Chemical Society* **2007**, 129, (30), 9429-9438.
143. Dubey, M.; Emoto, K.; Cheng, F.; Gamble, L. J.; Takahashi, H.; Grainger, D. W.; Castner, D. G., Surface analysis of photolithographic patterns using ToF-SIMS and PCA. *Surface and Interface Analysis* **2009**, 41, (8), 645-652.
144. Ogaki, R.; Alexander, M.; Kingshott, P., Chemical patterning in biointerface science. *Mater. Today* **2010**, 13, (4), 22-35.

145. Mishra, G.; Easton, C. D.; McArthur, S. L., Physical vs Photolithographic Patterning of Plasma Polymers: An Investigation by ToF-SSIMS and Multivariate Analysis. *Langmuir* **2009**, 26, (5), 3720-3730.
146. Thomas, R. K., Neutron reflectometry in solid state and materials science. *Current Opinion in Solid State & Materials Science* **1996**, 1, (5), 636-644.
147. Ott, F.; Cousin, F.; Menelle, A., Surfaces and interfaces characterization by neutron reflectometry. *Journal of Alloys and Compounds* **2004**, 382, (1-2), 29-38.
148. Förch, R.; Schönherr, H.; Jenkins, A. T. A., *Surface design: applications in bioscience and nanotechnology*. Wiley-VCH: 2009.
149. Hegemann, D.; Brunner, H.; Oehr, C., Plasma treatment of polymers for surface and adhesion improvement. *Nuclear Instruments and Methods in Physics Research Section B: Beam Interactions with Materials and Atoms* **2003**, 208, 281-286.
150. Ivanova, E. P., *Nanoscale structure and properties of microbial cell surfaces*. Nova Science Publishers: 2007.
151. Genzer, J.; Bhat, R. R., Surface-Bound Soft Matter Gradients. *Langmuir* **2008**, 24, (6), 2294.
152. Smith, J. T.; Tomfohr, J. K.; Wells, M. C.; Beebe, T. P.; Kepler, T. B.; Reichert, W. M., Measurement of Cell Migration on Surface-Bound Fibronectin Gradients. *Langmuir* **2004**, 20, (19), 8279.
153. Zelzer, M.; Majani, R.; Bradley, J. W.; Rose, F.; Davies, M. C.; Alexander, M. R., Investigation of cell-surface interactions using chemical gradients formed from plasma polymers. *Biomaterials* **2008**, 29, (2), 172-184.
154. Robinson, D. E.; Marson, A.; Short, R. D.; Buttle, D. J.; Day, A. J.; Parry, K. L.; Wiles, M.; Highfield, P.; Mistry, A.; Whittle, J. D., Surface gradient of functional heparin. *Advanced Materials* **2008**, 20, (6), 1166-1169.
155. Vasilev, K.; Mierczynski, A.; Hook, A.; Chan, J.; Voelcker, N. H.; Short, R. D., Creating gradients of two proteins by differential passive adsorption onto a PEG-density gradient. *Biomaterials* **2010**, 31, 392-397.
156. Jeong, B. J.; Lee, J. H.; Lee, H. B., Preparation and Characterization of Comb-like PEO Gradient Surfaces. *Journal of Colloid And Interface Science* **1996**, 178, (2), 757-763.
157. Wang, Q.; Bohn, P. W., Surface composition gradients of immobilized cell signaling molecules. Epidermal growth factor on gold. *Thin Solid Films* **2006**, 513, (1-2), 338-346.
158. Bhat, R.; Chaney, B.; Rowley, J.; Liebmann-Vinson, A.; Genzer, J., Tailoring Cell Adhesion Using Surface-Grafted Polymer Gradient Assemblies. *Advanced Materials* **2005**, 17, (23), 2802-2807.
159. Liedberg, B.; Wirde, M.; Tao, Y. T.; Tengvall, P.; Gelius, U., Molecular Gradients of omega-Substituted Alkanethiols on Gold Studied by X-ray Photoelectron Spectroscopy. *Langmuir* **1997**, 13, (20), 5329-5334.
160. Ekblad, T.; Andersson, O.; Tai, F. I.; Edeith, T.; Liedberg, B., Lateral control of protein adsorption on charged polymer gradients. *Langmuir* **2009**, 25, (6), 3755-3762.
161. Li, B.; Ma, Y.; Wang, S.; Moran, P. M., Influence of carboxyl group density on neuron cell attachment and differentiation behavior: Gradient-guided neurite outgrowth. *Biomaterials* **2005**, 26, (24), 4956-4963.

162. Iwasaki, Y.; Ishihara, K.; Nakabayashi, N.; Khang, G.; Jeon, J. H.; Lee, J. W.; Lee, H. B., Platelet adhesion on the gradient surfaces grafted with phospholipid polymer. *Journal of Biomaterials Science, Polymer Edition* **1998**, 9, (8), 801-816.
163. Lee, S. J.; Khang, G.; Lee, Y. M.; Lee, H. B., The effect of surface wettability on induction and growth of neurites from the PC-12 cell on a polymer surface. *Journal of Colloid and Interface Science* **2003**, 259, (2), 228-235.
164. Lee, T. G.; Shon, H. K.; Kim, M. S.; Lee, H. B.; Moon, D. W., ToF-SIMS imaging of gradient polyethylene and its amine-functionalized surfaces. *Applied Surface Science* **2006**, 252, (19), 6754-6756.
165. Shin, Y. N.; Kim, B. S.; Ahn, H. H.; Lee, J. H.; Kim, K. S.; Lee, J. Y.; Kim, M. S.; Khang, G.; Lee, H. B., Adhesion comparison of human bone marrow stem cells on a gradient wettable surface prepared by corona treatment. *Applied Surface Science* **2008**, 255, (2), 293-296.
166. Lee, J. H.; Lee, H. B., Platelet adhesion onto wettability gradient surfaces in the absence and presence of plasma proteins. *Journal of Biomedical Materials Research* **1998**, 41, (2), 304-311.
167. Morgenthaler, S.; Lee, S.; Zürcher, S.; Spencer, N. D., A Simple, Reproducible Approach to the Preparation of Surface-Chemical Gradients. *Langmuir* **2003**, 19, (25), 10459-10462.
168. Vasilev, K.; Mierczynski, A.; Hook, A.; Chan, J.; Voelcker, N. H.; Short, R. D., Creating gradients of two proteins by differential passive adsorption onto a PEG-density gradient. *Biomaterials* **2010**, 31, 392-397.
169. Ogumi, Z.; Abe, T.; Nakamura, S.; Inaba, M., Functionally gradient polymer electrolyte prepared by plasma polymerization. *Solid State Ionics* **1999**, 121, (1), 289-293.
170. Carter, S. B., Principles of Cell Motility: The Direction of Cell Movement and Cancer Invasion. *Nature* **1965**, 208, 1183-1187.
171. Elwing, H.; Welin, S.; Askendal, A.; Nilsson, U.; Lundström, I., A wettability gradient method for studies of macromolecular interactions at the liquid/solid interface. *Journal of Colloid and Interface Science* **1987**, 119, (1), 203-210.
172. Chaudhury, M. K.; Whitesides, G. M., How to Make Water Run Uphill. *Science* **1992**, 256, (5063), 1539-1541.
173. Genzer, J.; Fischer, D. A.; Efimenko, K., Fabricating Two-Dimensional Molecular Gradients via Asymmetric Deformation of Uniformly-Coated Elastomer Sheets. *Advanced Materials* **2003**, 15, (18), 1545-1547.
174. Liedberg, B.; Tengvall, P., Molecular Gradients of .omega.-Substituted Alkanethiols on Gold: Preparation and Characterization. *Langmuir* **1995**, 11, (10), 3821-3827.
175. Fuierer, R. R.; Carroll, R. L.; Feldheim, D. L.; Gorman, C. B., Patterning Mesoscale Gradient Structures with Self-Assembled Monolayers and Scanning Tunneling Microscopy Based Replacement Lithography. *Advanced Materials* **2002**, 14, (2), 154-157.
176. Kraus, T.; Stutz, R.; Balmer, T. E.; Schmid, H.; Malaquin, L.; Spencer, N. D.; Wolf, H., Printing Chemical Gradients. *Langmuir* **2005**, 21, (17), 7796-7804.

177. Hypolite, C. L.; McLernon, T. L.; Adams, D. N.; Chapman, K. E.; Herbert, C. B.; Huang, C. C.; Distefano, M. D.; Hu, W.-S., Formation of Microscale Gradients of Protein Using Heterobifunctional Photolinkers. *Bioconjugate Chemistry* **1997**, 8, (5), 658-663.
178. Jeon, N. L.; Dertinger, S. K. W.; Chiu, D. T.; Choi, I. S.; Stroock, A. D.; Whitesides, G. M., Generation of Solution and Surface Gradients Using Microfluidic Systems. *Langmuir* **2000**, 16, (22), 8311.
179. Choi, S. H.; Newby, B., Micrometer-Scaled Gradient Surfaces Generated Using Contact Printing of Octadecyltrichlorosilane. *Langmuir* **2003**, 19, (18), 7427-7435.
180. Venkateswar, R. A.; Branch, D. W.; B.C.Wheeler, An Electrophoretic Method for Microstamping Biomolecule Gradients. *Biomedical Microdevices* **2000**, 2, 255-264.
181. Ueda-Yukoshi, T.; Matsuda, T., Cellular Responses on a Wettability Gradient Surface with Continuous Variations in Surface Compositions of Carbonate and Hydroxyl Groups. *Langmuir* **1995**, 11, (10), 4135-4140.
182. Pitt, W. G., Fabrication of a continuous wettability gradient by radio frequency plasma discharge. *Journal of Colloid and Interface Science* **1989**, 133, (1), 223-227.
183. Lee, J. H.; Kim, H. G.; Khang, G. S.; Lee, H. B.; Jhon, M. S., Characterization of wettability gradient surfaces prepared by corona discharge treatment. *Journal of Colloid and Interface Science* **1992**, 151, (2), 563-570.
184. Tomlinson, M. R.; Efimenko, K.; Genzer, J., Study of Kinetics and Macroinitiator Efficiency in Surface-Initiated Atom-Transfer Radical Polymerization. *Macromolecules* **2006**, 39, (26), 9049-9056.
185. Meredith, J. C.; Karim, A.; Amis, E. J., High-Throughput Measurement of Polymer Blend Phase Behavior. *Macromolecules* **2000**, 33, (16), 5760-5762.
186. Xu, C.; Wu, T.; Mei, Y.; Drain, C. M.; Batteas, J. D.; Beers, K. L., Synthesis and Characterization of Tapered Copolymer Brushes via Surface-Initiated Atom Transfer Radical Copolymerization. *Langmuir* **2005**, 21, (24), 11136-11140.
187. Xu, C.; Barnes, S. E.; Wu, T.; Fischer, D. A.; DeLongchamp, D. M.; Batteas, J. D.; Beers, K. L., Solution and Surface Composition Gradients via Microfluidic Confinement: Fabrication of a Statistical-Copolymer-Brush Composition Gradient. *Advanced Materials* **2006**, 18, (11), 1427-1430.
188. Tomlinson, M. R.; Genzer, J., Formation of Grafted Macromolecular Assemblies with a Gradual Variation of Molecular Weight on Solid Substrates. *Macromolecules* **2003**, 36, (10), 3449-3451.
189. Wu, T.; Efimenko, K.; VlÅek, P.; Åubr, V.; Genzer, J., Formation and properties of anchored polymers with a gradual variation of grafting densities on flat substrates. *Macromolecules* **2003**, 36, (7), 2448-2453.
190. Wu, T.; Efimenko, K.; Genzer, J., Combinatorial Study of the Mushroom-to-Brush Crossover in Surface Anchored Polyacrylamide. *Journal of the American Chemical Society* **2002**, 124, (32), 9394-9395.
191. Zhao, B., A Combinatorial Approach to Study Solvent-Induced Self-Assembly of Mixed Poly(methyl methacrylate)/Polystyrene Brushes on Planar Silica Substrates: Effect of Relative Grafting Density. *Langmuir* **2004**, 20, (26), 11748-11755.
192. Ionov, L.; Zdyrko, B.; Sidorenko, A.; Minko, S.; Klep, V.; Luzinov, I.; Stamm, M., Gradient Polymer Layers by "Grafting To" Approach. *Macromolecular Rapid Communications* **2004**, 25, (1), 360-365.

193. Mougin, K.; Ham, A. S.; Lawrence, M. B.; Fernandez, E. J.; Hillier, A. C., Construction of a Tethered Poly(ethylene glycol) Surface Gradient For Studies of Cell Adhesion Kinetics. *Langmuir* **2005**, 21, (11), 4809-4812.
194. Chang, W. C.; Sretavan, D. W., Novel High-Resolution Micropatterning for Neuron Culture Using Polylysine Adsorption on a Cell Repellant, Plasma-Polymerized Background. *Langmuir* **2008**, 24, (22), 13048-13057.
195. Garrod, R. P.; Harris, L. G.; Schofield, W. C. E.; McGettrick, J.; Ward, L. J.; Teare, D. O. H.; Badyal, J. P. S., Mimicking a stenocara beetle's back for microcondensation using plasmachemical patterned superhydrophobic-superhydrophilic surfaces. *Langmuir* **2007**, 23, (2), 689-693.
196. Goessl, A.; Garrison, M. D.; Lhoest, J. B.; Hoffman, A. S., Plasma lithography - thin-film patterning of polymeric biomaterials by RF plasma polymerization I: Surface preparation and analysis. *Journal of Biomaterials Science. Polymer Edition* **2001**, 12, (7), 721-738.
197. Nie, Z.; Kumacheva, E., Patterning surfaces with functional polymers. *Nat Mater* **2008**, 7, (4), 277-290.
198. Gather, M. C.; Kohnen, A.; Falcou, A.; Becker, H.; Meerholz, K., Solution-processed full-color polymer organic light-emitting diode displays fabricated by direct photolithography. *Advanced Functional Materials* **2007**, 17, (2), 191-200.
199. Renak, M. L.; Bazan, G. C.; Roitman, D., Microlithographic process for patterning conjugated emissive polymers. *Advanced Materials* **1997**, 9, (5), 392-&.
200. Yang, Y.; Chang, S. C.; Bharathan, J.; Liu, J., Organic/polymeric electroluminescent devices processed by hybrid ink-jet printing. *Journal of Materials Science-Materials in Electronics* **2000**, 11, (2), 89-96.
201. Chen, C. S.; Mrksich, M.; Huang, S.; Whitesides, G. M.; Ingber, D. E., Geometric control of cell life and death. *Science* **1997**, 276, (5317), 1425-1428.
202. DeForest, C. A.; Polizzotti, B. D.; Anseth, K. S., Sequential click reactions for synthesizing and patterning three-dimensional cell microenvironments. *Nat Mater* **2009**, 8, (8), 659-664.
203. Tavana, H.; Jovic, A.; Mosadegh, B.; Lee, Q. Y.; Liu, X.; Luker, K. E.; Luker, G. D.; Weiss, S. J.; Takayama, S., Nanolitre liquid patterning in aqueous environments for spatially defined reagent delivery to mammalian cells. *Nat Mater* **2009**, 8, (9), 736-741.
204. Engelmayer, G. C.; Cheng, M.; Bettinger, C. J.; Borenstein, J. T.; Langer, R.; Freed, L. E., Accordion-like honeycombs for tissue engineering of cardiac anisotropy. *Nat Mater* **2008**, 7, (12), 1003-1010.
205. Yang, J.; Rose, F., R. A. J. ; Gadegaard, N.; Morgan, A. R., A High-Throughput Assay of Cell-Surface Interactions using Topographical and Chemical Gradients. *Advanced Materials* **2009**, 21, (3), 300-304.
206. Ito, I.; Hayashi, M.; Imanishi, Y., Gradient micropattern immobilization of heparin and its interaction with cells. *J. Biomater. Sci.-Polym. Ed.* **2001**, 12, (4), 367-378.
207. Hahn, M. S.; Taite, L. J.; Moon, J. J.; Rowland, M. C.; Ruffino, K. A.; West, J. L., Photolithographic patterning of polyethylene glycol hydrogels. *Biomaterials* **2006**, 27, (12), 2519-2524.
208. Dillmore, W. S.; Yousaf, M. N.; Mrksich, M., A Photochemical Method for Patterning the Immobilization of Ligands and Cells to Self-Assembled Monolayers. *Langmuir* **2004**, 20, (17), 7223-7231.

209. Kane, R. S.; Takayama, S.; Ostuni, E.; Ingber, D. E.; Whitesides, G. M., Patterning proteins and cells using soft lithography. *Biomaterials* **1999**, 20, (23-24), 2363-2376.
210. Thissen, H.; Hayes, J.P.; Kingshott, P.; Johnson, G.; Harvey E.C. and Griesser H.J. , Nanometer thickness laser ablation for spatial control of cell attachment *Smart Materials & Structures* **2002**, 11, (5), 792.
211. Kim, D.-K.; Ganesan, R.; Jung, C.-H.; Hwang, I.-T.; Choi, J.-H.; Kim, J.-B.; Nho, Y.-C.; Suh, D.-H., Micropatterning of proteins on ion beam-induced poly(acrylic acid)-grafted polyethylene film. *Polymers for Advanced Technologies* 9999, (9999), n/a.
212. Jing, F. J.; Wang, L.; Fu, R. K. Y.; Leng, Y. X.; Chen, J. Y.; Huang, N.; Chu, P. K., Behavior of endothelial cells on micro-patterned titanium oxide fabricated by plasma immersion ion implantation and deposition and plasma etching. *Surface and Coatings Technology* **2007**, 201, (15), 6874-6877.
213. Yoshinobu, T.; Suzuki, J.; Kurooka, H.; Moon, W. C.; Iwasaki, H., AFM fabrication of oxide patterns and immobilization of biomolecules on Si surface. *Electrochimica Acta* **2003**, 48, (20-22), 3131-3135.
214. Piner, R. D.; Zhu, J.; Xu, F.; Hong, S. H.; Mirkin, C. A., "Dip-pen" nanolithography. *Science* **1999**, 283, (5402), 661-663.
215. Klajn, R.; Fialkowski, M.; Bensemann, I. T.; Bitner, A.; Campbell, C. J.; Bishop, K.; Smoukov, S.; Grzybowski, B. A., Multicolour micropatterning of thin films of dry gels. *Nat Mater* **2004**, 3, (10), 729-735.
216. Mishra, G.; Easton, C. D.; McArthur, S. L., Physical vs Photolithographic Patterning of Plasma Polymers: An Investigation by ToF⁺SSIMS and Multivariate Analysis. *Langmuir* **2009**, 26, (5), 3720-3730.
217. Malkov, G. S.; Martin, I. T.; Schwisow, W. B.; Chandler, J. P.; Wickes, B. T.; Gamble, L. J.; Castner, D. G.; Fisher, E. R., Pulsed-plasma-induced micropatterning with alternating hydrophilic and hydrophobic surface chemistries. *Plasma Processes and Polymers* **2008**, 5, (2), 129-145.
218. Bretagnol, F.; Kylian, O.; Hasiwa, M.; Ceriotti, L.; Rauscher, H.; Ceccone, G.; Gilliland, D.; Colpo, P.; Rossi, F., Micro-patterned surfaces based on plasma modification of PEO-like coating for biological applications. *Sensors and Actuators B-Chemical* **2007**, 123, (1), 283-292.
219. Muir, B.; Fairbrother, A.; Gengenbach, T.; Rovere, F.; Abdo, M.; McLean, K.; Hartley, P., Scanning Probe Nanolithography and Protein Patterning of Low-Fouling Plasma Polymer Multilayer Films. *Advanced Materials* **2006**, 18, (23), 3079-3082.
220. Lee, S. W.; Oh, B. K.; Sanedrin, R. G.; Salaita, K.; Fujigaya, T.; Mirkin, C. A., Biologically Active Protein Nanoarrays Generated Using Parallel Dip-Pen Nanolithography. *Advanced Materials* **2006**, 18, (9), 1133-1136.

Results Part 1:

Investigating the Properties of Uniform PEG-like Plasma polymers



Chapter 3:

A study into of the effects of plasma processing parameters on the production of uniform, low fouling PEG-like plasma polymer films

3. A study into of the effects of plasma processing parameters on the production of uniform, low fouling PEG-like plasma polymer films

3.1 Introduction

Chapter 3 investigates the effects of plasma processing conditions on the continuous wave, radio-frequency glow discharge plasma polymerisation of diethylene glycol dimethyl ether in terms of producing uniform, robust, low fouling PEG-like surfaces. The flow rate of the DG monomer was investigated and defined in the capacitively coupled plasma reactor, used for the deposition of the DGpp films discussed and presented in this thesis. Furthermore, the effect of the W/FM factor (Yasuda factor) on the resulting DGpp films was also investigated by producing a series of films deposited at systematically increasing load power, including 5, 10, 20, 30, 40 and 50 W over a standard 60 second deposition period. The chemistry of the resulting uniform DGpp films were fully characterised, including analysis of film thickness and wettability, and a thorough chemical analysis of the films using a number of complimentary chemical analysis techniques, including grazing incidence-FTIR for analysis of the bulk chemistry of the films, and XPS combined with NEXAFS to characterise the surface chemistry. Furthermore, any structuring of the plasma polymer film chains was investigated by performing NEXAFS experiments with both horizontally and vertically polarised light. It was envisaged that this may have helped, in part, to explain higher degrees of protein resistance displayed by the DGpp films, in terms of steric repulsion of the PEG chains against approaching proteins. Furthermore, analysis of the degree of protein resistance of the films was observed by exposing the films to solutions of BSA and lysozyme, two

proteins of differing physical characteristics such as size and charge, as previously discussed in Chapter 1. A higher degree of protein resistance of the films was found to correlate primarily with the films residual ether content. Cell attachment studies using the anchorage dependent HeLa cells were also performed highlighting the low-fouling nature of DGpp films produced at a 5W load power, and their potential use in both the field of biomaterials and applied research.

3.2 Materials and Methods

3.2.1 Substrate Materials and Cleaning

Ultra-flat single crystal silicon wafers (<100>, 1 cm² x 0.5 mm thick, M.M.R.C P/L), thin copper shim (100µm thick) and indium tin oxide (ITO) coated (single sided) aluminosilicate glass, (thickness of 1.1 mm, Delta Technologies, Corning 1737, CB-50IN) were all used as substrates for the deposition of the diethylene glycol dimethyl ether (DG) pp films. All substrates were cleaned by immersion in a 2 % RBS-35 surfactant (Pierce) in a 2 % ethanol solution and ultrasonicated for 1 hour. Substrates were rinsed multiple times in Milli-Q water and dried in a high-pressure stream of high purity nitrogen.

3.2.2 Masking

Masked areas (for AFM step height film thickness analysis and cell growth contrasts) were prepared on cleaned silicon wafers by solvent casting a 10% (w/v) solution of poly(D,L-lactide) (Boehringer Ingelheim) in acetone onto part of the substrate prior to pp deposition, and dried in air. Following pp, the mask was gently lifted using tweezers without damaging the surrounding film producing well defined step heights for film thickness analysis.

3.2.3 Plasma Polymerisation

A custom-built plasma reactor was used to deposit films, using a radiofrequency glow discharge of diethylene glycol dimethyl ether (DG) (BDH, 99% purity), without further purification, to deposit the DGpp thin films. The plasma reactor is composed of a cylindrical glass chamber (height of 35 cm and diameter of 17 cm), with two capacitatively coupled circular electrodes, spaced 10 cm apart. The top electrode ($d = 9.5$ cm) was connected to a RF power supply (125 kHz), while the bottom electrode (diameter = 14 cm) was grounded. Substrates were placed on the lower electrode, and a rotary pump was used to evacuate the chamber. The DG monomer was degassed three times prior to deposition, when the DG vapours were fed into the chamber at a starting pressure of 20 Pa, and a continuous RF field was generated between the electrodes for a deposition time of 60 seconds. The plasma load power was varied for these experiments including depositions at 5, 10, 20, 30, 40 and 50W.

3.2.4 Monomer flow rate determination

Prior to pp deposition, the flow rate of DG vapours was calculated as a function of monomer starting pressure. To monitor the pressure change during outflow experiments, the plasma reactor was prepared as for a pp deposition. The coarse outlet valve was closed and the fine outlet valve opened. The monomer inlet valve was opened until the starting monomer pressure had reached 20, 30 and 32.3 Pa, respectively (the latter pressure being the highest possible using this system and monomer). The monomer inlet valve was then closed and the pressure recorded over a 90 second time period. The inflow of the DG vapours was monitored, by closing the fine and coarse outflow valves, opening the monomer valve to the pre-determined position and measuring the pressure

increase over 90 seconds. From the inflow data, the flow rate of DG vapour was calculated, from the following equation¹, which is derived from the ideal gas equation:

$$F = (dp/dt) \times 16172(V/T) \quad [1]$$

Where F = flow rate ($\text{cm}^3 \text{ min}^{-1}$) V = volume of reactor = 7.4 L

p = pressure (mbar) T = temperature = 293 K

t = time (seconds)

3.2.5 Protein Adsorption

Solutions of bovine serum albumin (BSA) and lysozyme (Lys) (1 mg/ml) were prepared in phosphate buffer saline (PBS) at pH 7.4 and the DGpp films were incubated in the solutions for 1 hour at room temperature, followed by multiple rinses in Milli-Q water. As a control, each sample was compared to its equivalent, which had been treated in the same manner by incubating in PBS without the protein solutions, followed by the same rinsing routine. An XPS survey analysis was used to detect any nitrogen present (which is absent on the DGpp), indicating adsorbed proteins on the DGpp. Due to sensitivity errors that occur in XPS measurements near the instrument detection limit of 0.1-0.5 atomic %, the detection limit of protein adsorption on a surface is 10 - 25 ng/cm^2 .

3.2.6 Atomic Force Microscopy

An Asylum Research MFP-3D atomic force microscope (Santa Barbara, CA, USA) was used to measure film thickness, via step height analysis from tapping mode images collected with ultrasharp silicon nitride tips (NSC15 noncontact silicon cantilevers, MikroMasch, Spain). The tips used in this study had a typical force constant of 40 N/m

and a resonant frequency of 320 kHz. Typical scan settings involved the use of an applied piezo deflection voltage of 0.8 V at a scan rate of 0.3 Hz.

3.2.7 Grazing Incidence Fourier Transform Infra Red Spectroscopy

Grazing incidence FT-IR spectra were performed on the DGpp films, using a Perkin Elmer FTIR Spectrophotometer Spectrum 2000, equipped with a SpectraTech FT80 specular reflectance attachment, with a fixed grazing angle of 80°. All spectra were acquired with 128 scans and an instrument resolution of 8.0 cm⁻¹. To quantify the relevant functional group ratio, spectra were manually baseline corrected and normalised to the peak representing CH stretching (at ~ 2928 cm⁻¹)². The resulting absorbance of the relevant functional peaks compared.

3.2.8 Contact Angle Goniometry

Static contact angles of Milli-Q water on the DGpp films were measured using the contact angle measurement system of the KSV CAM 200 (KSV Instrument LTD). The reported static contact angle is the average taken from triplicate measurements performed on each sample.

3.2.9 X-ray Photoelectron Spectroscopy

To investigate the chemical composition of the DGpp films, XPS analysis was performed using an AXIS HSi spectrometer (Kratos Analytical Ltd, Manchester, UK) equipped with a monochromated Al K_α X-ray source at a power of 144 W (12 mA, 12 kV) and a hemispherical analyser operating in the fixed analyser transmission mode and a standard aperture (1 mm x 0.5 mm). Charging of the samples during irradiation was compensated for by the internal flood gun, coupled with a magnetic immersion lens. The pressure in the main vacuum chamber during analysis was typically 5 x 10⁻⁶ Pa.

Each sample was analysed at an emission angle of 0° and 75° wrt the surface normal, providing a depth analysis of approximately the top 10 and 2–3 nm respectively. Survey spectra were acquired at a pass energy of 320 eV, to identify the elements present in the DGpp films. The atomic concentrations were calculated using integral peak intensities and the sensitivity factors supplied by the manufacturer. In addition, high-resolution C 1s spectra were obtained and quantified using a minimisation algorithm in order to calculate optimised curvefits and to determine the relative contributions from specified functional groups.

Five peak components (mixed Guassian/Lorentzian model functions) were used. Component C1 at the lowest binding energy (BE) was assigned to aliphatic hydrocarbons (neutral carbon) and the corresponding BE set accordingly to 285 eV. A second component, C2 was included at a slightly higher BE to account for all C 1s photoelectrons that underwent a secondary BE shift. Component C3 (286.3-286.6 eV) represents C-O based groups (eg ethers and alcohols), C4 (287.9 – 288.2 eV) accounts for all C=O based functional groups (eg aldehydes and ketones) and C5 (288.9 – 289.3 eV) accounts for O-C=O based groups (eg acids or esters)

3.2.10 Near Edge X-ray Absorption Fine Structure

Near Edge X-ray Adsorption Fine Structure (NEXAFS) spectroscopy was performed at the Australian Synchrotron on the soft X-ray beam line (SXR, 14-ID). Samples were loaded into a UHV chamber, where a vacuum of 2×10^{-8} kPa was maintained. The beam line is equipped with an Apple II undulator, which was set to produce horizontally

polarised light that is then passed through a monochromator (Peterson plane grating, 1200 lines mm^{-1}). The photon flux on the beam line was 2.7×10^{11} photons/sec/200 mA, and the beam spot size on the sample was approximately 0.6 x 0.6 mm. Spectra were acquired (with the beam at 90° wrt the sample surface) for both the C (270-320 eV) and O (520 -560 eV) K-edge in partial electron yield (PEY) mode. A retarding potential of -100 eV and -400 eV for the C and O scans respectively was applied to the entrance of the detector to eliminate any contributions from lower energy electrons. To investigate any preferred orientation of the surface bound plasma polymer, spectra were also acquired at 45° wrt to the surface for the 5 W uniform films)

Multiple spectra on the same spot retained the same spectral features, indicating that the films are not subject to radiation damage. To account for contributions to the O 1s and C 1s spectra from internal contamination from the beamline itself, a clean sputtered Au foil was measured as a reference. Spectra were then normalised according to the method discussed by Watts et al.³ WinXAS version 2.34 was used to process the NEXAFS spectra where a background subtraction was performed at the pre-edge and a first order polynomial normalisation performed at the post-edge.

3.2.11 Cell Attachment Study

Individual sample replicates (three per treatment) were transferred to wells in a 24-well tissue culture tray and sterilised in a sterile solution of PBS (pH 7.4) containing penicillin and streptomycin (120 $\mu\text{g/mL}$ and 200 $\mu\text{g/mL}$, respectively) overnight at 4°C . A single masked example of each treatment condition and four TCPS control wells were also set up under the identical conditions.

To analyse the attachment behaviour of the HeLa cells on the DGpp surfaces, cells were seeded onto individual samples and TCPS control surfaces at a concentration of 2×10^5 cells/well in a culture medium composed of DMEM/Hams F12 supplemented with 10% (v/v) foetal bovine serum (FBS). The relative number of cells attached to the test surfaces was measured by incubating the cells on two of the three replicates per sample with the tetrazolium dye MTT for the final four hours of incubation. Viable cells convert the dye into an insoluble coloured formazan product that was solubilised with DMSO and the absorbance read on a plate reader at 595 nm. Cell attachment was then calculated by expressing the respective absorbance as a percentage of that read for cells on the TCPS control surface after taking into account the respective area differences between the TCPS control surfaces and the individual sample areas.

Visualisation of cell presence and morphology on the silicon wafers was achieved by exposing cells from the remaining sample replicate not used for the MTT assay to CellTracker Green™ (CTG, Molecular Probes, Invitrogen) for the final hour of incubation. The single masked sample per treatment was also exposed to the CTG solution. Digital images were taken from UV fluorescence microscopy of the CTG stained samples (Nikon Eclipse 90i).

3.3 Results and Discussion

3.3.1 Plasma Polymerisation

Plasma polymerisation has a number of variable parameters that can affect the resulting chemistry and physical properties of the pp film such as flow rate, plasma load power, electrode geometry, and temperature, pressure and deposition times.⁴⁻⁷ One in particular is the ‘Yasuda factor’, or W/FM parameter (where W is the radiofrequency power input, F is the flow rate and M is the molecular weight of the monomer), and can be defined as the plasma power input per monomer mass unit.^{1, 8, 9} A low W/FM value is reported to result in plasma polymer (pp) films with a high retention of the original monomer structure, while films deposited under conditions of a high W/FM value result in films with a more complex chemistry and less like the original monomer structure.¹ Before preparing the DGpp films for experimental analysis, the inflow and outflow pressures of DG vapours were monitored and flow rate calculated as a function of starting monomer pressure (where the corresponding position of the monomer control valve had been pre-determined to match the three monomer starting pressures) over a 90 second time period. Figures 3.3.1 and 3.3.2 present the pressure against time plots for the outflow and inflow of DG vapours respectively measured at three different monomer valve settings corresponding to starting monomer pressures of 20, 30 and 32.3 Pa. The outflow of the DG vapours (figure 3.3.1) decreases most significantly over the first 20 seconds, before steadily declining over the remaining 70 seconds. After the initial 20 to 30 second period the outflow pressure values were relatively similar irrespective of the initial monomer starting pressure.

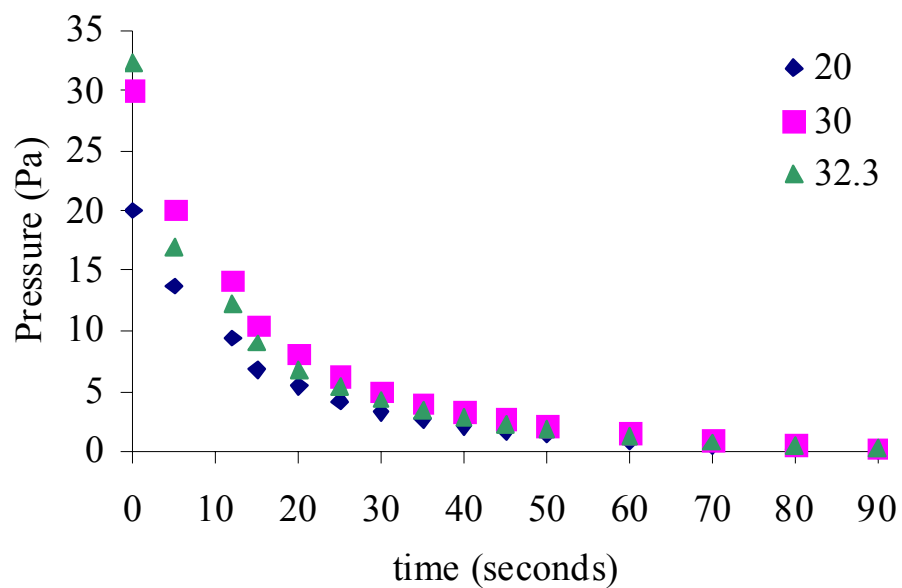


Figure 3.1 Outflow rates of DEGDME at initial monomer pressures of 20, 30 and 32.3 Pa

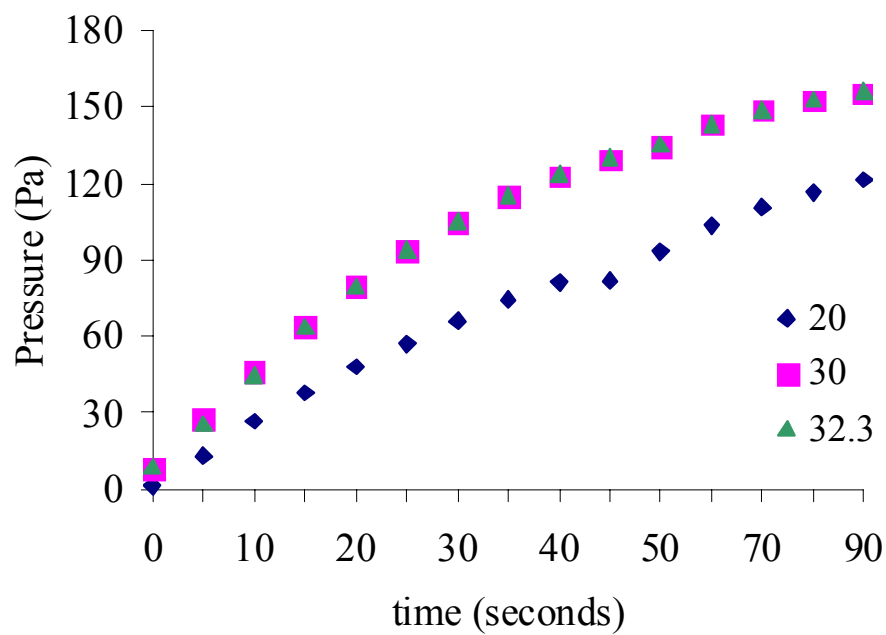


Figure 3.2 Inflow rates of DEGDME at initial monomer pressures of 20, 30 and 32.3 Pa

The inflow data shows a significant difference in the pressure increase over time when the monomer flow valve was set to the equivalent of an initial monomer pressure of 20 Pa, compared with 30 and 32.3 Pa, which resulted in similar pressure values over time. This indicates that at an initial monomer pressure of 20 Pa, the number of species flowing into and out of the reactor is less than at a starting pressure of 30 Pa or higher. Using the data obtained from the inflow pressure measurements (figure 3.3.2), flow rates ($F = \text{cm}^3 \text{ min}^{-1}$) of the DG vapours (Figure 3.3.3) were calculated from equation [1], (derived from the ideal gas equation)^{1, 8} as a function of starting monomer pressure. The average flow rate (calculated over a 90 second period) of the DG vapours was shown to be greater when the monomer starting pressure was 30 and 32.3 Pa ($F = 9.74$ and $9.07 \text{ cm}^3 \text{ sec}^{-1}$ respectively), compared with 20 Pa ($F = 7.03 \text{ cm}^3 \text{ sec}^{-1}$). While a higher flow rate is associated with less time spent between the electrodes and hence a lesser degree of fragmentation, the DGpp films deposited for this work were done at an initial monomer pressure of 20 Pa, as previous work performed by our group has identified this parameter to produce good adherent DGpp films (data unpublished).

To investigate the effect of varying the W/FM parameter on the resulting DGpp film chemistry the plasma load power was systematically varied during pp deposition from 5 to 50 W, at an initial monomer pressure of 20 Pa. The pressure increase during deposition was monitored, enabling an observation of the state of equilibrium within the system at each power.

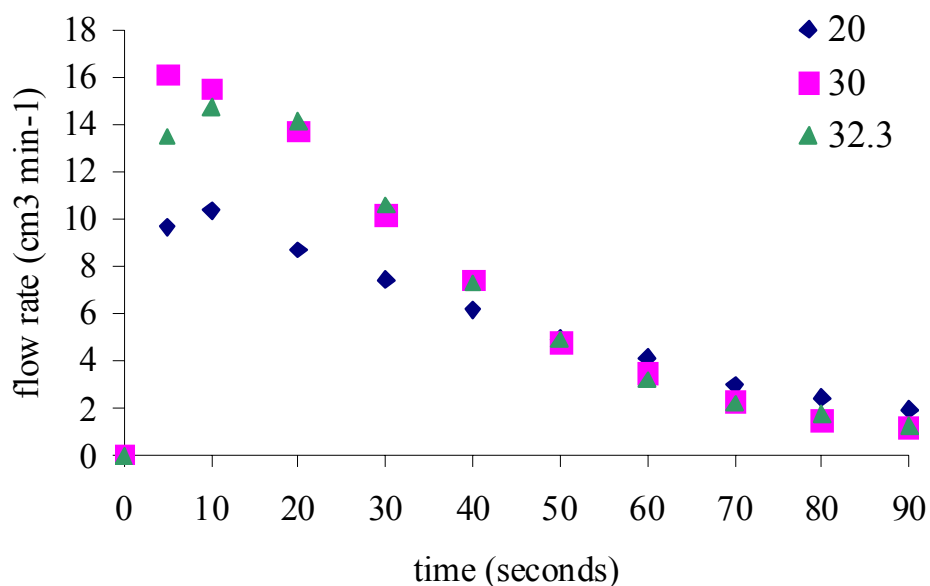


Figure 3.3 Flow rates of DEGDM vapour ($\text{cm}^3 \text{sec}^{-1}$) at initial monomer pressures of 20, 30 and 32.3 Pa

Figure 3.3.4 shows that higher load powers used for deposition of DG vapours results in an increased pressure range in the system with higher load powers, a maximum of 26.1 Pa for the films deposited at 5W compared to a maximum of 65.6 Pa when DG was deposited at the highest power used for this study, 50 W. An estimation of the average number of scissions per monomer unit can be related to pressure range in the reactor during pp deposition, by the following equation ¹:

$$(P_{\text{max}}/P_{\text{initial}}) - 1 = \text{average number of scissions per monomer unit} \quad [2]$$

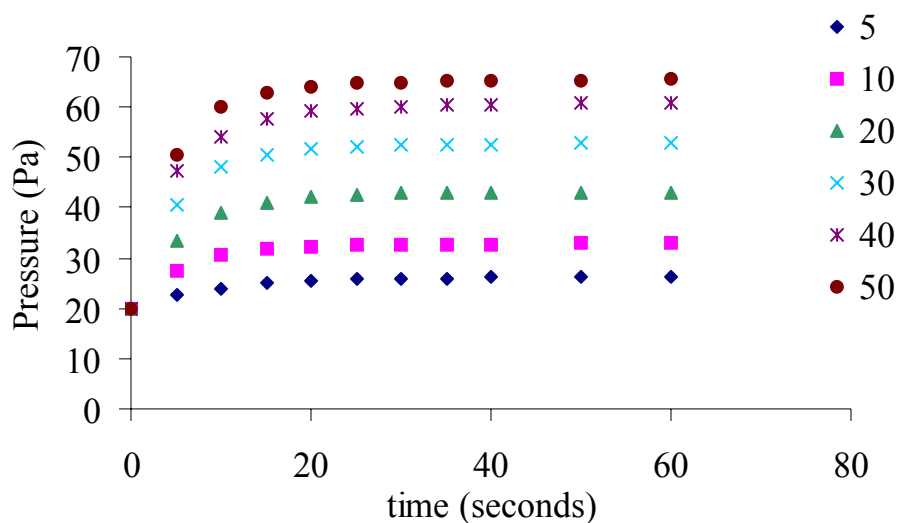


Figure 3.4 Reactor pressure as a function of RF power (W) and time.

Using equation [2], it was calculated that the average number of scissions during a 5W DGpp deposition (0.3 scissions) was approximately 7 times less than during a 50 W DGpp deposition (2.3 scissions). The implications of these results are consistent with Bretagnol et al.¹⁰, who reported that increasing the load power during deposition of PEO-like coatings resulted in more fragmentation of the monomer, and therefore, resulted in films with less PEO-like character.

Observation of the pressure vs. time plot (Figure 3.3.4), indicated that conditions in the plasma reactor reached equilibrium around the 25-30 second time point across all powers, and the rate of monomer inflow and outflow was equivalent to the rate of deposition.

3.3.2 Film Thickness and Wettability

To analyse the resulting chemical and physical properties of the DGpp films deposited at varied load power, a number of complimentary techniques were used, including AFM to analyse film thickness, contact angle goniometry to analyse film wettability and XPS, FTIR and NEXAFS to analyse the resulting film chemistries. The thickness of the DGpp films increased with higher deposition powers (Table 3.3.1) ranging from 21.2 nm thickness of DGpp film deposited under a load power of 5 W, to 92.8nm from the 50W DGpp film. The film wettability of the DGpp films (Table 3.3.1), measured from the static contact angles using MilliQ water, decreased only slightly in films deposited under higher load powers, ranging from 59° to 64°, similar to those reported by Cheng et al. on diglyme plasma polymerised surfaces.¹¹ The slight increase in contact angle seen in higher powered films is associated with a loss of PEG-like character and the film becoming more carbon like. The wettability of a film is reported to affect the interactions between the surface and proteins,¹² where a higher level of oxygen functionality is reported to increase the wettability of a film.^{5, 13}

Table 3.1 Film thickness and static contact angles of DG films deposited for 60 seconds

DGpp Load Power (W)	Film thickness (nm)	Static contact angle (°) ± SD
5	21.2	59.0 ± 1.8
10	49.6	61.5 ± 0.2
20	65.4	60.0 ± 1.4
30	81.9	63.0 ± 0.3
40	85.0	63.5 ± 0.3
50	92.8	64.0 ± 0.6

3.3.3 Film Chemistry

3.3.3.1 Grazing incidence FTIR

Analysis of the bulk chemistry of the DGpp films deposited at the varied load power was performed using grazing incidence FTIR. The overlaid spectra for each film is presented in Figure 3.3.5A showing the presence of three main functional groups including the stretching vibrations of COC (ethers) from ca. 1050-1200 cm^{-1} , carbonyls (C=O) at 1690-1780 cm^{-1} and hydrocarbon (CH_2CH_2 , CH_3) from ~ 2850 -3000 cm^{-1} . There is also an absorption in the spectra in the higher IR absorption region around 3200-3600 cm^{-1} , most likely attributed to the presence of -OH groups representing the presence of hydroxyl, carboxylic acid and water groups. However, due to the noisy nature of the spectra in this region, acquired on the bench top FTIR on these very thin films, the hydroxyl peaks have not been quantified for this discussion. It is worth noting, however, that hydroxyl contributions of DGpp film chemistry are very low compared to the presence of the other functionalities. Another point of interest to note from the FTIR spectra is the absence of an alkene stretch ($\sim 1621 \text{ cm}^{-1}$), indicating that no detectable concentration of C=C bonds was observed using the gi-FTIR technique. The absence of the alkene stretch absorption from FTIR analysis has also recently been reported by Cheng et al.¹¹ in an FTIR study of pulsed plasma deposited bulk chemical DGpp thin films. A comparison of the integrated areas of the COC and C=O functionalities plotted as a ratio to that of the hydrocarbon content for the DGpp films deposited at different load powers is presented in Figure 3.3.5B. In accordance with results reported by other researchers analysing DGpp films^{10, 11}, results from the FTIR data show that when the DGpp deposition occurs under lower load power, the chemistry of the resulting films

remains more like the original monomer structure. The ether content was shown to be highest in films deposited at 5 W, systematically decreasing (in relation to the hydrocarbon content) as the load power was increased. In contrast, the carbonyl content was lowest in the lower powered DGpp films, systematically increasing in content in films deposited at higher load powers.

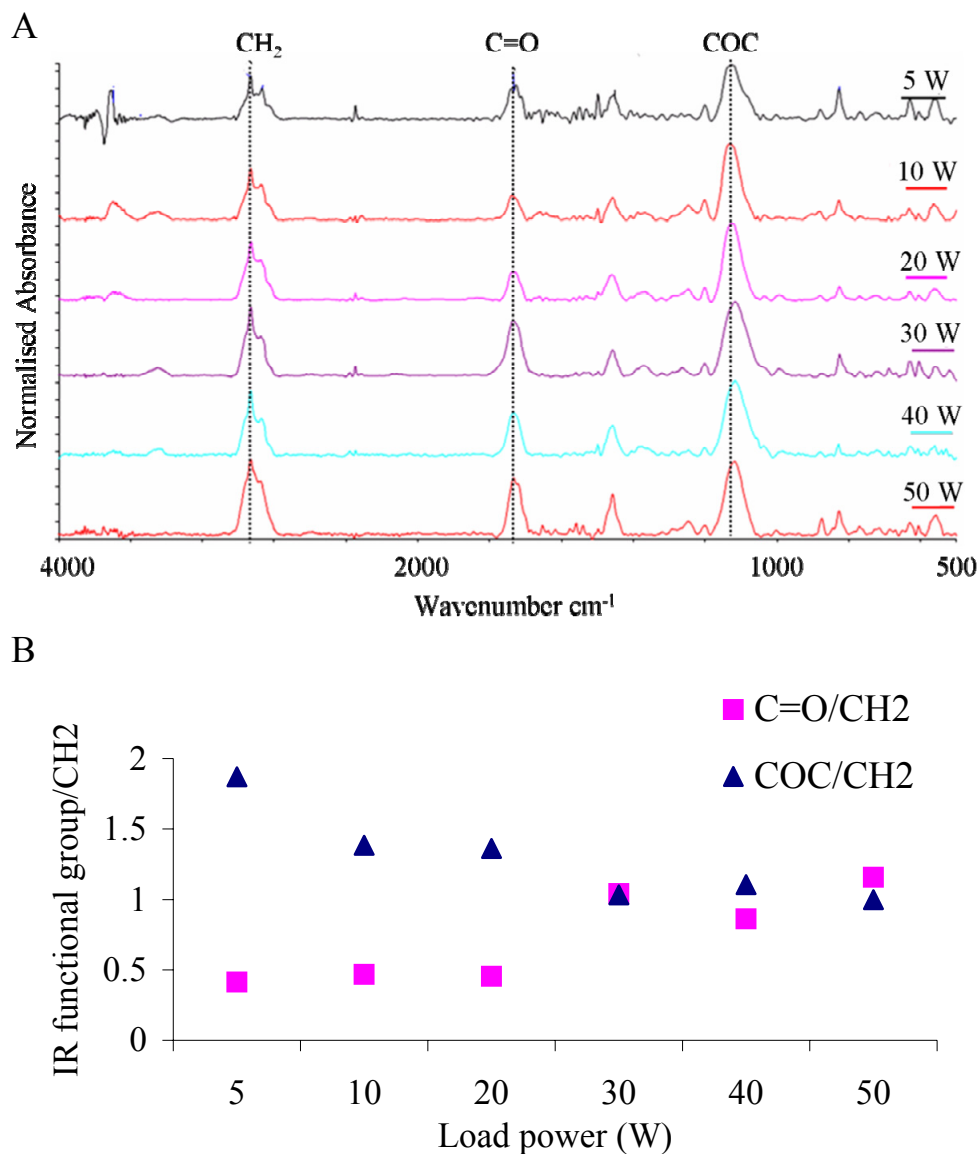


Figure 3.5 A: Overlay of FTIR spectra of DGpp films, with normalised absorbance units

B: Plot of the ratio of the integrated ether and carbonyl areas, to hydrocarbon

3.3.3.2 XPS

While FTIR analysis considers the bulk chemistry of the films, XPS enables analysis of the surface chemistry, which is the interface region that most dictates material-biological interactions. In general, it is agreed that XPS in normal emission mode (ie 90° wrt the surface) considers the top 10 nm of the film, while changing the angle of incidence of the X-ray to 45° wrt the surface enables analysis of the top ca. 3-4 nm of the film. Therefore, to gain a greater understanding of the films chemistries and their resulting effect on protein and cell interactions, a depth profiling XPS analysis of the DGpp films for this study has been performed at both normal and grazing angle emission.

Analysis of the elemental content of the DGpp films was conducted via XPS survey scans, which detected the presence of both carbon and oxygen. It is well reported in the analysis of PEG-like films that a higher O:C ratio is indicative of a film retaining more PEG-like qualities.^{10, 14} As such, the ratio of oxygen to carbon (O/C) in the DGpp films are plotted in Figures 3.3.6 A and B at both normal and grazing angle emission, respectively (for both air and pre- PBS exposed films), and decreases in films deposited at higher load powers. This indicates that the DGpp films have a higher oxygen content when they are deposited under lower load powers which is consistent with previous literature reports on DG-based plasma polymerised films.^{15, 16} Comparison of the O/C ratio from films analysed both dry and after incubation in PBS showed oxygen levels decreased following water exposure. This could be attributed to such events as a loss of material, chemical reactions¹⁷, or again even surface contamination. Furthermore, comparison of the normal and grazing angle emission O:C data (Figures 3.3.6 A and B,

respectively) suggests that the bulk of these films are more highly oxygenated than the surface, with higher O/C ratios detected at normal emission XPS.

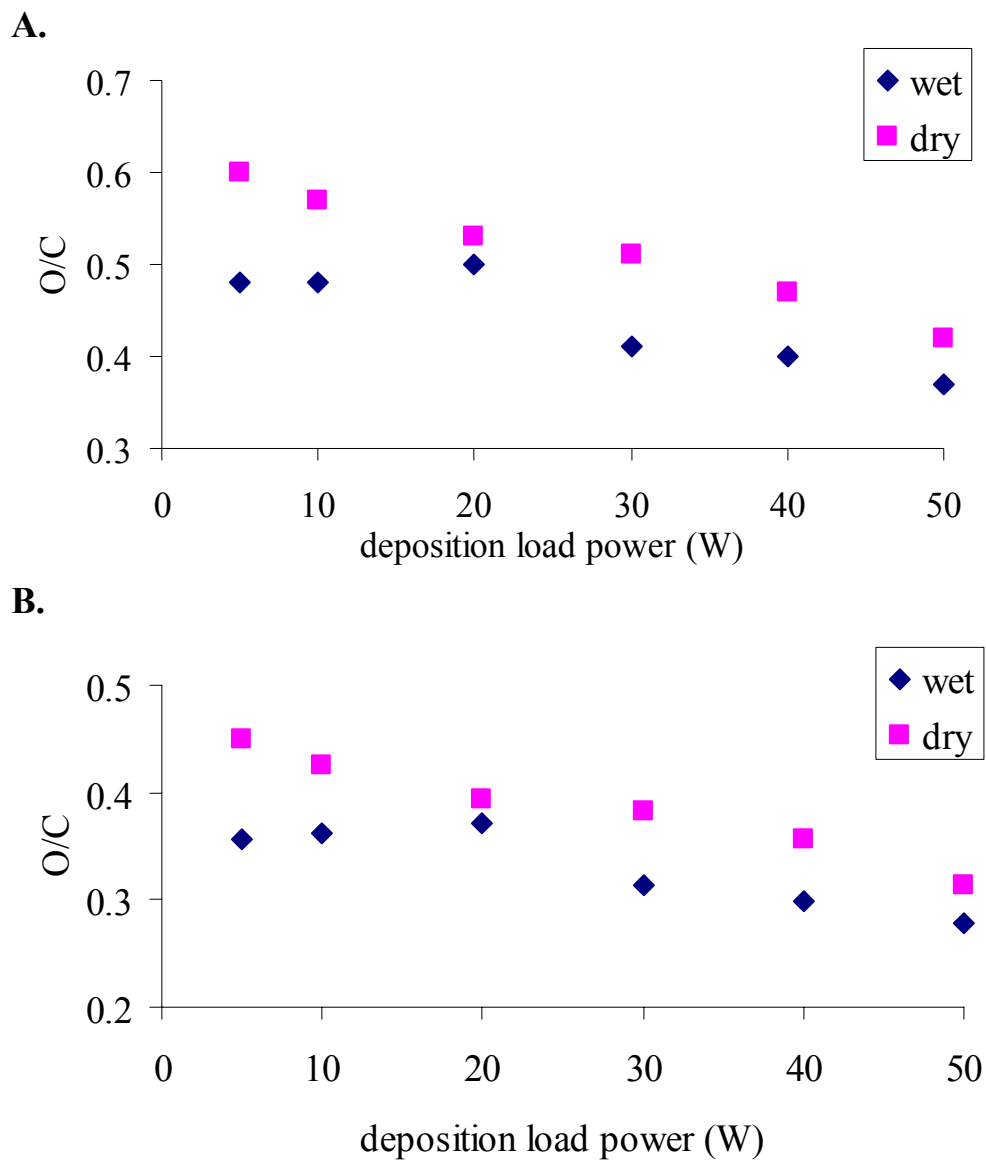


Figure 3.6 A: O/C ratio from normal emission XPS elemental analysis of DGpp

B: O/C ratio from grazing angle XPS elemental analysis of DGpp

While the oxygen content measured from the survey spectra considers all oxygenated species present, within the depth of the analysis, it does not however provide information on the type of oxygenated functionality present. It is well reported in the literature that a high retention of ether groups within PEG-like films is associated with its ability to resist non-specific protein adsorption.^{4, 16} Therefore, to identify the types of oxygenated species present in the DGpp films and measure their relative amounts, high resolution C 1s XPS analysis was performed on each of the DGpp films deposited at varied load power, both dry and after incubation in PBS. The C 1s curves were fitted into 4 components including CC;CH, COR, C=O and O-C=O species, and their relative contributions to the DGpp films quantified (C 1s curves presented in Figures 3.3.7 A and B, with the bottom 5 W spectra both show the fitted C 1s components). While it is important to note that the COR component of the C 1s XPS could be attributed from both ether and alcohol species, FT-IR analysis showed very low contributions of OH groups (Fig. 3.3.5A). In addition large contributions from aliphatic ether groups at 1122 cm^{-1} are observed and therefore it may be assumed that a large proportion of the COR component from the C 1s XPS is due to the ether functionality. The C=O component may be attributed to aldehydes and ketone functionalities.

The most obvious information to be extracted from observation of the XPS C 1s curves of the DGpp films deposited from 5 to 50 W, is the decrease in the COR component and subsequent increase in hydrocarbon species, as depicted in Figures 3.3.8. When comparing the spectra of the DGpp films deposited at each power attained from their dry state to those that had been previously incubated in PBS, once again the trend of loss of

monomer like ether content and subsequent increase in hydrocarbon content is apparent, between samples deposited at the same load power.

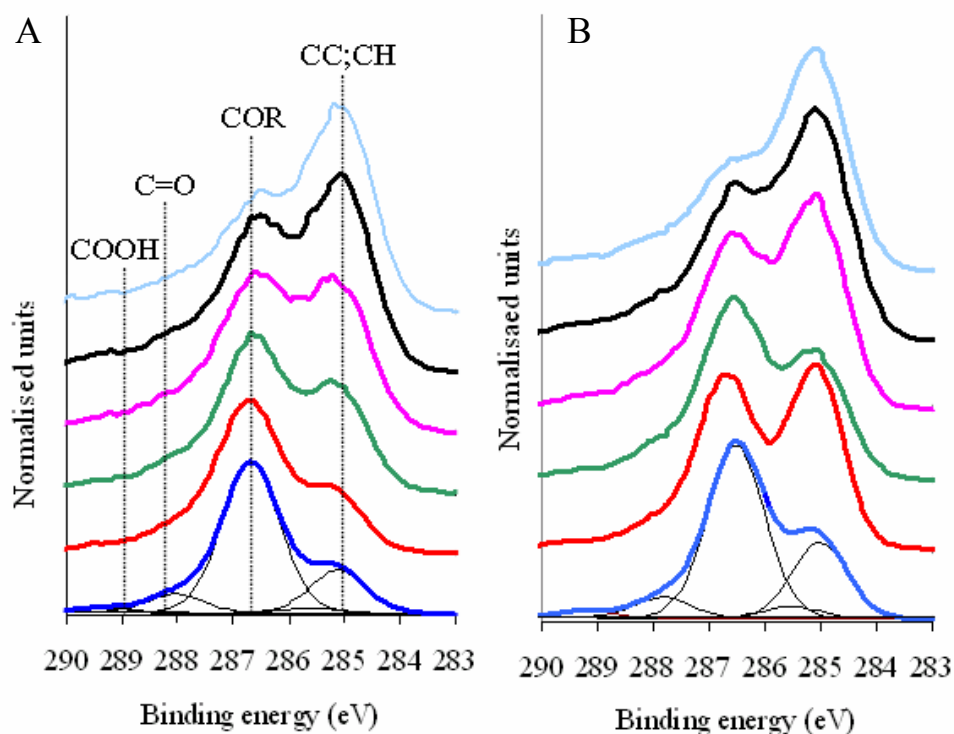


Figure 3.7 XPS C 1s curve fit for 5 (bottom spectra) to 50 W (top spectra) DGpp's (dry; left spectra) and after immersion in PBS (wet; right spectra)

Comparison of the COR/CH ratios (Figure 3.3.8) from the C 1s XPS spectra of the DGpp films shows a significant decrease in the COR content when the rate of monomer fragmentation within the plasma reactor was greater during deposition (at higher load powers). There was also a slight decrease in C=O and O-C=O species within the DGpp films deposited under higher load powers, relative to the CH component (Figure 3.3.8). This decrease in functionality was apparent both at normal and grazing angle emission (data not shown), indicating that it is the hydrocarbon content of the films increasing in the films when higher deposition powers are used. Furthermore, when comparing the

COR:CH ratio of the DGpp films attained at normal compared to grazing emission XPS (Figure 3.3.8 A and B respectively), it can be seen that the top surface (ie 3-4 nm) of the 5 and 10 W DGpp contains less ether functionality, than the top ca. 10 nm of the films, most apparent in the 5 W films, however this effect is not apparent in films deposited at 20W and higher. This finding could potentially relate to the higher stability of films, and lower amounts of lower molecular weight oligomers deposited at the surface of films when higher load powers are employed.

The differences in the percentage of the CC;CH and COR C1s components from the C 1s curves once after the film had been incubated in PBS (compared to those only exposed to air) has been plotted and is presented in Figure 3.3.9. This change in film chemistry following PBS incubation may be attributed to a loss of material such as short chain oligomers at the surface, however chemical reactions (such as reactions with trapped radicals or oxidation), and surface contamination cannot be ruled out. More importantly this data provides an insight into the relative stability of DGpp films deposited at the varying load power and indicates that DGpp films deposited at 20 W remain the most stable, while the film deposited at 10 W showed the greatest change in chemistry.

Bretagnol et al.¹⁰ analysed the stability of PEG-like pp films by immersing them in water, then re-analysing their chemical composition using XPS, as well as re-measuring their refractive index. They reported no significant atomic loss or addition, with the elemental composition remaining the same (within 5%), however a change in the refractive index of the films was observed, indicating a change in film chemistry.

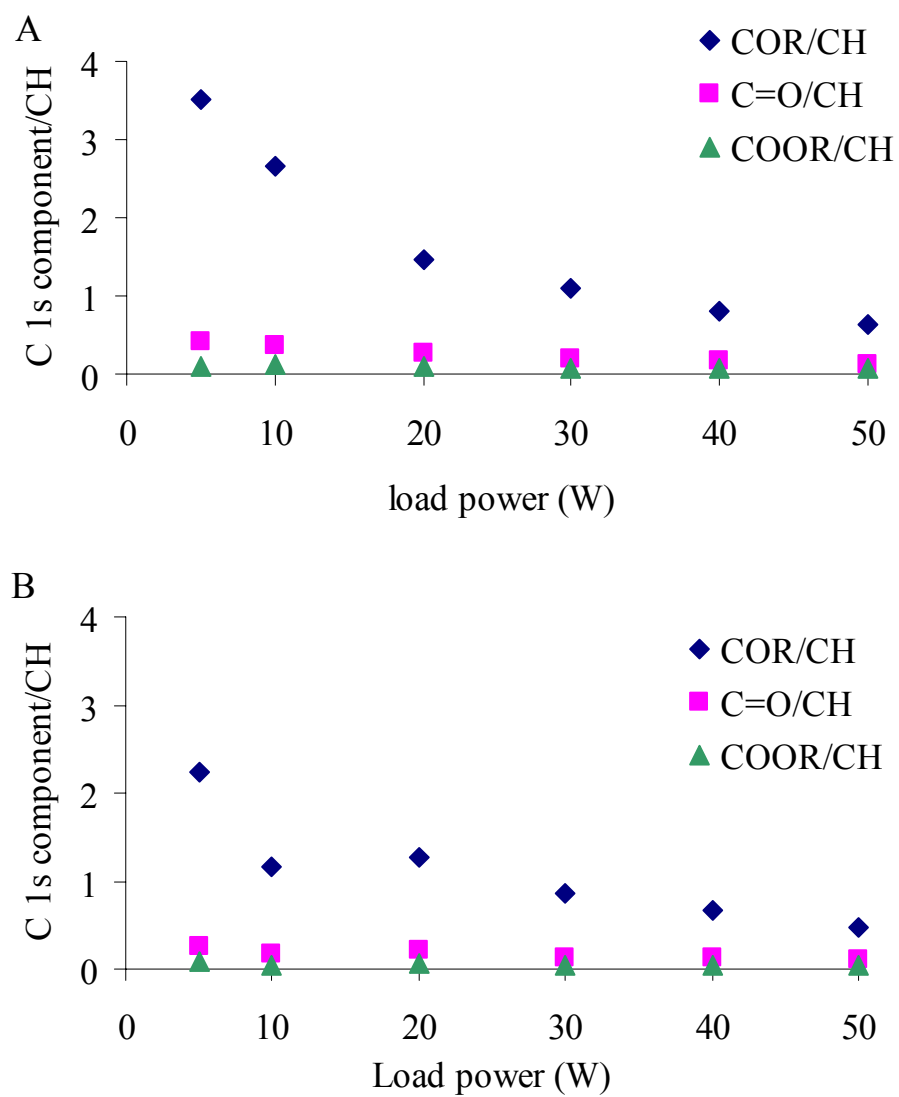


Figure 3. 8 C 1s component/CH ratios of DGpp films from C 1s normal (A) grazing angle (B) emission XPS analysis

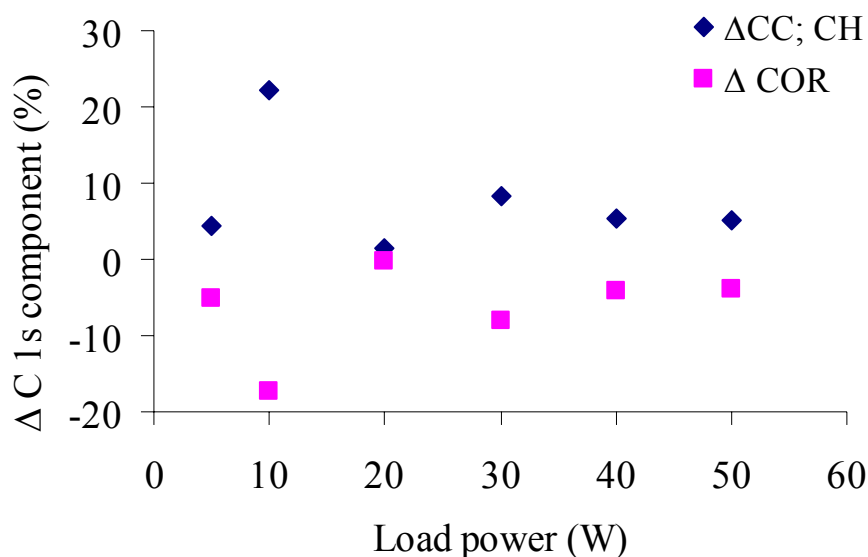


Figure 3.9 The change in COR and CC;CH species from DGpp films exposed to air, compared to those previously incubated in PBS prior to XPS analysis

3.3.3.3 NEXAFS

To further analyse the chemistry across the DGpp films, and detect any the orientation of terminal chains across the DGpp gradients, a C and O K-edge PEY NEXAFS spectroscopy study was performed on DGpp films deposited at 5 and 50 W load power. Analysis of the C 1s spectra revealed four main resonance feature (Figure 3.3.10A) including C 1s $\rightarrow \pi^*$ (C=O) excitation at ~ 285.7 eV (a), C 1s $\rightarrow \sigma^*$ (C-H) at ~ 287.3 eV (b), C 1s $\rightarrow \sigma^*$ (C-O) at ~ 289.9 eV (c) and a broader C 1s $\rightarrow \sigma^*$ (C-C;C-O) feature at ~ 294.4 eV (d). Due to the multiphoton resonance absorptions and the broader nature of the higher energy σ -bonded species, only the two lower energy features (C=O π^* and C-H σ^*) will be compared and discussed. A comparison of the two C 1s spectra indicate, in accordance with the FTIR and XPS data, that films deposited at higher load power have a higher amount of hydrocarbon and unsaturated (C=O) species. This finding is also

consistent with information reported by Swaraj *et al.*¹⁸, who analysed pulsed-plasma deposited ethylene samples using NEXAFS and reported that films deposited under higher load powers contained higher levels of unsaturation.

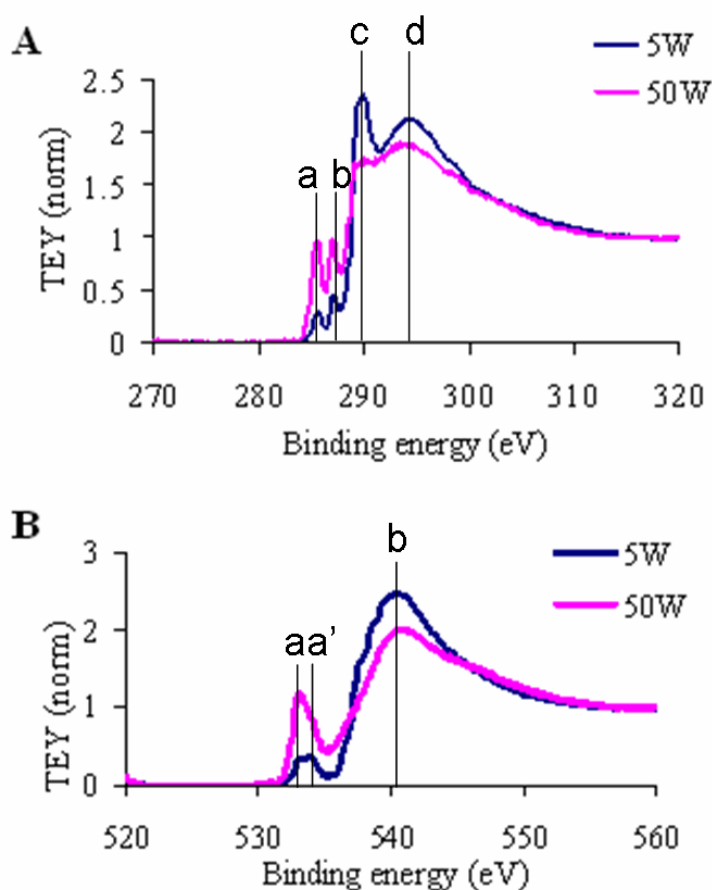


Figure 3.10 C and O K-edge (A and B respectively) NEXAFS spectra of DGpp films deposited at 5 and 50 W load powers. The peaks for the carbon 1s spectra are a: C=O π^* , b: C-H σ^* , c: C-O σ^* and d: C-C;C-O σ^* . For the Oxygen 1s spectra peaks are represented by a and a': C=O π^* and b: C-O σ^* .

The O 1s K-edge spectra (Figure 3.3.10B) for the 5 and 50 W DGpp films showed two main resonance features; firstly, the O 1s $\rightarrow \pi^*$ (C=O), an unresolved doublet peak with two components at ~ 533.4 and 534.1 eV (a and a', believed to be attributed to carbonyl and terminal aldehyde species, respectively) and secondly the O 1s $\rightarrow \sigma^*$ (C-O) transition

at ~540.8 eV (b). Analysis of the O 1s spectra support the findings from the C 1s spectra, again showing a higher level of unsaturation in films deposited at higher deposition load powers, with the a higher PEY signal for the C=O π^* resonance in the 50 W compared to the 5 W DGpp. As with the C 1s, the higher energy σ^* (C-O) resonances were not suitable for quantification of the relative concentrations of C-O bonded species due to the broad nature of the peaks and contributions from multiphoton resonance absorptions.

The use of NEXAFS as a tool for the analysis of plasma polymers¹⁹⁻²² and PEG-like films is in its infancy. Zwahlen et al.²³ reported a C and O K-edge NEXAFS analysis of oligo(ethylene glycol) (OEG) terminated alkanethiol SAMs on gold and their reported peak assignments are consistent with those reported in Figures 3.3.10. They investigated the degree of order in OEG-SAMs films made from different length oligomers and found that only shorter length oligomers showed a weak angular dependence. Due to the fragmentation, polymerisation and cross-linking processes that occur during plasma polymerisation, both the C 1s and O 1s NEXAFS spectra obtained for the DGpp gradients have the additional C=O π^* resonance features when compared to OEG SAMs. A number of researchers have used NEXAFS spectroscopy as part of a combinatorial approach to the analysis of surface gradients by mapping the surface chemistry as well as varying the polarisation of the light source, in order to detect any preferred orientation of surface bound materials.^{24, 25} We performed similar experiments to test for any possible orientation of polymer chains in the DGpp film gradients analysing C and O K-edge NEXAFS spectra using both horizontally and vertically polarised light. No difference was seen in spectra obtained from horizontally or vertically polarised light, indicating no

preferred orientation of the pp film chains, presumably due to the amorphous and cross-linked nature of the plasma polymer (dry) films in vacuum when analysed.

3.3.3 Protein Adsorption Studies

To analyse the ability of the DGpp films to resist non-specific protein adsorption, films were incubated in solutions of bovine serum albumin (BSA) and Lysozyme (Lys) (1 mg/mL in PBS, pH 7.4). The absence of elemental nitrogen in the DGpp films (confirmed by use of a control), allows the use of XPS elemental survey analysis to investigate protein adsorption on these films. Results presented in Figure 3.3.11 indicate that DGpp films deposited under lower load powers adsorbed less protein than those deposited under higher load powers, which correlate with film chemistry, most obviously the retention of a higher residual ether content. The 5 W DGpp film adsorbed very low levels of both Lys and BSA (less than 1 %), with a systematic increase in protein adsorption in correlation with the films deposition load power, increasing up to ~9 % for the Lys on the 50 W DGpp. Higher nitrogen contributions were detected on all DGpp films exposed to Lys compared with BSA, suggesting that Lys had a greater propensity to adsorb onto the DGpp films than BSA. From previous streaming potential measurements performed on similar DGpp films by our group,²⁶ it was found that the surface of the DGpp films possessed a slight negative charged, which would result in greater electrostatic interactions between the positively charged Lys (pI = 11) at pH 7.4. While BSA residues also contain positively charged domains, it has an overall neutral charge which may explain why lysozyme adsorbed more onto the DGpp films than the BSA proteins.

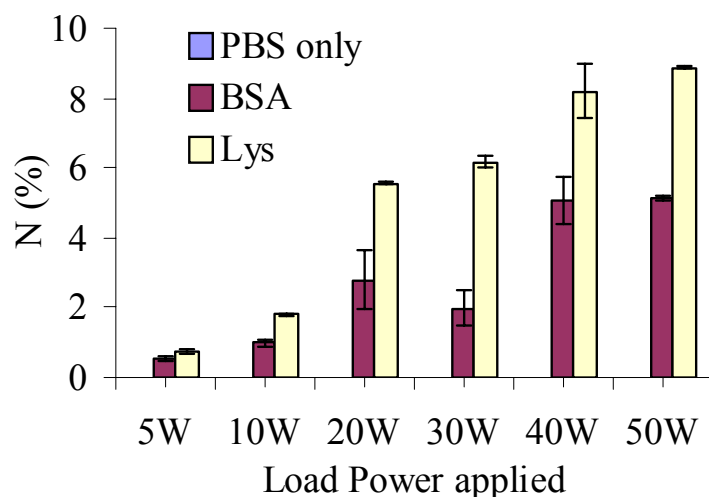


Figure 3.11 Protein adsorption of DGpp films as measured by N content from XPS elemental analysis, indicating lower powered DGpp films adsorb less BSA and lysozyme

The correlation between higher levels of protein resistance exhibited by PEG-like pp and the residual ether content has been previously reported and well discussed within the literature.^{10, 27} For example, Bretagnol et al.²⁸ used pulsed plasma polymerisation of a mixture of DEGDME vapours (15%) and argon to deposit PEG-like thin films at a load power of 1, 5 and 15 W. Quartz crystal microbalance with dissipation (QCM-d) monitoring was used to quantify the adsorption of BSA (50 µg/mL) on the DGpp films, which ranged from 0.02 to 0.14 µg/cm² respectively. They concluded that the load power used during pp deposition affected the films ability to resist protein adsorption due to its effect on monomer fragmentation and the residual PEO-character. Coatings that retained 40% of their PEO character (deposited at 15W) resulted in a 75% reduction of BSA adsorption compared with the control (AT-cut 5 MHz quartz covered with SiO₂). They further noted that there was little difference in protein adsorption between the DGpp films deposited at 1 and 5W, which retained 70% and 55% PEO character

respectively. DGpp films (used in this study) deposited at a load power of 5W using continuous wave pp retained 70% of their PEO character.

3.2.4 Cell adhesion studies

Anti-fouling surfaces are critical for the ongoing development of biocompatible biomedical devices and implants as well in the production of micro-patterned surfaces for the enhancement of fundamental cell based research²⁹ discussed in greater detail in chapter 6 of this thesis. The interaction between a surface and a cell, cellular proliferation and the body's inflammatory response are highly dictated by initial protein adsorption.³⁰ As such, the ability to create surfaces with specific cell attachment or cell repulsive areas is particularly attractive from a research perspective. Consequently, the attachment response of the anchorage dependent HeLa cell line on the DGpp films deposited at varied load powers was analysed. Results of the cell attachment study are presented in Table 3.3.3 and Figure 3.3.12. Very few cells attached to the 5 W DGpp, with 28% growth detected compared to that on the polystyrene tissue culture control surface (100%). Those cells that did attach displayed a rounded morphology and were often clumped together. It was also noted that the cell growth measured/observed on the 5W DGpp film (Figure 3.3.12) might have attached to an area of exposed Si, due to the fact that a very small number of cells can be seen growing on the 5W surface when compared to the entirety of the 500 x 500 um image presented in Figure 3.2.12A. This may have resulted from a blemish or scratch in the film, rather than cell attachment on the DGpp film itself. The attachment and growth of HeLa cells on the DGpp films deposited at a power of 20W and 50W showed no significant difference in the level of cell attachment (80% and 65%, respectively) (t-test, $p = 0.0816$), however showed an obvious

increase in the density of cell attachment. HeLa cells attached well to these surfaces and also showed signs of spreading Table 3.3.3 and Figure 3.3.13 (labelled 20 and 50 W).

Table 3.3.3 Percent HeLa cell attachment on DGpp films compared to TCPS (100%)

Sample	Attachment (%)	SD
Control (TCPS)	100	5.7
5W DGpp	28	7.6
20W DGpp	80	6.3
50W DGpp	65	6.6

The attachment of HeLa cells correlates with the residual ether content and wettability of the films, as seen with the protein adsorption on the DGpp films. Furthermore, as the cell attachment studies were performed in the presence of serum proteins, it is possible that cell attachment on these surfaces is mediated or influenced by the serum proteins. PEG-like materials have been reported for their use in biomaterials to control cell attachment and have been prepared by a number of methods including physical adsorption, graft polymerisation,^{31,32} chemical and photo-induced coupling as well as plasma polymerisation.^{10, 16} Very little has been reported, however on the fabrication of cell repulsive surfaces via the use of continuous wave RFGD plasma polymerisation.

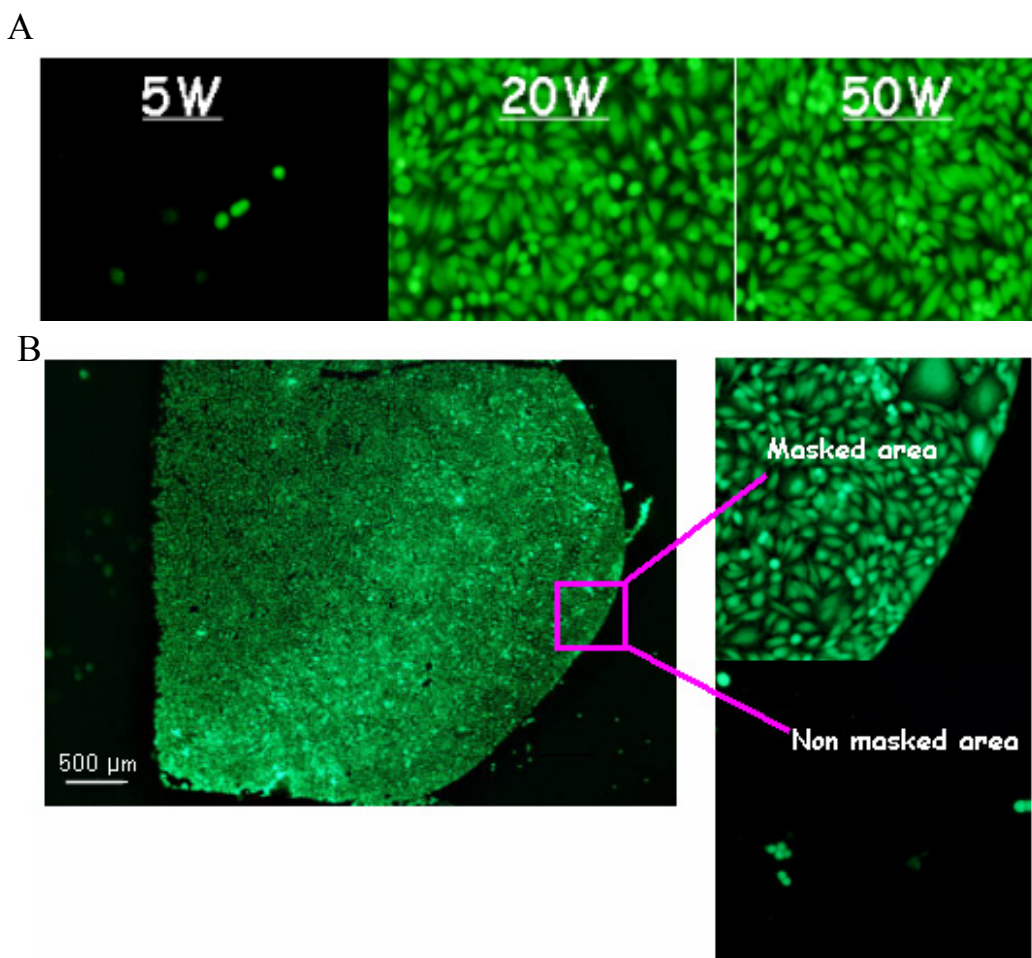


Figure 3.12 A; HeLa cell attachment on DGpp films, B; HeLa cell attachment on 5W DGpp film (non-masked area) compared to a pre-masked area (Si surface)

3.3 Conclusions

PEG-like thin films of systematically varied chemistry were prepared using continuous wave rfgd pp of DEGDME vapours. By analysing the films using XPS, FTIR and NEXAFS, it was shown that films deposited under higher load powers retained less of their PEG-like character, with the ether content ranging from 70% in the 5 W DGpp film to 34% in the 50 W DGpp. Films were also shown to be more unsaturated and contain more hydrocarbons when the rate of fragmentation was greater during pp deposition. An

AFM step height analysis showed the film thickness to increase with higher deposition powers and static contact angles increased slightly in films deposited at higher load power indicating a small decrease in wettability of the films.

The ability of the films to resist the adsorption of lysozyme and BSA was analysed and correlated with the ether content of the films. The higher nitrogen content measured on the DGpp films after exposure to lysozyme (compared to BSA) was attributed to higher electrostatic interactions between the positively charged lysozyme and the negative charges on the DGpp surfaces (as seen from previous streaming potential measurements on similar DGpp films). The ether content was also attributed to the attachment response of HeLa cells on the DGpp films. The 5W DGpp film surface appears inhibitory to HeLa cell attachment after 24 hours incubation in the presence of serum, while DGpp films prepared at load powers of 20 and 50 W were very supportive of HeLa cell attachment where cells showed signs of attachment and spreading, rather than the clumped rounded cells observed on the 5 W DGpp.³³

3.4 References

1. Gengenbach, T. R.; Griesser, H. J., Deposition conditions influence the postdeposition oxidation of methyl methacrylate plasma polymer films. *Journal of Polymer Science Part A: Polymer Chemistry* **1998**, 36, (6), 985-1000.
2. Menzies, J. D.; Cowie, C. C. B; Fong, C.; Forsythe, J.; Gengenbach, T.; Mc Lean, K.; Puskar, L.; Textor, M.; Thomsen L.; Tobin. M.; Muir, B., A one-step method for generating PEG-like plasma polymer gradients: Chemical Characterisation and Analysis of protein interactions. *Langmuir* **2010**.
3. Watts, J. F., *High resolution XPS of organic polymers: The Scienta ESCA 300 database*. G. Beamson and D. Briggs. 280pp., £65. John Wiley & Sons, Chichester, ISBN 0471 935921, (1992). 1993; Vol. 20, p 267.
4. Bremmell, K. E.; Kingshott, P.; Ademovic, Z.; Winther-Jensen, B.; Griesser, H. J., Colloid Probe AFM Investigation of Interactions between Fibrinogen and PEG-Like Plasma Polymer Surfaces. *Langmuir* **2006**, 22, (1), 313-318.
5. Biederman, H.; Slavínská, D., Plasma polymer films and their future prospects. *Surface and Coatings Technology* **2000**, 125, (1-3), 371-376.
6. Kühn, G.; Retzko, I.; Lippitz, A.; Unger, W.; Friedrich, J., Homofunctionalized polymer surfaces formed by selective plasma processes. *Surface and Coatings Technology* **2001**, 142-144, 494-500.
7. Swaraj, S.; Oran, U.; Lippitz, A.; Friedrich, J. F.; Unger, W. E. S., Study of influence of external plasma parameters on plasma polymerised films prepared from organic molecules (acrylic acid, allyl alcohol, allyl amine) using XPS and NEXAFS. *Surface & Coatings Technology* **2005**, 200, (1-4), 494-497.
8. Ward, A. J.; Short, R. D., A t.o.f.s.i.m.s. and x.p.s. investigation of the structure of plasma polymers prepared from the methacrylate series of monomers: 2. The influence of the W/F parameter on structural and functional group retention. *Polymer* **1995**, 36, (18), 3439-3450.
9. Retzko, I.; Friedrich, J. F.; Lippitz, A.; Unger, W. E. S., Chemical analysis of plasma-polymerized films: The application of X-ray photoelectron spectroscopy (XPS), X-ray absorption spectroscopy (NEXAFS) and fourier transform infrared spectroscopy (FTIR). *Journal of Electron Spectroscopy and Related Phenomena* **2001**, 121, (1-3), 111-129.
10. Brétagnol, F.; Lejeune, M.; Papadopoulou-Bouraoui, A.; Hasiwa, M.; Rauscher, H.; Ceccone, G.; Colpo, P.; Rossi, F., Fouling and non-fouling surfaces produced by plasma polymerization of ethylene oxide monomer. *Acta Biomaterialia* **2006**, 2, (2), 165-172.
11. Cheng, Q.; Komvopoulos, K., Synthesis of Polyethylene Glycol-Like Films from Capacitively Coupled Plasma of Diethylene Glycol Dimethyl Ether Monomer. *The Journal of Physical Chemistry C* **2008**, 113, (1), 213-219.
12. Xu, L. C.; Siedlecki, C. A., Effects of surface wettability and contact time on protein adhesion to biomaterial surfaces. *Biomaterials* **2007**, 28, (22), 3273-3283.
13. Hegemann, D.; Brunner, H.; Oehr, C., Plasma treatment of polymers for surface and adhesion improvement. *Nuclear Instruments and Methods in Physics Research Section B: Beam Interactions with Materials and Atoms* **2003**, 208, 281-286.

14. Johnston, E. E.; Bryers, J. D.; Ratner, B. D., Plasma Deposition and Surface Characterization of Oligoglyme, Dioxane, and Crown Ether Nonfouling Films. *Langmuir* **2005**, 21, (3), 870-881.
15. Beyer, D.; Knoll, W.; Ringsdorf, H.; Wang, J. H.; Timmons, R. B.; Sluka, P., Reduced protein adsorption on plastics via direct plasma deposition of triethylene glycol monoallyl ether. *Journal of Biomedical Materials Research* **1997**, 36, (2), 181-189.
16. Brétagnot, F.; Ceriotti, L.; Lejeune, M.; Papadopoulou-Bouraoui, A.; Hasiwa, M.; Gilliland, D.; Cecccone, G.; Colpo, P.; Rossi, F., Functional Micropatterned Surfaces by Combination of Plasma Polymerization and Lift-Off Processes. *Plasma Processes and Polymers* **2006**, 3, (1), 30-38.
17. Förch, R.; Zhang, Z.; Knoll, W., Soft Plasma Treated Surfaces: Tailoring of Structure and Properties for Biomaterial Applications. *Plasma Processes and Polymers* **2005**, 2, (5), 351-372.
18. Swaraj, S.; Oran, U.; Lippitz, A.; Schulze, R. D.; Friedrich, J. F.; Unger, W. E. S., Surface analysis of plasma-deposited polymer films, 4a: In situ characterization of plasma-deposited ethylene films by XPS and NEXAFS. *Plasma Processes and Polymers* **2005**, 2, (4), 310-318.
19. Kim, Y.; Kim, K. J.; Lee, Y., Surface analysis of fluorine-containing thin films fabricated by various plasma polymerization methods. *Surface and Coatings Technology* **2009**, 203, (20-21), 3129-3135.
20. Oran, U.; Swaraj, S.; Lippitz, A.; Unger, W. E. S., Surface Analysis of Plasma Deposited Polymer Films, 7. *Plasma Processes and Polymers* **2006**, 3, (3), 288-298.
21. Shard, A. G.; Whittle, J. D.; Beck, A. J.; Brookes, P. N.; Bullett, N. A.; Talib, R. A.; Mistry, A.; Barton, D.; McArthur, S. L., A NEXAFS Examination of Unsaturation in Plasma Polymers of Allylamine and Propylamine. *The Journal of Physical Chemistry B* **2004**, 108, (33), 12472-12480.
22. Friedrich, J. F.; Geng, S.; Unger, W.; Lippitz, A.; Erdmann, J.; Gorsler, H. V.; Wöll, C.; Schertel, A.; Bierbaum, K., Plasma functionalization and reorientation of macromolecules at polymer surfaces. *Surface and Coatings Technology* **1995**, 74-75, (Part 2), 664-669.
23. Zwahlen, M.; Herrwerth, S.; Eck, W.; Grunze, M.; Hahner, G., Conformational Order in Oligo(ethylene glycol)-Terminated Self-Assembled Monolayers on Gold Determined by Soft X-ray Absorption. *Langmuir* **2003**, 19, (22), 9305-9310.
24. Genzer, J.; Fischer, D. A.; Efimenko, K., Combinatorial near-edge x-ray absorption fine structure: Simultaneous determination of molecular orientation and bond concentration on chemically heterogeneous surfaces. *Applied Physics Letters* **2003**, 82, (2), 266-268.
25. Fischer, D. A.; Efimenko, K.; Bhat, R. R.; Sambasivan, S.; Genzer, J., Mapping Surface Chemistry and Molecular Orientation with Combinatorial Near-Edge X-Ray Absorption Fine Structure Spectroscopy. *Macromolecular Rapid Communications* **2004**, 25, (1), 141-149.
26. Muir, B. W.; Tarasova, A.; Gengenbach, T. R.; Menzies, D. J.; Meagher, L.; Rovere, F.; Fairbrother, A.; McLean, K. M.; Hartley, P. G., Characterization of Low-Fouling Ethylene Glycol Containing Plasma Polymer Films. *Langmuir* **2008**, 24, (8), 3828-3835.

27. Ademovic, Z. Z., Surface modification of PET films using pulsed AC plasma polymerisation aimed at preventing protein adsorption. *Plasma processes and polymers* **2005**, 2, (1), 53-63.
28. Bretagnol, F.; Lejeune, M.; Papadopoulou-Bouraoui, A.; Hasiwa, M.; Rauscher, H.; Ceccone, G.; Colpo, P.; Rossi, F., Fouling and non-fouling surfaces produced by plasma polymerization of ethylene oxide monomer. *Acta Biomaterialia* **2006**, 2, (2), 165-172.
29. Anderson, J. M., Biological responses to materials. *Annual Review of Materials Science* **2001**, 31, 81-110.
30. Zhang, M.; Desai, T.; Ferrari, M., Proteins and cells on PEG immobilized silicon surfaces. *Biomaterials* **1998**, 19, (10), 953-960.
31. Branch, D. W.; Wheeler, B. C.; Brewer, G. J.; Leckband, D. E., Long-term stability of grafted polyethylene glycol surfaces for use with microstamped substrates in neuronal cell culture. *Biomaterials* **2001**, 22, (10), 1035-1047.
32. Knerr, R.; Weiser, B.; Drotleff, S.; Steinem, C.; Göpferich, A., Measuring cell adhesion on RGD-modified, self-assembled PEG monolayers using the quartz crystal microbalance technique. *Macromolecular Bioscience* **2006**, 6, (10), 827-838.
33. Khoo, X.; Hamilton, P.; O'Toole, G. A.; Snyder, B. D.; Kenan, D. J.; Grinstaff, M. W., Directed Assembly of PEGylated-Peptide Coatings for Infection-Resistant Titanium Metal. *Journal of the American Chemical Society* **2009**, 131, (31), 10992-10997.

Chapter 4:

An X-ray and neutron reflectometry study of 'PEG-like' plasma polymer films

PART B: Suggested Declaration for Thesis Chapter

Monash University

Declaration for Thesis Chapter 4

Declaration by candidate

In the case of Chapter 4, the nature and extent of my contribution to the work was the following:

Nature of contribution	Extent of contribution (%)
Experimental design and conduct , data processing, manuscript writing	70 %

The following co-authors contributed to the work. Co-authors who are students at Monash University must also indicate the extent of their contribution in percentage terms:

Name	Nature of contribution	Extent of contribution (%) for student co-authors only
Hsin-Hui Chen	Assisted in Data processing	
Andrew Nelson	Assisted in Experimental and Data processing	
John Forsythe	Assisted planning and manuscript correction	
Thomas Gengenbach	Manuscript correction	
Keith McLean	Manuscript correction	
Celesta Fong	Manuscript correction	
Ben Muir	Assisted in Experimental design, data processing and manuscript writing and correction	

Candidate's
Signature



Date

30/05/2011

Declaration by co-authors

The undersigned hereby certify that:

- (1) the above declaration correctly reflects the nature and extent of the candidate's contribution to this work, and the nature of the contribution of each of the co-authors.
- (2) they meet the criteria for authorship in that they have participated in the conception, execution, or interpretation, of at least that part of the publication in their field of expertise;
- (3) they take public responsibility for their part of the publication, except for the responsible author who accepts overall responsibility for the publication;
- (4) there are no other authors of the publication according to these criteria;
- (5) potential conflicts of interest have been disclosed to (a) granting bodies, (b) the editor or publisher of journals or other publications, and (c) the head of the responsible academic unit; and
- (6) the original data are stored at the following location(s) and will be held for at least five years from the date indicated below:

Location(s)

CSIRO, Materials Science and Engineering, Clayton

		Date
Hsin-Hui Chen CSIRO, Materials Science and Engineering		30/5/2011
Andrew Nelson ANSTO		28/6/2011
John Forsythe Materials Science, Monash University		5/7/11
Thomas Gengenbach CSIRO, Materials Science and Engineering		4/7/2011
Keith McLean CSIRO, Materials Science and Engineering		30/5/11
Celesta Fong CSIRO, Materials Science and Engineering		30/5
Ben Muir CSIRO, Materials Science and Engineering		30/5/11

.....

4. An X-ray and neutron reflectometry study of ‘PEG-like’ plasma polymer films

Donna Menzies¹, Andrew Nelson², Hsin-Hui Shen¹, Keith M. McLean¹, John S. Forsythe³, Thomas Gengenbach¹, Celesta Fong¹, Benjamin W. Muir*¹

¹CSIRO Molecular and Health Technologies, Clayton South, Vic. 3169, Australia

²Australian Nuclear Science and Technology Organisation (ANSTO), New Illawarra Rd, Menai, NSW 2234, Australia

³ Monash University, Department of Materials Engineering, Clayton South, VIC, 3169, Australia

4.1 Abstract

Plasma enhanced chemical vapor deposited films of di(ethyleneglycol) dimethyl ether were analysed by a combination of XPS, AFM, QCM-D, X-ray and neutron reflectometry. The combination of these techniques enabled a systematic study of the impact of plasma deposition conditions upon resulting film chemistry (Empirical formula), mass densities, structure and water solvation which has been correlated with the films’ efficacy against protein fouling. All films were shown to contain substantially less hydrogen than the original monomer and absorb a vast amount of water, which correlated with their mass density profiles. A proportion of the plasma polymer hydrogen atoms were shown to be exchangeable, while QCM-D measurements were inaccurate in detecting associated water in lower power films that contained loosely bound material. The higher protein resistance of the films deposited at a low load power was attributed to its greater chemical and structural similarity to that of PEG graft surfaces. These studies

demonstrate the utility of using X-ray and neutron reflectometry analysis techniques in furthering the understanding of the chemistry of these films and their interaction with water and proteins.

Keywords: reflectometry, plasma polymer, composition, mass density

4.2 Introduction

The study of plasma polymer coatings that could potentially be used in biomedical devices is an area of increasing research interest.¹⁻⁵ One of the most common classes of thin film treatments employed in biomaterial devices is that of ‘low fouling’ or ‘stealth’ coatings.⁶ These coatings need to be able to resist or inhibit protein adsorption within the body. In the biomedical materials field the most common surface coating used to render a material resistant against protein fouling is through the use of poly(ethylene oxide) (PEO), also known as poly(ethylene glycol) (PEG).⁷ PEG polymers have a number of properties which have been implicated in their low-fouling nature. ‘Steric repulsion’ and the effect of the ‘water barrier’ resulting from the structuring of water in the near environment of the PEG chains are two of the most commonly described theories in the literature.⁸⁻¹⁰ To date the largest effort in the plasma polymer field to produce PEG-like films has been through the use of monomers containing ethylene oxide units, typically glycol diethers, which are also commonly known as the ‘glyme’ family of monomers.¹¹ Within this class of molecules, the preferred thin film deposition technique utilized has involved the use of pulsed plasmas with the monomer tetraethylene glycol dimethyl ether or ‘tetraglyme’.¹¹⁻¹³ Lopez and Ratner et al.¹¹ first described the use of ‘glyme’ monomers to deposit low protein fouling plasma polymer surfaces. It is believed that the

molecular structure of PEG-like plasma polymer films consists of randomly cross-linked methyl-terminated ethylene oxide chains. By controlling the plasma power during deposition, the ether content of PEG plasma polymer films can be controlled to an extent. Previous studies have shown that plasma polymer PEG-like films produced with monomers consisting of two or more ethylene oxide units can exhibit low fouling properties while monomers with one ethylene oxide unit do not.¹⁴ Recent studies by Johnston et al.¹⁵ have found that films produced from higher molecular weight precursors retain longer fragments of intact monomer. Protein adsorption results suggested that in general, protein resistance improves as the number of ethylene oxide units in the monomer precursor increases.

During the plasma deposition process an activated monomer introduced in the gas phase under vacuum undergoes fragmentation, excitation and ionisation. These fragments rearrange and react to form a cross-linked polymer matrix. The physico-chemical properties of a plasma polymer deposited from a specific monomer may be quite different to those of a conventional polymer. For example, the hydrogen content of plasma polymer films is low in comparison to the polymer of the corresponding monomer due to considerable cross-linking.¹⁶ It is therefore highly unlikely that low fouling plasma polymer films produced via the plasma polymerization of 'glyme' monomers will exactly reproduce the polymer surface chemistry generated from the more commonly used PEG polymer graft surfaces.^{9, 17-19} Plasma polymer chemistries generated from a particular monomer may vary substantially depending on the operational conditions used (reactor geometry, monomer flow rate, pressure, mode and strength of power delivery and frequency).²⁰

A number of surface characterization techniques have been used to investigate the physical and chemical properties of PEG-like plasma polymer films to aid in elucidating their surface properties. Techniques such as X-ray Photoelectron Spectroscopy (XPS), Fourier Transform Infra Red Spectroscopy (FTIR), Raman spectroscopy and mass spectrometry methods (e.g. TOF-SIMS), are typically used to deduce the amount of residual ether groups in these plasma polymerized surfaces. However, no report on the full chemical composition (including hydrogen) of these ‘glyme’ plasma polymer films and their solvation in water has been reported to the best of our knowledge. Conventional surface characterisation techniques that are commonly employed in the field do not quantify the amount of hydrogen remaining in plasma polymer films after plasma polymer deposition. Reflectometry techniques are now becoming increasingly important in the characterization of these nano-scale interfaces.²¹⁻²⁴ X-ray reflectometry (XRR) is ideally suited to the study of the internal properties of layered film structures on surfaces, yielding data on sub-surface structure and material properties. The use of Neutron Reflectometry (NR) in combination with XPS and XRR allows the full chemical composition of plasma deposited films to be determined.

In this work, we have performed a systematic study of the impact of plasma deposition conditions upon resulting film chemistry, structure and water solvation which has been correlated with the films’ efficacy against protein fouling. The combination of analysis techniques has provided a powerful toolbox for further examination of the specific chemical composition of these plasma polymer films, including hydrogen. Such detailed structure-property correlations may enable a more sophisticated approach to the design of protein resistant plasma polymer films. Specifically, the surface chemistry of the plasma

polymer coatings was characterised by XPS with surface morphology being characterised by AFM. A combination of XPS data with XRR and NR measurements on the plasma polymer film versus air enabled the stoichiometric composition and mass densities of the films to be obtained. Examination of the same films in an aqueous environment using NR and quartz crystal microbalance with dissipation monitoring (QCM-D) highlighted the degree to which the films absorb water. These measurements also showed a substantial exchange of hydrogen atoms between the film and solution, indicating that a large number of hydrogen atoms within the film are labile. Protein adsorption and water uptake studies were performed using (QCM-D) measurements and a correlation between the stoichiometric composition of the films (as calculated from reflectivity measurements) and the level of protein adsorption and water uptake were made. These studies demonstrate the utility of using XRR and NR analysis techniques in furthering the understanding of the chemistry of these films and their interaction

4.3 Materials and Methods

4.3.1 Substrates

Ultra-flat single crystal, silicon wafers (<111>, 10 cm diameter, 1 cm thick, *Silrec Corporation*, San Jose and <100>, 1 cm² x 0.5 mm thick, from *M.M.R.C Pty Ltd*, Melbourne, Australia) were used as substrates for the deposition of plasma polymer thin films. Smaller wafers (1 cm² x 0.05 cm thick) were used as substrates for AFM and XPS characterisation. Plasma deposition on the large and small wafers was performed simultaneously. Prior to plasma deposition, the wafers were rinsed with ethanol and cleaned in aqua regia (3:1 HCl:HNO₃) for an hour to remove any inorganic contaminants. The wafers were further treated with piranha solution (20 % H₂SO₄ in concentrated

H₂O₂) for three hours to remove residual organic contaminants. The wafers were thoroughly rinsed with Milli-Q water and blown dry with nitrogen gas after each step. This procedure did not introduce any measurable roughening of the surface as assessed by AFM (data not shown). The cleaning protocol produces a hydrophilic surface.

4.3.2 Plasma Polymer Deposition

Plasma polymerisation of di(ethyleneglycol) dimethyl ether (DG, 99 %, BDH) was carried out in a custom-built reactor described elsewhere.²⁵ Briefly, a cylindrical reactor chamber is used, with a height of 35 cm and a diameter of 17 cm. Within this chamber sit two circular electrodes (10.3 cm diameter), spaced 15 cm apart. Samples were placed on the lower grounded electrode and a continuous radiofrequency pulse was generated at the upper electrode. The monomer vapours were supplied to the reactor chamber from the liquid monomer contained in a round-bottom flask via a stainless steel line and a manual valve for fine control of the flow. The DG monomer flasks were kept on ice and in ambient air, respectively, during the experiments. The monomer liquid was degassed before plasma deposition.

The plasma deposition of DG was performed using a frequency of 200 kHz, load powers of 10, 20 and 50 W and an initial monomer pressure of 20 Pa for a treatment time of 35, 20 and 10 seconds respectively in order to produce films of appropriate thicknesses for reflectivity measurements. The final monomer pressures for the 10, 20 and 50 W plasma depositions were 33, 42 and 60 Pa respectively. After deposition, the reactor was immediately pumped down to base pressure before venting. The samples were stored in clean tissue culture grade petri dishes under ambient conditions until further analysis.

4.3.3 Atomic Force Microscopy

An Asylum Research MFP-3D atomic force microscope (Santa Barbara, CA, USA) was used to measure surface topography and roughness in tapping mode with ultrasharp silicon nitride tips (NSC15 noncontact silicon cantilevers, MikroMasch, Spain). The tips used in this study had a typical force constant of 40 N/m and a resonant frequency of 320 kHz. Typical scan settings involved the use of an applied piezo deflection voltage of 0.8 V at a scan rate of 0.3 Hz.

4.3.4 X-ray Photoelectron Spectroscopy

To investigate the chemical composition of the plasma polymer coatings X-ray photoelectron spectroscopy (XPS) was employed. XPS analysis was performed using an *AXIS HSi* spectrometer (*Kratos Analytical Ltd.*), equipped with a monochromated Al-K α source at a power of 144 W (12 mA, 12 kV). Charging of the samples during irradiation was compensated by the internal flood gun. The pressure in the main vacuum chamber during analysis was typically 5×10^{-6} Pa. Spectra were recorded with the photoelectron detection normal to the sample surface. All elements present were identified from survey spectra (acquired at a pass energy of 320 eV). High resolution spectra were recorded from individual peaks (C 1s, O 1s) at 40 eV pass energy (yielding a typical peak width for polymers of 1.0 – 1.1 eV). The atomic concentrations of the detected elements were calculated using integral peak intensities and the sensitivity factors supplied by the manufacturer. High resolution C 1s spectra were quantified using a minimisation algorithm in order to calculate optimised curvefits and thus determine the contributions from specific functional groups. Five peak components (mixed Gaussian/Lorentzian model functions) were used. Component C1 at the lowest binding energy (BE) was assumed to represent aliphatic hydrocarbons (“neutral” carbon) and the corresponding BE

set accordingly to 285.0 eV. A second component at a slightly higher BE was included to account for all C 1s photoelectrons that underwent a secondary BE shift. Component C3 at 286.3 – 286.6 eV represents C-O based groups (ethers and alcohols), C4 at 287.9 – 288.2 eV accounts for all C=O and O-C-O based groups (e.g. carbonyls, amides) and C5 at 288.9 – 289.3 eV represents O-C=O based groups (e.g. acids or esters). It is important to note that XPS does not detect light elements such as hydrogen and helium.

4.3.5 Contact angle measurements

Water contact angles were determined using a Dataphysics OCA20 goniometer, a photo of the drop was digitised and the profile fitted to the equation of Young and Laplace.²⁶ Once the drop profile had been determined, the contact angle was calculated from the intersection of the theoretical profile with the baseline. The contact angles presented are the mean of three separate measurements on different regions of the same plasma polymer sample.

4.3.6 Quartz crystal microbalance measurements

Real time monitoring of protein adsorption was performed at 25° C using a quartz crystal microbalance equipped with dissipation monitoring (QCM-D, Q-Sense, Gothenburg, Sweden). Shifts of the oscillating frequency (Df) were detected and plotted in real time using the resonance frequency at 5 MHz and the third, and fifth harmonic. DGpp films were deposited on gold 5 MHz quartz crystal chips. The chips were cleaned prior to DGpp film deposition by immersion in a piranha solution (sulphuric acid, hydrogen peroxide and MilliQ water (1:1:5 volume ratio)) and heated to 70° C for 5 minutes. The crystals were then thoroughly rinsed with MilliQ water before being dried with a high pressure stream of purified nitrogen. The DGpp coated chips were first hydrated in the

QCM-D over a 19 hour period in phosphate-buffered saline (PBS) (flow rate of 10 uL/min) in order to obtain a stable baseline prior to introduction of the protein. Bovine serum albumin (BSA, Sigma Aldrich) solution in PBS (1 mg/mL, pH = 7.45) was then flowed through the measuring chamber in contact with the DGpp coated crystal for 60 minutes, before re-flowing PBS over the DGpp coated crystals to wash away any loosely adsorbed protein. The frequency shift (Df) of the quartz crystal was converted into mass change (Dm) on the electrode surface, calculated using the Sauerbrey equation (Equation 1, mass sensitivity: 5 ng/cm²) were $C = 17.7 \text{ ng Hz}^{-1} \text{ cm}^{-2}$ for a 5 MHz quartz crystal and the overtone number, n , is equal to 1, 3, 5, 7. This equation enables an approximate calculation of the amount of protein adsorbed after rinsing.

$$\Delta m = -\frac{C\Delta f}{\eta} \quad [\text{Equation 1}]$$

4.3.7 Reflectometry Measurements

XRR data were collected using a Panalytical X'Pert Pro instrument ($\lambda = 1.5406 \text{ \AA}$). The specular X-ray reflectivity, R , (the ratio between the reflected and the incident intensity) was measured over the Q -range $0.01 \text{ \AA}^{-1} < Q < 0.4 \text{ \AA}^{-1}$, where $Q = 4\pi\sin\theta/\lambda$ is the momentum transfer and θ is the angle of incidence/reflection. NR data was collected on the NIST NG7 vertical scattering plane reflectometer over the Q range $0.007 \text{ \AA}^{-1} < Q < 0.15 \text{ \AA}^{-1}$. The data was analysed using least squares (differential evolution) in the Motofit program, weighting data on a logarithmic scale and using the instrumental resolution functions. An initial attempt to model the film with a single layer of uniform scattering length density (SLD) indicated that the films were not of a homogenous composition/density perpendicular to the interface (SLD being dependent on mass density and chemical composition). Therefore each film was modeled as a composite of

up to 12 layers, with each layer having the same thickness but differing in SLD. For NR datasets an additional native oxide layer was utilized (although this is sometimes hard to resolve). Normally the use of so many layers creates a jagged SLD profile due to over parameterisation of the system. However, in circumstances where the SLD gradient is roughly known it is possible to smooth such a profile by taking the arithmetic mean of the parameters obtained by fitting the data repeatedly. By using the SLD values from the XRR and NR measurements in tandem it is possible to determine both the mass density and hydrogen content of each of the sublayers, if one assumes that the atomic compositions from the XPS measurements are constant through the film.²⁴

The 20W and 50W films were also measured against aqueous solution using NR, with the neutron beam reflecting from the film/water surface. Three different solvents ('contrasts') were used for the 20 and 50W films, H₂O, D₂O and a mix of H₂O/D₂O (with an SLD of $3.3 \times 10^{-6} \text{ \AA}^{-2}$). Changing the deuteration level of the solution changes the refractive index of the water and therefore the scattering contrast of the system. An analysis identical to that carried out on the dry films was performed. By using the average SLD of the dry film, and the SLD of the films in water, the amount of absorbed water can be quantified, as well as the exchange of H atoms from within the film with those of the solvent. For such an analysis two water contrasts are required.

4.4 Results and Discussion

4.4.1 Characterisation of the films using Atomic Force Microscopy (AFM)

The surface topography and roughness of the deposited plasma polymer films were determined by AFM in air. Figure 4.1 shows tapping mode height and phase contrast

images of the films in air. The images illustrate the flat, smooth and defect-free nature of these films which makes them ideal for studies using reflectivity measurements. Analysis of the images reveals that all of the films were very smooth (RMS values between 0.45 and 0.57 nm). The size of the topographical height variations in the X and Y dimensions are in the order 20-50 nm. The film deposited at 10 W displayed minimal phase contrast with the 20 W being intermediate between the high and low power films.

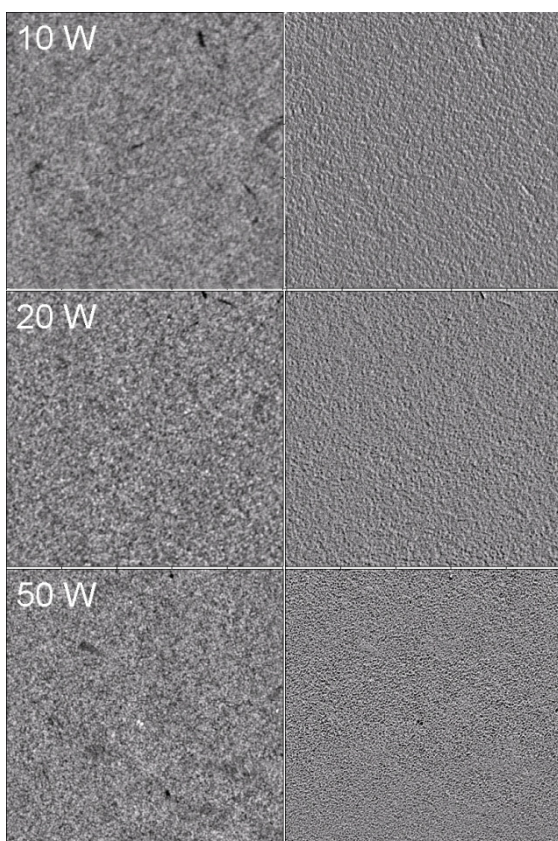


Figure 4.1 AFM tapping mode height images (left) and phase contrast images (right) of the DGpp films produced at load powers of 10, 20 and 50 W, scan size 5 μm , z height range 5 nm, phase scale 7°.

The static water contact angles of the three films produced at 10, 20 and 50 W were measured immediately after deposition of each film, and were found to be very similar at

$65^{\circ} \pm 2^{\circ}$, $60^{\circ} \pm 4^{\circ}$ and $66^{\circ} \pm 4^{\circ}$ respectively. The contact angles observed for these films compares similarly to the values reported in a recent study of di(ethyleneglycol) dimethyl ether plasma polymer films deposited on silicon at plasma load powers of 10 and 20 W by Cheng et al.²⁷

4.4.2 Film stability, water uptake and protein resistant properties of the DGpp films characterised by QCM-D

The protein resistant nature of the three films was evaluated against bovine serum albumin (BSA) using QCM-D. Initially the films were pre-equilibrated in a flow of PBS for 1000 minutes to allow them to fully hydrate and remove any loosely bound, low molecular weight material before incubation with protein (1mg/ml at pH 7.4). Figure 4.2A shows the QCM-D frequency responses of the films over the 1000 minute hydration period. A substantial loss of low molecular weight material is seen in the 10 W film as evident by the increase in frequency response over time. It is not uncommon for films produced at lower powers or under pulsed conditions to result in the formation of such low molecular weight material.¹⁴ The 10 W film rapidly loses material over the first few hours of PBS flow and then appears to stabilize. Conversely, a decrease in frequency response over time is observed for the 50 W film indicating a substantial amount of mechanically coupled mass (water and buffer salts). Interestingly from QCM-D analysis the 20 W film appears to be very stable during the flow of PBS solution and no significant increase or decrease is observed in its frequency response over time. This finding will be discussed further when NR data in water of the 20 W plasma polymer film is reported. Analysis of the dissipation response (Figure 4.2B) of the 10, 20 and 50 W films over the 1000 minute hydration period, confirms the higher uptake of water seen in the 50 W film, with increasing dissipation ($\Delta D = 8 \text{ E}^{-6}$) compared to no dissipation change

seen for the 20 W film. Furthermore, a decrease in the dissipation ($\Delta D = -30 \text{ E}^{-6}$) of the 10 W film is not only representative of a more rigid film than the 20 and 50 W films, but also reflects a lower amount of absorbed and coupled water compared to the 20 and 50 W films.

The frequency response, indicative of the mass change of the three plasma polymer films after flowing a solution of BSA is shown in Figure 4.2C. It can be seen that the level of protein adsorption clearly increases with plasma deposition power. If one makes an approximation on the amount of protein adsorbing in the films using the Sauerbrey equation (Equation 1), we calculate the levels of protein fouling to be 15, 60 and 80 ng/cm^2 on the 10, 20 and 50 W plasma polymer films respectively. We acknowledge the limitations of using this equation in accurately quantifying protein adsorption within these plasma polymer films. Bretagnol et al. has reported a similar study of protein adsorption on diglyme plasma polymerized surfaces. The level of BSA adsorption on the DGpp films deposited at 1, 5 and 15 W was measured using QCM-D, and using the Sauerbrey equation they reported BSA adsorption of ~ 20 , 25 and 110 ng/cm^2 respectively, compared to $\sim 600 \text{ ng}/\text{cm}^2$ measured on the control SiO_2 coated quartz crystal.²⁸

In addition to QCM-D analysis, protein adsorption experiments were performed on the plasma polymer surfaces at the same concentration of BSA (1 mg/mL) for one hour followed by repeated rinsing in PBS and then milli-Q water. An emerging nitrogen (N) signal was used to monitor protein adsorption on the surfaces. The atomic % nitrogen in

the films after BSA incubation were $0.6 \% \pm 0.2$, $2.7 \% \pm 0.2$ and $4.3 \% \pm 0.4$ for the 10, 20 and 50 W films respectively (data not shown). It is clear that significantly less protein absorption was observed on the 10 W film compared to the higher power films. In another study reported by Bretagnol et al, BSA adsorption on a diglyme plasma polymerized surface deposited under pulsed plasma discharge conditions yielded a similar value (0.5 %) to that reported to the 10 W film in this study (0.6 %). This was compared to BSA adsorption measured on a silicon wafer control, which yielded 12 % N content after incubation in BSA (100 $\mu\text{g/mL}$ for 1 hour). A comparison of the C-O (ether related) component as measure by XPS for the diglyme surface in Bretagnol's study was higher at 73 % compared to the 10 W film reported in this study which was 62 %.²⁹ Salim et al. however, have reported substantially lower protein adsorption on tetraglyme plasma coated microfluidic channels, using pulsed plasma discharge conditions with N 1s levels of 0 – 0.1 % after incubation in 50 $\mu\text{g/mL}$ solution of Human fibrinogen. The low protein adsorption in this study compared with those reported in the current study could be attributed to a higher C-O component (84 %), lower protein concentrations and differences in plasma processing parameters such as the pulsed plasma conditions and the use of a tetraglyme monomer.³⁰ Previous studies have shown that tri and tetraglyme plasma polymer films are extremely effective in reducing surface protein adsorption.^{15, 20}

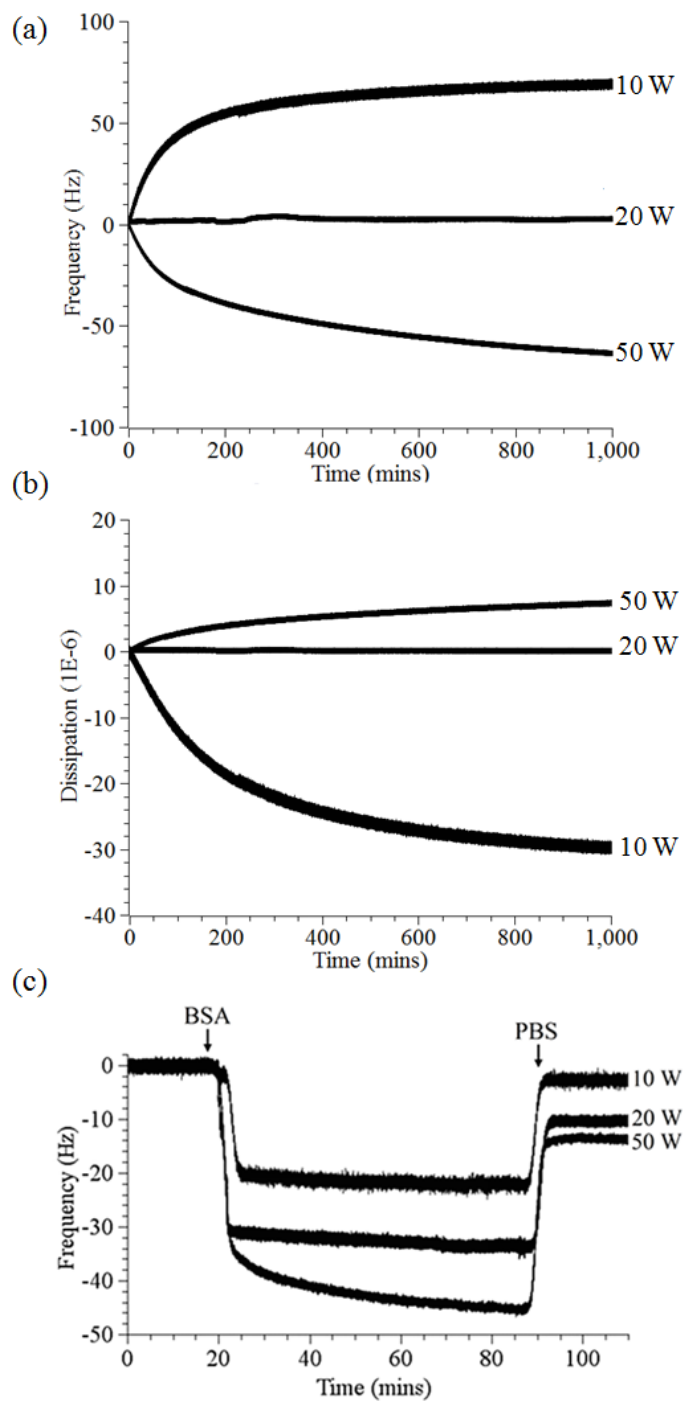


Figure 4.2 A and B: QCM-D frequency and dissipation response respectively, on the 10, 20 and 50 W plasma polymer films after incubation in PBS for 1000 minutes. Significant loss of material is seen in the 10 W film and water uptake is observed in the 50 W film. C: QCM-D frequency response of the third overtone on the 10, 20 and 50 W films after incubation with BSA for one hour (1 mg/mL, PBS, pH=7.4). The arrows indicate when the BSA and PBS solutions were flowed over the coated crystals.

4.4.3 Surface Chemistry

The results of XPS elemental analysis of freshly deposited films of di(ethyleneglycol) dimethyl ether plasma polymers at load powers of 10, 20 and 50 W are summarized in Table 1. The corresponding quantitative results and atomic ratios relative to total carbon are also compiled in Table 4.1. Elemental analysis by XPS reveals films comprising both carbon and oxygen with atomic concentrations varying from 69 - 76 % and 31 - 24 % respectively across the load power range consistent with previous studies of these di(ethyleneglycol) dimethyl ether plasma polymers.³¹ The chemical composition of the 20 and 50 W films differs substantially from the monomer ($C_2H_4.7O_1$), for which the oxygen content is higher (33 % O, 67 % C). It is clear that higher power glow discharges result in the deposition of plasma polymer films that contain less oxygen and a greater degree of hydrocarbon containing species. The absence of silicon in the recorded spectra suggests a plasma polymer film thickness in excess of the XPS analysis depth of 10 nm. Fitting of the high resolution carbon (C1s) spectra (Figure 4.3) reveals films that are rich in carbon-oxygen moieties such as ether, alcohol, aldehyde, ketone, ester and acid species. The presence of a higher C-O component suggests the incorporation of a high level of ether functionality in the low power films consistent with recent work investigating the gas phase discharge of di(ethylene glycol) vinyl ether and di(ethyleneglycol) dimethyl ether plasmas.^{27, 31-33} The ionisation/dissociation rate of the monomers ether units increases dramatically with plasma power resulting in films that contain significantly less ether units. The 10 W film retained the highest C-O component compared to the 20 and 50 W films. This indicates that depositions performed at 10 W load power are more effective in retaining the ether functionality of the starting monomer, when compared to the other deposition conditions investigated in this work.

Films deposited at 20 and 50 W load powers had a higher introduction of neutral hydrocarbon (C-C/C-H) species and a decreased retention of C-O ether and alcohol functionalities.

Table 4.1 Elemental compositions (atomic %) of DG plasma polymer films derived from high resolution XPS survey spectra. The theoretical monomer composition is shown for comparison. Also presented are results from quantification of the high resolution XPS C 1s surface composition (atomic ratios relative to total carbon, X/C) of the 10, 20 and 50 W films.

	% Composition		Atomic ratio relative to total carbon, X/C			
	C 1s	O 1s	C-C;C-H	C-O	C=O	O-C=O
Diethylene glycol dimethyl ether (DG) monomer	66.6	33.3	-	-	-	-
DGpp (10 W)	69.0	31.0	28.4	62.2	7.3	2.1
DGpp (20 W)	72.0	28.0	35.9	51.3	8.9	3.9
DGpp (50 W)	76.0	24.0	52.9	35.6	7.5	4.0

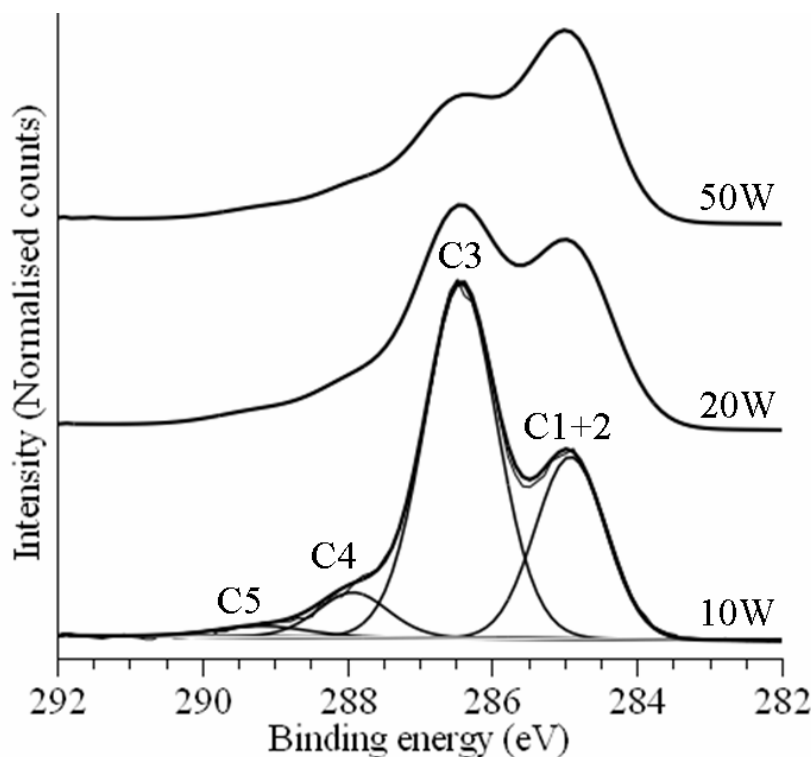


Figure 4.3 XPS C 1s high resolution spectra of the DG plasma polymer (DGpp) films produced at 10, 20 and 50 W load powers. Curve fits for the 10 W DGpp film are shown. Labeled components correlate to C1, C2 hydrocarbons; C3, C-O based groups (ethers and alcohols); C4, C=O and O-C-O based groups (e.g. aldehyde, ketone); C5, O-C=O based groups (e.g. acid, ester)

4.4.4 Characterisation of the films using X-ray and neutron reflectometry in air

The air-solid reflectivity measurements from the plasma polymer films are shown in Figure 4.4, while the structural parameters of each film are given in Table 4.2. The large number of Kiessig fringes in the X-ray reflectivity data for 10 W and 20 W which persist to high Q_z ($= 0.4 \text{ \AA}^{-1}$), indicates that the films are smooth and provides confidence for the precise determination of film thickness. However, these fringes fade quickly for the 50 W film, indicating that there is a steep gradient in scattering length density (SLD) through the film. This is consistent with the observation of a rapid increase in pressure of 40 Pa during the plasma deposition of di(ethyleneglycol) dimethyl ether at a load power of 50 W over ten seconds. As the pressure is rapidly increasing during plasma polymer

deposition of the 50 W film (4 Pa per second), it would be expected that a significant gradient in film composition with thickness would occur in this plasma polymer thin film which was deposited at a rate of approximately 2 nm per second. For comparison, the 10 W load power film only resulted in a 13 Pa increase in pressure over 35 seconds correlating to a pressure change of 0.4 Pa per second and a deposition rate of approximately 1 nm per second.

The coherent neutron scattering length (b) of H (-3.739 fm) is significantly different (both in sign and magnitude) to the other atoms (C: 6.646 fm; O: 5.803 fm) found in these plasma polymers. As the hydrogen content of these plasma polymer films is increased the neutron SLD decreases much more quickly than the X-ray SLD increases (at constant molecular volume). However, both SLD's are proportional to mass density. By simultaneously fitting the composition and mass density to the average X-ray and neutron SLD values determined for these plasma polymer films along with the XPS results (Table 1, XPS is not sensitive to H content) it is possible to calculate the average density of the film and the full atomic composition for the films (Table 4.2). There is an assumption involved in these calculations, namely the surface composition (atomic ratios) determined by XPS are similar to those in the bulk. The first layer (closest to the air) was ignored in the calculation of the average film properties. This is because the film roughness can be coupled to the mass density/atomic composition. Thus, if the fit underestimates the roughness of the film, then the fitting process can compensate by having a low mass density, or high H content, for the surface layer. It is clear that for all plasma polymers produced, there is a loss of oxygen and most significantly hydrogen during the radio

frequency glow discharge plasma polymerization of the di(ethyleneglycol) dimethyl ether monomer. This loss of hydrogen during the deposition of plasma polymers has been observed by us previously for other reactive functional monomer species.^{23, 24} The differences between the resulting plasma polymer film chemistry and the starting monomer composition are most significant for the higher power films, for which there is the most hydrogen depletion.

Interestingly, the density of poly(ethylene glycol) polymers varies from around 1.1 to 1.2 gcm^{-3} and increases with molecular weight. The density of the plasma polymer film produced at 10 W which was found to be the lowest protein fouling film is within the reported density range of this class of polymer at 1.19 gcm^{-3} . The atomic composition of the 10 W film ($\text{C}_2\text{H}_{3.3}\text{O}_{0.9}$) was closest to that of the starting monomer ($\text{C}_2\text{H}_{4.7}\text{O}_1$) and similar to that of PEG polymers ($\text{C}_2\text{H}_4\text{O}_1$). This highlights the possible similarities in both chemistry and structure of the lowest power plasma polymer thin film with that of PEG graft polymers. The outermost layer of the 10 W film also has the greatest H/C ratio near the air interface of all three plasma polymer films analyzed in this study which decreased systematically with power at the air interface. We therefore infer that the 10 W film is the most PEG-like in terms of film chemistry of the three films studied in this work, in particular at the surface (air interface) where interactions with proteins (when the films are placed in solution) are most relevant from both XPS and reflectivity measurements in air.

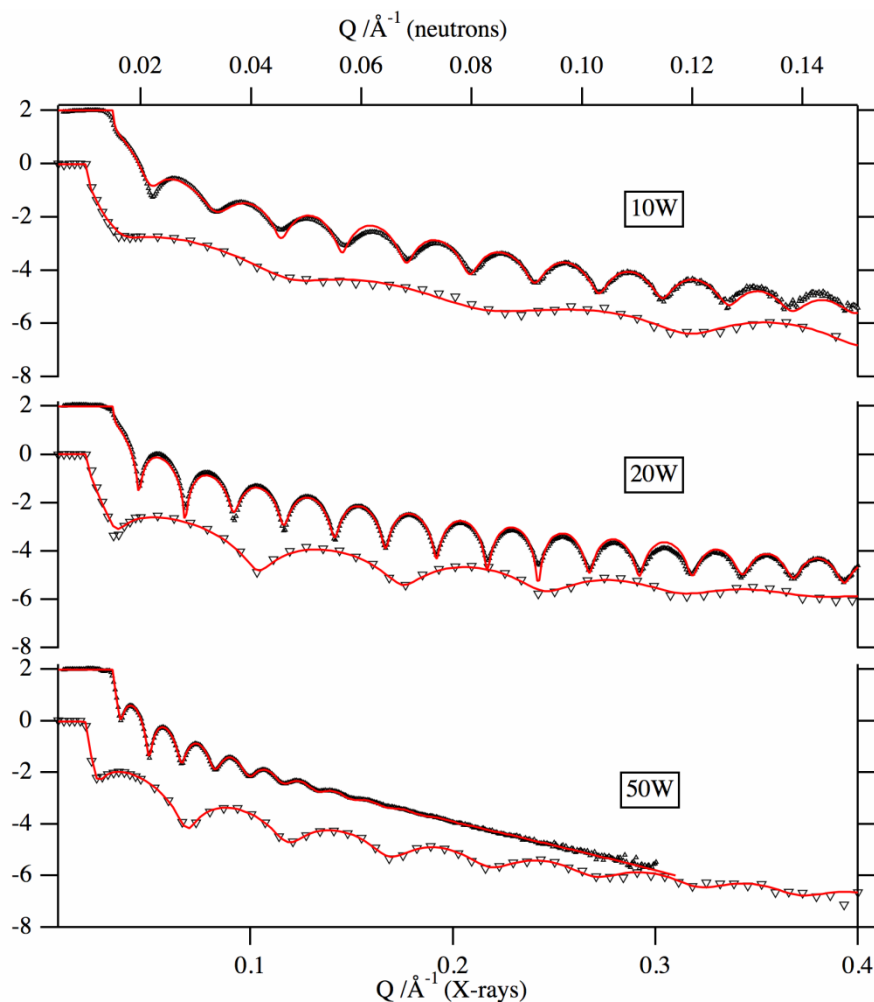


Figure 4.4 X-ray (top traces) and neutron reflectivity spectra (bottom traces) from the air-DGpp-silicon system for the a) 10, b) 20 and c) 50 W load power films. The lines represent fits to the data. XRR data is offset by a factor of 10^2 from the neutron spectra.

It can be seen from Figure 4.5 that the 50 W film has the lowest H/C ratio of all the films which is to be expected considering that a greater degree of monomer fragmentation occurs during the glow discharge polymerization of di(ethyleneglycol) dimethyl ether at 50 W. This is evident by the increase in pressure and deposition rate during plasma polymerisation at this load power compared to the lower power films. Interestingly, the 50 W film has the lowest average mass density of all the films produced. Strikingly, the mass density of the 50 W film at the air interface (the first 5 nm) is dramatically lower

than that of its bulk and compared to the bulk of both the 10 W and 20 W films (Figure 4.5). This may in part, be due to the rougher surface of the 50 W film. It is also possible that there may be a substantial amount of polymerization occurring in the higher powered plasma glow, within the plasma reactor system. If this was to occur, it is likely that the longer chain species could deposit on the silicon substrate during plasma polymerization and this may result in a less dense film being produced. In light of this finding, and taking into account the film chemistry of the 50 W film, it is not surprising that the 50 W film adsorbs a greater amount of protein than the lower power films.

Table 4.2. Average film thickness, roughness, scattering length density and composition of DG plasma polymer films as determined by AFM, X-ray and neutron reflectometry. ^{a)} excluding layer closest to air

	DGpp (10 W)	DGpp (20 W)	DGpp (50 W)
Film Thickness (Å)			
X-ray Reflectometry	358	248.5	198
Neutron Reflectometry	369	245.5	202.6
Scattering Length Density^a (ρ) ($\times 10^6$ Å⁻²)			
X-ray Reflectometry	10.94	11.30	8.91
Neutron Reflectometry	1.09	1.00	1.56
Monomer Atomic Composition	C ₂ H _{4.7} O ₁		
Plasma polymer Atomic Composition^a	C ₂ H _{3.3} O _{0.9}	C ₂ H _{3.3} O _{0.78}	C ₂ H _{2.0} O _{0.6}
Mass Density (gcm⁻³)^a	1.19	1.23	0.99

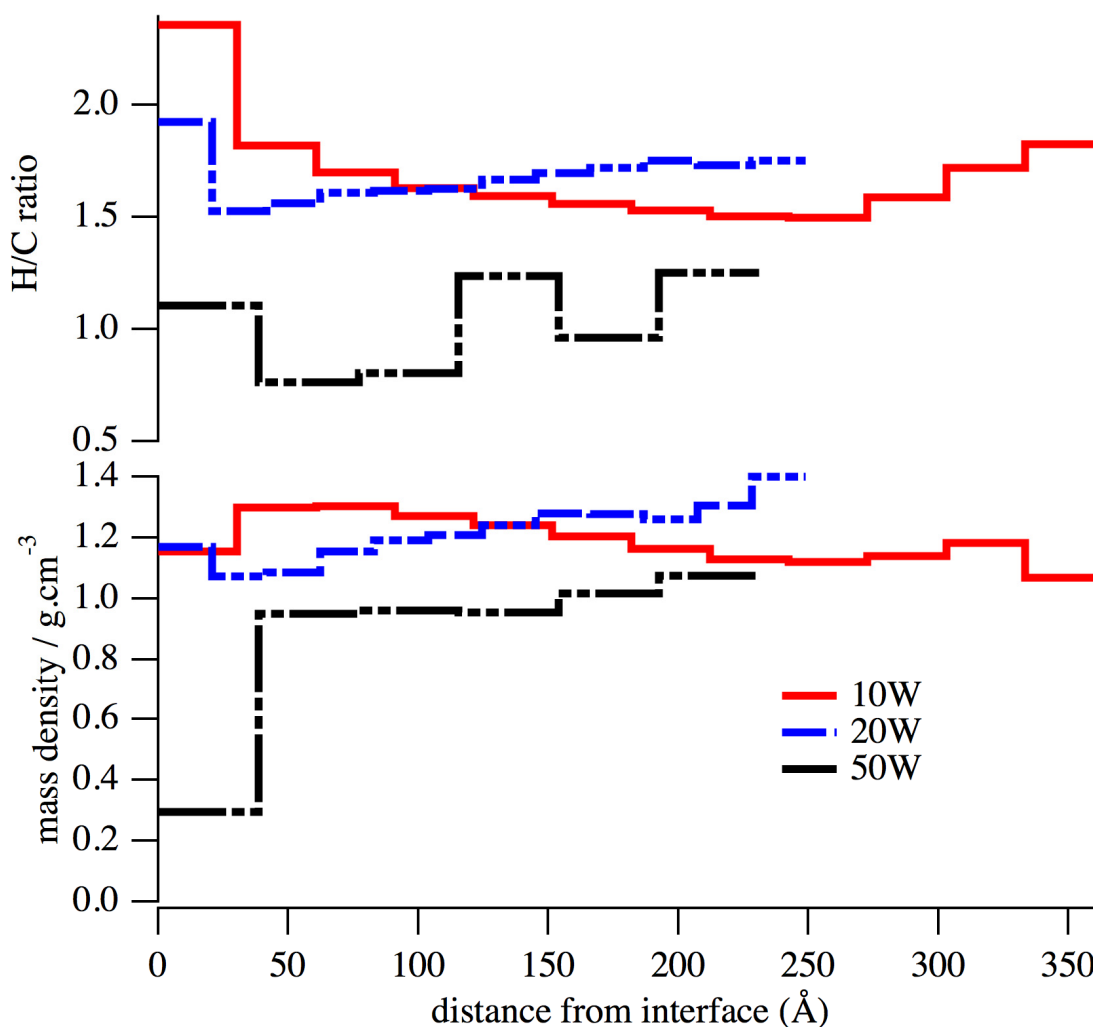


Figure 4.5 Plasma polymer: a) H/C ratio, b) film density as a function of distance from the substrate for 10, 20 and 50 W load power DGpp films (as determined from XRR and NR measurements)

The reflectivity data for the 20 W and 50 W films against various H₂O/D₂O mixes are shown in Figure 4.6. From inspection of the 20 W film in each of the D₂O/H₂O mixtures it is obvious that the films absorb a significant amount of water, as the SLD of the film changes substantially. By using the average SLD of the film in H₂O and the average SLD scattering length of the film against air, one can calculate the amount of absorbed water in the film. For the 20 W film this corresponds to 22 % v/v water ingress. For the

50 W film the amount of absorbed water is much higher, at 40 % v/v. When placed in water both films swelled by a significant amount, a 9 % increase in film thickness for the 20 W film was observed and a 10 % increase in film thickness for the 50 W film was measured. It is important to note here that QCM-D measurements (Figure 4.2A) confirmed that the 50 W film absorbed a substantial amount of water but this was not indicated from QCM-D measurements in the 20 W film. This has important implications in the use of QCM-D measurements in probing the hydration of plasma polymer films. We propose that in the 20 W film, as no increases in mass was detected after incubation in PBS, that the amount of low molecular weight material being removed in this film over time was balanced by water ingress into the film. The NR measurements in water in combination with QCM-D measurements provide strong evidence of this mechanism. It is not uncommon for films produced at lower powers or under pulsed conditions to result in the formation of such low molecular weight material. The implications of this low molecular weight material, in terms of the lower power films protein resistant nature, may be significant. The fact that the 50 W film adsorbs substantially more water than the film deposited at 20 W is interesting. Both films have very similar water contact angles and therefore surface hydrophilicity. We propose the discrepancy in water absorption is due to the lower average mass density of the 50 W film. This film therefore allows for greater water adsorption and diffusion throughout its bulk when compared to the 20 W film with the greater mass density. The level of water absorption in these films is far higher than we have observed in previous NR and XRR studies of amine containing plasma polymerized allylamine films.²³ In comparing our previous study of an allylamine plasma polymer film which had a water contact angle of 55° and a fitted mass density of

1.46 gcm⁻³, it only absorbed 3 % v/v water compared to 40 % v/v for the 50 W di(ethyleneglycol) dimethyl ether plasma polymer film, which has a similar water contact angle of 66° and a significantly lower mass density of 0.99 gcm⁻³. This previous work would seem to support our hypothesis that the mass density of these di(ethyleneglycol) dimethyl ether plasma polymers films plays a significant role in their water uptake. It appears that water contact angle measurements are not a good determinant of the solvation properties of these thin films. One cannot rule out the important influence of the film chemistry in addition to their mass densities in the extent of hydration of these plasma polymer films. It is well known that the ether units in PEG based polymers are extremely good at hydrogen bonding and are extremely well hydrated under most conditions. By this rationale however, one would expect the plasma polymer deposited at 20 W to absorb more water than the 50 W film as it contains a higher concentration of ether groups which is not the case.

Since we measured the 20 W film against two other D₂O/H₂O mixtures it is also possible to calculate the proportion of protons that exchange with solution. For the 20 W film, approximately 15 % of the protons exchange with solution. In general, labile hydrogen atoms are more commonly found on carboxyl and hydroxyl species that we have previously shown to be present in these plasma polymer films contain to an extent.³⁴ Hydrogen atoms bonded to carbon are generally much less labile. From analysis of the XPS C 1s high resolution spectra curve fits (Table 4.1) it can be seen that a minimum of 13 % of the oxygen groups in the 20 W film are not related to ether species. It is reasonable to assume that a small component of the C-O curve fitted species are hydroxyl

species as shown in our previous work. Therefore the fact that we are seeing 15 % of the protons in the 20 W film, can be rationalized by taking into consideration its significant degree of solvent penetration and the observation of residual ‘non-ether’ chemical species within the film. Unfortunately this analysis cannot be repeated for the 50 W film, as the D₂O and D₂O/H₂O solvents possessed similar SLD’s to the swollen film.

The proposed mechanisms of non-specific protein adsorption include electrostatic, van der Waals, hydrophobic and hydrogen bonding interactions.⁸ The 10, 20 and 50 W films had very similar static water contact angles of approximately 60°. It appears that with regards to the di(ethyleneglycol) dimethyl ether plasma polymer films, surface tension effects are not a significant discriminating factor in their relative water solvation and protein fouling characteristics as has been previously reported.^{15, 31} In a study on plasma polymer films deposited from ethylene glycol containing monomers, Johnston et al.¹⁵ have shown that molecular surface structure primarily affects the ability of PEG-like plasma polymer films to resist protein adsorption. Little correlation was observed between the contact angles measured and protein adsorption suggesting that surface tension and interfacial tension effects are not the primary factors that influence protein adsorption and water solvation in these types of plasma polymer thin films.

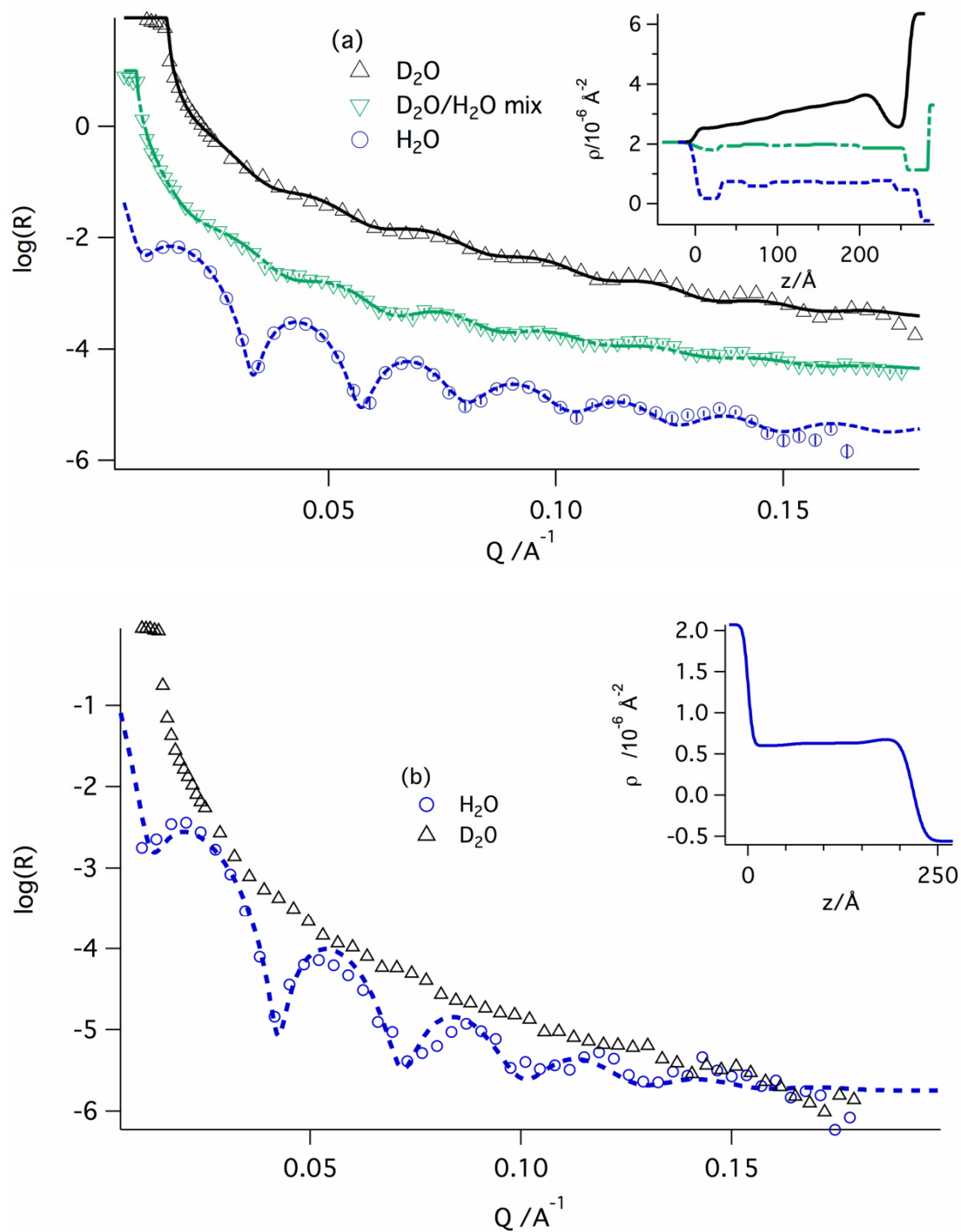


Figure 4.6 Neutron reflectivity spectra from the water-DGpp system for the a) 20 W and b) 50 W load power films measured against various $\text{H}_2\text{O}/\text{D}_2\text{O}$ mixtures. The lines represent fits to the data.

Based on the XPS data presented in Table 4.1, there are some clear differences in the composition of the di(ethyleneglycol) dimethyl ether plasma polymer coatings prepared under different deposition conditions. The composition of the 10 and 20 W films are high in ether (C-O) carbon species. However, the composition of the 50 W film was very different to that of these lower power films and likely relates to the degree of monomer fragmentation. This is supported by the observations of pressure rise and deposition rates during the plasma polymerisation of di(ethyleneglycol) dimethyl ether at different powers. Prior to incubation in the protein solutions we have one plasma polymer coating which contain a high C-C/C-H content of over 50 % (50 W) and two coatings which contain a high C-O content (10 and 20 W) of over 50 %. The relative amount of BSA adsorption was significantly reduced on the 10 W film (Figure 4.2) which was the most PEG-like. A similar result was found by Bretagnol et al.³² in a study of di(ethyleneglycol) dimethyl ether plasma polymer thin films produced at load powers of 1 and 5 W.

It is becoming clear that chain density and, thus, conformation are a critical factor in the successful low protein fouling properties of PEG and PEG-like films.^{19, 35-37} In a study by Fick et al.¹⁷ PEG-SAMs were reported be highly protein resistant when they contain a solvated densely grafted brush of only 40 Å in thickness which correlates to a chain length of only 11 ethylene glycol units. Our fitted reflectivity measurements point to the presence of such thin PEG-like plasma polymer films when they are produced at lower powers and QCM-D measurements in correlation with NRR measurements in water have shown that the films lose mass in water due to the presence of low molecular weight

material. It is reasonable to assume that the 10 W and 20 W films are crosslinked to some extent, with a high degree of residual ether containing chains at the surface and some low molecular weight material. Although we could not unambiguously confirm it experimentally, we expect the 10 W film to contain a greater amount of low molecular weight material than the 20 W film. We hypothesise that the reasons why these particular films are lower fouling than the 50 W film are the higher density of residual ether containing functional groups in these films, along with the film structure appearing similar to that of PEG graft surfaces and perhaps some low molecular weight material. It is clear from XPS analysis that the 50 W film has the lowest concentration of surface ether groups and the highest hydrocarbon component which was also observed in the neutron and X-ray reflectometry compositional fits. Therefore, the reason for its greater propensity to adsorb proteins must be at least in part due to this greater hydrocarbon component and oxygenated species when compared to the lower power films.

4.5 Conclusions

Thin films of di(ethyleneglycol) dimethyl ether have been generated by plasma polymerisation and studied using X-ray Photoelectron Spectroscopy (XPS), Quartz Crystal Microbalance with dissipation monitoring (QCM-D), X-ray and neutron reflectometry (NR). Using combinations of these techniques we were able to accurately determine the film thickness, RMS roughness, and decouple the films composition from their mass densities. All films result in a substantial loss of hydrogen when compared to the starting monomer, with H/C values at the air interface being higher in films deposited at lower load power. Similarly, XPS and reflectivity measurements showed that the chemical composition of the 10 W was most similar to that of PEG-grafted surfaces and

to the starting monomer, particularly at the surface (air interface) where the interactions with proteins is dictated (when the films are placed in solution).

The films were found to absorb a significant amount of water (~22 – 40 % v/v) and their degree of solvation appears to be dependent on both film chemistry and mass density profile. Films deposited at higher load powers resulted in lower mass densities and hence higher amounts of absorbed water. At the air interface, the mass densities of the 10 and 20 W films were most similar to PEG polymers while the 50W film had a very low mass density. A combination of the lower mass density and less PEG-like surface chemistry of the 50 W plasma polymer film was correlated with the higher amount of protein adsorbed, compared to the 10 and 20 W films. Surface hydrophilicity was shown to be a poor determinant of solvation and protein resistance in these thin films. A substantial proportion of the hydrogen atoms within the di(ethyleneglycol) dimethyl ether plasma polymer film deposited at 20 W were 'reactive' and exchangeable with solution, explaining their high degree of absorbed water. QCM-D measurements were found to be inaccurate in detecting associated water in the lower power films that contained loosely bound, low molecular weight material.

The lower powered plasma polymer film that contained a high ether content displayed significantly reduced adsorption of bovine serum albumin from concentrated protein solution. Plasma polymer films with low residual ether content that contained low molecular weight material adsorbed much greater levels of protein from solution. Reflectivity measurements show that the film with the greatest chemical similarity to that

of poly(ethylene glycol) grafted surfaces was the least fouling to proteins. In addition, the low fouling 10 W film was also found to have the highest H/C content at the air interface. Therefore, the higher protein resistance of the di(ethyleneglycol) dimethyl ether plasma polymer film deposited at a plasma load power of 10 W was attributed to its greater chemical and structural similarity to that of poly(ethylene glycol) graft surfaces. Interestingly, the degree of protein adsorption did not positively correlate with films that absorbed higher amounts of water, as is often suggested by the water barrier theory. This work shows the utility of combining NRR and XRR measurements of plasma polymer thin films in parallel with techniques such as XPS and QCM-D.

4.6 Acknowledgements

We thank the CSIRO OCE scheme for funding D. Menzies' PhD scholarship and the Access to Major Research Facilities Project (AMRFP) for funding. We thank the National Institute of Science and Technology, USA for providing the grant time to use the neutron Reflectometer (NG7).

4.7 References

1. Moustafa, M.; Simpson, C.; Glover, M.; Dawson, R. A.; Tesfaye, S.; Creagh, F. M.; Haddow, D.; Short, R.; Heller, S.; MacNeil, S., A new autologous keratinocyte dressing treatment for non-healing diabetic neuropathic foot ulcers. *Diabetic Medicine* **2004**, 21, (7), 786-789.
2. Colley, H. E.; Mishra, G.; Scutt, A. M.; McArthur, S. L., Plasma Polymer Coatings to Support Mesenchymal Stem Cell Adhesion, Growth and Differentiation on Variable Stiffness Silicone Elastomers. *Plasma Processes and Polymers* **2009**, 6, (12), 831-839.
3. Hoene, A.; Walschus, U.; Patrzyk, M.; Finke, B.; Lucke, S.; Nebe, B.; Schroeder, K.; Ohl, A.; Schlosser, M., In vivo investigation of the inflammatory response against allylamine plasma polymer coated titanium implants in a rat model. *Acta Biomaterialia* 6, (2), 676-683.
4. Simovic, S.; Losic, D.; Vasilev, K., Controlled drug release from porous materials by plasma polymer deposition. *Chemical Communications* 46, (8), 1317-1319.
5. Vasilev, K.; Sah, V.; Anselme, K.; Ndi, C.; Mateescu, M.; Dollmann, B.; Martinek, P.; Ys, H.; Ploux, L.; Griesser, H. J., Tunable Antibacterial Coatings That Support Mammalian Cell Growth. *Nano Letters* 10, (1), 202-207.
6. Muir, B. W.; Fairbrother, A.; Gengenbach, T. R.; Rovere, F.; Abdo, M. A.; McLean, K. M.; Hartley, P. G., Scanning probe nanolithography and protein patterning of low-fouling plasma polymer multilayer films. *Advanced Materials* **2006**, 18, (23), 3079-3082.
7. Israelachvili, J., The Different Faces of Poly(Ethylene Glycol). *Proceedings of the National Academy of Sciences of the United States of America* **1997**, 94, (16), 8378-8379.
8. Latour, R. A., Thermodynamic Perspectives on the Molecular Mechanisms Providing Protein Adsorption Resistance That Include Protein-Surface Interactions. *Journal of Biomedical Materials Research Part a* **2006**, 78A, (4), 843-854.
9. Mc Pherson, T.; Kidane, A.; Szleifer, I.; Park, K., Prevention of Protein Adsorption by Tethered Poly(Ethylene Oxide) Layers: Experiments and Single-Chain Mean-Field Analysis. *Langmuir* **1998**, 14, (1), 176-186.
10. Pertsin, A. J.; Grunze, M., Computer Simulation of Water Near the Surface of Oligo(Ethylene Glycol)-Terminated Alkanethiol Self-Assembled Monolayers. *Langmuir* **2000**, 16, (23), 8829-8841.
11. Lopez, G. P.; Ratner, B. D.; Tidwell, C. D.; Haycox, C. L.; Rapoza, R. J.; Horbett, T. A., Glow-Discharge Plasma Deposition of Tetraethylene Glycol Dimethyl Ether for Fouling-Resistant Biomaterial Surfaces. *Journal of Biomedical Materials Research* **1992**, 26, (4), 415-439.
12. Goessl, A.; Bowen-Pope, D. F.; Hoffman, A. S., Control of shape and size of vascular smooth muscle cells in vitro by plasma lithography. *Journal of Biomedical Materials Research* **2001**, 57, (1), 15-24.
13. Mishra, G.; Easton, C. D.; McArthur, S. L., Physical vs Photolithographic Patterning of Plasma Polymers: An Investigation by ToF-SSIMS and Multivariate Analysis. *Langmuir* 26, (5), 3720-3730.
14. Wu, Y. J.; Timmons, R. B.; Jen, J. S.; Molock, F. E., Non-Fouling Surfaces Produced by Gas Phase Pulsed Plasma Polymerization of an Ultra Low Molecular

Weight Ethylene Oxide Containing Monomer. *Colloids and Surfaces B: Biointerfaces* **2000**, 18, (3-4), 235-248.

15. Johnston, E. E.; Bryers, J. D.; Ratner, B. D., Plasma Deposition and Surface Characterization of Oligoglyme, Dioxane, and Crown Ether Nonfouling Films. *Langmuir* **2005**, 21, (3), 870-881.

16. Gengenbach, T. R.; Chatelier, R. C.; Griesser, H. J., Characterization of the Ageing of Plasma-Deposited Polymer Films: Global Analysis of X-Ray Photoelectron Spectroscopy Data. *Surface and Interface Analysis* **1996**, 24, (4), 271-281.

17. Fick, J.; Steitz, R.; Leiner, V.; Tokumitsu, S.; Himmelhaus, M.; Grunze, M., Swelling Behavior of Self-Assembled Monolayers of Alkanethiol-Terminated Poly(Ethylene Glycol): a Neutron Reflectometry Study. *Langmuir* **2004**, 20, (10), 3848-3853.

18. Ostuni, E.; Chapman, R. G.; Liang, M. N.; Meluleni, G.; Pier, G.; Ingber, D. E.; Whitesides, G. M., Self-Assembled Monolayers That Resist the Adsorption of Proteins and the Adhesion of Bacterial and Mammalian Cells. *Langmuir* **2001**, 17, (20), 6336-6343.

19. Unsworth, L. D.; Sheardown, H.; Brash, J. L., Protein-resistant poly(ethylene oxide)-grafted surfaces: Chain density-dependent multiple mechanisms of action. *Langmuir* **2008**, 24, (5), 1924-1929.

20. Moisan, M.; Barbeau, C.; Claude, R.; Ferreira, C. M.; Margot, J.; Paraszczak, J.; Sa, A. B.; Sauve, G.; Wertheimer, M. R., Radio frequency or microwave plasma reactors? Factors determining the optimum frequency of operation. *Journal of Vacuum Science & Technology B: Microelectronics and Nanometer Structures* **1991**, 9, (1), 8-25.

21. James, M., Characterization of Thin-Film Surfaces and Interfaces Using Neutron Reflectometry. *Australian Journal of Chemistry* **2001**, 54, (8), 487-491.

22. Jeon, H. S.; Wyatt, J.; Harper-Nixon, D.; Weinkauf, D. H., Characterization of thin polymer-like films formed by plasma polymerization of methylmethacrylate: A neutron reflectivity study. *Journal of Polymer Science Part B-Polymer Physics* **2004**, 42, (13), 2522-2530.

23. Muir, B. W.; Nelson, A.; Fairbrother, A.; Fong, C.; Hartley, P. G.; James, M.; McLean, K. M., A Comparative X-Ray and Neutron Reflectometry Study of Plasma Polymer Films Containing Reactive Amines. *Plasma Processes and Polymers* **2007**, 4, (4), 433-444.

24. Nelson, A.; Muir, B. W.; Oldham, J.; Fong, C.; McLean, K. M.; Hartley, P. G.; Oiseth, S. K.; James, M., X-Ray and Neutron Reflectometry Study of Glow-Discharge Plasma Polymer Films. *Langmuir* **2006**, 22, (1), 453-458.

25. Muir, B. W.; Thissen, H.; Simon, G. P.; Murphy, P.; Griesser, H. J., Factors affecting the adhesion of microwave plasma deposited siloxane films on polycarbonate. *Thin Solid Films* **2006**, 500, (1-2), 34-40.

26. Jennings, J. W.; Pallas, N. R., An efficient method for the determination of interfacial-tensions from drop. *Langmuir* **1988**, 4, (4), 959-967.

27. Cheng, Q.; Komvopoulos, K., Synthesis of Polyethylene Glycol-Like Films from Capacitively Coupled Plasma of Diethylene Glycol Dimethyl Ether Monomer. *The Journal of Physical Chemistry C* **2009**, 113, (1), 213-219.

28. Brétagne, F.; Lejeune, M.; Papadopoulou-Bouraoui, A.; Hasiwa, M.; Rauscher, H.; Ceccone, G.; Colpo, P.; Rossi, F., Fouling and non-fouling surfaces produced by

plasma polymerization of ethylene oxide monomer. *Acta Biomaterialia* **2006**, 2, (2), 165-172.

29. Bretagnol, F.; Kylian, O.; Hasiwa, M.; Ceriotti, L.; Rauscher, H.; Ceccone, G.; Gilliland, D.; Colpo, P.; Rossi, F., Micro-patterned surfaces based on plasma modification of PEO-like coating for biological applications. *Sensors and Actuators B-Chemical* **2007**, 123, (1), 283-292.

30. Salim, M.; Mishra, G.; Fowler, G. J. S.; O'Sullivan, B.; Wright, P. C.; McArthur, S. L., Non-fouling microfluidic chip produced by radio frequency tetraglyme plasma deposition. *Lab on a Chip* **2007**, 7, (4), 523-525.

31. Muir, B. W.; Tarasova, A.; Gengenbach, T. R.; Menzies, D. J.; Meagher, L.; Rovere, F.; Fairbrother, A.; McLean, K. M.; Hartley, P. G., Characterization of low-fouling ethylene glycol containing plasma polymer films. *Langmuir* **2008**, 24, (8), 3828-3835.

32. Bretagnol, F.; Lejeune, M.; Papadopoulou-Bouraoui, A.; Hasiwa, M.; Rauscher, H.; Ceccone, G.; Colpo, P.; Rossi, F., Fouling and non-fouling surfaces produced by plasma polymerization of ethylene oxide monomer. *Acta Biomaterialia* **2006**, 2, (2), 165-172.

33. Padron-Wells, G.; Jarvis, B. C.; Jindal, A. K.; Goeckner, M. J., Understanding the synthesis of DEGVE pulsed plasmas for application to ultra thin biocompatible interfaces. *Colloids and Surfaces B-Biointerfaces* **2009**, 68, (2), 163-170.

34. Menzies, J. D., Cowie, C. C. B, Fong, C., Forsythe, J., Gengenbach, T., Mc Lean, K., Puskar, L., Textor, M., Thomsen L., Tobin, M., Muir, B., A one-step method for generating PEG-like plasma polymer gradients: Chemical Characterisation and Analysis of protein interactions. *Langmuir* **2010**.

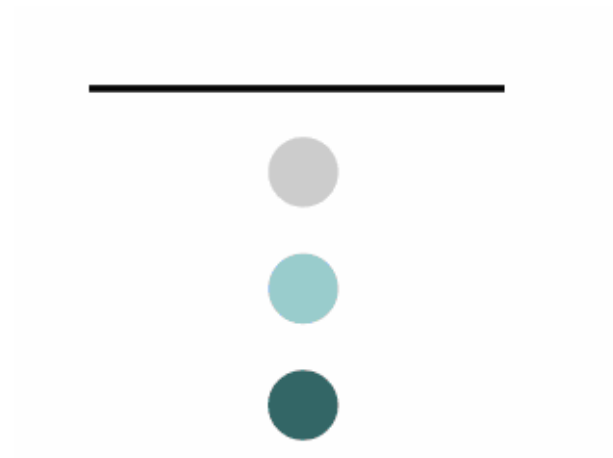
35. Feldman, K.; Hähner, G.; Spencer, N. D.; Harder, P.; Grunze, M., Probing Resistance to Protein Adsorption of Oligo(Ethylene Glycol)-Terminated Self-Assembled Monolayers by Scanning Force Microscopy. *Journal of the American Chemical Society* **1999**, 121, (43), 10134-10141.

36. Unsworth, L. D.; Tun, Z.; Sheardown, H.; Brash, J. L., Chemisorption of thiolated poly(ethylene oxide) to gold: surface chain densities measured by ellipsometry and neutron reflectometry. *Journal of Colloid and Interface Science* **2005**, 281, (1), 112-121.

37. Unsworth, L. D.; Tun, Z.; Sheardown, H.; Brash, J. L., In situ neutron reflectometry investigation of gold-chemisorbed PEO layers of varying chain density: Relationship of layer structure to protein resistance. *Journal of Colloid and Interface Science* **2006**, 296, (2), 520-526.

Part 2:

Generation and Characterisation of Gradient PEG-like Plasma polymers



Chapter 5:

**A one-step method for generating PEG-like
plasma polymer gradients: Chemical
characterisation and analysis of protein
interactions**

PART B: Suggested Declaration for Thesis Chapter

Monash University

Declaration for Thesis Chapter 5

Declaration by candidate

In the case of Chapter 5, the nature and extent of my contribution to the work was the following:

Nature of contribution	Extent of contribution (%)
Experimental design and conduct, data processing, manuscript writing	85 %

The following co-authors contributed to the work. Co-authors who are students at Monash University must also indicate the extent of their contribution in percentage terms:

Name	Nature of contribution	Extent of contribution (%) for student co-authors only
Bruce Cowie	Experimental advice	
Celesta Fong	Assisted in experimental conduct and manuscript correction	
John Forsythe	Assisted in experimental design and manuscript correction	
Thomas Gengenbach	Assisted in experimental conduct and manuscript correction	
Keith McLean	Manuscript correction	
Ljiljana Puskar	Experimental advice	
Marcus Textor	Experimental design and manuscript correction	
Lars Thomsen	Experimental advice	
Mark Tobin	Experimental advice	
Ben Muir	Experimental design, manuscript correction	

Candidate's
Signature



Date

30/05/2011

Declaration by co-authors

The undersigned hereby certify that:

- (1) the above declaration correctly reflects the nature and extent of the candidate's contribution to this work, and the nature of the contribution of each of the co-authors.
- (2) they meet the criteria for authorship in that they have participated in the conception, execution, or interpretation, of at least that part of the publication in their field of expertise;
- (3) they take public responsibility for their part of the publication, except for the responsible author who accepts overall responsibility for the publication;
- (4) there are no other authors of the publication according to these criteria;
- (5) potential conflicts of interest have been disclosed to (a) granting bodies, (b) the editor or publisher of journals or other publications, and (c) the head of the responsible academic unit; and
- (6) the original data are stored at the following location(s) and will be held for at least five years from the date indicated below:

Location(s)

CSIRO, Materials Science and Engineering

Signatures		Date
Bruce Cowie Australian Synchrotron		31/5/2011
Celesta Fong CSIRO, Materials Science and Engineering		30/5
John Forsythe Materials Engineering, Monash University		5/7/11
Thomas Gengenbach CSIRO, Materials Science and Engineering		4/7/2011
Keith McLean CSIRO, Materials Science and Engineering		30/5/11
Ljiljana Puskar Australian Synchrotron		21.06. 2011
Marcus Textor Dept of Materials, ETH, Switzerland		
Lars Thomsen Australian Synchrotron		30/05/11
Mark Tobin Australian Synchrotron		
Ben Muir CSIRO, Materials Science and Engineering		30/5/11

.....

5. A one-step method for generating PEG-like plasma polymer gradients: Chemical characterisation and analysis of protein interactions

Donna J. Menzies^{1,2}, Bruce Cowie⁴, Celesta Fong¹, John S. Forsythe², Thomas R. Gengenbach¹, Keith M. McLean¹, Ljiljana Puskar⁴, Marcus Textor³, Lars Thomsen⁴, Mark Tobin⁴, Benjamin W. Muir^{1*}

1. CSIRO, Molecular and Health Technologies, Clayton, VIC, 3168, Australia

2. Monash University, Dept of Materials Engineering, Clayton, VIC, 3800, Australia

3. Laboratory for Surface Science and Technology, Dept of Materials, ETH, 8093 Zurich, Switzerland

4. Australian Synchrotron, Clayton, VIC, 3168, Australia



5.1 Abstract

In this work we report a one-step method for the fabrication of poly(ethylene glycol) PEG-like chemical gradients, which were deposited via continuous wave radio-frequency glow discharge plasma polymerisation of diethylene glycol dimethyl ether (DG). A knife edge top electrode was used to produce the gradient coatings at plasma load powers of 5 and 30W. The chemistry across the gradients was analysed using a number of complementary techniques including spatially resolved synchrotron source grazing incidence FTIR microspectroscopy, X-ray photoelectron spectroscopy (XPS) and synchrotron source near edge X-ray absorption fine structure (NEXAFS) spectroscopy. Gradients deposited at lower load power retained a higher degree of monomer like functionality as did the central region directly underneath the knife edge electrode of each gradient film. Surface derivatisation experiments were employed to investigate the concentration of residual ether units in the films. In addition, surface

derivatisation was used to investigate the reactivity of the gradient films towards primary amine groups in a graft co-polymer of poly (L-Lysine) and poly(ethylene glycol) (PLL-g-PEG copolymer) which was correlated to residual aldehyde, ketone and carboxylic acid functionalities within the films. The protein adsorption characteristics of the gradients were analyzed using three proteins of varying size and charge. Protein adsorption varied and was dependent on the chemistry and the physical properties (such as size and charge) of the proteins. A correlation between the concentration of ether functionality and the protein fouling characteristics along the gradient films was observed. The gradient coating technique developed in this work allows for the efficient and high-throughput study of biomaterial gradient coating interactions.

Keywords: PEG gradient, plasma polymer, protein adsorption, NEXAFS

5.2 Introduction

The use of surface chemistry gradients to interrogate and optimize material-biological interactions in a high-throughput manner has become an increasingly popular tool in the field of biomaterials research. The generation of surface chemistry gradients can provide information on multiple compositions in a single experiment. Factors such as chemical functionality¹⁻³, wettability⁴⁻⁶, topography^{5, 7}, surface charge⁸, molecular structure^{9, 10} and the resulting physical properties^{11, 12} that may influence the interaction of biomolecules and cells, can be tested while minimizing experimental error. Furthermore, there are a number of physiological and biological processes which are driven by chemical gradient stimuli, such as the maintenance of homeostatic equilibrium, chemotaxis¹³ and embryonic development via gradient induced cell proliferation and differentiation. Tissue formation and neuronal development^{14, 15} are also controlled by a gradient distribution of specific biological cues¹⁵,

¹⁶ *in vivo*. Therefore surfaces that are able to mimic this physiological organization *in vitro* are of considerable interest to the life sciences.

Gradient surfaces are those which have a gradual, spatiotemporal variation of one or more chemical, physical or topographical property. A variety of methods have been reported for the fabrication of surface gradients¹⁷⁻¹⁹ including UV-initiated free-radical polymerisation⁸ and grafting²⁰, corona discharge²¹⁻²³, corona-induced graft copolymerisation²⁴, diffusion techniques^{13, 25}, adsorption²⁶ and plasma co-polymerisation.²⁷ The use of radio frequency plasma polymerisation (RFpp) has also been reported for gradient generation^{1, 28-30}, but to date have required the use of a moving sample stage or shutter. Our one-step method of gradient generation uses RFpp without the need for any moving components.

Gradient surfaces have been used to study the interaction and function of both cells and biomolecules, such as proteins. Wettability gradients formed by treating various polymeric substrates such as polyethylene³¹ and polylactide-glycolide³² films in air with corona discharge from a knife-type electrode, have been used to investigate the effect of wettability on protein adsorption^{33, 34}, platelet adhesion⁶ and cell adhesion, spreading and growth.^{32, 34, 35} Chemical gradients presenting various chemical functionalities have also been used to study many biological interactions *in vitro*. Robinson et al.³⁰ used plasma polymerisation of octadiene and allylamine monomers to form compositional gradients that enable the formation of immobilized, functional heparin gradients. Similarly, Zelzer et al.¹ formed chemical gradients using plasma polymerisation of hexane and allylamine to investigate the optimal surface chemistry and wettability for the attachment and differentiation of fibroblasts. A number of researchers have also used surface chemical gradients as a high throughput

approach to screening and identifying the critical parameters involved in the interaction of, or resistance to, various proteins and platelets.^{36, 37}

The use of poly(ethylene glycol) based materials to impart protein resistance is well described and the use of PEG-based gradients provides an ideal surface to interrogate the important chemical and physical characteristics that impart PEG's protein resistant nature. The mechanisms of PEG's protein resistance have been extensively investigated^{38, 39} and two of the most well regarded explanations include 'steric stabilization'^{40, 41} and the 'water barrier' theories. Latour⁴² recently encompassed these theories into a thermodynamic approach, where he suggests that the enthalpic (favoured H-bonding of the tethered chains to water molecules rather than to the functional groups on the proteins) and entropic effects resulting from protein adsorption cause a net increase in the free energy of the system upon protein adsorption. However, this theory assumes the presence of PEG surfaces with long flexible surface-tethered chains having both a low packing density (to allow a high mobility) yet providing full coverage on the surface. These assumptions are not particularly relevant however, to the highly cross-linked PEG-like surfaces produced from plasma polymerisation described in this study.

We have produced 2D surface bound PEG-like chemical gradients in one step, using continuous wave radio frequency glow discharge (rfgd) plasma polymerisation of diethylene glycol dimethyl ether (DG). The 2D effect of the gradient was displayed by combinatorial chemical analysis techniques and thickness measurements. Using a knife edge upper electrode, a non uniform plasma glow discharge was generated around the upper electrode resulting in the deposition of a chemical gradient on substrates placed directly underneath the plasma glow. The chemistry across the DGpp gradients was analysed using grazing-

incidence FTIR (gi-FTIR) microspectroscopy to provide a chemical map of the bulk chemistry across the gradients. X-ray Photoelectron Spectroscopy (XPS) and Near Edge X-ray Absorption Fine Structure (NEXAFS) provided complementary surface sensitive chemical analysis of these gradients. NEXAFS has been shown to be an excellent combinatorial tool for studying surface bound gradients due to its ability to analyse both surface chemistry and molecular orientation^{9, 10}. The adsorption of three model proteins (bovine serum albumin (BSA), lysozyme and γ -globulin) was measured across the gradients, and these demonstrated marked variability in their ability to resist protein adsorption that correlated with changes in surface chemistry.

5.3 Materials and Methods

5.3.1 Substrates Preparation

DGpp gradients were deposited onto ultra-flat single crystal silicon wafers (<100>, 1 cm² x 0.5 mm thick, MMRC P/L), cleaned by ultrasonication in a 1% RBS-35 surfactant (Pierce) in (2% ethanol in MilliQ) for 1 hour. Substrates were then rinsed multiple times in Milli-Q water before being dried in a high-pressure stream of high purity nitrogen. Indium tin oxide coated aluminosilicate glass (Delta Technologies, Corning 1737, CB-50IN) were used for the giFTIR analysis to provide a reflective surface, and were cleaned as described above.

5.3.2 Plasma Polymerisation

Radio frequency glow discharge plasma polymerisation was used to deposit PEG-like gradient films in a custom-built plasma reactor. The reactor consists of a cylindrical glass chamber (height of 35 cm and diameter of 17 cm) and is fitted with two capacitively coupled electrodes. The top electrode (a razor) was connected to a RF power supply (125 kHz) and lowered to sit ~ 1mm above the substrate, while the bottom electrode (diameter = 14 cm) was grounded (see Appendix 1, Figure 1). The monomer, diethylene glycol dimethyl ether, often referred to as 'diglyme' (DG) (BDH, 99% purity) was fed into the reactor from a round

bottom flask attached to a stainless steel line and a manual valve to control the flow. Substrates were placed on the lower electrode, and a rotary pump was used to evacuate the chamber. The DG vapours were fed into the chamber at a starting pressure of 20 Pa, and a continuous RF field was generated between the electrodes for a deposition time of 180 seconds. Gradients were deposited at two different load powers, 5 and 30W.

5.3.3 Profilometry

Film thickness across the gradient was measured using a Veeco Dektak 6M stylus profilometer. Briefly, the stylus (diameter 12.5 μm) force was set to 10 mg across a distance of 1000 μm over 10 seconds. A thin line of the DGpp gradient was removed in the direction of the gradient by scratching the surface with a sharp needle to expose the silicon substrate. Measurements were then taken over the scratch across the gradient at 1 mm interval to assess film thickness

5.3.4 Grazing incidence FTIR microspectroscopy

Chemical maps across the DGpp gradients were measured using a FTIR microscope at the infrared beamline at the Australian Synchrotron. A Bruker Vertex 80v FTIR spectrometer with a KBr beam splitter and vacuum windows is coupled to a Bruker Hyperion 2000 IR microscope (Bruker Optik GmbH, Ettlingen, Germany) which is equipped with a liquid nitrogen cooled single point MCT detector and motorised sample stage which allows for point by point raster scanning of the sample. Spectra were collected in grazing incidence mode using a Bruker Grazing Angle Objective (GAO) at 15x magnification. An IR polarizer was used to ensure the perpendicular polarisation vector of the incident radiation to the sample surface. All data were collected using the Bruker Opus software version 6.5 with the video mapping package used for generation of two dimensional grazing angle absorbance maps. FTIR spectra were acquired at a spectral resolution of 6.0 cm^{-1} with 256 scans co-added and normalized to the alkane stretch (~ 2850 to 3000 cm^{-1}) to compensate for any

thickness effects across the gradient. A 20 x 20 μm aperture was used and spectra acquired at step intervals of 250 μm across the gradients.

5.3.5 X-ray Photoelectron Spectroscopy (XPS)

To investigate the chemical composition of the DGpp films, XPS analysis was performed using an AXIS HSi spectrometer (Kratos Analytical Ltd, Manchester, UK) equipped with a monochromated Al K_{α} X-ray source at a power of 144 W (12 mA, 12 kV). A hemispherical analyser was used, operating in the fixed analyser transmission mode with a standard aperture (1.0 mm x 0.5 mm). Charging of the samples during irradiation was compensated for by the internal flood gun, coupled with a magnetic immersion lens. The pressure in the main vacuum chamber during analysis was typically 5×10^{-6} Pa. Survey spectra were acquired at a pass energy of 320 eV to identify the elements present in the DGpp films. The atomic concentrations were calculated using integral peak intensities and the sensitivity factors supplied by the manufacturer. High-resolution C 1s spectra were also obtained and quantified using a minimisation algorithm in order to calculate optimised curvefits and determine the relative contributions from specified functional groups.

Five peak components (mixed gaussian/Lorentzian model functions) were used. Component C1 at the lowest binding energy (BE) was assigned to aliphatic hydrocarbons (neutral carbon) and the corresponding BE set accordingly to 285 eV.²²⁴ A second component at a slightly higher BE was included to account for all C 1s photoelectrons that underwent a secondary BE shift. Component C3 (286.3-286.6 eV) represents C-O based groups (eg ethers and alcohols), C4 (287.9 – 288.2 eV) accounts for all C=O based functional groups (eg aldehydes and ketones) and C5 (288.9 – 289.3 eV) accounts for O-C=O based groups (eg acids or esters). These components were applied to the analysis of the DGpp gradients prior to protein adsorption.

5.3.6 Near Edge X-ray Adsorption Fine Structure (NEXAFS) spectroscopy

Near Edge X-ray Adsorption Fine Structure (NEXAFS) spectroscopy was performed at the Australian Synchrotron on the soft X-ray beam line (SXR, 14-ID). Samples were loaded into a UHV chamber, where a vacuum of 2×10^{-8} kPa was maintained. The beam line is equipped with an Apple II undulator, which was set to produce horizontally polarised light that is then passed through a monochromator (Peterson plane grating, 1200 lines mm⁻¹). The photon flux on the beam line was 2.7×10^{11} photons/sec/200 mA, and the beam spot size on the sample was approximately 0.6 x 0.6 mm. Spectra were acquired (with the beam at 90° wrt the sample surface) for both the C (270-320 eV) and O (520 -560 eV) K-edge in partial electron yield (PEY) mode. A retarding potential of -100 eV and -400 eV for the C and O scans respectively was applied to the entrance of the detector to eliminate any contributions from lower energy electrons.

Multiple spectra on the same spot retained the same spectral features, indicating that the films are not subject to radiation damage. To account for contributions to the O 1s and C 1s spectra from internal contamination from the beamline itself, a clean sputtered Au foil was measured as a reference. Spectra were then normalised according to the method discussed by Watts et al.⁴⁴. A MatLab based curve fitting program, Whooshka was used to curve-fit the NEXAFS spectra, where a series of Gaussian peaks were assigned to fit the resonance features along with a step edge.

5.3.7 Surface Derivatisation

Using the method described by Shard et al.⁴⁵ surface derivatisation of the hydroxyl groups across the DGpp gradient films was performed using gas phase reaction with trifluoroacetic anhydride (TFAA). Briefly, a small volume TFAA was placed in a vial and the gradient film attached to the lid of the vial. The sample was gently agitated for approximately 30 seconds

and left for approximately 1 hour for the reaction to take place. Samples were then analyzed for their atomic composition and using the equation below, the concentration of hydroxyl groups was calculated.

$$X_{C-OH} = 1/(3(I_c S_f/I_f S_c)-2) \quad [1]$$

Where: I = intensity (of C and F)

S = sensitivity factor (of C and F)

To determine the degree and manner the proteins were bound to the gradient surfaces, the grafting capability of the co-polymer poly(L-lysine)-poly(ethylene glycol) (PLL-g-PEG) with the primary amine (1°) functionalities of the protein was assessed. Two mechanisms of reaction are possible, namely covalent or electrostatic. Covalent bonding involves attachment of the 1° amines via either aldehyde or ketone groups; whereas electrostatic interactions react via residual acid functionalities within the gradient surfaces. Samples were incubated overnight at room temperature with 1 mg/ml PLL-g-PEG solutions in water (pH 5) and were rinsed with MilliQ water prior to analysis of the N content using XPS.

5.3.8 Protein adsorption

To assess the relative adsorption of various proteins across the DGpp gradients, fresh samples were incubated in solutions of bovine serum albumin, lysozyme and γ -globulins proteins (1 mg/ml in PBS, pH 7.4 for 1 hour). Samples were then thoroughly rinsed with MilliQ water before being blown dry with a high-velocity, ultra pure nitrogen stream. Samples were then analysed using XPS where protein adsorption was indicated by the presence of elemental N on the DGpp gradient surface.

5.4 Results and Discussion

5.4.1 Plasma Deposition

In this work, PEG like gradient plasma polymer (pp) thin films were deposited via radio frequency glow discharge plasma polymerisation of diethylene glycol dimethyl ether (DG) at two different load powers, 5 and 30W. Using a knife edge upper electrode within the plasma reactor, a non-uniform plasma glow discharge was created around the upper electrode (razor), resulting in DGpp gradient films with a systematic variation in both their surface chemistry and thickness. Photographic images of the DGpp gradients deposited on a Si substrate are presented in Figure 5.1A, where the colour changes occurring across the DGpp coated substrate are indicative of the variation in film thickness.

Profilometry measurements were performed across the DGpp gradients to measure film thickness (Figure 5.1B). The central region of the DGpp gradients, deposited directly under the knife edge electrode will be referred to '0 mm' throughout this paper. The 5W DGpp gradient showed an increasing film thickness from 0 mm to a distance of 5 mm and then a systematic decrease when measured out to 10 mm. Similarly, the film thickness across the 30W gradient increased between 0 to 4 mm and then decreased out to 10 mm but produced thicker gradients in comparison to the 5W coatings, indicating a faster film deposition rate at higher load power. XPS elemental analysis of the DGpp films showed the presence of both oxygen and carbon, with the oxygen content remaining highest at the centre of the gradients (data not shown). A similar trend was observed for both the 5 and 30 W gradient films; however films deposited at 30W retained lower levels of oxygen. Analysis of the O/C atomic ratio (Figure 5.1B) across the gradients ranged from 0.46 (at 0mm) to 0.42 (10mm) in the case of the 5W films and from 0.33 (0mm) to 0.27 (10mm) in the case of the 30W film. The O/C ratio of the starting diglyme monomer is 0.5.

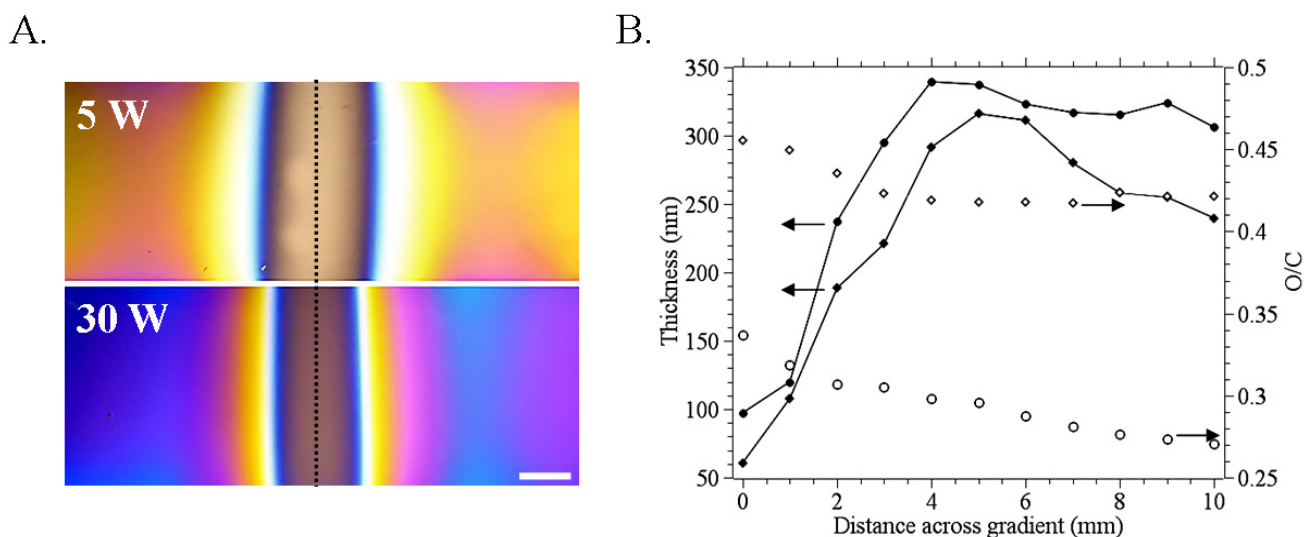


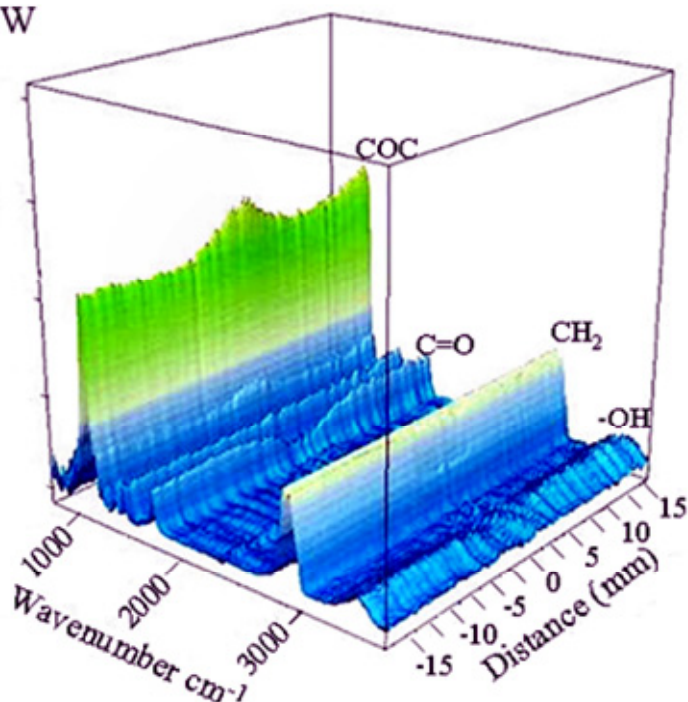
Figure 5.1 A. Photographic images of DGpp gradients deposited on Si at 5 and 30 W load powers. The colour change across the gradient films is indicative of changing film thickness with distance. The broken vertical line indicates the projected position of the knife-edge electrode during deposition. Quantify scale bar B. Film thickness (dark symbols, lines are a guide for the eye) and O/C elemental ratio (hollow symbols) plotted across the 5 (◇) and 30 W (●) DGpp gradients as a function of distance. Arrows indicate to which axis the data relates to.

5.4.2 giFTIR microspectroscopy

The variation of the bulk plasma polymer thin film gradient chemistries produced during the rfgd of DG at load powers of 5 and 30 W was investigated using gi-FTIR microspectroscopy with a synchrotron radiation source. FTIR spectra from 20x20 μm sample regions were acquired to 15 mm either side of the gradient centre (0 mm), at a spatial distance of 250 μm intervals across the gradients. Figure 5.2 presents 3-dimensional FTIR spectral plots taken across the 5 and 30W gradient films. The dominant peak observed in the spectra was the ether stretch at $\sim 1052\text{ cm}^{-1}$. It is possible that some contribution to this stretch may also be from residual ester groups in the gradient films. It was shown that the gradients retain the greatest monomer-like functionality (high ether content) in the central region (0 mm) of the gradient that is deposited directly underneath the knife edge electrode. The formation of new chemical species after plasma polymer deposition is well documented and generally occurs as a result of post oxidation reactions and scission of the starting monomer or oligomer species in the plasma glow discharge. A systematic decrease in the absorbance of the ether stretch

(OCO) extending out from the central region of the gradient was observed, which was even more pronounced in the 30 W DGpp gradient. The carbonyl stretch at $\sim 1735\text{ cm}^{-1}$ showed the opposite trend to the ether stretch with lower carbonyl intensity observed at the centre of the gradients where fragmentation of the monomer species appears to be occurring to a lesser extent. The spectra, normalized to the alkane stretch (~ 2850 to 3000 cm^{-1} , which incorporates the stretch vibrations from both CH_2CH_2 and CH_3 groups) indicate that very low levels of carbonyl containing species are present in the centre of the 5 W gradient, although compared to the 30 W film it has a much greater concentration of residual ether present. This region of the 5W gradient film has a much greater concentration of residual ether functionality present when compared to the 30 W film. It is difficult to assign the exact origin of the carbonyl species in this work due to the closeness of acid, ester, aldehyde and ketone stretches in this region and the inherently broader nature of the DGpp films spectral peaks in comparison to small molecule FTIR spectra. In the gradient deposited at the 30W plasma load power, higher levels of carbonyl functionality were observed but again remained lowest in the centre of the gradient at 0 mm. Analysis of the hydroxyl stretch ($\sim 3450\text{ cm}^{-1}$) showed a variation in intensity across the 5W gradient with lower levels seen at the central region, however no systematic trend was observed across the 5W gradient. Another point of interest to note from the FTIR spectra is the absence of an alkene stretch ($\sim 1621\text{ cm}^{-1}$), indicating that no detectable concentration of $\text{C}=\text{C}$ bonds was observed using the gi-FTIR technique. The absence of the alkene stretch absorption from FTIR analysis has also recently been reported by Cheng et al.⁴⁶ in an FTIR study of pulsed plasma deposited bulk chemical DGpp thin films.

5 W



30 W

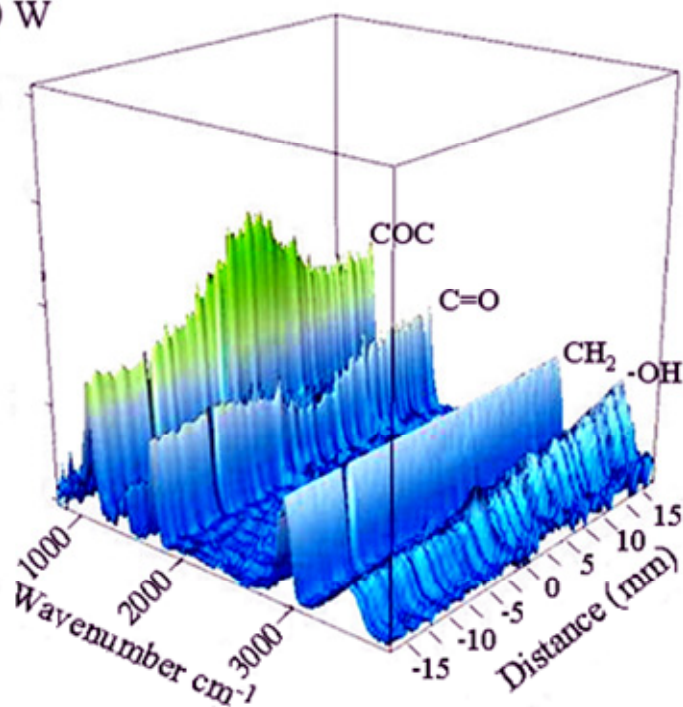


Figure 5.2 3D grazing incidence synchrotron source FTIR spectroscopy surface plots measured along the 5 and 30 W DGpp gradients. The spectra show the major functional groups observed are ether, carbonyl and hydroxyl groups (approx 1052, 1735 and 3450 cm^{-1} respectively). To avoid thickness effects contributing to the relative absorption of various functionalities, all peaks measured were relative to the normalized alkane stretch (~ 2850 to 3000 cm^{-1}).

5.4.3 X-Ray Photoelectron Spectroscopy

High resolution C 1s XPS analyses were performed across the two DGpp gradients to characterise their surface chemistry, and was compared to the bulk functional group analysis generated from the gi-FTIR microspectroscopy data. Figure 5.3 presents 3D plots of data generated from high-resolution C 1s analyses of the 5 and 30W gradient films. Analysis of the C 1s spectra revealed four main contributing chemical components including C-C and C-H (hydrocarbon), C-OR (ether and alcohol), C=O (ketone and aldehyde) and COOR (carboxylic acid and ester). The central region of both the 5W and 30W gradients, retained the highest concentration of COR groups (~ 286.6 eV) indicating a higher retention of the monomer ether functionality. A systematic decrease in the ether (C-OR) functionality from the centre and across the gradient was observed, consistent with the gi-FTIR analysis of the bulk DGpp gradient film chemistries. The FTIR and XPS data show that the ether content of the 5 W gradient changes more dramatically at the surface than the bulk of the film. The opposite is true for the 30 W film with the gradient showing a stronger chemical spatial variation compared to the interfacial chemistry. C 1s analysis also revealed that the C-C/C-H (~ 285 eV), C=O (288 eV) and COOR (289.1 eV) functionalities were lowest in the centre (0 mm) and increased across the gradients. Gradients deposited at a 5 W load power retained more monomer-like functionality compared with the 30 W gradient, with higher concentrations of C-OR groups and lower concentrations of the C-C/C-H, C=O and COOR functionalities. The 5W gradient film yielded C-OR concentrations ranging from 79 % at the centre (0 mm) to 57 % at 10 mm, compared with 46% (0mm) to 25 % (10mm) for the 30W films. The loss of COR functional groups corresponded with an increase in hydrocarbon species and in the 30W gradient film, the concentration of COR units in the central region is equivalent to the concentration of hydrocarbon (CC/CH) units. There was a small variation in the concentration of C=O and COOR functionalities between gradients; however aldehyde and ketone C=O groups were present at a higher concentration in both gradients compared to

the acidic and ester (COOR) groups. The central region of each gradient also had lower levels of C=O and COOR species.

Bretagnol *et al.*⁴⁷ reported on DGpp films deposited via pulsed rfgd plasma polymerisation yielding surfaces composed of 70-74% COR functionalities at a load power of 1W. While using continuous wave rfgd plasma polymerisation at a load power of 15 W, they report a final film COR content of just 40 %. This finding is interesting as it demonstrates that the geometry of the electrodes used in plasma polymer film deposition can have a significant influence over the final film chemistry and that using a continuous rfgd plasma polymerisation process we are able to obtain comparable results to that of a pulsed plasma technique. Similarly, Cheng *et al.*⁴⁶ recently reported the deposition of DG vapours using pulsed rfgd plasma polymerisation where the highest COR content was reported to be 72 % at a load power of 1 W. The 5 W gradients deposited for this study yielded COR contents of > 70 % within 2 mm either side of the gradient centre, decreasing to 57 % at a distance of 10 mm. Our generic approach therefore provides a one step deposition method for generating a gradient composition of COR functionalities and a high throughput platform for studying the chemical nature of these films. Previous studies of these types of plasma polymer films have necessitated the deposition of multiple samples to investigate their protein resistance and surface chemistries.

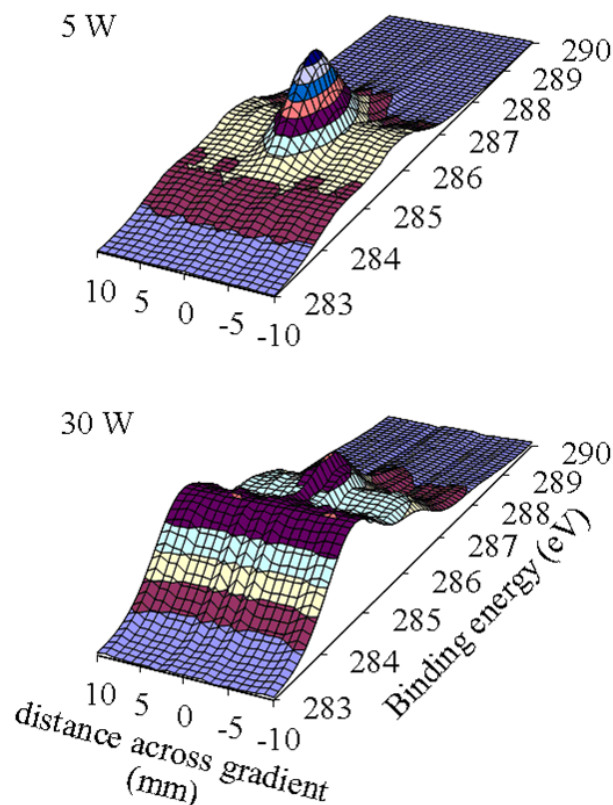


Figure 5.3 3D plot of high-resolution C 1s XPS spectra (Distance from centre of the gradient vs binding energy) taken across the DGpp gradients deposited at 5 and 30W. The spectra indicate that the central region of all the gradients retains the highest C-O component (C 1s binding energy of 286.6 eV). The C-O component concentration systematically decreases along the gradients and correlates to a parallel gain in C-C and C-H species.

3.4.4 NEXAFS spectroscopy

To further analyse the chemistry across the DGpp gradients, and detect any the orientation of terminal chains across the DGpp gradients, a C and O K-edge PEY NEXAFS spectroscopy study was performed. Analysis of the C 1s spectra revealed four main resonance features (Figure 5.4) including C 1s $\rightarrow \pi^*$ ($\text{C}=\text{O}$) excitation at ~ 285.7 eV (A), C 1s $\rightarrow \sigma^*$ ($\text{C}-\text{H}$) at ~ 287.3 eV (B), C 1s $\rightarrow \sigma^*$ ($\text{C}-\text{O}$) at ~ 289.9 eV (C) and a broader C 1s $\rightarrow \sigma^*$ ($\text{C}-\text{C};\text{C}-\text{O}$) feature at ~ 294.4 eV (D). Due to the multiphoton resonance absorptions and the broader nature of the higher energy σ -bonded species, only the two lower energy features ($\text{C}=\text{O} \pi^*$ and $\text{C}-\text{H} \sigma^*$) will be compared and discussed. To quantify and compare the relative concentration of these various bonded species, spectral features were integrated using a curve fitting procedure (discussed in the methods section) and the area compared across the gradients and between the gradients

deposited at the two load powers (see Appendix 1 for example curve fits and O K-edge NEXAFS results and analysis)

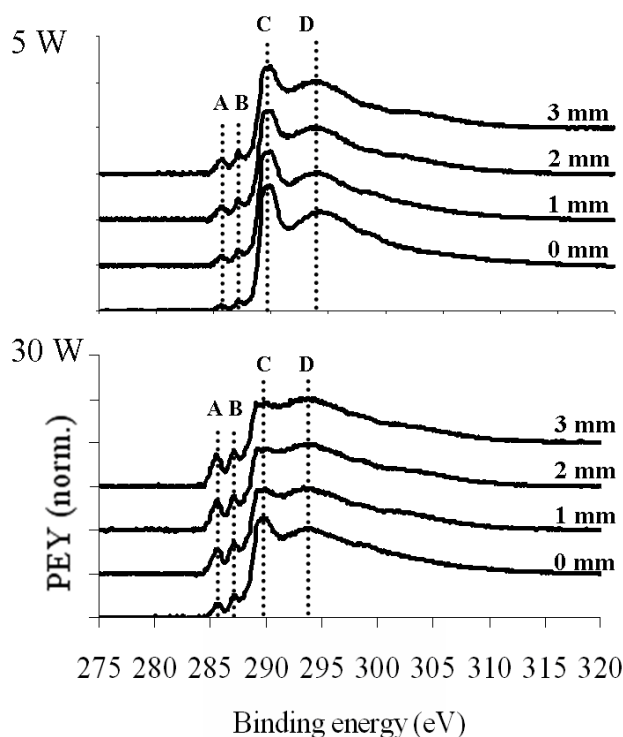


Figure 5.4 C 1s K-edge NEXAFS spectra plotted across the 5W and 30W DGpp gradient films between 0 and 3 mm. (A= C 1s \rightarrow π^* (C=O), B= C 1s \rightarrow σ^* (C-H), C= C 1s \rightarrow σ^* (C-O), D= C 1s \rightarrow σ^* (C-C;C-O)). The central region of each gradient and films deposited at lower load power retained lower C=O and CH species, which systematically increase outwards.

Results presenting the integrated area plots of the C=O π^* and C-H σ^* resonance features from the C 1s K-edge spectra, plotted across the two DGpp gradients (5 and 30 W) 3mm either side of the centre (0 mm) show that the centre of each gradient had lower concentrations of carbonyl (C=O) and hydrocarbon species (Appendix 1), systematically increasing outwards. This is consistent with the data obtained from XPS and gi-FTIR analysis. Higher levels of carbonyl and hydrocarbon species were introduced into the gradients as the load power was increased during plasma deposition. This is also consistent with information reported by Swaraj *et al.*⁴⁸, who analysed pulsed-plasma deposited ethylene

samples using NEXAFS and reported that films deposited under higher load powers contained higher levels of carbonyls.

The use of NEXAFS as a tool for the analysis of plasma polymers^{45, 49-51} and PEG-like films is in its infancy. Zwahlen et al.⁵² reported a C and O K-edge NEXAFS analysis of oligo(ethylene glycol) (OEG) terminated alkanethiol SAMs on gold and their reported peak assignments are consistent with those reported in Figures 5.4. They investigated the degree of order in OEG-SAMs films made from different length oligomers and found that only shorter length oligomers showed a weak angular dependence. Due to the fragmentation, polymerisation and cross-linking process that occur during plasma polymerisation, both the C 1s and O 1s NEXAFS spectra obtained for the DGpp gradients have the additional C=O π^* resonance features when compared to OEG SAMs. A number of researchers have used NEXAFS spectroscopy as part of a combinatorial approach to the analysis of surface gradients by mapping the surface chemistry as well as varying the polarisation of the light source, in order to detect any preferred orientation of the surface bound materials.^{9, 10} We performed similar experiments to test for any possible orientation of polymer chains in the DGpp film gradients analysing C and O K-edge NEXAFS spectra using both horizontally and vertically polarised light. No difference was seen in spectra obtained from horizontally or vertically polarised light, indicating no preferred orientation, presumably due to the amorphous and cross-linked nature of the plasma polymer (dry) films in vacuum when analysed.

5.4.5 Surface Derivatisation

Spectroscopic analysis of the DGpp gradient films revealed contributions from a number of chemical functionalities. To further deduce specific chemical functionalities that may have been present in the films such as residual hydroxyl, aldehyde/ketone and acid groups, a chemical derivatisation study was performed on the 5 and 30 W DGpp gradient films. Derivatisation of surface functionalities with reactive fluorinated compounds has been well reported and discussed^{53, 54} in the literature for use as XPS markers, since XPS cannot, for example, differentiate between certain chemical functionalities such as hydroxyls and ethers in the COR C1s component. By using a gas phase reaction between any potential surface hydroxyl species along the DGpp gradients with trifluoroacetic anhydride (TFAA),⁵⁵ it is possible to deduce the concentration (Equation 1) of residual hydroxyl groups on the surface and therefore the actual concentration of surface ether groups. It is important to note, however that surface derivatisation might only access the reactive groups at the top surface whereas the C-O-R XPS signal originates from a 5 – 10 nm thick surface layer. Figure 5.5A presents the F/C plots from quantified XPS survey spectra across the 5 and 30W DGpp gradient films after derivatisation with TFAA. Interestingly the two films show opposite trends in terms of their hydroxyl content with distance from the centre of the film. Results indicate a higher total surface concentration of hydroxyl functionalities across the 5W DGpp gradient with a slightly lower level in the centre (0 mm) of the gradient. The 30W DGpp gradient displayed a high concentration of hydroxyl species in the centre of the gradient which systematically decreased moving outwards across the gradient. Using this data the normalised surface ether concentration was calculated across the 5 and 30 W gradients and Figure 5.5B shows the ether concentration plotted both before and after subtracting the hydroxyl contributions (to the COR C 1s component). The actual ether concentration across the 5 W gradients was then calculated ranging from 74 % (0 mm) to 51 % (10 mm) while the 30 W ranged from 41 % (0 mm) to 23 % (10 mm). Although the 5 W DGpp gradient films

may contain more surface hydroxyl species, overall it has a far greater concentration of 'monomer like' ether functionalities retained in the film when compared to the 30 W gradient films. This result highlights the fact that as the plasma power is increased a greater number of oxygen containing chemical functionalities are being generated during and possibly after thin film deposition, within the surface and bulk of the DGpp gradient coatings.

Spectroscopic analysis of the films alluded to possible reactive chemical functionalities such as aldehyde, ketone and acidic groups. Their presence may have significant consequences for biomedical coatings produced using DGpp and their possible reactivity towards biological species such as proteins. Surface bound aldehydes and ketones may readily react with amine groups located on many proteins. Residual acid groups on the DGpp surface which we have investigated previously on bulk DGpp surface coatings⁵⁶ may also aid in enhancing electrostatic interactions with biomolecules and possibly hinder the performance of these types of coatings *in vivo* and *in vitro*. To investigate further any possible reactivity of these residual chemistries the 5 and 30 W gradients (Fig 5C) were incubated with the amine functional graft co-polymer of poly(L-lysine) and poly(ethylene glycol) (PLL-g-PEG).⁵⁷ It was envisioned that any covalent coupling through covalent reactions of the PLL-g-PEG primary amine groups with either aldehydes or ketones and electrostatic interactions with residual acid functionalities may be observed via XPS through the appearance of a nitrogen signal. XPS and NEXAFS surface analysis confirmed that the central region of each gradient was shown to have the lowest aldehyde/ketone and acid/ester components with the 30W generated gradient having the greatest concentration of these species. The assembly on the 5 and 30 W gradients of the polycationic PLL-g-PEG (e.g. oppositely charged to the carboxylate presenting DGpp) follows a similar trend to that found for these functionalities indicating there is indeed an interaction of the polymer with these species.

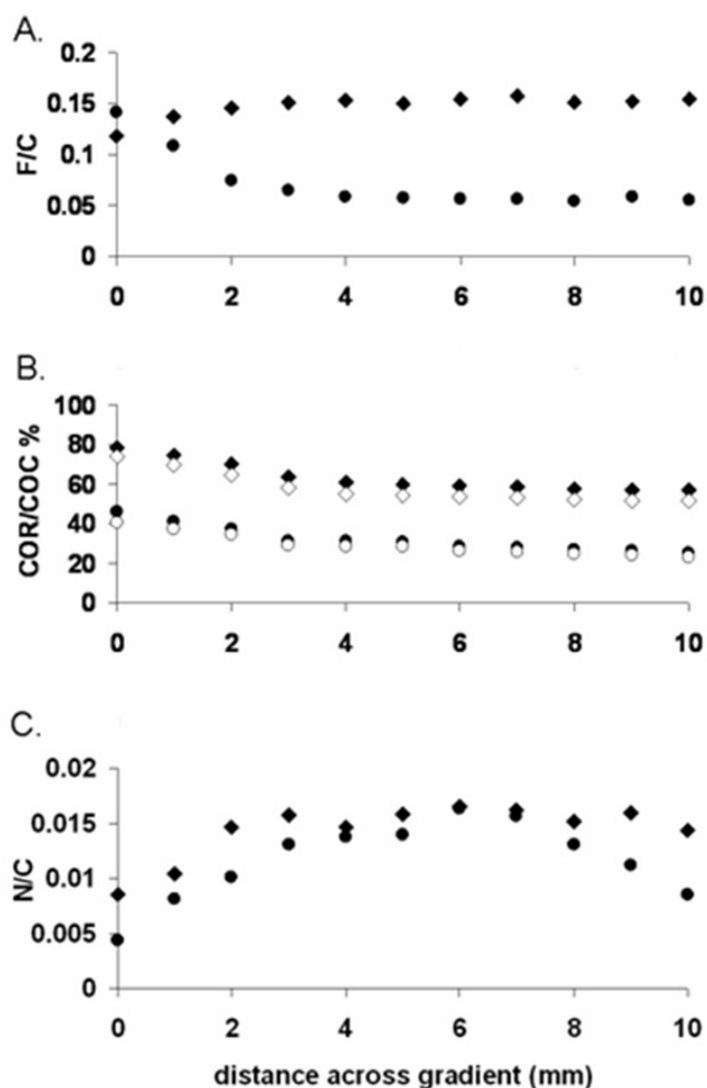


Figure 5.5 XPS elemental and chemical species analysis from C 1s curve fits and survey spectra of the 5 and 30 W gradient DGpp thin films; A. The resulting F/C values plotted across the 5 (◆) and 30W (●) gradient films after gas phase derivatisation of surface hydroxyl groups using TFAA. B. The ‘actual’ surface ether content was calculated across the gradients before and after chemical derivatisation of surface hydroxyl groups from the COR component of the C 1s curve-fit (hollow symbols represent the normalised ether content after surface derivatisation). C. The resultant N/C values plotted across the 5 and 30 W gradient films after incubation with PLL-g-PEG.

It is difficult to categorically deduce whether the polymer is interacting electrostatically, through hydrophobic forces or by formation of covalent bonds with the gradient surfaces. The formation of covalent bonds without specific activation of the carboxylic acid surface functionalities with amine functionalities in the PLL-g-PEG is rather unlikely. However, it is

possible that there are hydrophobic-hydrophobic interactions occurring between the side chains of the lysine residues with local hydrophobic domains in the DGpp surfaces. The use of PLL-g-PEG as a low fouling coating is well documented in the literature and has been reported useful for reducing protein adsorption onto metal oxide surfaces^{57, 58}, as well as inhibiting bacteria adhesion. Using the surface functionalities introduced across the DGpp gradients during polymerisation, we have effectively formed gradients of PLL-g-PEG that could be useful in studying the interactions of various proteins, bacteria and cells and shows the versatility of these PEG-like chemical gradients.

5.4.6 Protein Adsorption

To test the protein adsorption properties of the DGpp gradients, the adsorption of three proteins of varied size and charge (bovine serum albumin, (BSA) lysozyme, (Lys) and γ -globulin, (IgG)) was analysed via the appearance of nitrogen with XPS (protein detection limit ~ 10 ng/cm²). The N/C ratio measured across the 5 and 30 W DGpp gradients was plotted as a function of the actual ether content (COC) of the gradient films (after subtraction of the C-OH contributions via TFAA derivitisation) (Figure 5.6). By using proteins of varying charge and size at a concentration of 1 mg/ml in PBS, it was hypothesized that we could more thoroughly interrogate the critical parameters related to the production of low fouling PEG-like plasma polymer films. BSA has a net negative charge at physiological pH (pI = 4.7) and a Mw of ~ 69 kDa, lysozyme has a net positive charge at physiological pH (pI = 11.1) and is a smaller molecule with a molecular weight of ~ 14.6 kDa, while the IgGs are larger proteins with a molecular weight of ~ 150 kDa, an overall neutral charge at physiological pH and (pI of 7.3). The adsorption of each protein systematically increased across the gradients correlating with regions of lower ether content and higher carbonyl, carboxylic acid and hydrocarbon species, forming adsorbed protein gradients.

The 5W gradient adsorbed no BSA as measured by XPS across its entirety. Lysozyme adsorption was not detected in the central region of the 5 W gradients, however, the N/C ratio increased across the surface gradient at an ether content of less than 70%. The IgGs adsorbed across both the 5 and 30 W gradients with significantly higher amounts detected on the 30 W gradient film. We believe this is in part due to the inherently ‘sticky’ nature of these molecules, their larger size and the lack of any small contribution from electrostatic repulsion effects under the conditions used in this work. In the centre of the 5 W gradient only a small amount of IgG was detected.

A comparison of the adsorption behaviour of BSA and lysozyme on the 30W gradient showed an opposite situation to that of the 5 W film with more BSA adsorbing than lysozyme for the former surface. BSA was detected in slightly greater amounts across the 30W gradient with N/C values ranging from 0.012 to 0.056 over a 10mm distance when compared to the 5 W DGpp gradient. Lysozyme adsorption as measured via the N/C varied from ~ 0.04 to 0.07. The difference in adsorption behaviour of lysozyme and BSA between the 5 and 30 W gradients may be attributed to such phenomena as increased hydrophobic and electrostatic interactions between the surfaces and proteins. Previous work performed by our group⁵⁶ has shown that uniform DGpp films possess an overall negative charge at physiological pH, which in part helps explain one of the mechanisms involved in the low fouling nature of these DGpp coatings along with a high residual ether and low hydrocarbon content. Furthermore, we also highlighted the minimal electrostatic interactions of lower powered DGpp films, where the thickness of the films was shown to be less than the Debye length in low ionic strength solution.⁵⁶ Pasche et al.⁵⁷ has shown that lysozyme proteins behave in a similar manner to hard, positively charged particles, being attracted by negatively charged surfaces and repelled by positively charged surfaces (on PEGylated Nb₂O₅ surfaces). Analysis of the

surface charge across the DGpp gradients should be considered in the future and may confirm stronger negatively charged surfaces in gradients deposited at higher load power, which would help to confirm if it is the electrostatic interactions that are primarily driving the higher lysozyme adsorption across the 30 W DGpp gradient.

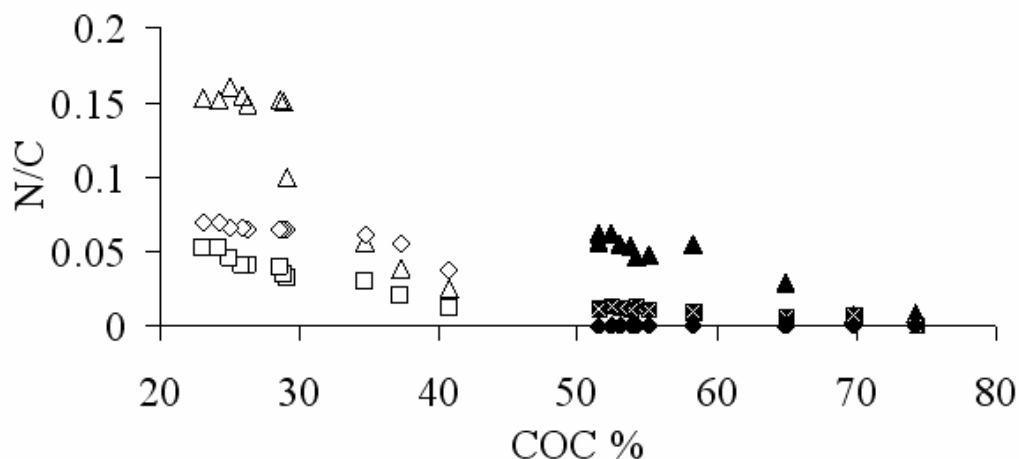


Figure 5.6 XPS N/C ratios measured after adsorption of BSA (◆), lysozyme (◻) and γ-globulins (▲) as a function of normalized residual ether content in the 5 W (solid symbols) and 30 W (hollow symbols) gradients.

It is clear from the spectroscopic characterization of the films that the 30 W gradient has significantly less ether and more hydrocarbon species along its length. It may be that higher adsorption of BSA across the 30 W gradient coating is driven by hydrophobic-hydrophobic interactions, which may overpower the electrostatic repulsions that occur between BSA proteins and the residual carboxylic acid species across the DGpp gradients. Also, the larger size of BSA compared to lysozyme, may contribute to a larger number of reactive terminal amine groups that could possibly interact covalently with the residual aldehyde and ketone groups shown to be present across the DGpp gradients from our spectroscopic studies. Further, when lysozyme does interact with surface defects and chemical entities that are not protein resistant and adsorb on the gradient surfaces, the smaller protein may be more effective at ‘blocking’ these sites and resisting further immobilization and interaction with additional lysozyme from solution than BSA.

5.5 Conclusions

A series of PEG-like chemical gradients were prepared using continuous wave radio-frequency glow discharge plasma polymerisation of diethylene glycol dimethyl ether (DG) at load powers of 5 and 30 W. A knife edge upper electrode was employed to produce the defined chemical gradients studied. Complementary surface analysis techniques were used to characterise the gradients, including grazing incidence-FTIR microspectroscopy, X-ray photoelectron spectroscopy and near edge X-ray absorption fine structure spectroscopy. We have found that the ether functionality systematically varies across the gradients with the highest 'PEG like' characteristics in the central region of the films deposited directly underneath the razor electrode. It was found that the hydrocarbon, ketone, aldehyde, acid and ester content varied across the gradients, being lowest in the central region increasing radially outwards. Films deposited at 5W retained higher ether contents and had lower levels of hydrocarbon and carbonyl functionalities than the 30W gradient films. Adsorbed protein gradients were formed and correlated well with the residual ether content from XPS analysis, with the central region of the gradients being the most protein resistant. Interestingly the observed adsorption trends of the negatively charged BSA and positively charged lysozyme was reversed across the 5 W and 30 W DGpp films. This simple, time-efficient and reproducible method of gradient generation not only produces surfaces that are ideal for the study and characterisation of low-fouling films and potentially their subsequent interaction with biomolecules and cells, but could potentially be useful in the generation of gradients presenting other surface functionalities by careful selection of the monomer species used.

5.6 Acknowledgements

This research was undertaken on the soft X-ray, (NEXAFS, BL6) and infra-red microscope (giFTIR microspectroscopy, BL8) beamlines at the Australian Synchrotron, Victoria,

Australia. We thank Kevin Prince for his helpful discussions towards interpretation of the NEXAFS data. We acknowledge the use of ‘Whooshka’ software program to perform the curve-fitting of the NEXAFS data. Ms Donna Menzies thanks the CSIRO OCE Scheme for funding her PhD scholarship stipend. Professor Marcus Textor acknowledges support from CSIRO’s OCE Distinguished Visiting Scientist Program.

5.7 References

1. Zelzer M, Majani R, Bradley JW, Rose F, Davies MC, Alexander MR. 2008 Investigation of cell-surface interactions using chemical gradients formed from plasma polymers. *Biomaterials*.**29**(2):172-184
2. Busscher HJ, Ruardy TG, Van der Mei HC, Schakenraad JM. 1997 Preparation and characterization of chemical gradient surfaces and their application for the study of cellular interaction phenomena. *Surface Science Reports*.**29**(1):3-30
3. Parry KL, Shard AG, Short RD, White RG, Whittle JD, Wright A. 2006 ARXPS characterisation of plasma polymerised surface chemical gradients. *Surface and Interface Analysis*.**38**(11):1497-1504
4. Shin YN, Kim BS, Ahn HH, Lee JH, Kim KS, Lee JY, et al. 2008 Adhesion comparison of human bone marrow stem cells on a gradient wettable surface prepared by corona treatment. *Applied Surface Science*.**255**(2):293-296
5. Yang J, Rose F, R. A. J. , Gadegaard N, Morgan AR. 2009 A High-Throughput Assay of Cell-Surface Interactions using Topographical and Chemical Gradients. *Advanced Materials*.**21**(3):300-304
6. Lee JH, Lee HB. 1998 Platelet adhesion onto wettability gradient surfaces in the absence and presence of plasma proteins. *Journal of Biomedical Materials Research*.**41**(2):304-311
7. Blondiaux N, Morgenthaler S, Pugin R, Spencer ND, Liley M. 2008 Gradients of topographical structure in thin polymer films. *Applied Surface Science*.**254**(21):6820-6825
8. Ekblad T, Andersson O, Tai FI, Edeith T, Liedberg B. 2009 Lateral control of protein adsorption on charged polymer gradients. *Langmuir*.**25**(6):3755-3762
9. Fischer DA, Efimenko K, Bhat RR, Sambasivan S, Genzer J. 2004 Mapping Surface Chemistry and Molecular Orientation with Combinatorial Near-Edge X-Ray Absorption Fine Structure Spectroscopy. *Macromolecular Rapid Communications*.**25**(1):141-149
10. Genzer J, Fischer DA, Efimenko K. 2003 Combinatorial near-edge x-ray absorption fine structure: Simultaneous determination of molecular orientation and bond concentration on chemically heterogeneous surfaces. *Applied Physics Letters*.**82**(2):266-268
11. Wong JY, Velasco A, Rajagopalan P, Pham Q. 2003 Directed movement of vascular smooth muscle cells on gradient-compliant hydrogels. *Langmuir*.**19**(5):1908-1913
12. Pelham Jr RJ, Wang YL. 1997 Cell locomotion and focal adhesions are regulated by substrate flexibility. *Proceedings of the National Academy of Sciences of the United States of America*.**94**(25):13661-13665
13. Smith JT, Tomfohr JK, Wells MC, Beebe TP, Kepler TB, Reichert WM. 2004 Measurement of Cell Migration on Surface-Bound Fibronectin Gradients. *Langmuir*.**20**(19):8279
14. Singh M, Berkland C, Detamore MS. 2008 Strategies and applications for incorporating physical and chemical signal gradients in tissue engineering. *Tissue Engineering - Part B: Reviews*.**14**(4):341-366

15. Vasilev K, Mierczynska A, Hook AL, Chan J, Voelcker NH, Short RD. Creating gradients of two proteins by differential passive adsorption onto a PEG-density gradient. *Biomaterials*.**31**(3):392-397
16. DeLong SA, Gobin AS, West JL. 2005 Covalent immobilization of RGDS on hydrogel surfaces to direct cell alignment and migration. *Journal of Controlled Release*.**109**(1-3):139-148
17. Morgenthaler S, Zink C, Spencer ND. 2008 Surface-chemical and -morphological gradients. *Soft Matter*.**4**(3):419-434.(10.1039/b715466f)
18. Genzer J, Bhat RR. 2008 Surface-Bound Soft Matter Gradients. *Langmuir*.**24**(6):2294
19. Bhat RR, Tomlinson MR, Wu T, Genzer J. Surface-grafted polymer gradients: Formation, characterization, and applications. Surface- Initiated Polymerization II. Berlin: Springer-Verlag Berlin; 2006. p. 51-124.
20. Li B, Ma Y, Wang S, Moran PM. 2005 Influence of carboxyl group density on neuron cell attachment and differentiation behavior: Gradient-guided neurite outgrowth. *Biomaterials*.**26**(24):4956-4963
21. Iwasaki Y, Ishihara K, Nakabayashi N, Khang G, Jeon JH, Lee JW, et al. 1998 Platelet adhesion on the gradient surfaces grafted with phospholipid polymer. *Journal of Biomaterials Science, Polymer Edition*.**9**(8):801-816
22. Lee SJ, Khang G, Lee YM, Lee HB. 2003 The effect of surface wettability on induction and growth of neurites from the PC-12 cell on a polymer surface. *Journal of Colloid and Interface Science*.**259**(2):228-235
23. Lee TG, Shon HK, Kim MS, Lee HB, Moon DW. 2006 ToF-SIMS imaging of gradient polyethylene and its amine-functionalized surfaces. *Applied Surface Science*.**252**(19):6754-6756
24. Jeong BJ, Lee JH, Lee HB. 1996 Preparation and Characterization of Comb-like PEO Gradient Surfaces. *Journal of Colloid And Interface Science*.**178**(2):757-763
25. Liedberg B, Wirde M, Tao YT, Tengvall P, Gelius U. 1997 Molecular Gradients of omega-Substituted Alkanethiols on Gold Studied by X-ray Photoelectron Spectroscopy. *Langmuir*.**13**(20):5329-5334
26. Morgenthaler S, Lee S, Zürcher S, Spencer ND. 2003 A Simple, Reproducible Approach to the Preparation of Surface-Chemical Gradients. *Langmuir*.**19**(25):10459-10462
27. Vasilev K, Mierczynsk A, Hook A, Chan J, Voelcker NH, Short R D. 2010 Creating gradients of two proteins by differential passive adsorption onto a PEG-density gradient. *Biomaterials*.**31**:392-397
28. Wells N, Baxter MA, Turnbull JE, Murray P, Edgar D, Parry KL, et al. 2009 The geometric control of E14 and R1 mouse embryonic stem cell pluripotency by plasma polymer surface chemical gradients. *Biomaterials*.**30**(6):1066-1070
29. Ogumi Z, Abe T, Nakamura S, Inaba M. 1999 Functionally gradient polymer electrolyte prepared by plasma polymerization. *Solid State Ionics*.**121**(1):289-293
30. Robinson DE, Marson A, Short RD, Buttle DJ, Day AJ, Parry KL, et al. 2008 Surface gradient of functional heparin. *Advanced Materials*.**20**(6):1166-1169
31. Lee JH, Lee HB. 1993 A wettability gradient as a tool to study protein adsorption and cell adhesion on polymer surfaces. *Journal of Biomaterials Science Polymer Edition*.**4**(5):467-481

32. Khang G, Rhee JM, Lee JH, Lee I, Lee HB. 2000 Interaction of Different Types of Cells on Poly(L-lactide-co-glycolide) Surface with Wettability Chemogradient. *Korea Polymer Journal*.**8**(6):276-284
33. Spijker HT, Bos R, van Oeveren W, de Vries J, Busscher HJ. 1999 Protein adsorption on gradient surfaces on polyethylene prepared in a shielded gas plasma. *Colloids and Surfaces B: Biointerfaces*.**15**(1):89-97
34. Xu LC, Siedlecki CA. 2007 Effects of surface wettability and contact time on protein adhesion to biomaterial surfaces. *Biomaterials*.**28**(22):3273-3283
35. Li B, Ma Y, Wang S, Moran PM. 2005 A technique for preparing protein gradients on polymeric surfaces: Effects on PC12 pheochromocytoma cells. *Biomaterials*.**26**(13):1487-1495
36. Spijker HT, Bos R, Busscher HJ, van Kooten TG, van Oeveren W. 2002 Platelet adhesion and activation on a shielded plasma gradient prepared on polyethylene. *Biomaterials*.**23**(3):757-766
37. Corum LE, Hlady V. Screening platelet-surface interactions using negative surface charge gradients. *Biomaterials*.**31**(12):3148-3155
38. Sheth SR, Leckband D. 1997 Measurements of attractive forces between proteins and end-grafted poly(ethylene glycol) chains. *Proceedings of the National Academy of Sciences of the United States of America*.**94**(16):8399-8404.(10.1073/pnas.94.16.8399)
39. Szleifer I. 1997 Protein adsorption on tethered polymer layers: effect of polymer chain architecture and composition. *Physica A*.**244**(1-4):370-388
40. Kingshott P, Thissen H, Griesser HJ. 2002 Effects of cloud-point grafting, chain length, and density of PEG layers on competitive adsorption of ocular proteins. *Biomaterials*.**23**(9):2043-2056
41. Li L, Chen S, Zheng J, Ratner BD, Jiang S. 2005 Protein Adsorption on Oligo(ethylene glycol)-Terminated Alkanethiolate Self-Assembled Monolayers: The Molecular Basis for Nonfouling Behavior. *The Journal of Physical Chemistry B*.**109**(7):2934-2941
42. Latour RA. 2006 Thermodynamic perspectives on the molecular mechanisms providing protein adsorption resistance that include protein-surface interactions. *Journal of Biomedical Materials Research Part A*.**78A**(4):843-854
43. Watts JF. High resolution XPS of organic polymers: The Scienta ESCA 300 database. G. Beamson and D. Briggs. 280pp., £65. John Wiley & Sons, Chichester, ISBN 0471 935921, (1992)1993.
44. Watts B, Thomsen L, Dastoor PC. 2006 Methods in carbon K-edge NEXAFS: Experiment and analysis. *Journal of Electron Spectroscopy and Related Phenomena*.**151**(2):105-120
45. Shard AG, Whittle JD, Beck AJ, Brookes PN, Bullett NA, Talib RA, et al. 2004 A NEXAFS Examination of Unsaturation in Plasma Polymers of Allylamine and Propylamine. *The Journal of Physical Chemistry B*.**108**(33):12472-12480
46. Cheng Q, Komvopoulos K. 2009 Synthesis of Polyethylene Glycol-Like Films from Capacitively Coupled Plasma of Diethylene Glycol Dimethyl Ether Monomer. *The Journal of Physical Chemistry C*.**113**(1):213-219
47. Brétagne F, Lejeune M, Papadopolou-Bouraoui A, Hasiwa M, Rauscher H, Ceccone G, et al. 2006 Fouling and non-fouling surfaces produced by plasma polymerization of ethylene oxide monomer. *Acta Biomaterialia*.**2**(2):165-172

48. Swaraj S, Oran U, Lippitz A, Schulze RD, Friedrich JF, Unger WES. 2005 Surface analysis of plasma-deposited polymer films, 4a: In situ characterization of plasma-deposited ethylene films by XPS and NEXAFS. *Plasma Processes and Polymers*.**2**(4):310-318
49. Kim Y, Kim KJ, Lee Y. 2009 Surface analysis of fluorine-containing thin films fabricated by various plasma polymerization methods. *Surface and Coatings Technology*.**203**(20-21):3129-3135
50. Oran U, Swaraj S, Lippitz A, Unger WES. 2006 Surface Analysis of Plasma Deposited Polymer Films, 7. *Plasma Processes and Polymers*.**3**(3):288-298
51. Friedrich JF, Geng S, Unger W, Lippitz A, Erdmann J, Gorsler HV, et al. 1995 Plasma functionalization and reorientation of macromolecules at polymer surfaces. *Surface and Coatings Technology*.**74-75**(Part 2):664-669
52. Zwahlen M, Herrwerth S, Eck W, Grunze M, Hahner G. 2003 Conformational Order in Oligo(ethylene glycol)-Terminated Self-Assembled Monolayers on Gold Determined by Soft X-ray Absorption. *Langmuir*.**19**(22):9305-9310.(10.1021/la0350610)
53. Buchholz V, Adler P, Bäcker M, Hölle W, Simon A, Wegner G. 1997 Regeneration and Hydroxyl Accessibility of Cellulose in Ultrathin Films. *Langmuir*.**13**(12):3206-3209
54. Chilkoti A, Castner DG, Ratner BD, Briggs D. 1990 Surface characterization of a poly(styrene/p-hydroxystyrene) copolymer series using x-ray photoelectron spectroscopy, static secondary ion mass spectrometry, and chemical derivatization techniques. *Journal of Vacuum Science & Technology A*.**8**(3):2274-2282
55. Friedrich J, Unger W, Lippitz A, Geng S, Koprinarov I, Kühn G, et al. 1998 Modelling plasma-induced reactions on polymer surfaces using aliphatic self-assembling and LB layers. *Surface and Coatings Technology*.**98**(1-3):1132-1141
56. Muir BW, Tarasova A, Gengenbach TR, Menzies DJ, Meagher L, Rovere F, et al. 2008 Characterization of Low-Fouling Ethylene Glycol Containing Plasma Polymer Films. *Langmuir*.**24**(8):3828-3835
57. Blättler TM, Pasche S, Textor M, Griesser HJ. 2006 High Salt Stability and Protein Resistance of Poly(l-lysine)-g-poly(ethylene glycol) Copolymers Covalently Immobilized via Aldehyde Plasma Polymer Interlayers on Inorganic and Polymeric Substrates. *Langmuir*.**22**(13):5760-5769
58. Pasche S, De Paul SM, Janos V, Spencer ND, Textor M. 2003 Poly(l-lysine)-graft-poly(ethylene glycol) Assembled Monolayers on Niobium Oxide Surfaces: A Quantitative Study of the Influence of Polymer Interfacial Architecture on Resistance to Protein Adsorption by ToF-SIMS and in Situ OWLS. *Langmuir*.**19**(22):9216-9225.(10.1021/la034111y)
59. Pasche S, Voros J, Griesser HJ, Spencer ND, Textor M. 2005 Effects of ionic strength and surface charge on protein adsorption at PEGylated surfaces. *Journal of Physical Chemistry B*.**109**(37):17545-17552.(10.1021/jp050431+)

Chapter 6:

**An XPS and TOF-SIMS study of protein
and cell adsorption across PEG-like plasma
polymer films with lateral compositional
gradients**

PART B: Suggested Declaration for Thesis Chapter

Monash University

Declaration for Thesis Chapter 6

Declaration by candidate

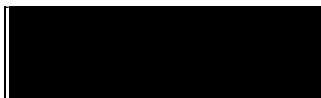
In the case of Chapter 6, the nature and extent of my contribution to the work was the following:

Nature of contribution	Extent of contribution (%)
Experimental design and conduct, data processing, manuscript writing	70 %

The following co-authors contributed to the work. Co-authors who are students at Monash University must also indicate the extent of their contribution in percentage terms:

Name	Nature of contribution	Extent of contribution (%) for student co-authors only
Marek Jasieniak	Assisted in experimental conduct and data processing	
Hans Griesser	Assisted in experimental design and manuscript corrections	
John Forsythe	Assisted in experimental design and manuscript corrections	
Graham Johnson	Assisted in experimental conduct and data processing	
Gail McFarland	Assisted in experimental conduct and data processing	
Ben Muir	Assisted in experimental design and manuscript corrections	

Candidate's
Signature



Date

30/05/2011

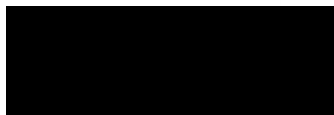

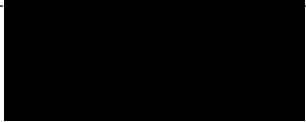
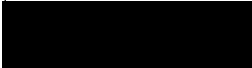
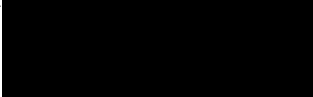
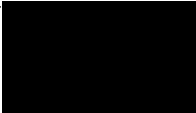
Declaration by co-authors

The undersigned hereby certify that:

- (1) the above declaration correctly reflects the nature and extent of the candidate's contribution to this work, and the nature of the contribution of each of the co-authors.
- (2) they meet the criteria for authorship in that they have participated in the conception, execution, or interpretation, of at least that part of the publication in their field of expertise;
- (3) they take public responsibility for their part of the publication, except for the responsible author who accepts overall responsibility for the publication;
- (4) there are no other authors of the publication according to these criteria;
- (5) potential conflicts of interest have been disclosed to (a) granting bodies, (b) the editor or publisher of journals or other publications, and (c) the head of the responsible academic unit; and
- (6) the original data are stored at the following location(s) and will be held for at least five years from the date indicated below:

Location(s)

CSIRO, Materials Science and Engineering

Signature	Date
Marek Jasieniak Ian Wark Research Institute, University of South Australia	
Hans Griesser Ian Wark Research Institute, University of South Australia	
John Forsythe Materials Engineering, Monash University	
Graham Johnson CSIRO, Materials Science and Engineering	
Gail McFarland CSIRO, Materials Science and Engineering	
Ben Muir CSIRO, Materials Science and Engineering	

30/5/2011
30 May 2011
5/7/11
31/5/2011
31.05.2011
30/5/11

.....

6. An XPS and TOF-SIMS study of protein and cell adsorption across PEG-like plasma polymer films with lateral compositional gradients

Donna J. Menzies^{1,2}, Marek Jasieniak³, Hans J. Griesser³, John Forsythe², Graham Johnson¹, Gail McFarland¹, Benjamin W. Muir^{1*}

1. CSIRO, Molecular and Health Technologies, Clayton, VIC, 3168, Australia

2. Monash University, Materials Engineering, Clayton, VIC, 3800, Australia

3. University of South Australia, SA, Australia

6.1 Abstract

In this work we report a detailed X-ray photoelectron spectroscopy (XPS) and time-of-flight secondary ion mass spectroscopy (TOF-SIMS) study of poly(ethylene glycol) PEG-like chemical gradients deposited via plasma enhanced chemical vapour deposition (PECVD) using diethyleneglycol dimethyl ether (DG) as a monomer. Principal component analysis (PCA) was applied to the TOF-SIMS data both before and after protein adsorption on the plasma polymer thin films. Results of the PCA loadings indicated a higher content of positive related hydrocarbon fragments across the 30 W gradient, which adsorbed higher amounts of proteins. Gradients deposited at lower load power retained a higher degree of monomer like functionality as did the central region directly underneath the knife edge electrode. Analysis of the adsorption of serum proteins (human serum albumin and fetal bovine serum) was monitored across the gradient films and increased with decreasing ether (PEG-like) film chemistries. The effect of protein

incubation time on the levels adsorbed in the plasma polymer films was critical with significantly more protein adsorbing after 24 hour incubation times. The attachment of HeLa cells on the gradients was observed and appeared to be dictated not only by the surface chemistry, but also by the adsorption of serum proteins.

Keywords: plasma polymer, PEG, gradient, TOF-SIMS, protein adsorption, diglyme, cell attachment

6.2 Introduction

In the field of biomaterials the host bodies' acceptance and ultimate performance of various implants and biomedical devices can be critically dependant on resisting or controlling the non-specific adsorption of proteins and cells. The irreversible adsorption of proteins onto these surfaces can severely affect their desired function and result in an inflammatory response or infection, in the case of tissue contacting via the promotion of macrophage adhesion¹ and surface induced thrombosis in the case of blood contacting devices. Furthermore, it has been suggested that cell attachment is governed by the adsorption of serum proteins containing cell signaling sequences and their resulting, adsorbed conformation.² Biosensor and diagnostic devices are among other numerous *in vitro* materials that rely heavily on reducing non specific protein adsorption for their success.³

The chemistry of a surface largely dictates biological interactions and can also result in variations of other physical properties of the film/surface such as wettability, cross-link density, swelling, solvation and roughness. As such it is critical that a thorough analysis

of a biomaterials surface chemistry and an understanding of the complex physico-chemical properties that govern surface interface interactions with biological molecules is achieved. To this end, gradient surfaces provide an excellent platform in which to study many competing surface properties in an efficient manner. These gradient surfaces provide a high throughput and/or combinatorial approach for optimising the interactions of various proteins, biomolecules and cells with a material of interest⁴ while vastly reducing the need for multiple surface preparations. Furthermore, gradient surfaces provide a physiologically relevant environment for predicting the behaviors of specific biomolecules of interest in vitro and in vivo, since many physiological events such as cell migration, differentiation and chemotaxis are driven by gradients of specific proteins and peptides that provide directional cues.⁵ Since it is largely the surface interface that dictates the resulting biological interactions, it is important that the chemical analysis techniques employed are highly surface sensitive⁶ including techniques such as time of flight secondary ion mass spectroscopy (TOF-SIMS)⁷⁻¹⁰, X-ray photoelectron spectroscopy (XPS)^{11, 12} and near edge X-ray adsorption fine structure (NEXAFS).^{12, 13}

To date, a number of methods of generating surface gradients¹⁴⁻¹⁷ with various properties have been reported, including variations in chemistry, wettability, topography, molecular orientation, and surface charge. There are a number of methods used to produce surface chemical gradients and a vast number of these have relied on the modification of self assembled monolayer's (SAMs) via various diffusion process techniques.^{4, 18} The use of corona discharge¹⁹⁻²¹ and radio-frequency plasma treatment²²⁻²⁵ have also been reported, and these methods have the distinct advantage over other deposition methods since it is

not restricted to a specific substrate or attachment functionality.²⁶ In this work we have used a plasma polymer gradient using DG as a model monomer to study the effects of film chemistry on protein adsorption and cell attachment. The chemistry of the films generated (in particular the ether content) can be systematically varied by manipulation of the deposition parameters including load power and monomer flow rate and the films produced are generally extremely smooth, making them ideal model surfaces to investigate the effects of surface chemistry on protein and cellular interactions. This study was conducted as the performance of biomaterials vastly relies on their ability to resist non-specific protein adsorption, and many researchers have employed the “low-fouling” nature of PEG like materials to impart this property into the synthetic biomaterial²⁷⁻³³. PEG’s low protein fouling nature can be attributed to a combination of enthalpic and entropic effects.¹⁸ However the exact chemistries required to achieve these properties can be difficult to optimize in plasma polymer vacuum deposition equipment. We were interested to determine what DG plasma polymer surface chemistries if any, were resistant to protein and cell adhesion as well as determining what plasma polymer surface chemistries could be supportive of protein and cell adhesion.

Previous studies have shown the benefits of using plasma polymer gradients to study cell-surface interactions. Zelzer et al.²⁵ formed chemical gradients from the plasma polymerization of hexane and allylamine (via diffusion of the gaseous monomers under a fixed mask) and used them to investigate the attachment and proliferation of fibroblast cells. The study indicated that initial cell attachment density differed as a function of the specific chemistry across the gradient which contrasted with their attachment upon a

chemically equivalent, uniform surface. They suggest this could be due to differences in cell-cell signalling or greater number of proteins produced from the surrounding cells between the different substrate types. This is an interesting finding and is something that should be considered when using surface gradients as a high throughput method for optimizing surface-biological interactions. Robinson et al.²³ also reported on the generation of chemical gradients formed via plasma polymerization using a mixture of allylamine and octadiene monomers. They were able to form functional heparin gradients, where the adsorption and function (protein binding activity) varied as a product of the allylamine gradient. It was found that the adsorption of higher amounts of heparin did not correspond to a continued increase in functionality.

The use of PEG based gradients is becoming an increasingly popular tool for the study and optimization of cell attachment, proliferation and viability. Jeong et al.²¹ formed gradients in the density of comb-like PEO chains prepared on low density polyethylene (PE) sheets by corona discharge treatment that were subsequently grafted with poly(ethylene glycol) mono-methacrylate (PEG-MA). Wang et al.³⁴ utilized PEG molecules in the formation of a two component chemical gradient to control protein adsorption. A PEG thiol and 11-amino-1-undecanethiol was used to form covalently linked gradients of epidermal growth factor (EGF) a signaling molecule, via carbodiimide coupling chemistry. Lower EGF adsorption occurred at higher PEG concentrations. More recently Vasilev et al.²² has demonstrated the use of PEG density gradients to create gradients of two proteins of differing size (lysozyme and fibrinogen). Delong et al.³⁵ used PEG-based hydrogels with a gradient of covalently immobilized RGDS to

study the effect of fibroblast growth migration and alignment. It was found that the fibroblasts changed their morphology to align in the direction of increasing RGDS concentration and that the slope of the gradient further affected this response. Bhat et al.³⁶ used gradients of polymer molecular weight (Mw) and/or grafting density of surface bound Poly(2-hydroxyethyl methacrylate) (PHEMA) with physisorbed fibronectin to investigate changes in the behavior and morphology of osteoblastic cells as a function of their chemical environment. It is clear from an overview of the literature that while a number of methods have been described to generate surface gradients, there is room for optimising and expanding the range of materials and surface chemistries/properties that can be deposited to accelerate biomaterial and tissue engineering research.³⁷

In previous work we have introduced the technique of plasma polymer gradient deposition using a knife edge upper electrode to generate gradient surfaces.³⁸ Use of this electrode configuration within the plasma deposition process results in the generation of a chemical gradient on substrates placed directly underneath the plasma glow. In this work we have conducted a detailed study of the gradient plasma polymer film chemistry via X-ray Photoelectron Spectroscopy (XPS) and time-of-flight secondary ion mass spectroscopy (TOF-SIMS) with principle component analysis (PCA). The adsorption of serum proteins (human serum albumin (HSA) and fetal bovine serum (FBS)) was monitored across the gradients and was shown to be effected by the surface chemistry as well as protein incubation time, which demonstrated marked variability in the films ability to resist protein adsorption. Furthermore, the attachment of HeLa cells (in the presence of serum proteins) was monitored across the gradient and was shown to

correlate with the surface chemistry, but more importantly, cell attachment appeared to correlate strongly with the adsorption of serum proteins.

6.3 Materials and Methods

6.3.1 Substrate Preparation

DGpp gradients were deposited onto ultra-flat single crystal silicon wafers (<100>, 1 cm² x 0.5 mm thick, MMRC P/L), cleaned by ultrasonication in a 2% RBS-35 surfactant solution (Pierce, 2% ethanol in MilliQ) for 1 hour. Substrates were then rinsed multiple times in Milli-Q water before being dried in a high-pressure stream of high purity nitrogen. For the cell culture experiments, the glass slides were pre-coated with a heptylamine (Aldrich, 99% purity) HA-pp layer to enhance the adhesion of DGpp gradient to the glass substrate.³⁹ The parameters used for RFGD deposition of HA films were a frequency of 200 kHz, a load power of 30 W, an initial monomer pressure of 40 Pa (final pressure of 70 Pa), and a treatment time of 30 s.

6.3.2 Plasma Polymerisation

Radio frequency glow discharge plasma polymerisation was used to deposit PEG-like gradient films in a custom-built plasma reactor described previously¹². The reactor consists of a cylindrical glass chamber (height of 35 cm and diameter of 17 cm) and is fitted with two capacitively coupled electrodes. The top electrode (a razor) was connected to a RF power supply (125 kHz) and lowered to sit ~ 1mm above the substrate, while the bottom electrode (diameter = 14 cm) was grounded. The monomer diethylene glycol dimethyl ether, or 'diglyme' (DG) (BDH, 99% purity) was fed into the reactor from a round bottom flask attached to a stainless steel line and a manual valve to control the flow. Substrates were placed on the lower electrode, and a rotary pump was used to

evacuate the chamber. The DG vapors were fed into the chamber at a starting pressure of 20 Pa, and a continuous RF field was generated between the electrodes for a deposition time of 180 seconds. Gradients were deposited at two different load powers, 5 and 30W, with pressure ranging from 20-27.5 Pa for the 5 W gradient and 20-51.4 Pa for the 30 W gradient deposition.

6.3.3 X-Ray Photoelectron Spectroscopy (XPS)

To investigate the chemical composition of the DGpp films, XPS analysis was performed using an AXIS HSi spectrometer (Kratos Analytical Ltd, Manchester, UK) equipped with a monochromated Al K_{α} X-ray source at a power of 144 W (12 mA, 12 kV). A hemispherical analyser was used, operating in the fixed analyser transmission mode with a standard aperture (1.0 mm x 0.5 mm). Charging of the samples during irradiation was compensated for by the internal flood gun, coupled with a magnetic immersion lens. The pressure in the main vacuum chamber during analysis was typically 5×10^{-6} Pa. Survey spectra were acquired at a pass energy of 320 eV to identify the elements present in the DGpp films. The atomic concentrations were calculated using integral peak intensities and the sensitivity factors supplied by the manufacturer. High-resolution C 1s spectra were also obtained and quantified using a minimisation algorithm in order to calculate optimised curvefits and determine the relative contributions from specified functional groups. Five peak components (mixed gaussian/Lorentzian model functions) were used to fit the C 1s curves. Component C1 at the lowest binding energy (BE) was assigned to aliphatic hydrocarbons (neutral carbon) and the corresponding BE set accordingly to 285 eV⁴⁰ and normalised to 1 for presentation of the 3d C 1s XPS plots. A second component at a slightly higher BE was included to account for all C 1s photoelectrons

that underwent a secondary BE shift. Component C3 (286.3-286.6 eV) represents C-O based groups (eg ethers and alcohols), C4 (287.9 – 288.2 eV) accounts for all C=O based functional groups (eg aldehydes and ketones) and C5 (288.9 – 289.3 eV) accounts for O-C=O based groups (eg acids or esters). These components were applied to the analysis of the DGpp gradients prior to protein adsorption.

To investigate protein adsorption, survey scans were acquired across the DGpp gradients after protein incubation. Survey spectra were collected with a Kratos AXIS Ultra DLD spectrometer, using monochromatic AlK_{α} radiation ($h\nu = 1486.7$ eV). The scans were recorded with a pass energy of 160 eV and a 110 μm aperture. The scan centres were separated by 200 μm . Each gradient sample was characterised by 32 spectra corresponding to a total scan-length of ~ 6.5 mm.

6.3.4 Time-of-Flight Secondary Ion mass Spectroscopy (ToF-SIMS)

ToF-SIMS analyses were performed with a PHI TRIFT II model 2100 spectrometer (PHI Electronics Ltd.) equipped with a ^{69}Ga liquid metal ion gun. A pulsed primary ion beam was used to desorb and ionize species from sample surfaces. Pulsed low-energy electrons were used for charge compensation. Mass axis calibration was done with CH_3^+ , C_2H_5^+ , and C_3H_7^+ in positive mode of operation, the one employed in this study. A mass resolution $m/\Delta m$ of 4500 at nominal $m/z = 27$ amu (C_2H_3^+) was typically achieved. The ToF-SIMS technique is “destructive” by its nature; however, by applying an ion beam of low current, it is possible to derive data from a virtually intact surface. The primary ion fluxes used in this study were between 3×10^{11} and 6×10^{11} ions cm^{-2} , meeting the static conditions regime that for spectroscopy should be less than 1×10^{12} ions cm^{-2} . The gradient samples were characterized by multiple scans collected along a line

perpendicular to that defined by the razor electrode. The area of each scan was 100x100 μm and the scan centres were separated by 200 μm . Each gradient sample was characterised by 40 spectra resulting in a total scan-length of ~ 8.0 mm. The complex mass spectra were analysed by detecting differences in the fragmentation patterns. This was achieved with the aid of Principal Component Analysis (PCA).

6.3.5 Serum protein adsorption

To assess the relative adsorption of various proteins across the DGpp gradients, fresh samples were incubated in solutions of human serum albumin (0.1 mg/ml in PBS, pH 7.4 for 1 hour) and fetal bovine serum (FBS). DGpp gradients were incubated in 10% FBS (CSL) solutions in PBS (pH=7.4, 37 degrees) for both 1 and 24 hr incubation times at 37 °C. Samples were then thoroughly rinsed with MilliQ water before to remove excess salt being blown dry with a high-velocity, ultra pure nitrogen stream. Samples were then analysed using XPS and ToF-SIMS (for HSA attachment) where protein adsorption was indicated by the presence of elemental N or N containing fragments on the DGpp gradient surface.

6.3.6 Cell attachment

Sample preparation: DGpp gradient coated glass slides were transferred to separate chambers of a 4-chamber culture tray (Nunc, these culture trays are designed to hold one whole glass slide in each chamber) and then soaked in 7 ml of a sterile solution of 1xPBS containing penicillin (120 $\mu\text{g/ml}$) and streptomycin (200 $\mu\text{g/ml}$) overnight at 4°C.

Cell attachment: The sterilizing solution from the step above was removed and HeLa cells were seeded at a density of 5×10^5 cells/chamber in 7 ml of fresh DMEM/Hams F12 supplemented as usual (10% FBS, pen/strep, glut). This density was designed to give an

effective loading close to confluence after 24 hours attachment. Cells were incubated for 24 hours at 37°C in humidified air containing 5% CO₂. Visualisation of cell presence and morphology on the silicon wafers was achieved by exposing cells CellTracker Green™ (CTG, Molecular Probes, Invitrogen) for the final hour of incubation.

Microarray Scanner: An applied precision array WoRx microarray scanner was used to image stained and fixed cells across the plasma polymer gradient coated glass slides. No auto-fluorescence of the plasma polymer films was observed when using an Alexa 488 filter. The intensity vs distance profiles across the stained cells on the gradient were taken using 'Image J' software.

6.4 Results and Discussion

In this work, PEG like gradient plasma polymer (pp) thin films were deposited via radio frequency glow discharge plasma polymerisation of diethylene glycol dimethyl ether (DG) at two different load powers, 5 and 30 W. A knife edge upper electrode within the plasma reactor was used to generate the DGpp gradient films with a systematic variation in their surface chemistry.¹² In particular the concentration of surface ether groups (known to be critical to protein adsorption in PEG-like polymer films) can be systematically varied across the DG plasma polymer (DGpp) gradients. It was expected that differences in protein and cell adhesion may be evident along the ether surface chemistry created using this technique. The region of the gradient deposited directly underneath the knife edge electrode is defined throughout this paper as '0 mm' and the gradients are analysed either side of this central region, at increments across the gradient surfaces. Being able to precisely identify this central (0 mm) region of the gradient in

enclosed vacuum environments, such as those in the case of XPS and TOF-SIMs, can be difficult and care must be taken to carefully identify this region prior to analysis.

6.4.1 XPS analysis of gradient films

XPS survey scans performed across the gradients reveal the presence of elemental carbon and oxygen only. The oxygen to carbon ratio plotted as a function of distance is shown in Figure 6.1A. It can be seen that the central region of each gradient retains the highest oxygen content, which systematically decreases across the gradient, which we have reported previously.¹² Gradients deposited at 5 W retained O/C ratios most similar to that of the starting monomer (0.5)⁴¹, which was measured to be 0.46 in the central region, and decreased to 0.41 at a distance of 4 mm from the gradients centre. The 30 W gradient yielded O/C ratios ranging from 0.34 to 0.3 between 0 and 4 mm across the gradient respectively. These values are similar to other reported in the literature for diglyme plasma polymers. Bretagnol et al.⁴¹ reported O/C ratios for uniform DGpp films deposited using rfgd plasma polymerisation of DG at 1 to 15 W to be 0.44 to 0.31, respectively.

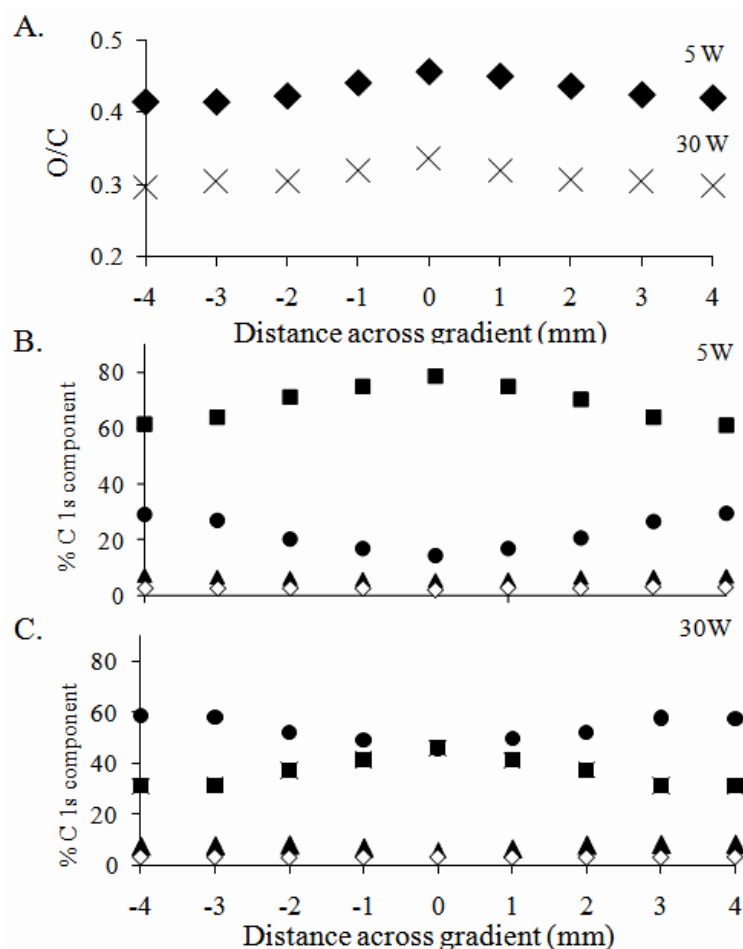


Figure 6.1 A. O/C elemental ratio across the 5 and 30 W gradients B. and C. Percentage of the relevant C 1s components plotted across the gradients from the high resolution C 1s XPS curves of the 5 W (B) and 30 W (C) DGpp gradient films. The components are C-C, C-H (●), C-O (■), C=O (▲) and O-C=O (◇) and percentages are relative to total carbon.

High resolution C 1s XPS analysis (data not shown) revealed four main chemical components contributing to the spectra including C-C and C-H (hydrocarbon), COR (ether and alcohol), C=O (ketone and aldehyde) and COOR (carboxylic acid and ester). Figure 6.1B and C presents the contribution of these components from high-resolution C 1s analyses across the 5 and 30W gradient films respectively. The central region of both the 5W and 30W gradients, retained the highest concentration of COR groups (~ 286.6 eV) indicating greater retention of the DG monomers native ether groups. Gradients

deposited at a 5 W load power retained more monomer-like functionality when compared with the 30 W gradient, with higher concentrations of COR (ether and alcohol related) groups. A systematic decrease in the COR functionality from the centre and across the gradients was observed, but the change in this component was most noticeable across the 5 W film, yielding a more concentrated chemical slope across the gradient surface, ranging from 79 % at the centre (0 mm) to 61 % at 4 mm, compared with 46% (0mm) to 31 % (4 mm) for the 30W films. Quantification of the C 1s analysis also revealed that the C-C/C-H, C=O and COOR functionalities were lowest in the centre (0 mm) and increased across both gradients. The loss of COR functional groups corresponded with an increase in hydrocarbon species.¹² Previous chemical mapping experiments performed across the 5 and 30 W DGpp gradients using synchrotron source grazing incidence FTIR microspectroscopy confirmed the presence of surface ether groups and that the chemical gradient occurs throughout the bulk of the films (rather than just the surface) and is strongest in the region of the film deposited on either side of the razor.¹² The ether content was found to remain highest at the centre of both of the gradients, however the 5 W gradient retained more monomer like functionality with a greater contribution to the giFTIR spectra from the ether stretch when compared to the 30 W gradient.

6.4.2 ToF-SIMS Chemistry

Positive ion TOF-SIMS spectra were acquired across the 5 and 30 W gradients and analysed using PCA to aid in the interpretation of the data. PCA is a statistical transformation of data, which when applied to the complex TOF-SIMS spectra, reduces the dimensionality and random variables of the raw data, enabling a more accurate

comparison of ion peak trends not necessarily apparent between datasets. Analysis of the TOF-SIMS positive ion spectra (Figure 6.2A-D) shows that in all cases the spectra contain the same major fragments but they differ in their relative intensities. The commonly reported ether fragments⁴²⁻⁴⁴ at $m/z = 31$ (CH_3O^+), $m/z = 45$ ($\text{C}_2\text{H}_5\text{O}^+$), $m/z = 59$ ($\text{C}_3\text{H}_7\text{O}^+$) and $m/z = 73$ ($\text{C}_3\text{H}_5\text{O}_2^+$) are shown to be more intense at the centre (0 mm) of the gradients, when compared to the intensity of well known hydrocarbon fragments, specifically $m/z = 15$ (CH_3^+), $m/z = 41$ (C_3H_5^+), $m/z = 43$ (C_3H_7^+) and $m/z = 55$ (C_4H_7^+). This effect is most noticeable at a distance of 3.5 mm across the 30 W gradient, as shown in Figure 6.2D, where the height of the hydrocarbon peaks are almost equivalent to the major PEG related peaks. The results of the PCA analysis across the 5 W and 30 W gradients are shown in figure 3, where both the PC1 scores (89.7 %) (6.3A and B) and the loadings plots of PC1 (6.3C and D) are presented respectively. Analysis of the scores plot of the 5 W gradient (Figure 6.3A) alludes to an oscillating variation in surface chemistry that was not apparent from analysis of the XPS data with negatively loaded peaks around either side of the centre of the gradient and a very narrow central region of positively loadings and negative loading out to around 2mm which then become positive again. The scores plot for the 30 W gradient (Figure 6.3B) shows a wider region of positive scores out to 2 mm either side of the central region which then become positive of the gradient more in keeping with the trends in gradient chemistry observed via XPS. Therefore there is an essentially opposite trend in the scores plot of the 5 and 30 W gradients after PCA however the peaks which are either positively or negatively loaded are the same in both powers indicating differences in surface chemistries in the top 2-3 nm.

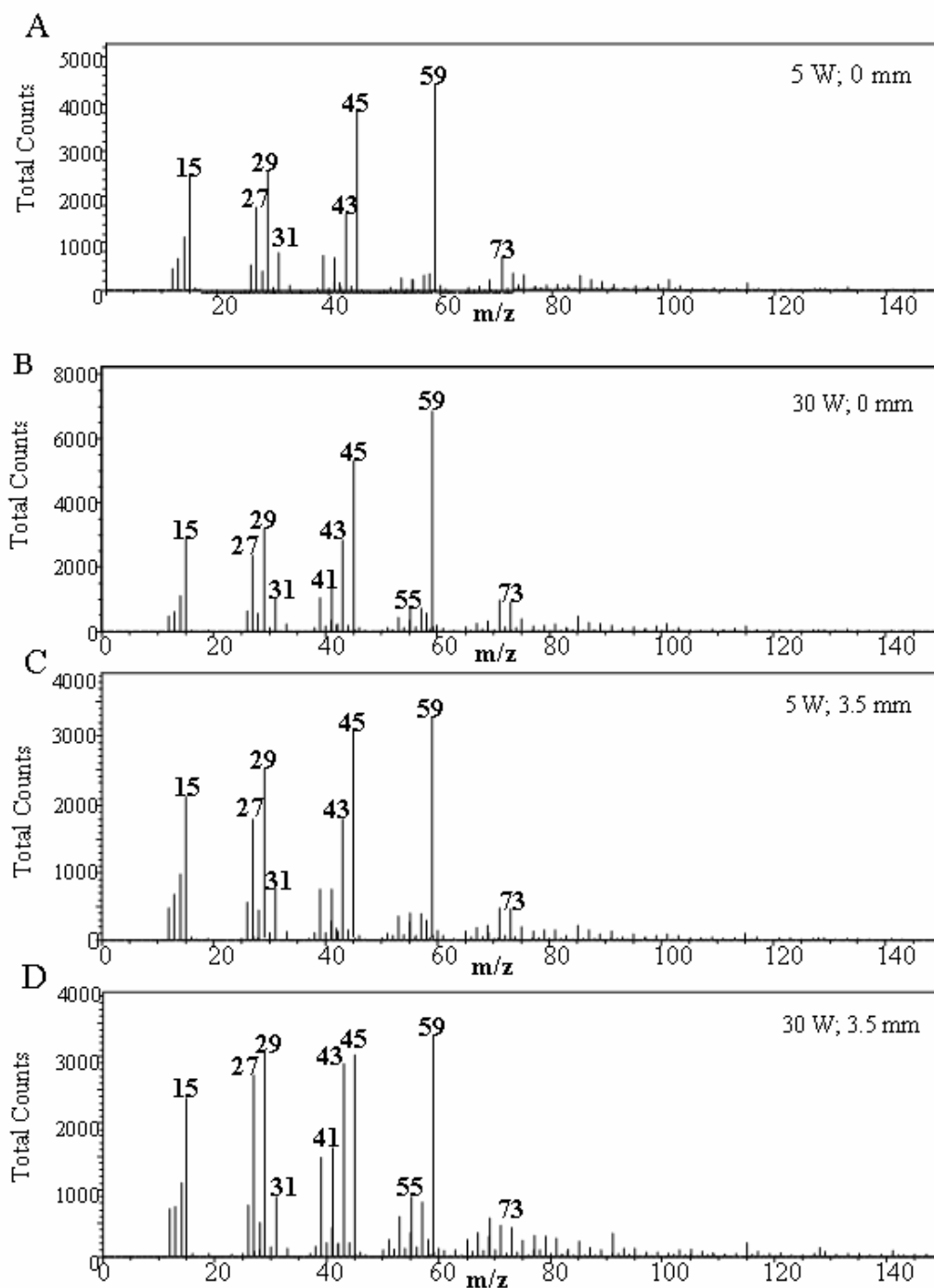


Figure 6.2 TOF-SIMS positive spectra of the 5 and 30 W gradients taken from the central region “0 mm” (A and B) and 3.5 mm across the gradient (C and D) for the 5 and 30 W gradients respectively.

The positive hydrocarbon related fragments were negatively loaded for both the 5 and 30 W gradients, while the ether related fragments loaded positively (Figures 6.3C and D). The positive ether related fragments include CH_3O^+ , $\text{C}_2\text{H}_5\text{O}^+$ and $\text{C}_3\text{H}_7\text{O}^+$ and as discussed previously, these are common to PEG-like surfaces.⁴²⁻⁴⁴ Furthermore, the intensity of the positively loaded ether related fragments are lower in the centre of the 5 W gradient compared to the 30 W gradient, indicating that the ether components are less prevalent in the centre of the 5W gradient which is in disagreement with XPS and previously reported FTIR data in the 5 W film. The finding that more ‘PEG-like’ surface chemistries are prevalent in the centre of the 30 W film is in keeping with XPS analysis of the films. The discrepancy in the XPS and FTIR data with PCA of the loadings in the 5 W film could be due to a number of reasons. It is possible that due to the lower depth penetration of the TOF-SIMS compared to XPS, that the TOF-SIMS analysis is identifying some possible oxidation or chemical re-arrangement occurring at the surface of the 5 W gradient. We know from previous studies that lower power DGpp films can result in the generation of low molecular weight material (as discussed in Chapter 4). In the ‘low power’ region of the plasma discharge directly underneath the knife edge electrode this material may contain more hydrocarbons and therefore make the surface look less ether like within the first 2-3 nm as analysed by TOF-SIMS when compared to the 10 nm sampling depth of XPS. Analysis of the scores plot for both the 5 and 30 W gradients does show a distinct change in films chemistry, however at approximately 2 mm either side of the gradients centre.

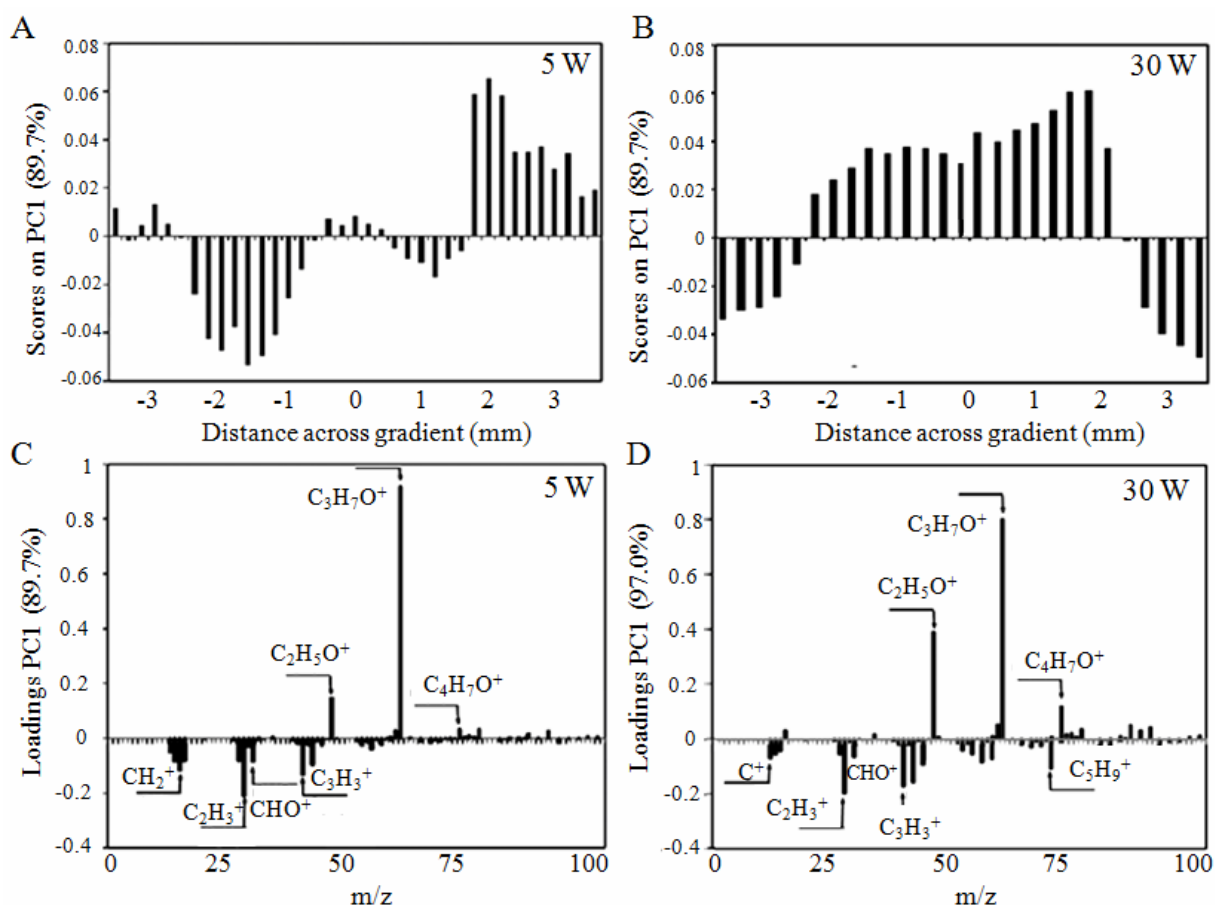


Figure 6.3 PCA analysis of positive TOF-SIMS mass spectra recorded on 5 W (A) and 30 W (B) DGpp gradients showing PC1 scores as a function of distance across the sample surface, with 0 denoting the approximate position of the knife-edge electrode. Loadings of hydrocarbon and oxygen-containing fragment ions on PC1 for the 5 (B) and 30 W indicate that gradients were deposited.

6.4.3 XPS and ToF-SIMS analysis of Protein Adsorption on gradient films (HSA)

Analysis of the PCA scores (Figures 6.4 A and B for the 5 and 30 W gradients respectively) and loadings plots (Figures 6.4 C and D for the 5 and 30 W gradients respectively) after the gradients were exposed to solutions of human serum albumin clearly indicate a higher relative amount of adsorbed proteins across the 30 W gradient than the 5 W gradient. The amount of N containing positive ions are negligible across the 5 W gradient, however it is interesting that the same oscillatory nature of the surface chemistry was revealed. One might initially interpret this as proteins adsorption varying

with the surface composition across the 5 W gradient, however it is the CHO and hydrocarbon ions that primarily load onto PC1, whereas the loadings of CHN ions are negligible (Figure 6.4C). Therefore, Figure 6.4C reproduces quite closely the surface chemistry observed in Figure 3C before adsorption and does not reveal whether or not the small amounts of adsorbed proteins follow the same banding as the positively loaded fragments seen could also possibly be due in part to fragmentation of adsorbed proteins. This data highlights the potential for reaching incorrect conclusions when analysing PCA data and thus the need for care in interpreting such results. For the 30 W gradient, the positive N containing fragments loaded negatively onto the PC 1 loading plot (Figure 6.4D), and the scores plot (Figure 6.4B) indicates that HSA adsorption is occurring either side of the gradient centre, consistent with the chemistry variation seen on the TOF-SIMS PC 1 scores plot in Figure 6.3B.

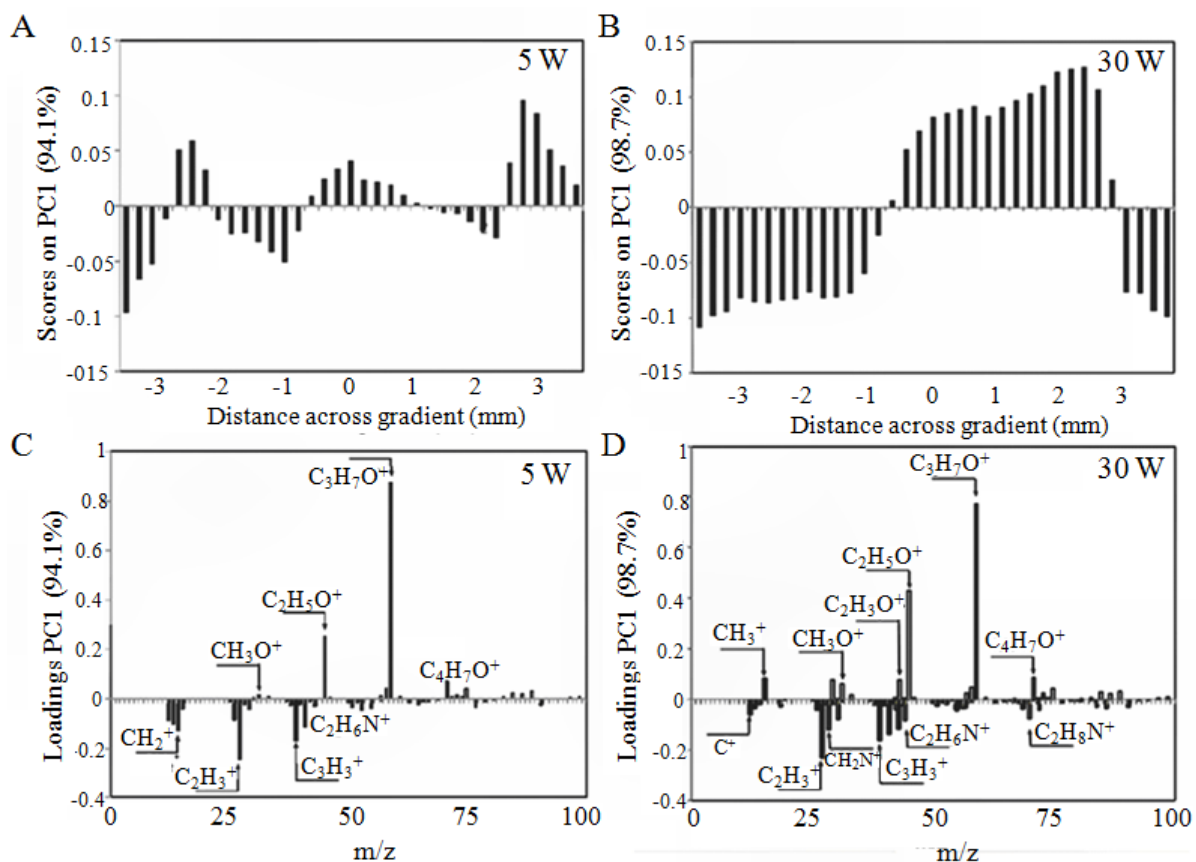


Figure 6.4 PCA analysis of positive TOF-SIMS mass spectra recorded on the gradients after exposure to HSA: (A) PC1 scores as a function of distance across the 5 (A) and 30 W (B) gradients, and (C) and (D) loadings of hydrocarbon, oxygen-containing and nitrogen-containing fragment ions on PC1 (note that loadings of immonium ions are negligible across the 5 W gradient; e.g., $\text{C}_2\text{H}_6\text{N}^+$). The score plots reveal the oscillating adsorption across the gradients (most pronounced across 5 W gradient), consistent with the spatial chemistry variations measured by TOF-SIMS prior to protein incubation (0 denotes the 'approximate' position of the knife edge electrode).

The total normalised intensity of positive CHN containing fragments (immonium ions from amino acids) was plotted from the TOF-SIMS data and is shown in Fig 6.5A. It shows that across the 5W pp gradient there is a very low level of protein related fragments detected. For the 30W sample there is substantially more nitrogen containing fragments on areas away from the centre of the gradient and less fragments near the gradient centre, in agreement with XPS data. From XPS analysis of the 5 W gradient (Figure 6.5 B) no N signal was detected across the entire sample area (-3 mm to 3mm) however it clear from the nitrogen containing fragments that some protein has indeed

adsorbed in the centre of the gradient that was not evident from XPS analysis. From XPS analysis of HAS adsorption in the 30W pp (Figure 6.5 B), there is substantial protein adsorption in the regions further away from the electrode whereas underneath and near the electrode, the pp resisted protein adsorption to below the detection limit of ~ 10 ng/cm² via XPS analysis. The lower protein fouling region spanned across a distance of approximately 2 mm either side of the gradient centre, consistent with the chemistry variation seen on the TOF-SIMS PC 1 scores plot in Figure 6.3B.

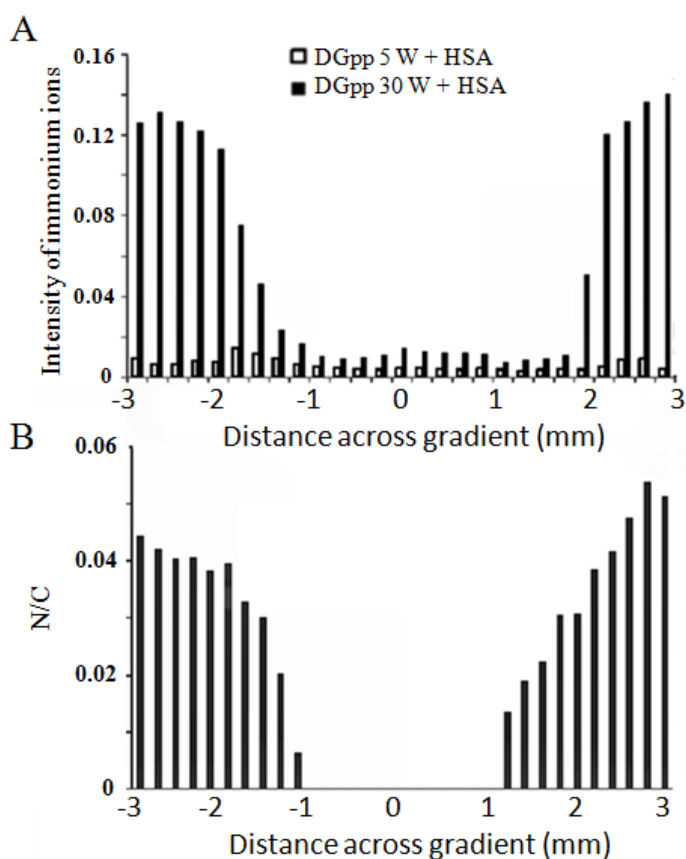


Figure 6.5 (A) Summated relative intensity of immonium ions across DGpp-5W and DGpp-30W surfaces after exposure to HSA measured by TOF-SIMS analysis (0 denotes the ‘approximate’ position of the knife edge electrode). (B) N/C elemental ratio from XPS analysis plotted across the DGpp gradients following incubation in HSA. The central region of the gradient remained resistant to HSA incubation, with adsorption increasing across the gradient. No N was detected across the 5 W gradient within the XPS detection limits

6.4.4 Fetal Bovine Serum Adsorption and HeLa cell attachment

In order to probe the relationship between the chemistry of the gradient surface, protein resistance/adsorption, and cell attachment, fetal bovine serum (FBS) was also used for protein adsorption studies across the 5 and 30 W gradient films. FBS was used in addition to the human serum albumin data already presented in figures 6.4 and 6.5, as this is commonly present during cell attachment/cell culture experiments. Analysis of FBS adsorption across the DGpp gradients was performed after 1 and 24 hour incubation times at 37° C (Figure 6.6 A and B), to detect any influence of protein exposure time on adsorption, and to compare with the cell attachment data which was performed over a 24 hour period. The adsorption of protein across the gradients was tracked by monitoring the emerging nitrogen component in the XPS survey spectra. The relative amount of FBS adsorbing across the gradients was found to correlate with the COR component in the films as measured from C1s XPS spectra curve fit data (Figure 6.1B and C) with regions of higher ether content adsorbing less FBS. Across the 5 W gradient, no adsorbed FBS proteins were detected at the centre of the gradients (0 to 2 mm) after 1 hour incubation. At 2 mm across the 5 W gradient, correlating to an XPS COR content of ~ 70 %, FBS proteins were detected and the N/C ratio increased to a maximum 0.035 (correlating to 2.4 atomic % N) at a distance of 4 mm from the central gradient region. After 1 hour, low levels of protein were observed in the 30 W film measured in their central region, increasing to maximum N/C contents of 0.08 (correlating to 5.9 atomic % N) at 4 mm across the gradient.

After 24 hours incubation of the gradients in the serum proteins, an increase in protein adsorption across both gradients was observed (Figure 6.6B) with FBS proteins adsorbing in the central region of both gradients. When comparing the adsorption of FBS across the gradients as a function of time (1 hour vs. 24 hours) the 5 W film results in a gradation of physisorbed FBS proteins, ranging from 0.49 to a maximum of 0.9 (correlating to 5.9 atomic % N) at 4 mm across the gradient. The 30 W gradient however, had a relatively uniform coverage of FBS across the entire surface with no gradient in protein adsorption visible after 24 hours. The adsorption of FBS proteins was also monitored across a bare silicon substrate as a control after both 1 and 24 hours incubation periods, where no difference was observed in the final N/C values, which were 0.24 (correlating to 9.8 atomic % N, data not shown).

In a time dependant study of ^{125}I plasminogen adsorption on lysine modified N-succinimidyl carbonate PEG grafted polyurethane (PU) surface (PU-PEG-NHS), Chen et al.⁴⁵ found that the adsorption of plasminogen from blood plasma continued to increase on the PEG-lysine modified surface until 7 hours. They suggested that the rate of plasminogen adsorption onto the PEG-lysine modified surface was slowed (compared to ungrafted controls) due to the inhibitory influence of the PEG. This further demonstrates the importance of time dependency in protein adsorption studies, where the effect of time is often a neglected.

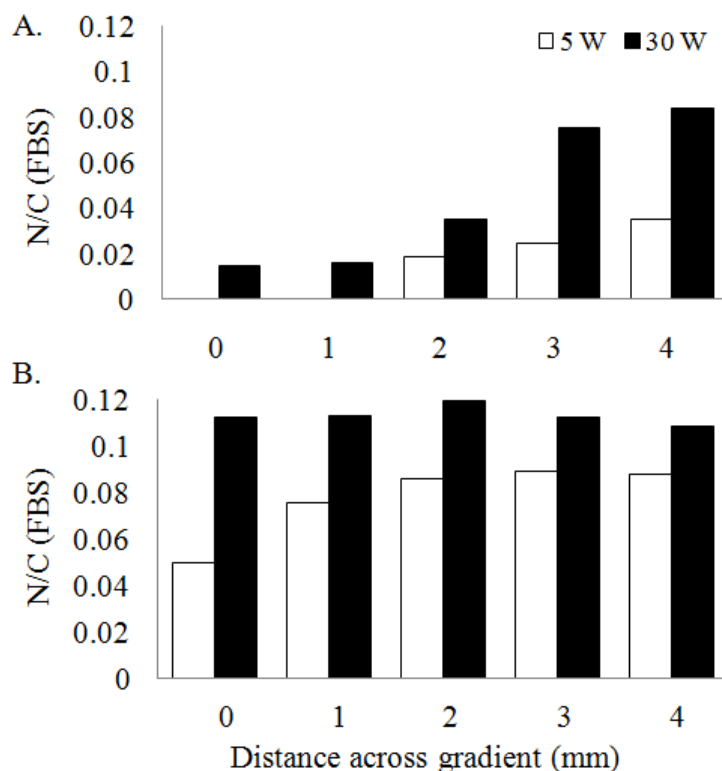


Figure 6.6 Adsorption of FBS proteins across DGpp gradients as a function of distance across the gradient after 1 hr and 24 hr (A and B, respectively) as measured by XPS elemental N detection.

Cell attachment across the DGpp gradients was observed using fluorescently labeled HeLa cells in the presence of FBS over a 24 hour incubation period. An overview of the attachment of the fluorescently labeled HeLa cells is shown in Figures 6.7A and B for the 5 and 30 W gradients respectively, while high resolution images of the attached cells are shown in Figures 6.7D and E. Furthermore, the normalised fluorescence intensity profile of the cells attached across the 5 and 30 W gradients is displayed in Figure 6.7E. The central region (~ 2 mm either side of the gradient) of the 5 W gradient remained relatively resistant to HeLa cell attachment, while cells attached across the entire 30 W DGpp gradient. This correlates not only with surface chemistry but primarily with the adsorption of FBS proteins as presented in figure 6.2B. HeLa cells began adsorbing onto

the 5 W surface when the chemistry XPS COR content dropped to $\sim 70\%$, while the central region of the 30 W gradient showed a maximum COR content across the gradient of just 46 % in part explaining the cell attachment across its entirety. Analysis of the high resolution images shows that HeLa cells attached across the 5 W gradient (Figure 6.7C) are rounded, clumped and not well attached, while those attached across the 30 W gradient (Figure 6.7D) are more dense, spread and confluent.

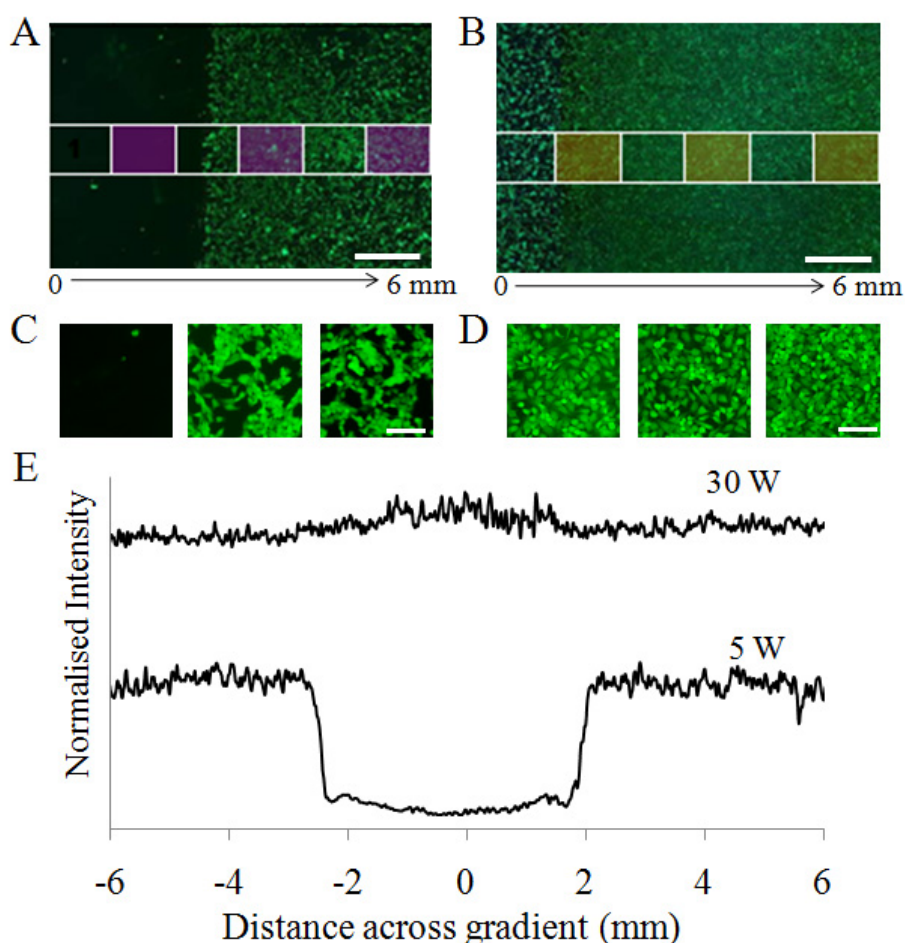


Figure 6.7 (A and B) Overview of the fluorescently labelled HeLa cells attached across the 5 and 30 W DGpp gradient films respectively, at low magnification (x2 objective) (scale bar represents 1 mm). (C and D) Higher resolution images (x10 objective) of the attached cells across the 5 and 30 W gradients respectively. Images were taken from regions across the gradients in the shaded highlighted boxes shown in Figures A and B (scale bars represent 100 μm). (E) Fluorescence intensity profile of stained HeLa cells across the 5 and 30 W gradients.

Results of cell adhesion studies of PEG like DGpp films, reported by Bretagnol et al.⁴¹ also concluded that there was strong correlation between cell resistance/adhesion and the ether content of the films. Samples were deposited at 1, 5 and 15 W yielding systematically decreasing surface ether contents and analysed for their resistance to the adsorption of BSA using QCM-D. Both the 1 and 5 W samples adsorbed extremely low levels of BSA (i.e. ~ 0.2 and $0.3 \mu\text{g}/\text{cm}^2$), while the 15 W sample and reference adsorbed higher levels. They suggested however, that the use of just one protein is not sufficient to predict cell response. The attachment of L929 fibroblast cells on the 1 W samples (72 % COR content) was reduced by $\geq 95\%$, while both the 5 and the 15 W (~ 54 and 40 % COR content) samples showed excellent cell adhesive properties, in contrast to the BSA adsorption studies. Other researchers using chemical gradients have also correlated the growth or activity of cells with the presence of media proteins. Lee et al.⁴⁶ prepared wettability gradient on polyethylene (PE) surfaces using a corona discharge treatment and detected the maximum adsorption of calf serum proteins across the gradients at a position which correlated with the attachment of PC-12 cells. Similarly, Bhat et al.⁴⁷ used orthogonal surface chemical gradients of grafted PHEMA (Mw and grafting density) to control and systematically vary the amount of adsorbed Fibronectin (FN), an ECM protein known to promote the attachment of MC-3T3 E1 cells. Cell coverage was found to correlate with both the coverage of PHEMA on the substrate and consequently, the adsorption of fibrinogen.⁴⁶ Our results indicate that by controlling and varying the adsorption of serum across a gradient (dictated largely by surface chemistry), the attachment cells across a surface may be controlled.

6.5 Conclusions

Plasma polymer (pp) PEG-like chemical gradients were generated using a one step continuous wave radio-frequency glow discharge plasma polymerisation of diethylene glycol dimethyl ether (DG), at load powers of 5 and 30 W. XPS showed that the ether functionality systematically varied across the length of the gradient, with the highest 'PEG like' characteristics retained in the central region of the films and in gradients deposited at lower load power. The presence of hydrocarbon, carbonyl and acid and hydroxyl functionalities also varied systematically across the gradients, being lower in the central region and increasing laterally outwards. TOF-SIMS data highlighted an oscillatory nature of the surface chemistry across the gradients that were not detected by XPS, indicating a depth variation to surface chemistry. The adsorption of both HSA and FBS was monitored across the gradients. XPS detected no HSA proteins across the 5 W gradient, while TOF-SIMS detected very low levels. HSA adsorption was shown to be higher on the 30 W gradient and correlated with a distinct chemical change (specifically higher amounts of positive hydrocarbon fragments) seen at approximately 2 mm either side of the gradient centre. The importance of protein incubation time in protein adsorption studies was highlighted, where no FBS proteins were detected in the central region of the 5 W gradient after a 1 hour incubation period, while after 24 hours proteins were detected across the entire gradient. Furthermore, the attachment of HeLa cells (in the presence of serum containing media) were used to investigate cell-surface interactions across the gradients which were found to correlate with the results of the adsorption of the FBS proteins in terms of cell density as a function of distance on the gradient.

6.6 References

1. Feng, W.; Nieh, M. P.; Zhu, S.; Harroun, T. A.; Katsaras, J.; Brash, J. L., Characterization of protein resistant, grafted methacrylate polymer layers bearing oligo(ethylene glycol) and phosphorylcholine side chains by neutron reflectometry. *Biointerphases* **2007**, 2, (1), 34-43.
2. Barry, J. J. A.; Howard, D.; Shakesheff, K. M.; Howdle, S. M.; Alexander, M. R., Using a core-sheath distribution of surface chemistry through 3D tissue engineering scaffolds to control cell ingress. *Advanced Materials* **2006**, 18, (11), 1406.
3. Muir, B.; Fairbrother, A.; Gengenbach, T.; Rovere, F.; Abdo, M.; McLean, K.; Hartley, P., Scanning Probe Nanolithography and Protein Patterning of Low-Fouling Plasma Polymer Multilayer Films. *Advanced Materials* **2006**, 18, (23), 3079-3082.
4. Genzer, J.; Bhat, R. R., Surface-Bound Soft Matter Gradients. *Langmuir* **2008**, 24, (6), 2294.
5. Smith, J. T.; Tomfohr, J. K.; Wells, M. C.; Beebe, T. P.; Kepler, T. B.; Reichert, W. M., Measurement of Cell Migration on Surface-Bound Fibronectin Gradients. *Langmuir* **2004**, 20, (19), 8279.
6. Belu, A. M.; Graham, D. J.; Castner, D. G., Time-of-flight secondary ion mass spectrometry: techniques and applications for the characterization of biomaterial surfaces. *Biomaterials* **2003**, 24, (21), 3635-3653.
7. Johnston, E. E.; Bryers, J. D.; Ratner, B. D., Plasma Deposition and Surface Characterization of Oligoglyme, Dioxane, and Crown Ether Nonfouling Films. *Langmuir* **2005**, 21, (3), 870-881.
8. Wagner, M. S.; Pasche, S.; Castner, D. G.; Textor, M., Characterization of poly(L-lysine)-graft-poly(ethylene glycol) assembled monolayers on niobium pentoxide substrates using time-of-flight secondary ion mass spectrometry and multivariate analysis. *Analytical Chemistry* **2004**, 76, (5), 1483-1492.
9. Dubey, M.; Emoto, K.; Cheng, F.; Gamble, L. J.; Takahashi, H.; Grainger, D. W.; Castner, D. G., Surface analysis of photolithographic patterns using ToF-SIMS and PCA. *Surface and Interface Analysis* **2009**, 41, (8), 645-652.
10. Takahashi, H.; Emoto, K.; Dubey, M.; Castner, D. G.; Grainger, D. W., Imaging surface immobilization chemistry: Correlation with cell patterning on non-adhesive hydrogel thin films. *Advanced Functional Materials* **2008**, 18, (14), 2079-2088.
11. Thissen, H.; Gengenbach, T.; du Toit, R.; Sweeney, D. F.; Kingshott, P.; Griesser, H. J.; Meagher, L., Clinical observations of biofouling on PEO coated silicone hydrogel contact lenses. *Biomaterials* 31, (21), 5510-5519.
12. Menzies, J. D.; Cowie, C. C. B.; Fong, C.; Forsythe, J.; Gengenbach, T.; Mc Lean, K.; Puskar, L.; Textor, M.; Thomsen, L.; Tobin, M.; Muir, B., A one-step method for generating PEG-like plasma polymer gradients: Chemical Characterisation and Analysis of protein interactions. *Langmuir* **2010**.
13. Liu, F.; Dubey, M.; Takahashi, H.; Castner, D. G.; Grainger, D. W., Immobilized Antibody Orientation Analysis Using Secondary Ion Mass Spectrometry and Fluorescence Imaging of Affinity-Generated Patterns. *Analytical Chemistry* 82, (7), 2947-2958.
14. Ballav, N.; Shaporenko, A.; Terfort, A.; Zharnikov, M., A Flexible Approach to the Fabrication of Chemical Gradients. *Advanced Materials* **2007**, 19, (7), 998-1000.

15. Busscher, H. J.; Ruardy, T. G.; Van der Mei, H. C.; Schakenraad, J. M., Preparation and characterization of chemical gradient surfaces and their application for the study of cellular interaction phenomena. *Surface Science Reports* **1997**, 29, (1), 3-30.
16. Jing, Y.; Felicity, R. A. J. R.; Nikolaj, G.; Morgan, R. A., A High-Throughput Assay of Cell-Surface Interactions using Topographical and Chemical Gradients. *Advanced Materials* **2009**, 21, (3), 300-304.
17. Morgenthaler, S.; Lee, S.; Zürcher, S.; Spencer, N. D., A Simple, Reproducible Approach to the Preparation of Surface-Chemical Gradients. *Langmuir* **2003**, 19, (25), 10459-10462.
18. Latour, R. A., Thermodynamic perspectives on the molecular mechanisms providing protein adsorption resistance that include protein-surface interactions. *Journal of Biomedical Materials Research Part A* **2006**, 78A, (4), 843-854.
19. Shin, Y. N.; Kim, B. S.; Ahn, H. H.; Lee, J. H.; Kim, K. S.; Lee, J. Y.; Kim, M. S.; Khang, G.; Lee, H. B., Adhesion comparison of human bone marrow stem cells on a gradient wettable surface prepared by corona treatment. *Applied Surface Science* **2008**, 255, (2), 293-296.
20. Lee, J. H.; Lee, H. B., Platelet adhesion onto wettability gradient surfaces in the absence and presence of plasma proteins. *Journal of Biomedical Materials Research* **1998**, 41, (2), 304-311.
21. Jeong, B. J.; Lee, J. H.; Lee, H. B., Preparation and Characterization of Comb-like PEO Gradient Surfaces. *Journal of Colloid and Interface Science* **1996**, 178, (2), 757-763.
22. Vasilev, K.; Mierczynski, A.; Hook, A.; Chan, J.; Voelcker, N. H.; Short, R. D., Creating gradients of two proteins by differential passive adsorption onto a PEG-density gradient. *Biomaterials* **2010**, 31, 392-397.
23. Robinson, D. E.; Marson, A.; Short, R. D.; Buttle, D. J.; Day, A. J.; Parry, K. L.; Wiles, M.; Highfield, P.; Mistry, A.; Whittle, J. D., Surface Gradient of Functional Heparin. *Advanced Materials* **2008**, 20, (6), 1166-1169.
24. Wells, N.; Baxter, M. A.; Turnbull, J. E.; Murray, P.; Edgar, D.; Parry, K. L.; Steele, D. A.; Short, R. D., The geometric control of E14 and R1 mouse embryonic stem cell pluripotency by plasma polymer surface chemical gradients. *Biomaterials* **2009**, 30, (6), 1066-1070.
25. Zelzer, M.; Majani, R.; Bradley, J. W.; Rose, F.; Davies, M. C.; Alexander, M. R., Investigation of cell-surface interactions using chemical gradients formed from plasma polymers. *Biomaterials* **2008**, 29, (2), 172-184.
26. Zelzer, M.; Scurr, D.; Abdullah, B.; Urquhart, A. J.; Gadegaard, N.; Bradley, J. W.; Alexander, M. R., Influence of the plasma sheath on plasma polymer deposition in advance of a mask and down pores. *Journal of Physical Chemistry B* **2009**, 113, (25), 8487-8494.
27. Archambault, J. G.; Brash, J. L., Protein resistant polyurethane surfaces by chemical grafting of PEO: amino-terminated PEO as grafting reagent. *Colloids and Surfaces B: Biointerfaces* **2004**, 39, (1-2), 9-16.
28. Beyer, D.; Knoll, W.; Ringsdorf, H.; Wang, J. H.; Timmons, R. B.; Sluka, P., Reduced protein adsorption on plastics via direct plasma deposition of triethylene glycol monoallyl ether. *Journal of Biomedical Materials Research* **1997**, 36, (2), 181-189.

29. Blättler, T. M.; Pasche, S.; Textor, M.; Griesser, H. J., High Salt Stability and Protein Resistance of Poly(l-lysine)-g-poly(ethylene glycol) Copolymers Covalently Immobilized via Aldehyde Plasma Polymer Interlayers on Inorganic and Polymeric Substrates. *Langmuir* **2006**, 22, (13), 5760-5769.
30. Bretagnol, F.; Kylian, O.; Hasiwa, M.; Ceriotti, L.; Rauscher, H.; Ceccone, G.; Gilliland, D.; Colpo, P.; Rossi, F., Micro-patterned surfaces based on plasma modification of PEO-like coating for biological applications. *Sensors and Actuators B-Chemical* **2007**, 123, (1), 283-292.
31. Cao, L.; Chang, M.; Lee, C. Y.; Castner, D. G.; Sukavaneshvar, S.; Ratner, B. D.; Horbett, T. A., Plasma-deposited tetraglyme surfaces greatly reduce total blood protein adsorption, contact activation, platelet adhesion, platelet procoagulant activity, and in vitro thrombus deposition. *Journal of Biomedical Materials Research Part A* **2007**, 81A, (4), 827-837.
32. Jin, Z.; Feng, W.; Zhu, S.; Sheardown, H.; Brash, J. L., Protein-resistant polyurethane via surface-initiated atom transfer radical polymerization of oligo(ethylene glycol) methacrylate. *Journal of Biomedical Materials Research - Part A* **2009**, 91, (4), 1189-1201.
33. Kim, J. H.; Kim, S. C., PEO-grafting on PU/PS IPNs for enhanced blood compatibility-effect of pendant length and grafting density. *Biomaterials* **2002**, 23, (9), 2015-2025.
34. Wang, Q.; Bohn, P. W., Surface composition gradients of immobilized cell signaling molecules. Epidermal growth factor on gold. *Thin Solid Films* **2006**, 513, (1-2), 338-346.
35. DeLong, S. A.; Gobin, A. S.; West, J. L., Covalent immobilization of RGDS on hydrogel surfaces to direct cell alignment and migration. *J. Control. Release* **2005**, 109, (1-3), 139-148.
36. Bhat, R.; Chaney, B.; Rowley, J.; Liebmann-Vinson, A.; Genzer, J., Tailoring Cell Adhesion Using Surface-Grafted Polymer Gradient Assemblies. *Advanced Materials* **2005**, 17, (23), 2802-2807.
37. Simon, C. G.; Yang, Y. Y.; Thomas, V.; Dorsey, S. M.; Morgan, A. W., Cell Interactions with Biomaterials Gradients and Arrays. *Combinatorial Chemistry & High Throughput Screening* **2009**, 12, (6), 544-553.
38. Menzies, D. J.; Cowie, B.; Fong, C.; Forsythe, J. S.; Gengenbach, T. R.; McLean, K. M.; Puskar, L.; Textor, M.; Thomsen, L.; Tobin, M.; Muir, B. W., One-Step Method for Generating PEG-Like Plasma Polymer Gradients: Chemical Characterization and Analysis of Protein Interactions. *Langmuir* 26, (17), 13987-13994.
39. Muir, B. W.; Tarasova, A.; Gengenbach, T. R.; Menzies, D. J.; Meagher, L.; Rovere, F.; Fairbrother, A.; McLean, K. M.; Hartley, P. G., Characterization of Low-Fouling Ethylene Glycol Containing Plasma Polymer Films. *Langmuir* **2008**, 24, (8), 3828-3835.
40. G. Beamson and D. Briggs, *High Resolution XPS of Organic Polymers*,. 1st edition ed.; John Wiley & Sons Ltd: Chichester, 1992.
41. Brétaganol, F.; Lejeune, M.; Papadopoulou-Bouraoui, A.; Hasiwa, M.; Rauscher, H.; Ceccone, G.; Colpo, P.; Rossi, F., Fouling and non-fouling surfaces produced by plasma polymerization of ethylene oxide monomer. *Acta Biomaterialia* **2006**, 2, (2), 165-172.

42. Brétagne, F.; Ceriotti, L.; Lejeune, M.; Papadopoulou-Bouraoui, A.; Hasiwa, M.; Gilliland, D.; Ceccone, G.; Colpo, P.; Rossi, F., Functional Micropatterned Surfaces by Combination of Plasma Polymerization and Lift-Off Processes. *Plasma Processes and Polymers* **2006**, 3, (1), 30-38.
43. Michel, R.; Pasche, S.; Textor, M.; Castner, D. G., Influence of PEG Architecture on Protein Adsorption and Conformation. *Langmuir* **2005**, 21, (26), 12327-12332.
44. Choi, C.; Jung, D.; Moon, D. W.; Lee, T. G., Surface analysis of protein-resistant, plasma-polymerized ethylene glycol thin films. *Surface and Interface Analysis* **2010**, 43, (1-2), 331-335.
45. Chen, H.; Zhang, Y. X.; Li, D.; Hu, X. Y.; Wang, L.; McClung, W. G.; Brash, J. L., Surfaces having dual fibrinolytic and protein resistant properties by immobilization of lysine on polyurethane through a PEG spacer. *Journal of Biomedical Materials Research Part A* **2009**, 90A, (3), 940-946.
46. Lee, S. J.; Khang, G.; Lee, Y. M.; Lee, H. B., The effect of surface wettability on induction and growth of neurites from the PC-12 cell on a polymer surface. *Journal of Colloid and Interface Science* **2003**, 259, (2), 228-235.
47. Bhat, R. R.; Chaney, B. N.; Rowley, J.; Liebmann-Vinson, A.; Genzer, J., Tailoring cell adhesion using surface-grafted polymer gradient assemblies. *Advanced Materials* **2005**, 17, (23), 2802-2807.

Part 3:

Generation and Characterisation of Chemically Micropatterned surfaces



Chapter 7:

One step multifunctional micropatterning of surfaces using asymmetric glow discharge plasma polymerisation

PART B: Suggested Declaration for Thesis Chapter

Monash University

Declaration for Thesis Chapter 7

Declaration by candidate

In the case of Chapter7, the nature and extent of my contribution to the work was the following:

Nature of contribution	Extent of contribution (%)
Experimental design and conduct, data processing, manuscript writing	70 %

The following co-authors contributed to the work. Co-authors who are students at Monash University must also indicate the extent of their contribution in percentage terms:

Name	Nature of contribution	Extent of contribution (%) for student co-authors only
Thomas Gengenbach	Experimental advice and Manuscript corrections	
John Forsythe	Assisted in experimental design and manuscript correction	
Nick Birbilis	Assisted in experimental conduct	
Christine Charles	Assisted in experimental conduct	
Graham Johnson	Assisted in experimental conduct	
Gail McFarland	Assisted in experimental conduct	
Patrick Leech	Assisted in experimental conduct	
Celesta Fong	Assisted in experimental conduct and manuscript corrections	
Richard Williams	Assisted in experimental conduct and manuscript corrections	
Keith McLean	Manuscript corrections	
Ben Muir	Experimental design, manuscript writing and correction	

Candidate's
Signature



Date

30/05/2011

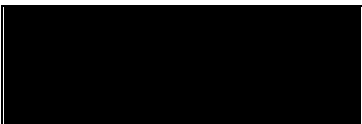
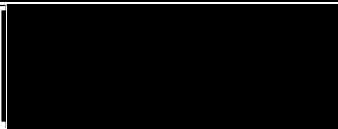
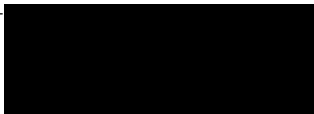
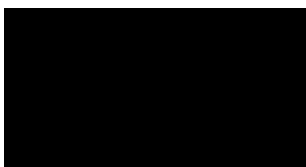

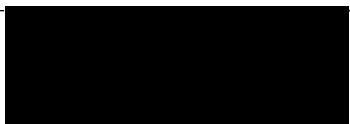
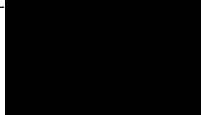
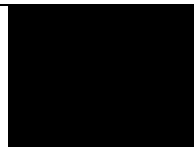

Declaration by co-authors

The undersigned hereby certify that:

- (1) the above declaration correctly reflects the nature and extent of the candidate's contribution to this work, and the nature of the contribution of each of the co-authors.

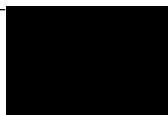
- (2) they meet the criteria for authorship in that they have participated in the conception, execution, or interpretation, of at least that part of the publication in their field of expertise;
- (3) they take public responsibility for their part of the publication, except for the responsible author who accepts overall responsibility for the publication;
- (4) there are no other authors of the publication according to these criteria;
- (5) potential conflicts of interest have been disclosed to (a) granting bodies, (b) the editor or publisher of journals or other publications, and (c) the head of the responsible academic unit; and
- (6) the original data are stored at the following location(s) and will be held for at least five years from the date indicated below:

Location(s)	CSIRO, Materials Science and Engineering
--------------------	---

Signature		Date
Thomas Gengenbach CSIRO, Materials Science and Engineering		4/7/2011
John Forsythe Materials Engineering, Monash University		5/7/11
Nick Birbilis Materials Engineering, Monash University		30/5/2011
Christine Charles Research School of Physics and Engineering, Australian National University		30/05/11
Graham Johnson CSIRO, Materials Science and Engineering		31/5/2011
Gail McFarland CSIRO, Materials Science and Engineering		31.05.2011
Celesta Fong CSIRO, Materials Science and Engineering		30/5
Richard Williams CSIRO, Materials Science and Engineering		30/5/2011
Keith McLean CSIRO, Materials Science and Engineering		30/5/11

Ben Muir

CSIRO, Materials Science
and Engineering



30/5/11

.....

7. One step multifunctional micropatterning of surfaces using asymmetric glow discharge plasma polymerisation

Donna J. Menzies, Thomas Gengenbach, John Forsythe, Nick Birbilis, Graham Johnson, Christine Charles, Gail McFarland, Richard Williams, Celesta Fong, Patrick Leech, Keith McLean and Benjamin W. Muir*

[*] Dr. B. W. Muir, D. J. Menzies, Dr. T. Gengenbach, Dr. G. Johnson, Dr. G. McFarland, Dr. R. Williams, Dr. C. Fong, Dr. P. Leech and Dr. K. McLean: CSIRO, Materials Science and Engineering, VIC 3169, Australia

E-mail: 

Dr. J. Forsythe, Dr N. Birbilis and D.J. Menzies: Monash University, Dept of Materials Engineering, VIC 3800, Australia

Dr. C. Charles: Australian National University, Research School of Physics and Engineering, Space Plasma, Power and Propulsion Laboratory, ACT 0200, Australia

7.1 Abstract

Micropatterning of surfaces with varying chemical, physical and topographical properties usually requires a number of fabrication steps and specific substrate materials, increasing complexity and production costs. Herein, we describe a technique based on plasma enhanced chemical vapour deposition which allows the substrate independent micropatterning of multifunctional, selective surface chemistries in one step without solvents. In this ‘top down’ method, which we have termed ‘Plasma induced patterning via Electrode Templates’ (PIPET), a patterned upper electrode is used to generate a non-uniform plasma in which film deposition is controlled to produce chemical micropatterns. We illustrate the versatility of this technique via the controlled adhesion of proteins, geometric confinement of cells and the spatial confinement of peptide self-assembly. This

multifunctional micropatterning technique has broad applicability in the fields of cell biology, tissue engineering and biomedical science. It could potentially form the basis of new applications in fields such as optics and electronics.

Keywords: Surface Modification, Thin Films, Self-Assembly, Polymeric Materials

7.2 Introduction

Micropatterning of surfaces with varying chemical, physical and topographical properties usually requires a number of fabrication steps and specific substrate materials. Herein, we describe a technique based on plasma enhanced chemical vapour deposition (PECVD) which allows the substrate independent micropatterning of multifunctional, selective surface chemistries in one step without solvents. In this method, which we have termed ‘Plasma Induced Patterning via Electrode Templates’ (PIPET), a patterned upper electrode is used to generate a non-uniform plasma in which film deposition is controlled to produce chemical micropatterns.

The generation of regular arrays of multiple polymer surface chemistries or features on a surface is routinely used in a number of research fields.¹⁻⁴ Polymer micropatterning techniques generally require a number of steps to produce the desired features. These methods include photochemical⁹ and lithographic¹⁰ techniques.¹¹ With the exception of a small number of emerging patterning techniques¹², these methods require further chemical derivatisation for optimal functionality.^{8, 12} The novel technique reported here is based on PECVD and is the first example of a substrate independent, solvent free, one-step process that allows the generation of stable multifunctional micropatterns. PECVD¹³

generates plasma polymer (pp) films that comprise cross-linked and fragmented combinations of the gaseous monomer. PECVD enables the modification of various substrate materials^{14,15} and is scalable for use in sterile environments.¹⁶ However, existing plasma based patterning methods such as etching¹³, plasma lithography,¹⁵ and microplasmas^{15, 17} require numerous production steps for use in biological applications where surface passivation and activation is necessary.

7.3 Materials and Methods

7.3.1 Plasma polymer deposition

Plasma polymerisations were performed in a custom-built reactor (see Appendix 2) on pre-cleaned ultra-flat single crystal, silicon wafers (<100>, 1 cm² x 0.5 mm thick,) and pre-cleaned glass slides (Biolab).¹⁹ Diethylene glycol dimethyl ether (BDH, 99% purity) was deposited at 125 KHz, a load power of 5 W, monomer pressure of 20 Pa for 120 seconds. Cell attachment and self-assembling peptide studies on the DGpp patterned surfaces were performed on glass substrates that were pre-coated with a heptylamine pp film (Aldrich,) (200 kHz, power of 30 W, monomer pressure of 40 Pa for 30 seconds.

7.3.2 Preparation of patterned plasma reactor electrodes

Patterned electrodes were produced via lithographic etching on thin copper. The electrodes comprised arrays of circles (0.9-1.6 mm diameter) or squares, and triangles with maximum cross dimension of 1.25-1.5 mm and an interspacing of approximately 2 mm.

7.3.3 Optical images of patterns

Optical images of the DGpp patterned features were collected using an “Infinity X” camera (Luminera) attached to a binocular Microscope (Kyowa) at 0.7x magnification.

7.3.4 Optical profilometry

Images of the patterned films were obtained using a Wyko NT1100 Optical Profilometer (Veeco) at 5x magnification using a field of view of 1.

7.3.5 giFTIR microspectroscopy

Chemical maps across the DGpp patterned spot were acquired using a synchrotron source FTIR microscope (Australian Synchrotron). Using a Bruker Vertex 80v FTIR spectrometer coupled to a Bruker Hyperion 2000 IR microscope, spectra were collected in grazing incidence mode using a Grazing Angle Objective at 15x magnification. Spectra (256 scans) were acquired using a 20 x 20 μm aperture and step size of 50 x 50 μm (spectral resolution of 6.0 cm^{-1}). Bruker Opus software version 6.5 equipped with video mapping was used to generate 2D absorbance maps. Data was converted to 3D chemical maps using the OPUS 6.5 software, corrected with an eight point baseline correction and normalized to the alkane stretch (~ 2850 to 3000 cm^{-1}).

7.3.6 ToF-SIMS measurements

ToF SIMS measurements were performed using an ION-TOF IV, with a reflectron time-of-flight analyser. Positive ion spectra were collected using a 25 keV Bi^+ primary-ion beam in high-current-bunched mode over a region of interest of 500 μm^2 at a resolution of 256 pixels².

7.3.7 Protein adsorption

Patterned films were incubated in BSA (Sigma) (in PBS (1 mg/mL at pH 7.4) for one hour at room temperature and thoroughly rinsed.

7.3.8 Cell culture

The micropatterned slides were sterilised overnight in 2 ml of 1xPBS containing 200 units/ml penicillin and 200 $\mu\text{g}/\text{ml}$ streptomycin (GIBCO). HeLa cells were seeded onto

the glass slides at a density of 1×10^6 cells/chamber in 7 ml of fresh Dulbecco's Modification of Eagle's Medium/Ham's F12 (MP Biomedicals) supplemented with 10% (v/v) FBS (ICP BiologicalsTM), 100 units/ml penicillin and 100 μ g/ml streptomycin. The cells were incubated for up to 7 days at 37° C in humidified air containing 5% CO₂. For the final hour of incubation (either day 1 or day 7) the medium was removed from each slide chamber and replaced with 7ml/slide of fresh complete medium containing CellTrackerTM Green (Molecular Probes,) at a dilution of 1:1,000. The culture medium was then removed and each slide rinsed with sterile 1x PBS pH 7.4. Cells were fixed for 30 minutes with 4 % formol saline at room temperature, then washed with PBS and deionised water. Fluorescent images of representative cells were obtained using a Nikon Eclipse 90i microscope equipped with epifluorescence illumination. The CellTrackerTM green stained cells were imaged at $\lambda = 488$ nm at 2x and 10x magnification.

7.3.9 Site specific growth of self assembling peptides

The patterned slides were incubated for 4 hours in Thermolysin from *Proteoloyticus rokko* (Sigma Aldrich, 2 mg/ml) before unbound enzyme was removed by rinsing. Reactants were prepared to a final concentration of 20 mM Fmoc-L and 40 mM Leu-Leu (Sigma Aldrich) by the addition of pH 8.5, 10 mM Tris buffer. The pH was then adjusted to 7.2 and Congo red stock solution was added to a final concentration of 10 mM. The reactant solution was then added to the surface of the slide, and left to incubate for 4 hours. Hydrogel spots were dried under nitrogen, and imaged using cross polarised microscopy.

7.4 Results and Discussion

The key innovation of PIPET is a patterned upper electrode (Figure 7.1a and Appendix 2), where an asymmetric glow discharge occurs, resulting in a spatial variation of the bulk plasma and sheath, which affects the chemical structure of the resulting plasma polymer. The versatility of this technique is illustrated via the controlled adhesion of proteins, geometric confinement of cells and the spatial confinement of peptide self-assembly. The performance of biomaterial devices is dependent on their ability to resist or control protein and cell adhesion.^{18, 19} The monomer diethylene glycol dimethyl ether (DG) was utilised in this work as it contains ether units which form the backbone of poly(ethylene glycol) (PEG) molecules.²⁰ The ether functionality of PEG polymers is critical to their low-fouling nature.²¹ The use of PIPET with DG, provides patterned surfaces with regions of both high ether (PEG-like) and low ether (non PEG-like) chemistries (Figure 7.1b). ‘Non-PEG-like’ chemistries occur directly under the holes of the patterned electrode which is attributable to greater monomer fragmentation in this region. The ‘PEG-like’ character of the surface increases radially from the centre of the patterned features.

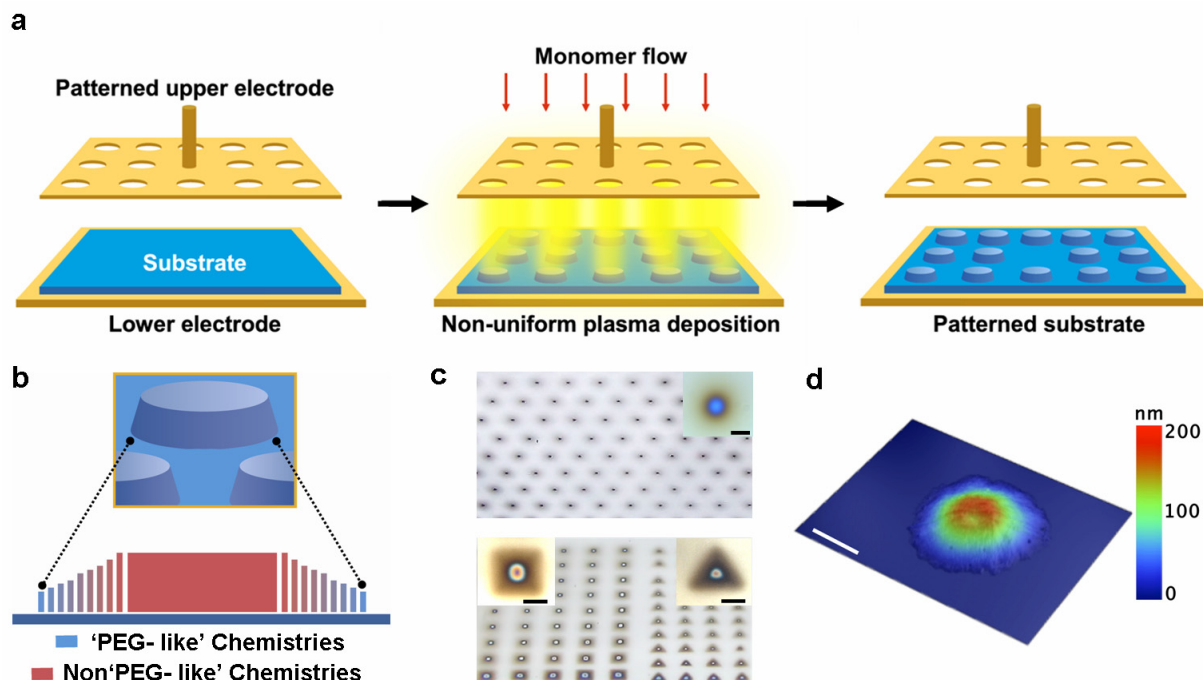


Figure 7.1. a, Schematic of the PIPET technique. b, Variation in film chemistry and crosslink density across a spot. Within a spot the chemistry is less ‘PEG-like’ compared to the surrounding film. c, Optical microscopy images of patterned surfaces on silicon wafers (scale bars are 200 μm). The colours inside the elevated features arise from interference of reflected light between the upper and lower film boundaries. Lighter areas in the optical images correlate with thinner ‘PEG-like’ film chemistries. d, Optical profilometry image across a spot (scale bar is 200 μm).

The size (microns to millimetres), thickness (nanometres) and shape of the patterned features can be easily varied by manipulation of the geometry of the upper electrode and PECVD conditions (Figure 7.1c). The features produced are the same size as the open holes in the upper electrode, displaying good fidelity. The increased thickness of the films within the centre of the patterned shapes was confirmed via analysis with optical profilometry (Figure 7.1d). The elevated features are approximately 200 nm above the surrounding PEG-like regions which are 60 nm in thickness, when using electrode patterned features 1 mm in size.

For PIPET to be useful in biological applications, it is necessary to have spatial control over surface chemistry in well-defined regions. Grazing incidence Fourier Transform Infra-Red (giFTIR) microspectroscopy and time-of-flight secondary ion mass spectroscopy (ToF-SIMS) was used to analyse patterned circles. Chemical maps (Figure 7.2 a-c) show a higher carbonyl and lower ether content within the circle compared with the surrounding PEG-like film. This suggests that the plasma discharge and hence, monomer fragmentation is more energetic in this region. The presence of these carbonyl functional groups originates from bond scission of the monomer and post oxidation reactions. Modelling of the plasma sheath physics using argon cross sections further validates these findings (see Appendix 2). The model estimated the main plasma parameters for comparison with the inter-electrode distance and the patterned hole size (Appendix 2, Table 1). The Debye length was calculated to be of the order of 100 μm which is comparable to the hole size in the upper electrode, and suggests that the limit to the pattern fidelity using PIPET is around 100 μm . Plasma sheaths are regions where charge separation can occur and strong electron and ion density gradients are present. The sum of the live (0.8 mm) and earth sheath (0.2 mm) thicknesses is comparable to the inter-electrode distance suggesting that the plasma bulk can be neglected and the process is dominated by the sheath at the patterned electrode. As the hole size is of the order of the Debye length, it is possible to have gradients in both the electron and ion density across the holes which spatially affects monomer fragmentation and ionisation. The non-uniformity of the plasma discharge conforms qualitatively with the hole patterns within the upper electrode.

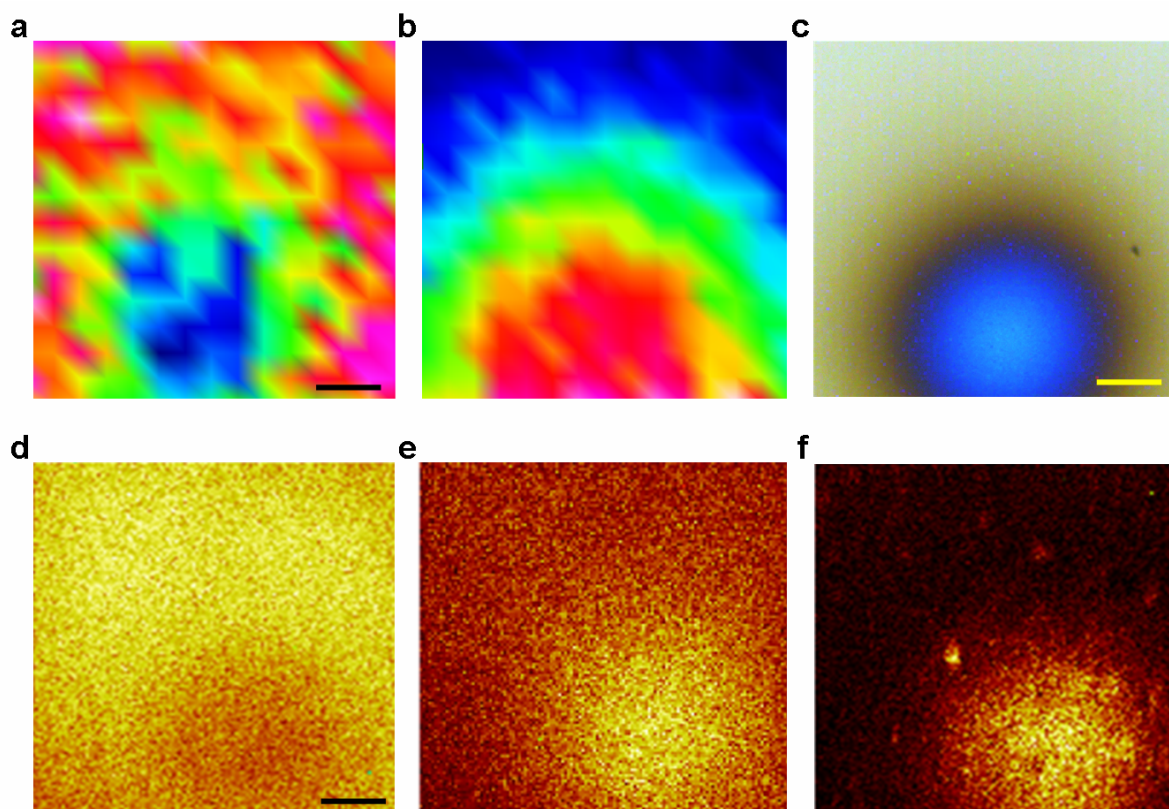


Figure 7.2 a-b, Synchrotron giFTIR plots of the intensity of ether & carbonyl stretches across a spot (high intensity is shown in red and low intensity in blue), c, Optical microscopy image of the spot, d-e, ToF-SIMS intensity plots of characteristic ether fragments ($C_3H_7O^+$, $C_3H_6O^+$, $C_3H_5O_2^+$, $C_4H_9O^+$, $C_4H_8O_2^+$, $C_5H_{10}O^+$, $C_5H_{11}O_2^+$) & hydrocarbon fragments ($C_4H_9^+$, $C_5H_5^+$, $C_6H_5^+$, $C_7H_7^+$) from a PIPET spot, f, ToF-SIMS intensity plots of characteristic nitrogen containing fragments ($C_5H_5N^+$, $C_3H_8N^+$, $C_5H_{10}N^+$, $C_5H_{12}N^+$) after incubation of a PIPET spot with protein (BSA). For ToF-SIMS images high intensity is shown in yellow and low intensity in black. Scale bar in all images is 100 μ m.

To demonstrate the utility of PIPET in biomedical research it was proposed that it should be possible to produce site-specific ‘islands’ for the containment of protein immobilisation, cell proliferation and enzyme assisted self-assembly in a microarray format. Imaging ToF-SIMS was used to map the surface chemistries before and after incubation with bovine serum albumin (BSA) (Figure 7.2d-f). Collective, images of positive ether related ion fragments commonly reported in PEG-like materials²² are shown in Figure 7.2d and hydrocarbon ion fragments in Figure 7.2e for a surface prior to incubation with BSA. Strong image contrast and good pattern fidelity is observed for all

of the ions, with higher concentrations of hydrocarbon fragments being localized in the centre of the circle. More ether or PEG-like ion fragments are observed in the surrounding film. BSA adsorption was strongly retained within the centre of the circle, as indicated by significantly more nitrogen containing ions (Figure 7.2f) in these regions. X-ray Photoelectron Spectroscopy (XPS) confirmed the spatial variation of surface chemistries (see Appendix 2).

In the second example we demonstrate the preferential confinement and growth of an adherent HeLa cell line. Optical images of the patterns used to confine cell growth are shown in Figure 7.3a and 3b for a planar array of HeLa cells, in which individual cells attach and spread in the centre of the patterns. The ‘PEG-like’ regions support minimal cell attachment. The long term stability and robustness under physiological conditions of such patterns is a key performance characteristic. To exemplify the robustness of the PIPET films, cells were incubated on circular patterns for 1 and 7 days (Figure 7.3c-d). After 7 days culture the cells have proliferated but remain constrained within the patterned boundary. The surrounding PEG-like regions of the film retained its biological inertness; although a small number of cells were observed initially, these were not viable after several days. This observation is consistent with the concept that the patterns have retained their ability to support both initial cell attachment and spreading, as well as subsequent proliferation.

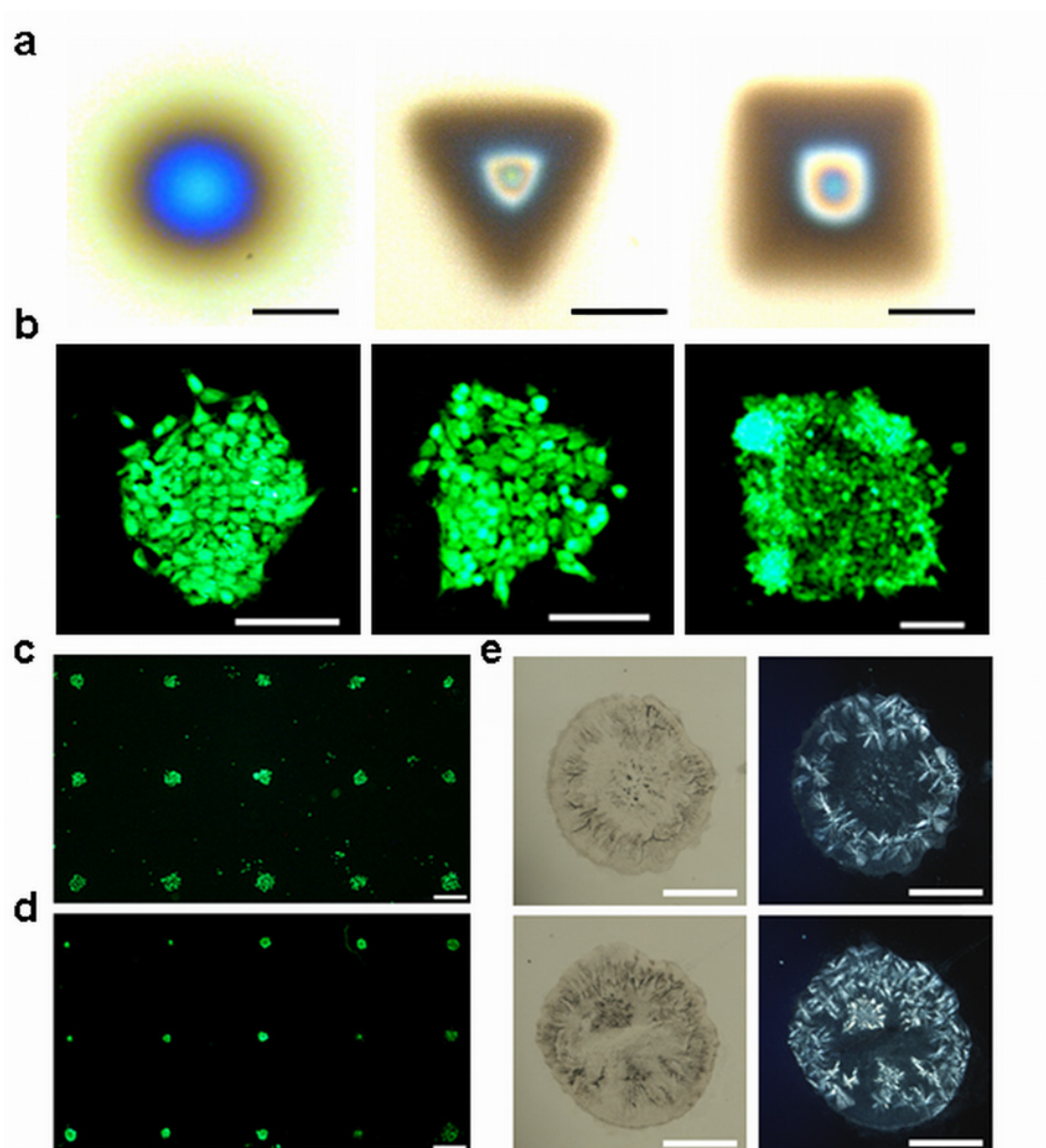


Figure 7.3 PCA analysis of positive ToF-SIMS mass spectra recorded on the gradients after exposure to HSA: (A) PC1 scores as a function of distance across the 5 (A) and 30 W (B) gradients, and (C) and (D) loadings of hydrocarbon, oxygen-containing and nitrogen-containing fragment ions on PC1 (note that loadings of immonium ions are negligible across the 5 W gradient; e.g., $C_2H_6N^+$). The score plots reveal the oscillating adsorption across the gradients (most pronounced across 5 W gradient), consistent with the spatial chemistry variations measured by ToF-SIMS prior to protein incubation

For microarray applications, an arrayed protein must remain functional. In order to explore the potential of PIPET for microfabrication, we utilised a system in which a localised enzyme was used to direct the self-assembly of a peptide hydrogel.²³ The formation of the self-assembling peptide was catalysed by a proteolytic enzyme and the self-assembly process occurred at the site of enzyme activity (Appendix 2). When the solution of peptide reactants is added, the self-assembly occurs in the vicinity of the enzyme adsorbed in the centre of the patterned circles (Figure 7.3e). Spots of hydrogel were observed around 500 μm in diameter, suggesting the enzymes are localised which yield nucleation sites, and the hydrogel ‘grows’ to cover an area greater than the spot of enzyme during the self-assembly. The presence of the self-assembled, peptide β - sheets were validated as birefringence (Figure 7.3e). We envisage that this technique could be used to form complex patterns of self-assembled peptide hydrogels or enzyme arrays for fabrication, tissue culture and sensing with potential applications in cell culture,²⁴ nanoelectronics, and signalling.

7.5 Conclusions

We have described a new approach for the generation of substrate independent, multifunctional surface chemistries that are cell and protein resistant/adherent in a single step. The patterning technique is extremely versatile, tunable, solvent free and scalable. We have demonstrated the broad utility of this strategy through the controlled adhesion of proteins, confinement of HeLa cells and enzyme-assisted peptide self-assembly. The method enables the production of various geometrical shapes and micropattern properties to be deposited with good spatial and chemical fidelity. This multifunctional

micropatterning technique has broad applicability in the fields of cell biology, tissue engineering and biomedical science. The technique has the potential for use with a range of different monomers depending on the application. This multifunctional micropatterning technique could potentially form the basis of new applications in additional fields such as optics, electronics, surface science and High-Throughput research which require the micropatterning of thin films.

7.6 References

1. M. L. Renak, G. C. Bazan, D. Roitman. Microlithographic process for patterning conjugated emissive polymers. *Advanced Materials* **1997**, 9, 392.
2. C. S. Chen, M. Mrksich, S. Huang, G. M. Whitesides, D. E. Ingber. Geometric control of cell life and death. *Science* **1997**, 276, 1425.
3. H. Tavana, A. Jovic, B. Mosadegh, Q. Y. Lee, X. Liu, K. E. Luker, G. D. Luker, S. J. Weiss, S. Takayama, *Nature Materials* **2009**, 8, 736.
4. G. C. Engelmayr, M. Cheng, C. J. Bettinger, J. T. Borenstein, R. Langer, L. E. Freed. Nanolitre liquid patterning in aqueous environments for spatially defined reagent delivery to mammalian cells. *Nature Materials* **2008**, 7, 1003.
5. Z. Nie, E. Kumacheva. Patterning surfaces with functional polymers. *Nature Materials* **2008**, 7, 277.
6. Q. Cheng, S. Li, K. Komvopoulos. Plasma-assisted surface chemical patterning for single-cell culture. *Biomaterials* **2009**, 30, 4203.
7. A. Goessl, M. D. Garrison, J. B. Lhoest, A. S. Hoffman. Plasma lithography - Thin-film patterning of polymers by RF plasma polymerization II: Study of differential binding using adsorption probes. *Journal of Biomaterials Science, Polymer Edition* **2001**, 12, 721.
8. F. Brétagne, O. Kylián, M. Hasiwa, L. Ceriotti, H. Rauscher, G. Ceccone, D. Gilliland, P. Colpo, F. Rossi. Micro-patterned surfaces based on plasma modification of PEO-like coating for biological applications. *Sensors and Actuators, B*. **2007**, 123, 283.
9. M. S. Hahn, L. J. Taite, J. J. Moon, M. C. Rowland, K. A. Ruffino, J. L. West. Photolithographic patterning of polyethylene glycol hydrogels. *Biomaterials* **2006**, 27, 2519.
10. R. S. Kane, S. Takayama, E. Ostuni, D. E. Ingber, G. M. Whitesides. Patterning proteins and cells using soft lithography. *Biomaterials* **1999**, 20, 2363.
11. R. D. Piner, J. Zhu, F. Xu, S. H. Hong, C. A. Mirkin. "Dip-pen" nanolithography. *Science* **1999**, 283, 661.
12. R. Klajn, M. Fialkowski, I. T. Bensemann, A. Bitner, C. J. Campbell, K. Bishop, S. Smoukov, B. A. Grzybowski. Multicolour micropatterning of thin films of dry gels. *Nature Materials* **2004**, 3, 729.
13. P. K. Chu, J. Y. Chen, L. P. Wang, N. Huang. Plasma-surface modification of biomaterials. *Materials Science and Engineering Reports* **2002**, 36, 143.
14. T. Desmet, R. Morent, N. De Geyter, C. Leys, E. Schacht, P. Dubruel. Nonthermal plasma technology as a versatile strategy for polymeric biomaterials surface modification: A review. *Biomacromolecules* **2009**, 10, 2351.
15. G. S. Malkov, I. T. Martin, W. B. Schwisow, J. P. Chandler, B. T. Wickes, L. J. Gamble, D. G. Castner, E. R. Fisher. Pulsed-plasma-induced micropatterning with alternating hydrophilic and hydrophobic surface chemistries. *Plasma Processes and Polymers* **2008**, 5, 129.
16. Y. N. Xia, G. M. Whitesides. Soft lithography. *Annual Review of Material Science* **1998**, 28, 153.
17. M. Leduc, S. Coulombe, R. L. Leask. Atmospheric Pressure Plasma Jet Deposition of Patterned Polymer Films for Cell Culture Applications. *IEEE Transactions on Plasma Science* **2009**, 37, 927.

18. R. G. Chapman, E. Ostuni, L. Yan, G. M. Whitesides. Preparation of Mixed Self-Assembled Monolayers (SAMs) That Resist Adsorption of Proteins Using the Reaction of Amines with a SAM That Presents Interchain Carboxylic Anhydride Groups. *Langmuir* **2000**, *16*, 6927.
19. B. Muir, A. Fairbrother, T. Gengenbach, F. Rovere, M. Abdo, K. McLean, P. Hartley. Scanning Probe Nanolithography and Protein Patterning of Low-Fouling Plasma Polymer Multilayer Films. *Advanced Materials* **2006**, *18*, 3079.
20. J. Israelachvili. The different faces of poly(ethylene glycol). *The National Academy of Sciences of the USA* **1997**, *94*, 8378.
21. R. A. Latour, Thermodynamic perspectives on the molecular mechanisms providing protein adsorption resistance that include protein-surface interactions. *Journal of Biomedical Materials Research Part A* **2006**, *78A*, 843.
22. F. Brétagnot, L. Ceriotti, M. Lejeune, A. Papadopoulou-Bouraoui, M. Hasiwa, D. Gilliland, G. Ceccone, P. Colpo, F. Rossi. Functional Micropatterned Surfaces by Combination of Plasma Polymerization and Lift-Off Processes. *Plasma Processes and Polymers* **2006**, *3*, 30.
23. R. J. Williams, A. M. Smith, R. Collins, N. Hodson, A. K. Das, R. V. Ulijn. Enzyme-assisted self-assembly under thermodynamic control. *Nature Nanotechnology* **2009**, *4*, 19.
24. V. Jayawarna, M. Ali, T. A. Jowitt, A. E. Miller, A. Saiani, J. E. Gough, R. V. Ulijn. Nanostructured hydrogels for three-dimensional cell culture through self-assembly of fluorenylmethoxycarbonyl-dipeptides. *Advanced Materials*. **2006**, *18*, 611.

Chapter 8:

Conclusions and Future Works

8. Conclusions and Future Works

8.1 Conclusions

In this work, the generation and characterization of low-fouling uniform and gradient coatings and chemically patterned surfaces capable of manipulating biomolecules and cell interactions has been reported. Radio frequency glow discharge plasma polymerization of diethylene glycol dimethyl ether (diglyme, DG) was employed for surface fabrication, with manipulation of the upper active electrode in terms of shape and dimensions performed to achieve the gradient and patterned surfaces, compared to the conventional uniform plasma polymer surface. The results component of this thesis was categorised into three main sections, including uniform, gradient and micropatterned surfaces, and as such I will discuss the findings and conclusions for each of these topics separately.

8.1.1 Uniform PEG like plasma polymers

Chapters 3 and 4 presented uniform DG plasma polymer surfaces that were extensively characterized for their chemical properties, as a function of the deposition load power and the resulting protein and cell repulsive capabilities. **Chapter 3** investigated the effects of plasma processing conditions on the continuous wave, radio-frequency glow discharge plasma polymerisation of diethylene glycol dimethyl ether in terms of producing uniform, robust, low fouling PEG-like surfaces. The flow rate of the DG monomer was investigated and defined in the capacitatively coupled plasma reactor, used for the deposition of the DGpp films discussed and presented in this thesis. The effect of the W/FM factor (Yasuda factor) on the resulting DGpp films was also investigated by producing a series of films deposited at

systematically increasing load power, including 5, 10, 20, 30, 40 and 50 W over a standard 60 second deposition period.

A thorough chemical analysis of the films was performed by a combination of complimentary techniques, including grazing incidence FTIR, XPS and NEXAFS. Results concluded that films deposited under lower load powers retained more of the original monomer PEG-like character both at the surface and throughout the bulk of the film. The XPS (COR) ether content ranged from 70% in the 5 W DGpp film, decreasing to 34% in the 50 W DGpp. Lower power films were also shown to contain lower amounts of unsaturated and hydrocarbon functionalities due to a lower rate of fragmentation during plasma polymer deposition. Polarised NEXAFS experiments were performed to investigate the role of any chemical surface structuring of the lower fouling plasma polymerised films, however no preferred orientation was observed (in the ultra high vacuum environment).

AFM step height analysis showed the film thickness to increase with higher deposition powers and static contact angles also increased slightly in films deposited at higher load power indicating a small decrease in wettability of the films. The adsorption of lysozyme and BSA increased on films deposited at higher load power and was correlated primarily with the ether content of the films. Only very low levels of proteins were detected on the high ether containing 5 W surface, (less than 1 % N detected from XPS). HeLa cell attachment response also appeared to be dictated by the films ether content with the 5 W DGpp film surface inhibiting cell attachment after 24 hours incubation in the presence of serum, while DGpp films prepared at load powers of 20 and 50 W were very supportive of

HeLa cell attachment. Of those cells that did attach on the 5 W film, cells showed a clumped and rounded morphology as opposed to the well attached and spread cells on the 50 W film.

In **Chapter 4**, which was based around the neutron reflectometry (NR) studies, surfaces were required to be approximately 200 Å in thickness (requirement for NR analysis). To achieve this, while surfaces were deposited at different load powers (10, 20 and 50 W), the time of deposition also had to be optimized/adjusted (45, 20 and 10 seconds respectively). The combination of XPS, neutron and X-ray reflectometry enabled the determination of film mass density, full chemical composition including analysis of hydrogen content (not attainable from XPS or NEXAFS) and degree of solvation. The atomic composition of the 10 W film ($C_2H_{3.3}O_{0.9}$) was closest to that of diglyme ($C_2H_{4.7}O_1$) and most similar to that of PEG polymers ($C_2H_4O_1$), while for the 20 and 50 W films the atomic composition was determined to be $C_2H_{3.3}O_{0.78}$ and $C_2H_{2.0}O_{0.6}$ respectively. All films result in a substantial loss of hydrogen when compared to the starting monomer, with H/C values at the air interface being higher in films deposited at lower load power. Mass density variation of the films was less systematic, however the 10 and 20 films densities were most similar to a typical PEG polymer (1.19 and 1.23 gcm⁻³ respectively), while the 50 W films was lower at 0.99 gcm⁻³.

NR showed that the films absorbed a substantial amount of water (~22 – 40 % v/v for the 20 and 50 W films), and their degree of solvation appeared to be dependent on both film chemistry and mass density profile. QCM-D hydration studies confirmed the higher uptake of water however QCM-D was unable to detect this change in the 20 W film. It was proposed that the surface was losing lower molecular weight surface species while hydration was

occurring and as such, no change in frequency or dissipation was detected. QCM-D was also used to measure protein (BSA) adsorption on the three surfaces, which showed the 10 W film containing a higher ether content to be the most efficient in reducing BSA adsorption. A combination of the lower mass density and less PEG-like surface chemistry of the 50 W plasma polymer film was correlated with the higher amount of protein adsorbed, compared to the 10 and 20 W films. In addition, the low fouling 10 W film was also found to have the highest H/C content at the air interface. Interestingly, the degree of protein adsorption did not positively correlate with films that absorbed higher amounts of water, as is often suggested by the water barrier theory.

8.1.2 PEG-like gradient plasma polymers

In **Chapter 5**, the generation and characterisation of 2-D PEG-like, surface bound chemical gradients deposited at 5 and 30 W is reported. A knife edge upper electrode was employed within the plasma reactor to produce the defined chemical gradients. The chemistry across the gradients was analysed by grazing incidence-FTIR microspectroscopy, XPS and NEXAFS. The ether functionality systematically varied across the gradients (both at the surface and the bulk of the film) with the highest 'PEG like' characteristics in the central region of the films deposited directly underneath the razor electrode. Hydrocarbon, ketone, aldehyde, acid and ester functionality varied across the gradients, being lowest in the central region and increasing radially outwards. Gradients deposited at 5W retained higher ether contents and had lower levels of hydrocarbon and carbonyl functionalities than the 30W gradient films.

Analysis of protein adsorption and interactions was performed using three proteins of varied size and charge, including BSA, lysozyme and IgG. Adsorbed protein gradients were formed and correlated well with the residual ether content from XPS analysis, with the central region of the gradients being the most protein resistant.

Chapter 6 furthered the work reported in chapter 5, by including a ToF-SIMS analysis of both gradient chemistry as well as protein adsorption. ToF-SIMS showed to be more sensitive in detecting lower amounts of adsorbed proteins (human serum albumin). Principal component analysis (PCA) was applied to the ToF-SIMS data both before and after protein adsorption, and highlighted a more oscillating variation to the surface chemistry across the gradients compared to XPS results. The ether related positive fragments were shown to load positively, while the positive hydrocarbon fragments loaded negatively. Very low amounts of N containing fragments (indicative of protein adsorption) was seen across the 5 W gradient, while the adsorption of HSA across the 30 W gradient correlated with a distinct chemical change (specifically higher amounts of positive hydrocarbon fragments) seen at approximately 2 mm either side of the gradient centre.

The adsorption of fetal bovine serum (FBS) across the gradients after 1 and 24 hour incubation was also monitored, as this is often present in cell attachment/culture protocols. Serum adsorption appeared to be influenced by the time of protein incubation and film chemistry. While the central region of the 5 W gradient resisted FBS adsorption after 1 hour, after a 24 hour incubation period, FBS proteins were detected across the entire gradient and this correlated with the attachment of HeLa cells. The central region of the gradients which

retained the highest ether content remained the most protein resistant, as did gradients deposited at lower load power.

8.1.3 Chemically patterned plasma polymer surfaces

The development, generation, characterisation and application of multifunctional micropatterned surfaces was described in **Chapter 7**. To the best of my knowledge, this is the first one-step method described in the literature to generate chemically patterned surfaces. To generate the patterns, a patterned upper electrode was designed with holes of varying shape and size, producing an asymmetric glow discharge during plasma deposition. This results in a spatial variation of the bulk diglyme plasma and sheath (as determined from mathematical modeling of the plasma processes), producing surfaces of distinct high and low ether content. The basis and functioning of micropatterned surfaces relies on a low-fouling background film. The chemistry across the patterned surfaces was analysed and/or imaged using, ToF-SIMS, *gi*-FTIR microspectroscopy and XPS, where the patterned features showed to contain a lower ether content and higher hydrocarbon and carbonyl functionality, while the surrounding coating was shown to be more PEG-like. Optical profilometry confirmed that the patterned features were thicker than the surrounding PEG-like surface. The diverse functioning of the patterned surfaces was displayed through the controlled adhesion of proteins (BSA), as well as the spatial confinement of HeLa cell attachment and enzyme-assisted peptide self-assembly.

8.2 Future Directions

While there has been a lot of work reported on the production and characterisation of low-fouling plasma polymerised uniform coatings, there is not a lot reported on the generation of

gradient and micropatterned surfaces. That is, with the exception of those requiring a moving internal component, for gradient generation, or multiple steps and the use of a physical mask for the case of micropatterned surfaces, as discussed in Chapter 2. The future direction of both the gradient and micro-patterned surfaces generally lends itself to their applications in the field of biomedical, biomaterial and regenerative medicine research.

As was displayed in chapter 5 by the systematically increased adsorption of a graft copolymer of poly(L-Lysine) and poly(ethylene glycol) (PLL-g-PEG copolymer) across the DGpp gradients, these gradients can be utilised to form gradients of other materials/biomolecules of interest, either by physic-sorption or alternatively, covalent coupling. Furthermore, plasma polymerisation of other monomers, such as heptylamine or acetylaldehyde should be investigated. It is envisaged that these would create gradients of chemical functionalities ideal for the chemical coupling of biomolecules of interest.

Another possibility for the advancement of the gradient surfaces includes their use in the generation of orthogonal gradients, where the chemical and or topographical features vary in 3 dimensions. This may enhance the applicability of these surfaces as a high throughput screening tool. Furthermore, the utility of these surfaces has not been extensively analysed. These surfaces should be capable of generating high throughput material-biological analysis with other biological matter such as stems cells and DNA.

In terms of micro-patterning, the future focus should be on pattern miniaturisation and distinction, by investigation into plasma processing parameters and electrode geometry. The technique has the potential for use with a range of different monomers depending on the

application and as with the gradients, the future of the patterned surfaces lies in their applications. This multifunctional micropatterning technique could potentially form the basis of new applications in additional fields such as optics, electronics, surface science and High-Throughput research which require the micropatterning of thin films. However in the fields of biomaterials and regenerative medicine, some important aspects which should be probed further, include the use of stem cell behavior, where the effect of inter-pattern distance and pattern size and shape should be used to investigate stem cell fate, function and differentiation.

Appendix 1

Supporting Information for Chapter 5

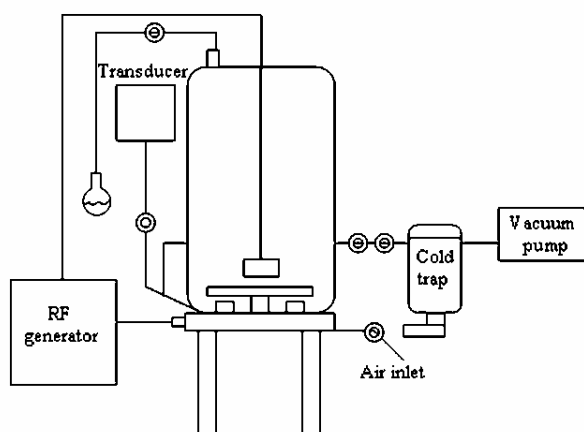


Figure 1. Schematic diagram of the radio-frequency plasma discharge reactor used for the fabrication of gradient PEG-like plasma polymer films. A knife-edge top electrode is attached to the RF source and lowered to 1 mm above the sample substrate.

Explanatory Note:

Using a knife edge razor within the plasma reactor lowered to sit ~ 1mm above the substrate (Figure 1) chemical gradients were deposited from diglyme monomer. Using the electrode configuration shown in the above figure, results in a variation to the plasma sheath surrounding the live electrode, generating PEG-like chemical plasma polymer gradients. The monomer was fed into the jar bell plasma reactor and the RF source ignited at a starting pressure of 20 Pa. Deposition continued for 180 seconds at a load power of 5 and 30 W.

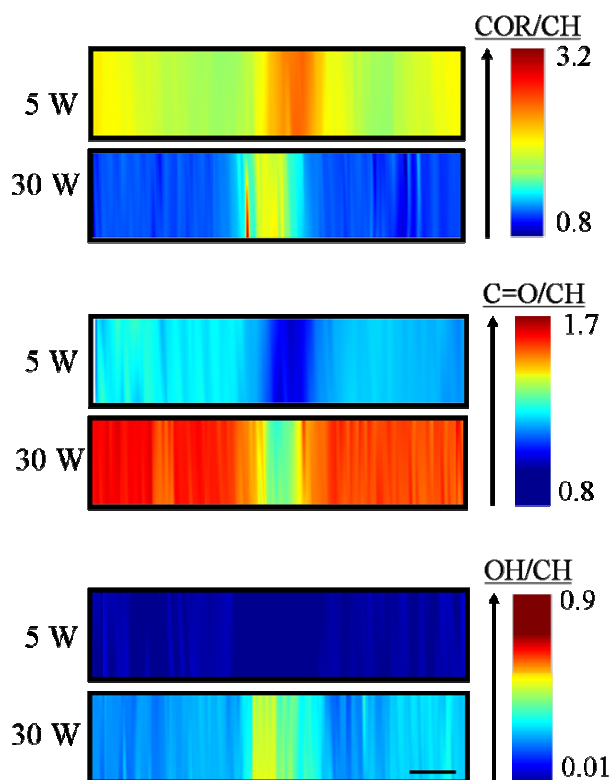


Figure 2. giFTIR surface plots for the 5 and 30 W gradient films were acquired at 500 x 250 μm in the X and Y directions respectively, and converted to 2D plots representing the relative concentration (calculated from area under each component stretch) of ether (COR), carbonyl (C=O) and hydroxyl (OH) stretches as a ratio to the hydrocarbon (CH) stretch (scale bar represents 1 mm)

Explanatory Note:

2D chemical mapping experiments performed across the 5 and 30 W DGpp gradients using synchrotron source giFTIR microspectroscopy indicates that the chemical gradient is strongest directly below the knife edge electrode. In this work we refer to this point as the centre of the gradient films. FTIR spectra were recorded across the DGpp gradients and were subsequently converted to area intensity plots. These plots represented the integrated area of the COC, C=O and –OH functionalities respectively as a ratio to that of the normalised CH stretch. The CH stretch was normalised to minimise any thickness effects contributing to a change in the absorption of the chemical functionalities across the gradients. Figure 2 compares the intensity plots related to the relative concentration of ether, carbonyl and hydroxyl functionality across the 5 and 30 W gradients. The ether content was found to be

highest at the centre of both of the gradients. The 5 W gradients retained more monomer like functionality with a greater contribution to the giFTIR spectra from the ether stretch when compared to the 30 W gradients. An opposing trend was observed when comparing the relative contribution to the giFTIR spectra from the carbonyl and hydroxyl stretches. In this case the central region of each gradient had lower amounts of carbonyl and hydroxyl groups compared to the outer regions of the gradient and the 5 W had lower levels of components when compared to the 30 W gradient films.

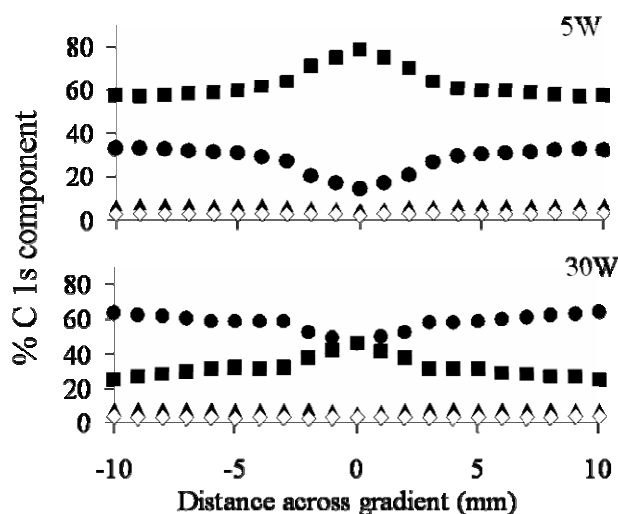


Figure 3. XPS C1s curve fitted component data presented as percentage C1s component vs. distance from the centre of the 5 W and 30 W gradient films. Fitted components are C-C, C-H (■), C-O (●), C=O (▲) and O-C=O (◇) and percentages are relative to total carbon.

Explanatory Notes:

To analyse the surface chemistries present across the DGpp gradients, high resolution C 1s XPS curves were acquired and four main chemical components including C-C;C-H (hydrocarbons), C-OR (ethers and alcohols), C=O (ketones and ketones) and COOR (carboxylic acids and esters) were fitted. These are presented as a function of distance vs percent C 1s component (relative to total C species) across the 5 and 30 W gradients. Within both gradient, the most noticeable variation was seen in the COR and C-C; CH components.

The presence of C-OR functionalities is highest at the centre under the knife edge electrode and systematically decreases extending outwards across the gradients. A higher C-OR content is indicative of a greater retention of ether units. FTIR analysis across these films revealed only a very small amount of hydroxyl groups in the bulk of the gradients (Figure 2). An opposing trend of increasing hydrocarbon content correlates with a subsequent loss of COR units. A slight variation of the C=O and COOR components was observed across the gradients and both species were found to be lowest at the centre of the gradients. The retention of C-OR units was also affected by the plasma load power applied during gradient film deposition. Films deposited at a load power of 5 W contained 78 % C-OR groups (relative to total carbon) at the centre of the gradient compared to only 46 % C-OR in 30W DGpp gradient films, showing that the COR to CC: CH also decreases in gradients deposited at higher load powers.

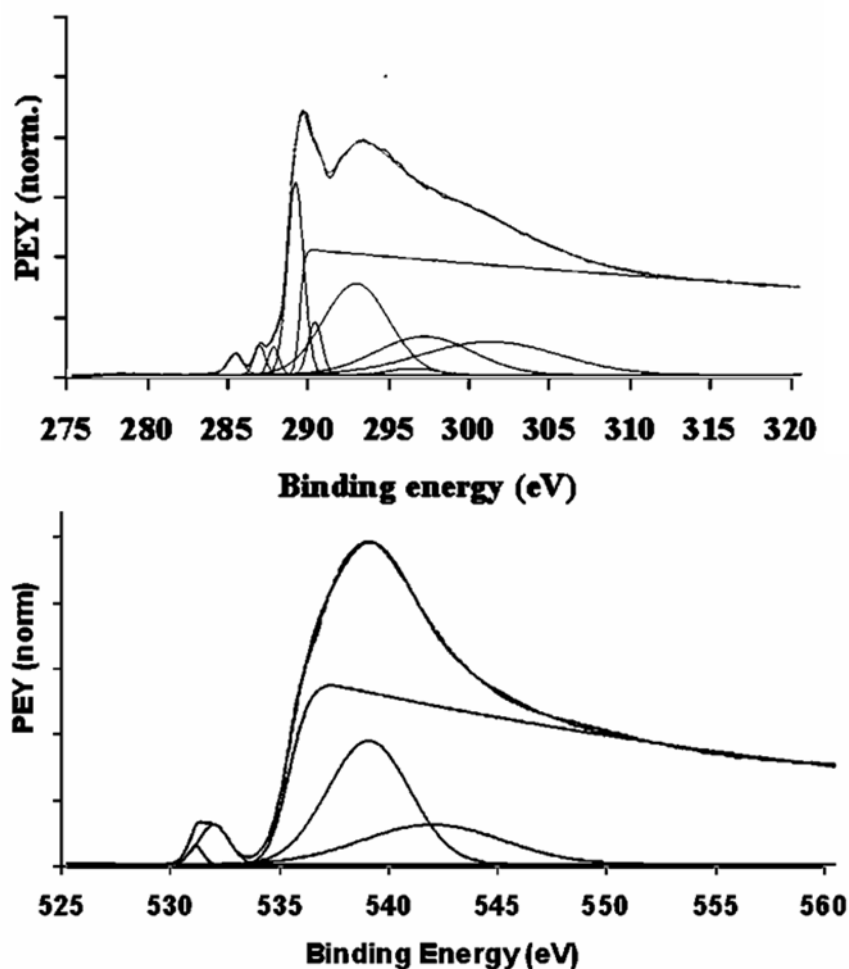


Figure 4. Example C 1s and O 1s curvefits shown for the centre of the 5 W gradient. A series of Gaussian peaks were fitted enabling a comparison of the integrated area of the relevant spectral features

Explanatory notes:

A MatLab based curve fitting program, Whooshka was used to curve-fit the NEXAFS spectra, where a series of Gaussian peaks were assigned to fit the area of the resonance features, along with a step edge. Example curve fits for both the C 1s and O 1s K-edge spectra are shown (Figure 4).

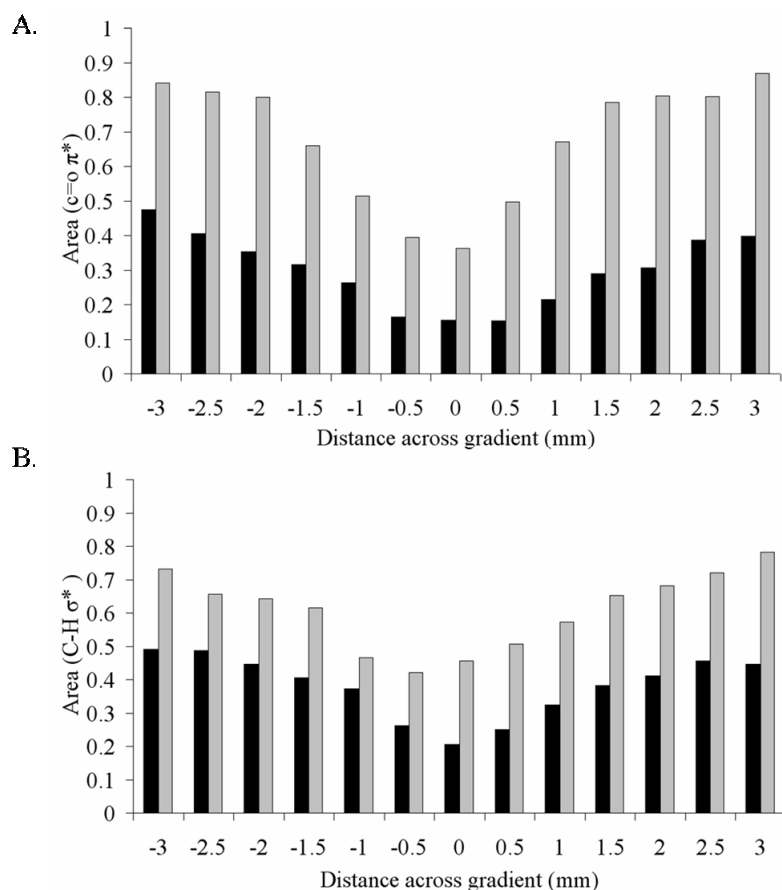


Figure 5. Area plots of the C=O π^* (A) and C-H σ^* (B) spectral features from the C 1s NEXAFS spectra. Results indicate that the presence of carbonyl and hydrocarbon species is lowest at the centre of the gradient and increases in films deposited at higher load power. The data is plotted across the 5 W (■) and 30W (□) DGpp gradients

Explanatory notes:

Results of the curve fitting procedure for the C=O π^* and C-H σ^* resonance of the C 1s K-edge spectra taken across the DGpp gradients are presented in Figure 5. Results for the two DGpp gradients (5 and 30 W) are plotted 3mm either side of the centre (0 mm) show that the central region of each gradient have lower concentrations of unsaturation (C=O) and hydrocarbon species, systematically increasing outwards. This is consistent with the data obtained from XPS and gi-FTIR analysis. Higher levels of unsaturation and hydrocarbon

species were introduced into the gradients as the load power was increased during plasma deposition.

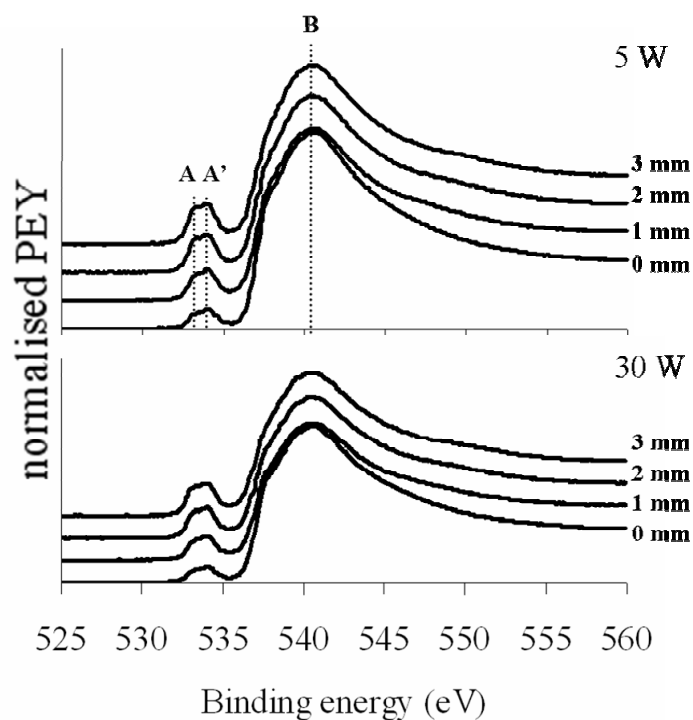


Figure 6. O 1s K-edge NEXAFS spectral Overlays taken between 0 and 3 mm across the 5 and 30 W DGpp gradients. The contribution of the C=O π^* transition unsaturated peak (A and A') increases with distance from the centre of the gradient and in gradients deposited at higher load power.

Explanatory notes:

Figure 6 presents the O K-edge NEXAFS spectra for the 5 and 30 W gradients between 0 and 3 mm across each film. The spectra for the DGpp gradients showed two main resonance features; firstly, the O 1s $\rightarrow \pi^*$ (C=O), exhibited as an unresolved doublet peak with two components at ~ 533.4 and 534.1 eV (A and A', believed to be attributed to carbonyl and aldehyde species, respectively) and secondly the O 1s $\rightarrow \sigma^*$ (C-O) transition at ~ 540.8 eV (B).

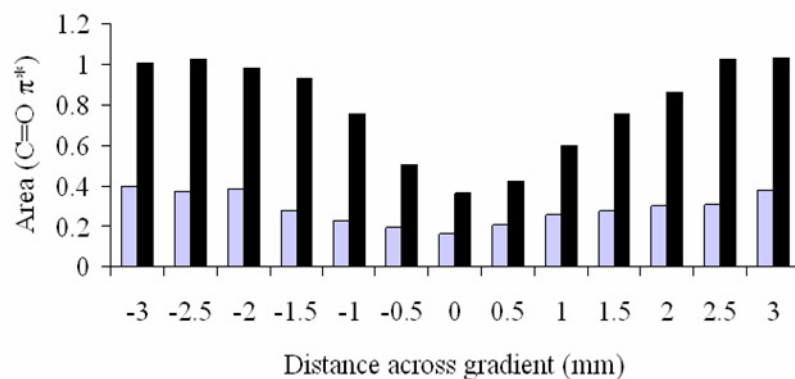


Figure 7. Area plots of the C=O π^* spectral feature from the O 1s NEXAFS spectra. Results indicate that the carbonyl functionality is lowest at the centre of the gradient and increases in films deposited at higher load powers. The data is plotted across the DGpp gradients for the 5 (■) and 30W (■) films

Explanatory notes:

Analysis of the spectra acquired across the 5W gradient indicate an increasing PEY signal for the C=O π^* resonance, (the same trend observed for the 30 W film) which is confirmed when the integrated area of both components (A and A') is plotted as a function of distance across the gradient (Figure 7). It can be seen that there is a trend of increasing unsaturation extending out from the centre across the gradients and as a function of deposition power, which correlates with the results obtained from the C K-edge spectral analysis. Once again, the higher energy $\sigma^*_{(C-O)}$ resonances were not suitable for quantification of the relative concentrations of C-O bonded species due to the broad nature of the peaks and contributions from multiphoton resonance absorptions.

Appendix 2

Supporting Information for Chapter 7

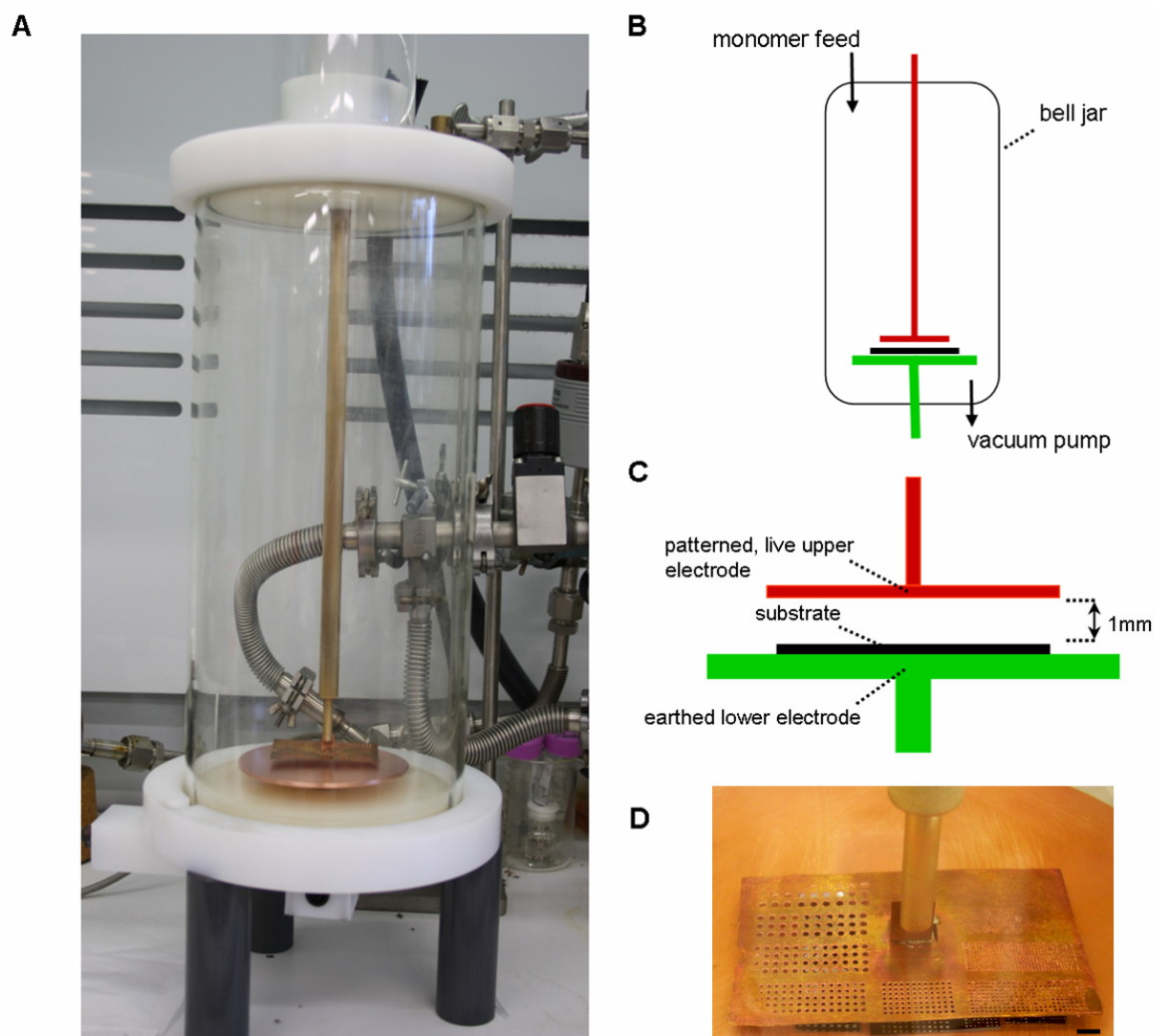


Figure 1. Reactor configuration for the deposition of micropatterned DGpp surfaces. A. Photograph of the reactor as used for the procedure. B. Schematic of the major components. C. Detailed schematic of the electrode region. The live, patterned electrode is red, whereas the earthed electrode is green. The patterned electrode is brought to 1mm of the substrate (black) upon which the patterns are to be deposited. D. A photographic image of the patterned electrode showing the specific electrode configurations (scale bar 5mm) The patterned holes allow for a variation in density of the plasma sheath and result in chemically patterned surfaces with a one step deposition.

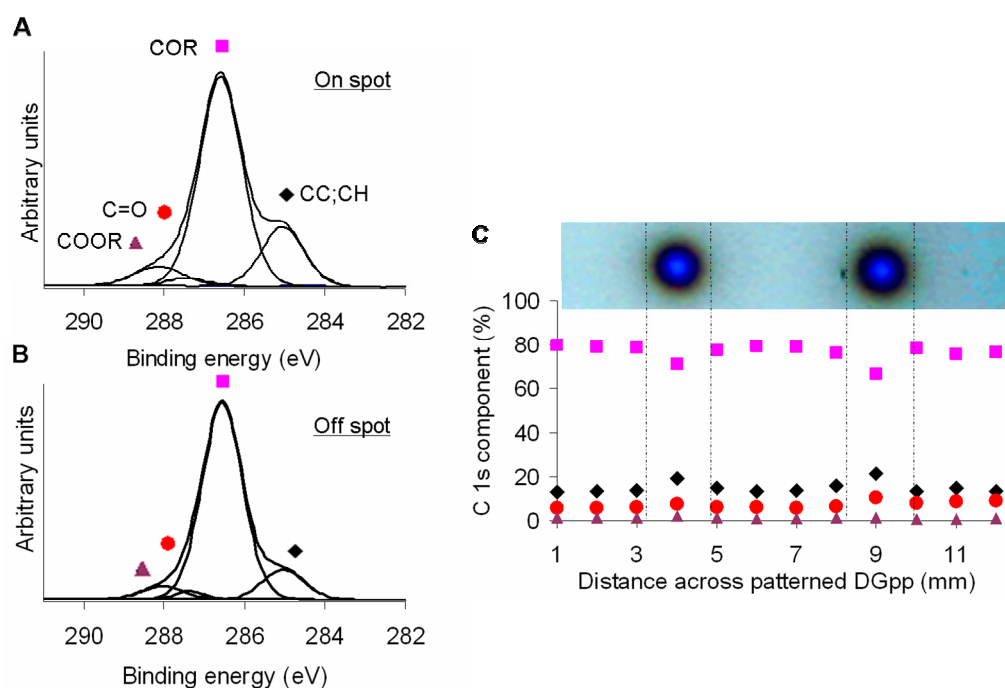


Figure 2. High resolution XPS C 1s scans were acquired across the DGpp patterned surfaces. A and B. The C 1s curves taken both on and off the spot respectively show the spots to contain lower ether related and higher hydrocarbon groups. C. The resulting C 1s components were plotted as a percentage of total C species, showing the patterned features to contain lower COR (■) surface groups, and higher CC;CH (◆) and C=O (●) groups, with relatively uniform level of COOR (▲) detected across the surface as determined within the analysis depth of XPS.

Explanatory Note: High resolution C 1s XPS spectra were acquired across the DGpp patterned surfaces and representative spectra taken both on and off the spot are presented in Figure 2 A and B. Four main chemical components were evident and fitted to the acquired C 1s curves, including C-C;C-H (hydrocarbons), C-OR (ethers and alcohols), C=O (aldehydes and ketones) and COOR (carboxylic acids and esters). Comparison of the two C 1s curves shows variation of the COR to CC;CH intensity ratio, indicating a higher retention of monomer-like chemistry on the surrounding film compared to a lower COR concentration within the spot. Furthermore, the percentage of each C 1s component relative to total carbon is plotted as a function of distance across the patterned surface (Figure 2 C) showing that the COR content drops by approximately 10 % on the patterned features compared to the

surrounding, low fouling, base film. A slightly higher level of CC;CH, C=O and COOR bonded species were evident within the patterned spot compared to the surrounding film.

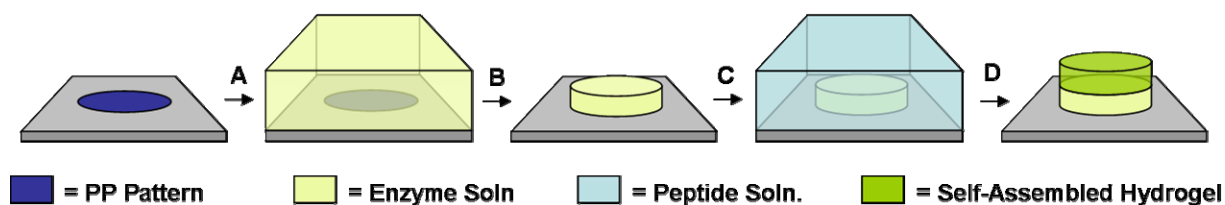


Figure 3. Schematic of enzyme immobilisation for peptide self-assembly. Patterned substrates were prepared as previously on glass microscope slides. A. the slide was incubated in a solution of thermolysin (from *Proteolyticus rokko*) at a concentration of 82 units/ml for a period of 24 hours. B. The slides were then washed multiple times to remove all unattached enzyme, leaving the functional enzyme only within the confines of the pattern. C. The patterns were then incubated in a solution of precursor (20mM fmoc-leucine and 40mM di-leucine) for 24 hours. During this incubation period, the enzyme performs a reversed hydrolysis reaction to form fmoc-tripeptide, which undergoes self-assembly.[1] D. Upon removal of the precursor solution, a self assembled hydrogel remains which is confined to the site of enzyme activity.

Explanatory Note: Modelling of the plasma discharge

The asymmetric discharge can be electrically modelled by two sheaths at the live (upper) and earth (lower) electrodes and via the plasma bulk. The geometric electrode area ratio is $A_{\text{earth}}/A_{\text{live}} \sim 2.8$ ($A_{\text{earth}} = 78 \text{ cm}^2$ and $A_{\text{live}} = 28 \text{ cm}^2$) and most of the applied voltage will be dropped in the live electrode sheath since its capacitance will be smaller than that of the earth sheath. For the present operating pressure of 26 Pa, we assume an electron temperature kT_e of $\sim 3 \text{ eV}$ [2] (k is the Boltzmann constant) which yields a plasma potential of about $V_p \sim (kT_e/e) \ln(M_i/2Pm)^{1/2} \sim 5 (kT_e/e) \sim 15 \text{ V}$ (e is the electronic charge, M_i is the argon ion mass and m is the electron mass). The presence of a ‘Pi’ resonant matching network with a blocking capacitor allows for the development of a self-bias potential $V_{\text{sb-live}}$ at the live electrode.[3]

The applied voltage at the live electrode can be written as:

$$V_{\text{live}} = Q(1.4U_{\text{rms}}) = 1.4Q(P_{\text{rms}}Z)^{1/2} \quad (1)$$

where Q is the quality factor of the resonant circuit ($Q \sim 3$), U_{rms} is the voltage at the entrance of the matching network, Z is the output impedance of the generator ($Z=50 \text{ Ohm}$), and P_{rms} is the input power ($P_{rms}=5 \text{ W}$). V_{live} is about 65 V which gives a self-bias of $V_{sb-live} \sim (V_p - V_{live}) \sim -50 \text{ V}$. A simple power loss estimate P_{loss} can be carried out assuming that the plasma escapes out through the two sheaths at the Bohm speed [4]:

$$P_{rms} = P_{loss} = en_{sheath} v_B \left[A_{live} (E_i + E_{exc} + V_p + |V_{sb-live}| + 2(kT_e/e)) + A_{earth} (E_i + E_{exc} + V_p + 2(kT_e/e)) \right] \quad (2)$$

where n_{sheath} is the plasma density next to the electrodes (sheath edge density), $v_B = (kT_e/M_i)^{1/2} \sim 2.7 \times 10^3 \text{ ms}^{-1}$ is the Bohm speed, $E_{ion} \sim 15 \text{ V}$ is the ionisation energy, $E_{exc} \sim 13 \text{ V}$ is the excitation energy, and it is assumed that each escaping electron carries $2(kT_e/e)$ of kinetic energy to the electrodes. For a 5 W input power, the calculated sheath density is $1.7 \times 10^{10} \text{ cm}^{-3}$.

The Debye length near the sheaths edge is:

$$\lambda_{De} = \sqrt{\frac{\epsilon_o kT_e}{e^2 n_{sheath}}} \sim 10^{-4} \text{ m} \sim 100 \mu\text{m} \quad (3)$$

where ϵ_o is the permittivity of free space ($\epsilon_o = 8.85 \times 10^{-12} \text{ Fm}^{-1}$).

To determine the live (S_{live}) and earth (S_{earth}) electrode sheath thickness we use the Child law for a collisionless DC sheath in an argon plasma capacitively coupled between two planar electrodes [2, 4]:

$$S = \left(\frac{K_i \epsilon_o}{e v_B} \sqrt{\frac{2e}{M_i}} \right)^{1/2} \frac{V^{3/4}}{n_{sheath}^{1/2}} \quad (4)$$

where $K_i = 4/9 = 0.44$ and V is the sheath potential (V_{live} and V_p , for the live and earth electrode, respectively). The calculated values for S_{live} and S_{earth} with an input power of 5 W

are 1 mm and 0.28 mm, respectively. At 26 Pa, the ion-neutral collision mean free path l_i is about 0.15 mm and the average number of collisions in the live and earth electrode sheaths is about 5 and 1.5, respectively. The sample is placed on the near collision-less earth electrode and the power deposited to the surface is about 0.04 Wcm^{-2} .

Table 1. Plasma parameters estimated from the argon plasma model for an input power of 5 W and an operating pressure of 26 Pa.

Electron temperature, T_e (eV)	3
Bohm velocity, v_B (m.s^{-1})	2700
Live Sheath potential, V_{live} (V)	65
Earth sheath potential, V_p (V)	15
Sheath edge density, n_{sheath} (m^{-3})	1.7×10^{16}
Debye length, l_{De} (m)	10^{-4}
Live sheath thickness, S_{live} (m)	7.8×10^{-4}
Earth sheath thickness, S_{earth} (m)	2.5×10^{-4}
Ion-neutral mean free path, l_i (m)	1.5×10^{-4}

References:

1. R. J. Williams, A. M. Smith, R. Collins, N. Hodson, A. K. Das, R. V. Ulijn. Enzyme-assisted self-assembly under thermodynamic control. *Nature Nanotechnology* **2009**, 4, 19.
2. M. A. Lieberman, A. J. Lichtenberg, in *Principles of plasma discharges and materials processing*, Wiley, New York **1994**.
3. H. B. Smith, C. Charles, R. W. Boswell, H. Kuwahara. Bias formation in a pulsed radiofrequency argon discharge. *Journal of Applied Physics* **1997**, 82, 561.
4. C. Charles, R. W. Boswell, M. A. Lieberman. Energy balance in a low pressure capacitive discharge driven by a double-saddle antenna. *Physics of Plasmas* **2003**, 10, 891.